ENHANCING ELECTRICAL DISCHARGE MACHINING PERFORMANCE THROUGH EMPLOYMENT OF TITANIUM NANOPOWDER MIXED DIELECTRIC AND SEVERE PLASTIC DEFORMATION OF ELECTRODE

HOURIYEH MARASHI

FACULTY OF ENGINEERING
UNIVERSITY OF MALAYA
KUALA LUMPUR

2016

University of Malaya

ENHANCING ELECTRICAL DISCHARGE MACHINING PERFORMANCE THROUGH EMPLOYMENT OF TITANIUM NANOPOWDER MIXED DIELECTRIC AND SEVERE PLASTIC DEFORMATION OF ELECTRODE

HOURIYEH MARASHI

THESIS SUBMITTED IN FULFILMENT OF THE REQUIREMENTS FOR THE DEGREE OF DOCTOR OF PHILOSOPHY

FACULTY OF ENGINEERING
UNIVERSITY OF MALAYA
KUALA LUMPUR

2016

University of Malaya

UNIVERSITY OF MALAYA

ORIGINAL LITERARY WORK DECLARATION

Name of Candidate: Houriyeh Marashi

Matric No: KHA130043

Name of Degree: Doctor of philosophy in Mechanical Engineering

Title of Project Thesis:

Enhancing Electrical Discharge Machining Performance through Employment of Titanium Nanopowder Mixed Dielectric and Severe Plastic Deformation of Electrode

Field of Study:

Mechanical Engineering, Advanced Manufacturing Processes

I do solemnly and sincerely declare that:

(1) I am the sole author/writer of this Work;
(2) This Work is original;
(3) Any use of any work in which copyright exists was done by way of fair dealing and for permitted purposes and any excerpt or extract from, or reference to or reproduction of any copyright work has been disclosed expressly and sufficiently and the title of the Work and its authorship have been acknowledged in this Work;
(4) I do not have any actual knowledge nor do I ought reasonably to know that the making of this work constitutes an infringement of any copyright work;
(5) I hereby assign all and every rights in the copyright to this Work to the University of Malaya ("UM"), who henceforth shall be owner of the copyright in this Work and that any reproduction or use in any form or by any means whatsoever is prohibited without the written consent of UM having been first had and obtained;
(6) I am fully aware that if in the course of making this Work I have infringed any copyright whether intentionally or otherwise, I may be subject to legal action or any other action as may be determined by UM.

Candidate's Signature Date:

Subscribed and solemnly declared before,

Witness's Signature Date:

Name:

Designation:

University of Malaya

ABSTRACT

Electrical Discharge Machining (EDM) is one of the most promising techniques for machining high-hardness materials with geometrically complex shape, which is implemented in various industrial fields such as die and mold, aerospace and biomedical. Despite the advantages, tool wear, relatively low material removal rate and its adverse effects on surface quality limit the applications of this technique. In this thesis two techniques are employed to overcome EDM disadvantages. The first technique is the addition of powder to dielectric, namely Powder Mixed Electrical Eischarge Machining (PMEDM). The aim of this research is firstly to enhance the characteristics of AISI D2 steel surface machined with EDM through adding Ti nanopowder to dielectric under various machining parameters, including discharge duration and current. Then surface characteristics and machining productivity were investigated in terms of morphology, topography, surface cracks susceptibility and MRR. It was indicated that addition of Ti nanopowder to dielectric notably enhanced the surface morphology and surface roughness at almost all machining parameters owing to discharge dispersion. The highest improvement of around 23 and 24% in average and peak-to-valley surface roughness were attained at 1 A current and 100 µs discharge duration, respectively. Furthermore, surface elemental analysis signified negligible Ti deposition on the machined surface while the atomic concentration of Ti was increased around the crack areas. Secondly, a novel technique for enhancing EDM electrode is proposed to reduce the electrode wear in EDM, which is challenging to overcome specially when it comes to producing geometrically complex components. This technique entails a new approach for developing pure copper electrode using Severe Plastic Deformation (SPD) to enhance the machining characteristics during EDM. Equal Channel Angular Pressing (ECAP) is selected as the most popular SPD method to process EDM electrodes. The results emphasize that electrodes subjected to ECAP enhance workpiece accuracy by decreasing

University of Malaya

Volumetric Overcut (VOC) and increasing corner sharpness. It is also revealed that nanohardness enhancement following ECAP leads to lower TWR. Lastly, combination of these techniques have been employed to realize the mutual effect of these techniques, employment of Ti nanopowder mixed dielectric and ECAP treatment of electrode. It was revealed that addition of powder to dielectric in all machining conditions leads to enhancing the machined surface quality in terms of morphology and average surface roughness. In overall, ECAP treatment of electrode improve the corner sharpness of produced components, however, addition of powder to dielectric deteriorates this effect through increasing the dielectric ionization. Formation of droplets on the surface close to the cavity walls was reduced after employment of Ti nanopowder mixed dielectric or/and ECAP treatment of electrode. Furthermore, addition of powder to dielectric increase the TWR for original and ECAP-treated electrodes due to increasing the ionization of dielectric fluid and there is a negligible amount of Ti element deposited on the machined surface when employing either of electrode types.

University of Malaya

ABSTRAK

Electrical Discharge Machining (EDM) adalah salah satu teknik yang paling menjanjikan untuk pemesinan bahan-kekerasan yang tinggi dengan bentuk geometri yang kompleks, yang dilaksanakan dalam pelbagai bidang industri seperti die dan acuan, aeroangkasa dan bioperubatan. Walaupun kelebihan, Kedar Kehausan meta-alat, kadar pembuangan bahan yang rendah dan kesan buruk terhadap kualiti permukaan menghadkan aplikasi teknik ini. Dalam tesis ini dua teknik diperkenalkan untuk mengatasi kelemahan EDM. Teknik pertama adalah penambahan serbuk untuk dielektrik, iaitu serbuk campuran pelepasan elektrik pemesinan (PMEDM). Tujuan kajian ini adalah pertama untuk meningkatkan ciri-ciri AISI D2 permukaan keluli dimesin dengan EDM melalui menambah Ti nanopowder untuk dielektrik di bawah pelbagai parameter pemesinan, termasuk tempoh pelepasan dan puncak semasa. Kemudian ciri-ciri permukaan dan pemesinan produktiviti telah disiasat dari segi morfologi, topografi, retak permukaan kecenderungan dan MRR. Ia telah menunjukkan bahawa penambahan Ti nanopowder untuk dielektrik terutamanya dipertingkatkan morfologi permukaan dan kekasaran permukaan di hampir semua parameter pemesinan kerana penyebaran pelepasan. Peningkatan tertinggi sekitar 23 dan 24% pada kekasaran purata dan permukaan puncak-ke-lembah telah mencapai pada 1.5 A Tempoh pelepasan semasa dan 100 μs puncak, masing-masing. Tambahan pula, analisis unsur permukaan menandakan diabaikan Ti pemendapan di permukaan dimesin manakala kepekatan atom Ti telah meningkat di sekitar kawasan retak. Kedua, satu teknik baru untuk meningkatkan EDM elektrod adalah dicadangkan untuk mengurangkan memakai elektrod dalam EDM, yang mencabar untuk mengatasi khas apabila ia datang untuk mengeluarkan komponen geometri kompleks. Teknik ini memerlukan pendekatan baru untuk membangunkan elektrod tembaga yang tulen menggunakan ubah bentuk plastik yang teruk (SPD) untuk meningkatkan ciri-ciri pemesinan semasa EDM. saluran sama sudut menekan (ECAP)

University of Malaya

dipilih sebagai kaedah SPD yang paling popular untuk memproses elektrod EDM. Keputusan menekankan bahawa elektrod tertakluk kepada ECAP meningkatkan ketepatan bahan kerja dengan mengurangkan VOC dan meningkatkan sudut ketajaman. Ia juga mendedahkan bahawa peningkatan nanohardness berikut ECAP membawa kepada menurunkan TWR. Akhir sekali, gabungan teknik-teknik ini telah digunakan untuk menyedari kesan bersama teknik-teknik ini, pekerjaan Ti nanopowder dielektrik bercampur dan rawatan ECAP elektrod. Ia telah mendedahkan bahawa penambahan serbuk untuk dielektrik dalam semua keadaan pemesinan membawa kepada meningkatkan kualiti permukaan yang dimesin dari segi morfologi dan purata kekasaran permukaan. Secara keseluruhannya, rawatan ECAP elektrod meningkatkan ketajaman sudut komponen dihasilkan, bagaimanapun, penambahan serbuk untuk dielektrik merosot kesan ini dengan meningkatkan pengionan dielektrik. Pembentukan titisan pada permukaan dekat dengan dinding rongga telah dikurangkan selepas penggajian Ti nanopowder bercampur dielektrik rawatan atau / dan ECAP elektrod. Tambahan pula, penambahan serbuk untuk dielektrik meningkatkan TWR untuk elektrod asal dan ECAP dirawat kerana meningkatkan pengionan cecair dielektrik dan terdapat jumlah yang sedikit unsur Ti disimpan di permukaan yang dimesin apabila menggunakan salah satu jenis elektrod.

University of Malaya

ACKNOWLEDGEMENTS

First and foremost, I would like to express my deeply indebted to my supervisor, Assoc. Professor Dr. Sarhan for his invaluable guidance, excellent supervision, insight and dedication throughout this project. Also, many thanks to Professor Dr. Hamdi for his indulgent support during the research.

I further express my gratitude to all the mechanical workshop technicians for their unlimited help and support in preparing samples and instruments. Besides, special thanks to my dearest family and my friends for being supportive and accompanying me along this thesis. My grateful thanks also extended to the Faculty of Engineering, University of Malaya for providing good facilities and sufficient resources that allowed me to complete this research.

University of Malaya

TABLE OF CONTENTS

University of Malaya

University of Malaya

University of Malaya

University of Malaya

LIST OF FIGURES

University of Malaya

University of Malaya

University of Malaya

University of Malaya

University of Malaya

University of Malaya

LIST OF TABLES

University of Malaya

LIST OF SYMBOLS AND ABBREVIATIONS

A	:	Plate area of capacitor
AFM	:	Atomic force microscopy
ARB	:	Accumulative roll bonding
C	:	Capacitor
C0	:	Ordinary electrode
C1	:	One pass ECAP treated electrode
C2	:	Two passes ECAP treated electrode
d	:	Distance between conductors
ε_0	:	Permittivity in free space
ε_r	:	Relative permitivity
E	:	Electrical field in capacitor
E_b	:	Dielectric breakdown strength
E_d	:	Discharge energy
ECAP	:	Equal channel angular pressing
EDX	:	Energy dispersive X-ray spectroscopy
ESEM	:	Environmental scanning electron microscopy
F_P	:	Pulse signal frequency
FESEM	:	Field emission scanning electron microscopy
Gr	:	Graphite
HPT	:	High pressure torsion
I	:	Current
I_a	:	Average Current
I_P	:	Peak current
κ	:	Dielectric constant

University of Malaya

MRR	:	Material removal rate
PMEDM	:	Powder mixed electrical discharge machining
Q	:	Charge stored in capacitor
Ra	:	Average surface roughness
Rz	:	Peak-to-valley surface roughness
SPD	:	Severe plastic deformation
SR	:	Surface roughness
t_d	:	Discharge duration
t_{delay}	:	Ignition delay time
T_{on}	:	Discharge duration
T_{off}	:	Charging duration
t_p	:	Pulse duration
TWR	:	Tool wear rate
U_0	:	Open gap voltage
U_b	:	Breakdown voltage
U_d	:	Discharge voltage
V	:	Voltage
VOC	:	Volumetric Overcut
V_a	:	Average voltage
W_t	:	Spark energy

University of Malaya

CHAPTER 1: INTRODUCTION

1.1 Background

Fabrication of machineries with high durability is a necessity for production of heavy-duty manufacturing components. Electrical Discharge Machining (EDM) is a non-traditional machining technique that is practical in various industries, including die and mold production, automotive, aerospace (Ho & Newman, 2003) and biomedicine (Masuzawa, 2000). Through conversion of electrical energy to thermal energy (K.-M. Tsai & Wang, 2001), a series of repeated sparks are generated on the workpiece surface facilitating (Mohd Abbas, Solomon, & Fuad Bahari, 2007) the material removal through surface material erosion. Not only prominent machinability of EDM, elimination of any mechanical stress (Y. Liu, Wang, Zhao, & Wang, 2010), vibration issues and chatter (Ho & Newman, 2003) are considered as some other advantages.

Despite the complex machining mechanism, EDM abilities have not been fully exploited due to its disadvantages. Primarily, the problem arises from the slow machining rate and poor surface quality (Houriyeh Marashi, Jafarlou, Sarhan, & Hamdi, 2016). Repetitive spark between tool and workpiece also causes an undesirable erosion of tool material increasing production cost and subsequently compromises the geometrical accuracy of the machined component. Furthermore, since the machined surface is exposed to heat and instant cooling by dielectric, surface cracks, heat affected zone and residual stress (Muhammad Pervej Jahan, Rahman, & Wong, 2010) are considered as other drawbacks. Hence, presenting new methods to develop EDM capabilities has always been center of attention. Several techniques have been introduced as an enhancement method to boost EDM performance such as implementation of ultrasonic vibration in EDM (L. Li, Zongwei, & Guangming, 2009), alternative tool materials (S. Singh, Maheshwari, & Pandey, 2004), introducing alternative dielectric mediums (Joshi,

University of Malaya

Govindan, Malshe, & Rajurkar, 2011) and Powder Mixed EDM (PMEDM) (Kansal, Singh, & Kumar, 2007b).

This thesis presents the enhancement of EDM process through two techniques. First, the addition of Ti nanopowder to dielectric namely Powder Mixed EDM (PMEDM). Powder particles in the machining gap prevent direct sparks between the tool and workpiece. In fact, the primary discharge occurs between the tool and powder particles, and then a series of small sparks melt and/or evaporate the surface material. Thus, the negative effect of direct spark between tool and workpiece is replaced by a series of small sparks, which results in a smoother surface. Second, employing severe plastic deformation of electrode to enhance its mechanical properties, which leads to enhancing EDM outcome. At last, two methods of Ti nanopowder mixed EDM and severe plastic deformation of electrode are employed to investigate their mutual influence on EDM performance measures.

1.2 Problem statement

Of the existing non-conventional methods, Electrical Discharge Machining (EDM) is a promising method for machining difficult-to-cut conductive materials with geometrically complex shapes (Srivastava & Pandey, 2013). Despite the advanced material removal system, EDM exhibits some limitations particularly when higher material removal rate (MRR) is necessary such as inappropriate surface quality, surface defects, layer susceptibility to heat and residual stress result in poor EDM performance (Ekmekci, 2007). In this study, the Ti nanopowder mixed dielectric has been employed to enhance the machined surface characteristics, which improves the MRR and surface quality simultaneously.

Tool wear rate (TWR) is another disadvantageous of EDM. Not only by affecting economical aspect of production, but TWR also compromises the machined component

University of Malaya

geometry through side or corner wear. To reduce the TWR during machining, this research for the first time proposes the severe plastic deformation of electrode to enhance its mechanical properties. In this method, the high machinability of electrode is preserved and the hardness property will increase which leads to lower TWR.

The aim of this study is to enhance EDM performance parameters such as MRR, TWR and surface roughness by employing the Ti nanaopowder mixed dielectric and severe plastic deformation of electrode.

1.3 Research objectives

- To determine the impact of Ti nanopowder addition on EDM performance characteristics under different machining conditions
- To determine the EDM process performance factors when equal channel angular pressing is employed to enhance mechanical properties of electrode
- To evaluate the mutual impact of Ti nanopowder addition to dielectric on EDM process performance factors when equal channel angular pressing is employed to enhance mechanical properties of electrode

1.4 Novelty statement

In this thesis, firstly, the influence of adding Ti nanopowder particles to dielectric in electrical discharge machining process is evaluated, to alternate the discharge attribute and achieve the optimized gap expansion for generating a surface with enhanced properties. The aim of this study is to determine how process performance factors mainly concerning surface quality are affected by the addition of Ti nanopowder. The new discharge characteristics result in the achievement of higher surface quality. The superior properties of the machined surface were achieved not only without declining the machining efficiency, but in fact with obtaining higher material removal rate with participation of the Ti nanopowder in the process.

University of Malaya

Secondly, a novel approach to enhance machining characteristics during electrical discharge machining is proposed through processing pure copper electrodes using severe plastic deformation (SPD). Equal channel angular pressing (ECAP) is selected as the most popular SPD method to process EDM electrodes. Using this method, the AISI D2 tool steel as one of the widely-used alloys in die and mold industry was machined using different electrode types and a product with promising characteristics was produced.

1.5 Thesis Overview

This thesis is mainly divided into five main chapters of introduction, literature review, methodology, results and discussion and conclusion. First chapter contains the introduction to the EDM problematic areas in which the research is concerned with, the aims and objectives of the study. The research approach mainly concerned with two main solutions proposed and practiced in this thesis, addition of Ti nanopowder to dielectric and severe plastic deformation of electrode to enhance the machining characteristics. Second chapter provides a critical assessment of the relevant literature mainly concerned with PMEDM, electrode enhancement techniques and metal strengthening methods. It consists of a critically written and comprehensive account of the published works by accredited scholars and researchers. Third chapter is the methodology including the experimental set up, base materials, conditions, procedure, instruments, analysis preparation and methods of analysis. Chapter four includes the obtained results and discussion on the topic and lastly chapter five points out the main achievements of this thesis for each employed technique and provides recommendation for future studies.

University of Malaya

CHAPTER 2: LITERATURE REVIEW

2.1 Introduction

The organization of this chapter is as follows. In section 2.2 and 2.3, the Electrical Discharge Machining (EDM) mechanism and the influence of input parameters on performance factors are discussed, respectively. In section 2.4, the Powder Mixed EDM (PMEDM) technology as one of the most promising techniques to enhance the machining performance is presented with subcategories including discharge characteristics after addition of powder, employed types of powder additives, detailed review of studies considering the performance and research trends of PMEDM. In section 2.5, tool electrode as an influential non-electrical parameter is considered. The idea of severe plastic deformation (SPD) as the most effective methods for strengthening materials implemented through grain refinement is presented in section 2.6. Additionally, in this section the most promising SPD techniques with emphasize on ECAP is presented which is the most successful SPD technique for processing bulk structural metallic materials. Furthermore, in section 2.6.4 major ECAP parameters including die geometry, extrusion force, friction and strain rate is discussed in detail. Finally, the conclusion of chapter 2 is presented in section 2.8.

2.2 Electrical discharge machining

The concept of EDM was introduced between world war I and WW II. Later, Boris R. and Natalie I. Lazarenko developed the RC-relaxation circuit and servo system unit, which transformed the EDM to a dependable machining technique (Sommer & Sommer, 2005). As EDM material removal mechanism is by melting and/or evaporating the surface, there is no mechanical stress applied on the workpiece. Which highlights the EDM as a viable tool to manufacture fragile components by avoiding the mechanical stress on the delicate parts in complex structures. The other outstanding capabilities of this technique include the ability to machine high-hardness conductive materials, produce

University of Malaya

complex geometrical shapes, poses simple tool-making process and eliminate the chatter phenomena (Ho & Newman, 2003).

Nowadays, EDM is transformed, as advanced and sophisticated generators, servo systems, controllers, etc. considerably enhanced its performance. EDM machine mainly consists of 5 main modules, control unit and generator, servo system, circulation system, dielectric reservoir and pump, machining tank with work piece holder as well as X-Y table. As illustrated in Figure 2.1 these components function side by side to provide a reliable machining platform.

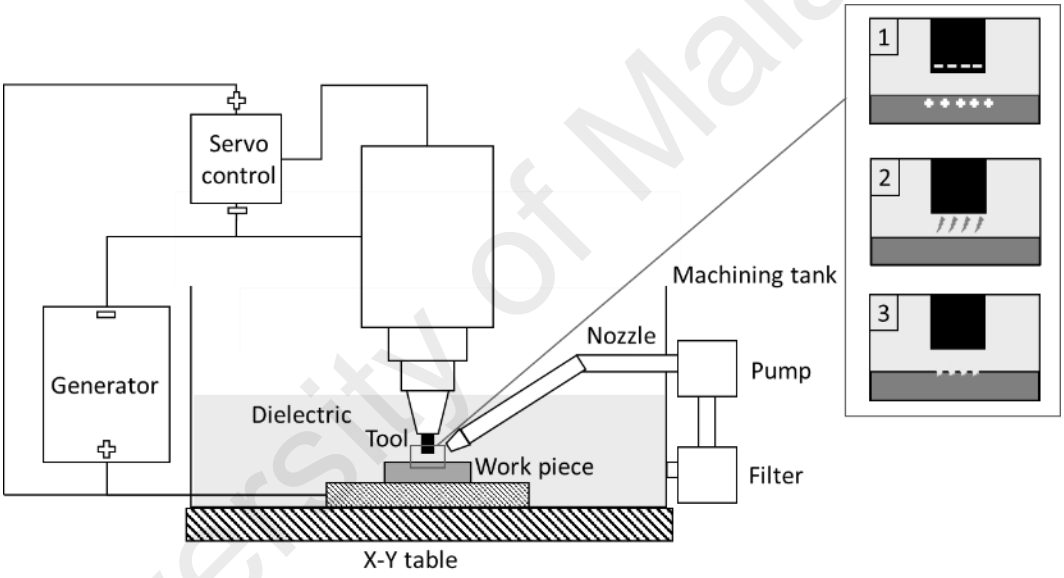

Figure 2.1: Schematic diagram of electrical discharge machine
1. Charging 2. Spark 3. Formation of crater

In order to understand the EDM spark characteristics, the material removal mechanism in conventional EDM is described. Conventional EDM undergoes continuous charging and discharging between tool and workpiece while immersed in dielectric fluid. According to explanations by Bernd M. Schumacher (2004), Muhammad P. Jahan (2013) and Hockenberry (1967), Formation of discharge channel which subsequently leads to material removal in EDM is described in three phases: (i) preparation, (ii) discharge and (iii) interval phases which are described schematically in Figure 2.2.

University of Malaya

In the first phase, followed by applying potential difference, the electrical field builds up between the electrodes (tool and workpiece). This strong electromagnetic field orients particles which are trapped in this field and polarize the dielectric molecules as well. This phenomenon subsequently forms a bridge to link the electrode and workpiece which leads to reduction of dielectric resistivity. Once the applied voltage exceeds the natural electrical resistivity of dielectric, the current gradually streams through the flux tube and hit the workpiece surface in the form of spark. During the second phase, while the current flow increase and voltage decrease, plasma channel forms and grows rapidly, generating an extreme amount of heat and pressure. The growth continues until an equilibrium is reached between energy supply, heat flow to tool and workpiece, evaporation of dielectric and internal pressure of formed bubble.

After the current pass through the flux and disrupts the arranged particles of dielectric and contamination including dielectric ionized molecules and workpiece re-solidified particles at second phase, the resistivity of dielectric increase quickly followed by rapid deionization of the plasma channel at the third phase. In the interval phase between discharges, the channel can no longer sustain a stable spark condition thus current drops to zero with a gradual increase in voltage. The gas bubble however demonstrated to stay 25 times longer than the pulse on-time (Hockenberry, 1967; B. M. Schumacher, 1965) while the over-heated molten material starts instantaneous boiling and releasing liquid globs. Low temperature of dielectric shocks the globs and hardened them from outside which result in hollow internal section due to contraction of metal (Yifan Liu et al., 2014).

Discharging occurs in a frequency range from 2,000 to 500,000 discharge per second (Jameson, 2001) repetitively to complete the machining agenda, printing the pattern of electrode on the workpiece surface. EDM machines require the tool electrode to have the opposite shape as the one going to be printed on workpiece.

University of Malaya

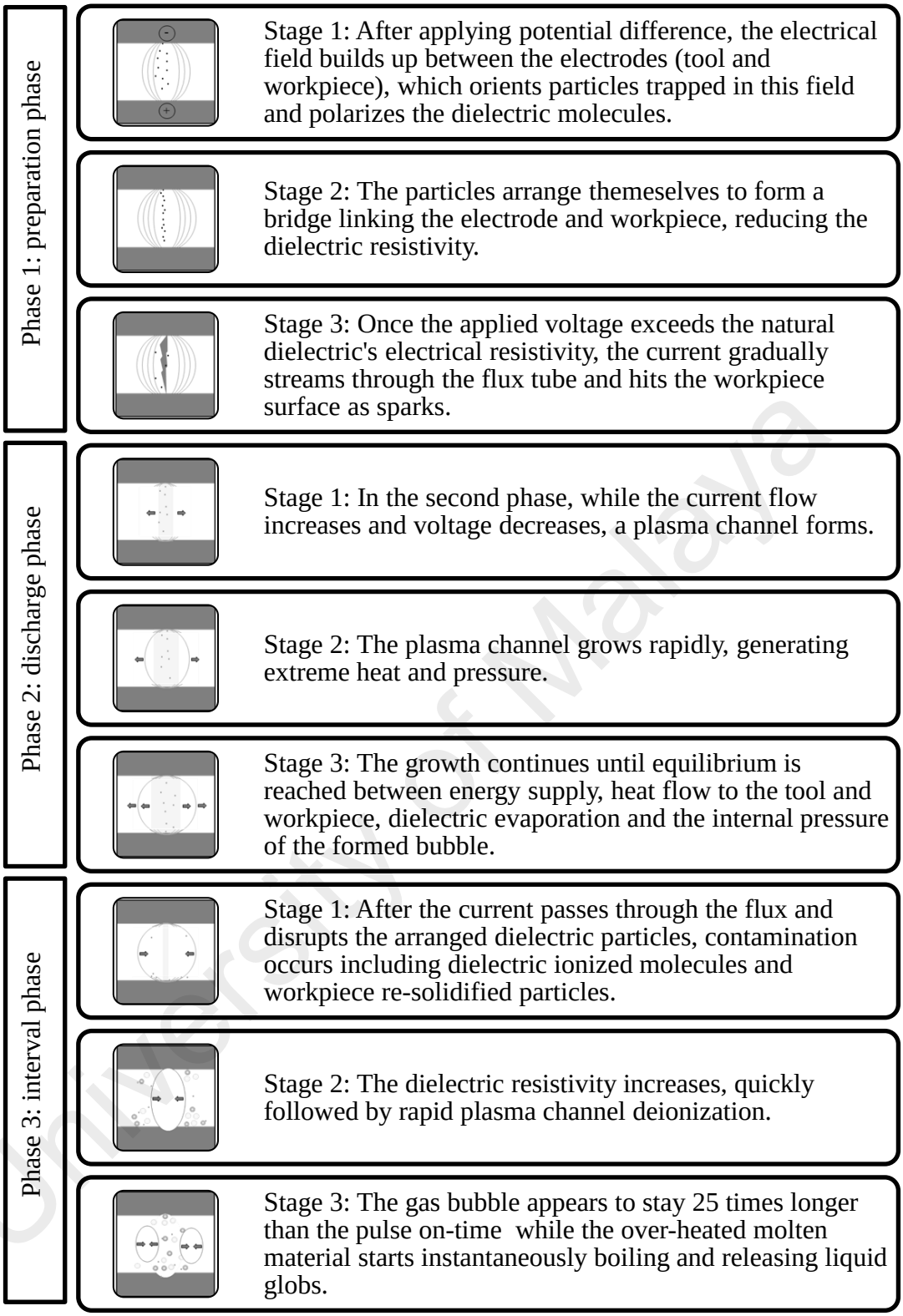

Figure 2.2: Schematic illustration of electrical discharge phases

University of Malaya

2.3 EDM input parameters and performance measures

EDM performance is evaluated through key performance measures, i.e. MRR, surface quality and TWR. These measures are significantly influenced by input machining parameters that are generally categorized as electrical and non-electrical parameters (Figure 2.3) (Muthuramalingam & Mohan, 2015). Electrical parameters are related to measurable electrical values that are regulated by the power supply unit (Jain, 2009), such as current (I), pulse-on-time (T_{on}), pulse-off-time (T_{off}), supply voltage (V) and polarity (Maradia, Boccadoro, Stirnimann, Kuster, & Wegener, 2015) and non-electrical input parameters including electrode lift time, working time, reciprocating speed, gain and nozzle flushing, and tool and workpiece rotation (Kansal, Singh, & Kumar, 2005).

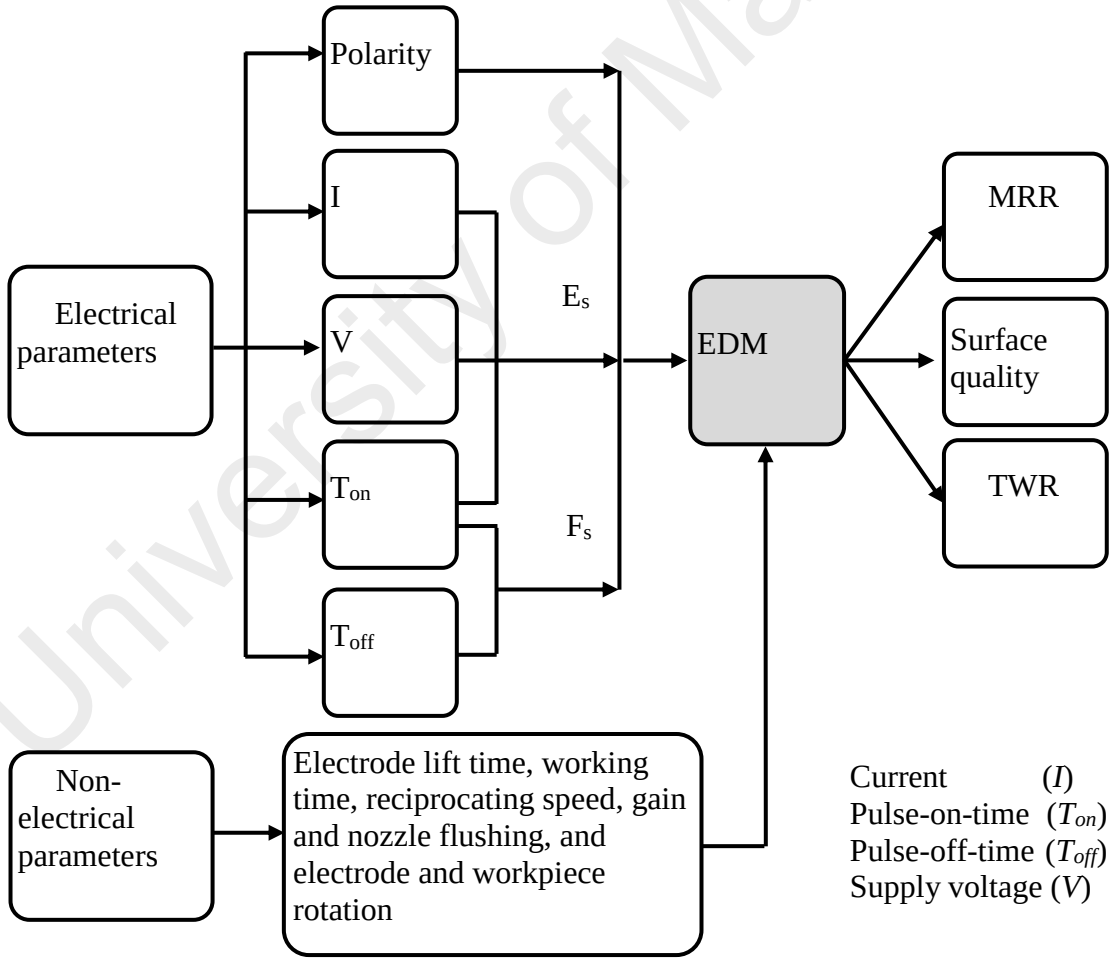

Figure 2.3: Key input parameters and performance measures of EDM (Based on (Garg et al., 2010))

University of Malaya

Material removal rate (MRR) in EDM is directly related to the economic aspect of production and is considered the highest priority (Muhammad P. Jahan, 2013). MRR reflects the process operational speed and is defined in two ways, as the volume (Torres, Puertas, & Luis, 2014) or weight (A. C. Wang, Tsai, & Lin, 2014) of material removed from the workpiece over the machining time.

The machined surface quality is evaluated through roughness, waviness and flaws. Among these, surface roughness measurement is the most employed technique and is commonly expressed as the average surface roughness (R_a). R_a is the average deviation from the mean surface by calculating the arithmetic average deviation of the ordinates of profile height increments from the centerline of that surface (Benbow, Elshennawy, & Walker, 2003).

Tool wear rate (TWR) is another performance measure that decreases EDM efficiency through increasing tool production cost and deteriorating the accuracy of produced component due to end, side and corner wear (Ao, Rieger, & Amouzegar, 2010). TWR is defined as the material weight (Subramanian, Marimuthu, & Sakthivel, 2012) or volume (Meena & Azad, 2012) removed from the tool over the machining time. Moreover, to assess the simultaneous effect of MRR and TWR, the tool wear ratio is introduced as TWR/MRR (Kansal et al., 2007b).

2.4 Powder mixed EDM Technology

Adding powder to dielectric, namely powder mixed electrical discharge machining (PMEDM) is an effective means of enhancing EDM performance owing to different spark attributes. Since PMEDM was introduced in 1980 (Kansal et al., 2007b), researchers have focused on improving the machining performance measures or introducing new PMEDM capabilities like surface modification to ultimately facilitate unique development for commercialization. Although several studies evaluate the PMEDM advancements over

University of Malaya

the years (Ho & Newman, 2003; Kansal et al., 2007b), no review article emphasizes the material, size and powder concentration. To fill this gap, an organized review of PMEDM is provided. First, the spark formation mechanism in conventional EDM besides important input parameters and performance measures is reviewed. Second, the significance of dielectric for EDM machining characteristics is discussed through a detailed review of various dielectric categories. Third, the role of powder addition in spark characteristics followed by the influence of various powder particles, materials, sizes and concentrations is comprehensively reviewed. Finally, powder materials are systematically studied to ease appropriate selection of powder parameters for further research studies.

2.4.1 Discharge characteristics in PMEDM

In conventional EDM, normal pulse discharges regularly cause arcing due to insufficient pure dielectric deionization and excessive local debris (Luo, 1997). However, adding sufficient powder to the dielectric increases the electrical conductivity and expands the gap, subsequently stabilizing the process through better flushing and servo-hunting (Wong, Lim, Rahuman, & Tee, 1998). Increased discharge gap width also decreases the heat flux (Kojima, Natsu, & Kunieda, 2008), which reduces the material removal of a single spark and enhances the surface quality. Yet such gap expansion is not feasible by using all powder materials, since powder density, electrical resistivity, and thermal conductivity along with particle size and concentration are highly determinative.

Besides, the increased electrical conductivity of dielectric enhances the ionization and spark frequency between tool and workpiece (Figure 2.4). The increased spark frequency appears to overcome the lower MRR of a single spark resulting from gap expansion. Therefore, multiple discharge patterns are evident from a single input pulse due to multiple discharge paths created, leading to discharge energy dispersion (Chow, Yan, Huang, & Hung, 2000; Wu, Yan, Huang, & Chen, 2005) in contrast to pure dielectric that

University of Malaya

produces a consistent waveform pattern (Figure 2.5). Moreover, discharge dispersion reduces the emergence of surface ridges due to the formation of shallower craters with lower borders (Ekmekci, 2009). Subsequently, smaller discharge craters and debris particles ease gap exhaust and accelerate MRR (Chow, Yang, Lin, & Chen, 2008).

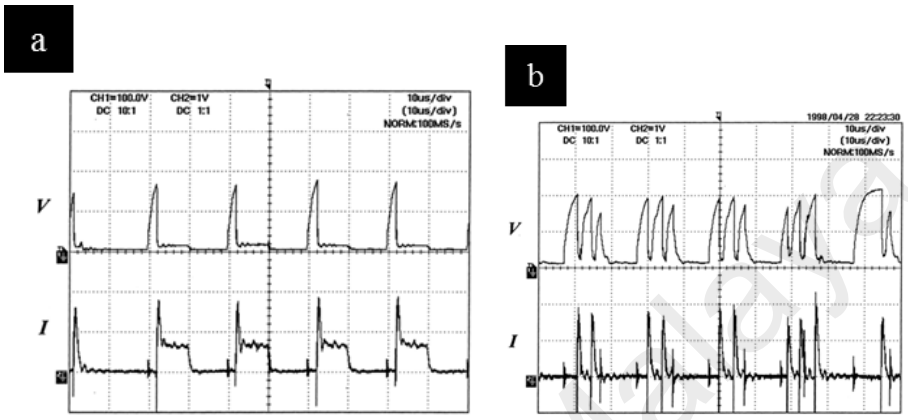

Figure 2.4: Typical waveforms of voltage and current for (a) kerosene and (b) kerosene with Al powder (Chow et al., 2000)

University of Malaya

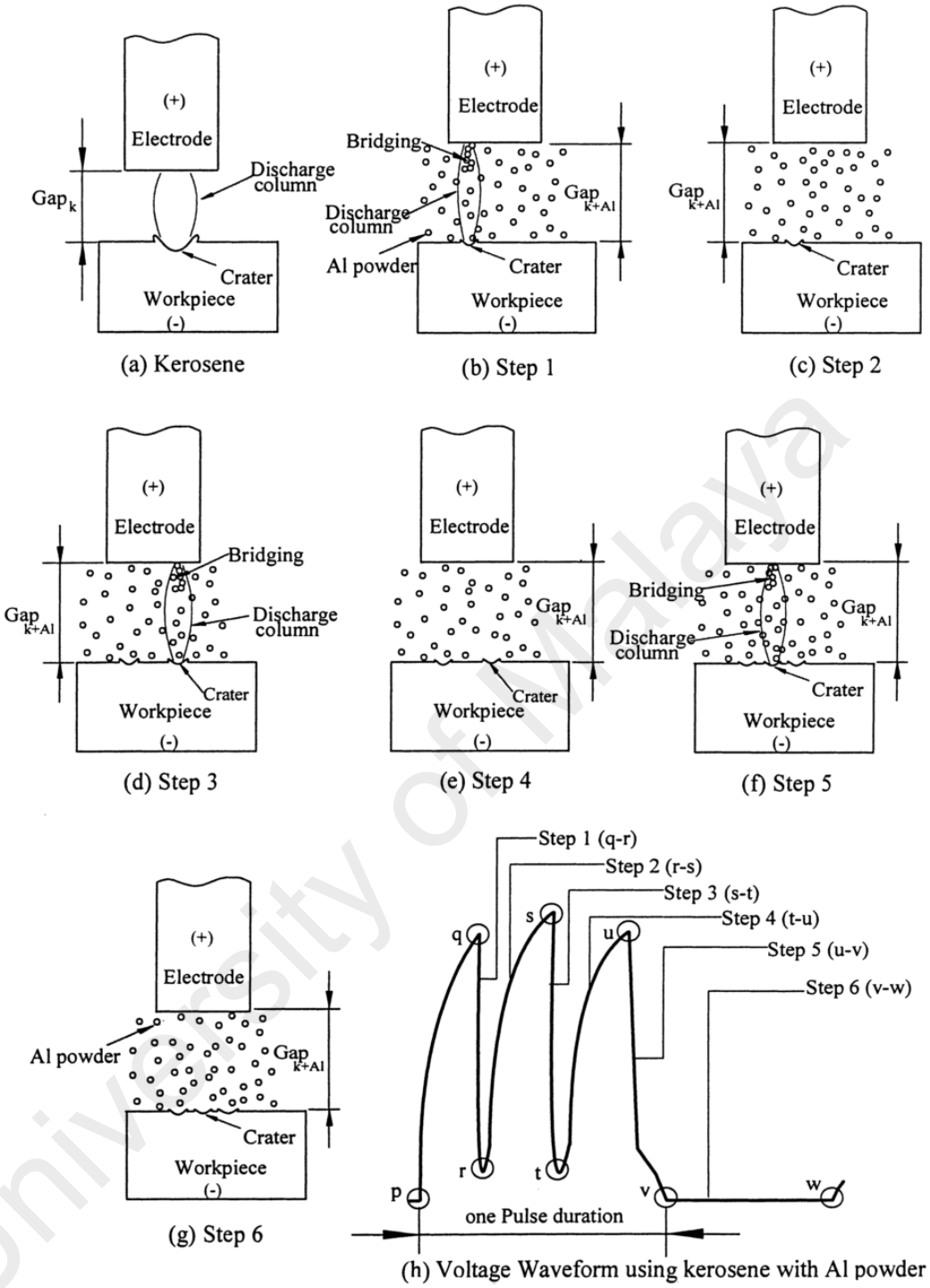

Figure 2.5: Effect of suspended Al powder on the sparking mechanism (Chow et al., 2000)

University of Malaya

2.4.2 Types of Powder additives

Powder thermo-physical properties, mainly particle density, and electrical and thermal conductivity highly influence the PMEDM discharge mechanism. Wong et al. (1998) examined the effect of a number of powders (Table 2.1) on PMEDM performance measures and observed that excluding crushed glass, all powders at least doubled the gap width. Among the powders, Al was found to generate a mirror-finish in machining SKH-51 by forming a surface with well-formed and small overlapping craters. Adding Al to dielectric expanded the gap by a factor of almost 12 due to its high electrical and thermal conductivity, which are the highest among the materials listed in Table 1. The gap expansion value is in agreement with the measurements obtained by Chow et al. (2000), proving that increasing T_{on} leads to an even wider gap when Al powder is added to dielectric; however, this was not the case for SiC powder additive due to its extremely high electrical resistivity. To clarify, when adding SiC and Al powder to kerosene dielectric during micro-slit EDM, the SiC powder enhanced MRR and increased TWR, whereas Al powder provided the best surface quality with the highest micro-slit expansion.

University of Malaya

Table 2.1: Powder additive properties and their relative discharge gap size in EDM (Wong et al., 1998)

Powder	Mesh size (degree of purity)	Thermal conductivity (W cm^{-1} K^{-1})	Electrical conductivity (mV cm^{-1})*	Gap size (µm)
No powder	NA	NA	NA	10-15
Gr	38±3 µm (purum powder of 99% purity, ash content: 0.05%)	1.5	3×10^{-3}	45-50
Si	45±3 µm (99.5%)	1.40	0.1 @ 0°	27-33
Al	45±3 µm (99.5%)	2.37	0.377	120-160
Crushed glass	2.0±0.07 µm	0.04	10^{-10}	10-15
SiC	2.36±0.08 µm	2.71	10^{-2}-10^{-12}	80-90
MoS_2	Typical particle size: 1-3 µm (max 40 µm)	1.38	10^{-6}	44-48

* At 20°

Tzeng and Lee (2001) indicated that among Al, SiC and Cr powders, using Cr leads to the highest MRR followed by Al and SiC; the most deteriorative effect on tool wear was observed for SiC, Al and Cr, respectively. The discrepancy between this research and Chow et al. (2000) results regarding the performance of Al and SiC powders is correlated to the machining scale, powder concentration or prescribed process parameters. Furthermore, among Al, Cr, SiC and Cu, Al powder generated the best SKD-11 surface finish and the thinnest recast layer (Yih-fong & Fu-chen, 2005). However, Cu powder did not contribute in the process due to high density, which caused this powder to deposit at the bottom of the tank (Tzeng & Lee, 2001; Yih-fong & Fu-chen, 2005).

University of Malaya

A comparative study on micro-sinking PMEDM by Klocke, Lung, Antonoglou, and Thomaidis (2004) revealed that for various I_p values, adding either Al or Si powder led to optimized performance measures. They found that particular combinations of powder and workpiece and appropriate setting of electrode polarity and pulse parameter can produce mirror-finish surfaces (Wong et al., 1998). Another powder material for PMEDM applications is Cr, which appeared to generate the second highest surface quality following Al. This is due to the higher Cr density than Al, which increases the particle impact on the melted zone, causing slightly higher surface roughness (Yih-fong & Fu-chen, 2005). Furthermore, Cr addition was found to cause a thicker recast layer compared to Al powder, which is attributed to Cr's lower thermal conductivity, as Cr takes less heat and applies more thermal input to the workpiece. The lower thermal conductivity of Cr compared to Al powder also resulted in higher MRR, because Al powder suspended dielectric absorbs more energy (Tzeng & Lee, 2001).

Graphite powder is another widely used additive powder that increases the electrical conductivity of dielectric and provides excellent lubricity. Graphite powder addition resulted in increasing MRR and decreasing TWR (Jeswani, 1981). Furthermore, graphite has shown to have a promising application especially in micro-PMEDM (Prihandana et al., 2013; Prihandana, Mahardika, Hamdi, Wong, & Mitsui, 2011). Adding graphite, MoS_2 and Si to dielectric seemed to provide glossy and mirror-like surfaces to varying degrees in PMEDM of SKH-54 (Wong et al., 1998). Despite roughness levels being lower in EDM (R_a=0.62 µm) than in suspended graphite PMEDM (R_a=0.75 µm), the surface quality was higher due to the higher machining and discharge dispersion rates. MoS_2, which is normally used as a commercial solid-state lubricant is another material used to produce high surface quality by increasing the wetting effect (Prihandana, Mahardika, Hamdi, Wong, & Mitsui, 2009).

University of Malaya

Titanium (Ti) and Tungsten (W) are other metallic powders employed as additives in PMEDM. Addition of Ti powder to dielectric appeared to increase the MRR (Houriyeh Marashi, Sarhan, & Hamdi, 2015), micro-hardness (Janmanee & Muttamara, 2012) and machined surface hydrophilicity and also increase the surface quality by reducing the R_a and surface crack density (S.-L. Chen, Lin, Huang, & Wang, 2014). Additionally, W powder mixed dielectric was shown to increase the machined surface micro-hardness by 100% (S. Kumar & Batra, 2012).

Beside SiC, ceramic powders such as TiC and B_4C have been utilized in PMEDM. Adding B_4C to deionized water was found to significantly increase the MRR and fabricate accurate micro-holes in machining Ti-6Al-4V (Kibria & Bhattacharyya, 2010; Kibria, Sarkar, Pradhan, & Bhattacharyya, 2009). Y.-F. Chen and Lin (2009) applied TiC powder mixed kerosene dielectric in machining Al–Zn–Mg. The results indicated that the decomposed titanium migrates to the machined surface and forms a TiC external layer with higher hardness than the base material.

2.4.3 Studies considering the performance of PMEDM

A wide range of materials are addressed in available PMEDM research articles. The main question raised in this regard pertains to what powder material would maximize the machining performance measures. Since the performance of powder in PMEDM varies depending on EDM derivation, machining scale, electrical parameter settings, workpiece material and many other factors, answering this question becomes difficult. Accordingly, in this section significant attention is directed to presenting a thorough review of powder materials used in PMEDM investigations and their influence on machining performance measures.

University of Malaya

Popularity of PMEDM among different variations is presented in Table 2.2. Evidently, powder addition has been most often implemented in conventional EDM and micro-EDM, followed by ultrasonic vibration assisted EDM/micro-EDM.

Table 2.2: Popularity of powder addition in various EDM techniques

EDM variation	Percentage of contribution	Investigations
Conventional EDM	68.9 %	Gr (Jeswani, 1981) (A. Kumar, Maheshwari, Sharma, & Beri, 2012) (A. K. Singh, Kumar, & Singh, 2015); Gr and surfactant (Kolli & Kumar, 2015); Gr, Si, Al, crushed glass, SiC, MoS_2 (Wong et al., 1998); Al (Zhao, Meng, & Wang, 2002) (Kung, Horng, & Chiang, 2007) (Hu et al., 2013) (Kansal, Singh, & Kumar, 2006); Al and surfactant (Wu et al., 2005); Al and Si (Klocke et al., 2004);Al, SiC; Cr, Cu (Tzeng & Lee, 2001) (Yih-fong & Fu-chen, 2005); Al and Gr (Bhattacharya, Batish, Singh, & Singla, 2011) (Batish, Bhattacharya, Singla, & Singh, 2012); Si (Kansal, Singh, & Kumar, 2007a) (Kansal et al., 2005) (Paulo Peças & Henriques, 2007) (P. Peças & Henriques, 2003); SiC (Ekmekci & Ersöz, 2012); Ti (Houriyeh Marashi et al., 2015) (Furutania, Saneto, Takezawa, Mohri, & Miyake, 2001b) (Janmanee & Muttamara, 2012); Cu and Gr (Sidhu, Batish, & Kumar, 2014);

University of Malaya

Table 2.2 continued

		Cr (Ojha, Garg, & Singh, 2011); W (S. Kumar & Batra, 2012); Si, Gr and W (Bhattacharya, Batish, & Kumar, 2013); Al and SiC (Chow et al., 2000); MoS_2 (Furutani & Shiraki, 2002); Si and Mn (Molinetti, Amorim, Soares, & Czelusniak, 2015); TiO_2 (Baseri & Sadeghian, 2015);
Micro EDM	13.3%	Gr nano-fibre(Liew, Yan, & Kuriyagawa, 2013); Gr (Prihandana et al., 2011); Gr (Muhammad Pervej Jahan et al., 2010); B_4C (Kibria et al., 2009) (Kibria & Bhattacharyya, 2010); Ti (S.-L. Chen et al., 2014);
Vibration assisted micro-EDM	7.0%	Gr (Micro-EDM with workpiece vibration) (Prihandana et al., 2013); Gr nano-fibre (micro-EDM with dielectric ultrasonic vibration) (Liew, Yan, & Kuriyagawa, 2014); MoS_2 (Tank ultrasonic vibration) (Prihandana et al., 2009);
Ultrasonic vibration assisted EDM	2.2%	TiC (EDM with tool ultrasonic vibration) (Y.-F. Chen & Lin, 2009);
Near dry EDM	4.4%	Si (Bai, Zhang, Yang, & Zhang, 2013); Si (Bai, Zhang, Zhang, Kong, & Yang, 2013);
Micro-slit EDM	4.4%	SiC (Chow et al., 2008); Al (Chow et al., 2000);

University of Malaya

Among the earliest investigations on PMEDM, Jeswani (1981) introduced the addition of 4 g/l of graphite powder with 10 µm average size to dielectric, which enhanced MRR by 60% and decreased TWR by 15%. Furthermore, Wong et al. (1998) revealed that addition of graphite powder (38±3µm) leads to mirror-finish surfaces for SKH-54 workpieces up to I_p of 2 A. A. Kumar et al. (2012) employed cryogenically treated copper tools in PMEDM of Inconel 718 in the presence of graphite powder in dielectric, which appeared effective in reducing both TWR and tool wear ratio during machining. A. K. Singh et al. (2015) investigated the addition of graphite powder to dielectric for improving the micro-hardness characteristics in EDM of superalloy Super Co 605. They specified that a significant amount of powder gets alloyed with the machined surface. Micro-hardness is influenced through current, polarity and pulse on-time for EDM and PMEDM.

Other than the investigation conducted by Wu et al. (2005) that used Al and surfactant addition to dielectric, Kolli and Kumar (2015) investigated the influence of surfactant and graphite (average size of 20 µm) in powder mixed EDM of Ti-6Al-4V. MRR was found to be the maximum with 6 g/l surfactant and 13.5 g/l graphite powder concentration at 20 A current. However, surface roughness was achieved at 4 g/l of surfactant and 4.5 g/l graphite powder concentration at 10 A current.

The addition of nano-size graphite powder to dielectric for enhancing micro-EDM was studied by Muhammad Pervej Jahan et al. (2010), Prihandana et al. (2011) and Prihandana et al. (2013). Adding graphite powder (55 nm average particle size) to dielectric oil was studied by Muhammad Pervej Jahan et al. (2010) for micro-EDM sinking and milling of cemented tungsten carbide (WC-Co), which was found to provide smooth and defect-free nano-surfaces. PMEDM milling showed a wider gap (Figure 2.6(a)) and lower MRR (Figure 2.6(b)) and tool wear ratio (Figure 2.6(c)). The spark gap in both milling and sinking demonstrated an increasing trend with increasing powder concentration, but MRR

University of Malaya

in PMEDM sinking appeared to have a peak at around 0.8 g/l. For concentrations over 0.2 g/l, R_a decreased due to settling and bridging. In order to increase the accuracy of micro-scale PMEDM, Prihandana et al. (2011) proposed ultrasonic vibration of dielectric (43 kHz frequency and 0.4 μm amplitude) and found that machining time reduced up to 35% by introducing 2 g/l of graphite powder (55 nm) to kerosene dielectric and micro-crack appearance on the machined surface diminished. graphite nanopowder addition also improved the R_a by around 15% (from 1.37 to 1.17 μm at 15 g/l concentration) compared to pure dielectric in micro-EDM of a Ti workpiece, and the machining time reduced by factor of 20 at 10 g/l concentration (Prihandana et al., 2013). Furthermore, the combination of added graphite nanopowder and workpiece vibration (1 kHz frequency and 1.5 μm amplitude) reduced the machining time from ~72 to ~3 min. This enhancement was greater than when using either one separately.

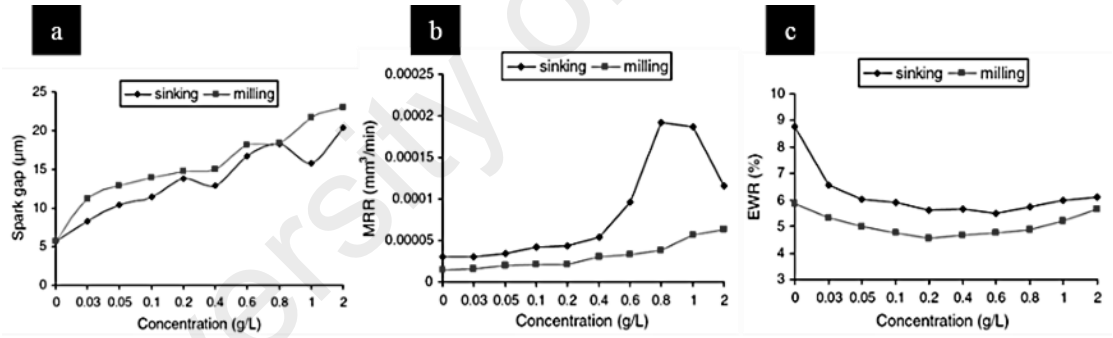

Figure 2.6: Variations of (a) spark gap, (b) MRR, and (c) tool wear ratio after addition of Gr powder to dielectric (Muhammad Pervej Jahan et al., 2010)

Compared to the abovementioned investigations, Liew et al. (2013) employed lower graphite nano-fiber concentrations (up to 0.3 g/l) in micro-EDM of reaction bonded SiC ceramic workpieces in time-controlled (10 min) and depth-controlled (20 μm) methods. Apparently, the electrical resistivity concern of this ceramic was resolved better during micro-EDM. A wider discharge gap (Figure 2.7(a)), higher MRR (Figure 2.7(b)), and lower surface roughness (Figure 2.7(c)) and tool wear ratio (Figure 2.7(d)) were observed

University of Malaya

at optimum powder concentration. Furthermore, the shape of machined profile improved significantly (Figure 2.7(e)).

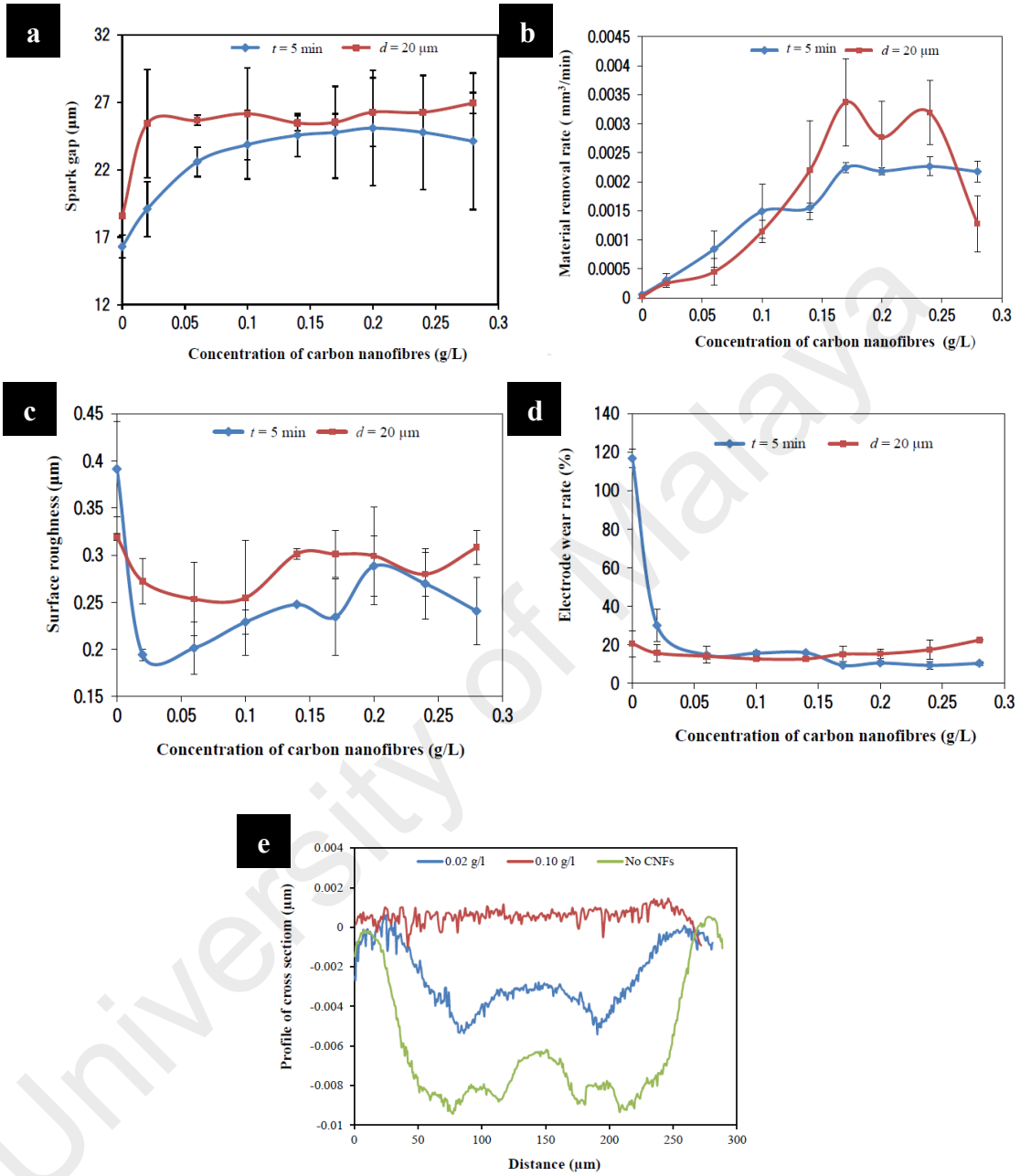

Figure 2.7: (a) Spark gap, (b) MRR, (c) surface roughness, (d) tool wear ratio, (e) cross-section (Liew et al., 2013)

Zhao et al. (2002) reported that adding 40 g/l Al powder (10 µm) to dielectric during machining steel workpiece optimized the MRR at T_{on}=10 µs and R_a at I_p=19 A. Figure 2.8(a) through 2.9 (i) show the influence of adding powder to kerosene dielectric on MRR, TWR, R_a and recast layer thickness at various T_{on}, particle concentration and size ranges.

University of Malaya

Tzeng and Lee (2001) and Yih-fong and Fu-chen (2005) revealed that among various Al powder sizes, adding 70-80 nm (the smallest) to kerosene dielectric provided the highest MRR at 0.5 cm^3/l powder concentration and T_{on}=25µs (Figure 2.8(a), (b) and (c)). Additionally, increasing the powder concentration or T_{on} leads to reduced tool wear ratio (Figure 2.8(d) and 2.10(e)). Moreover, the lowest R_a and thickest recast layer were observed for the smallest Al powder particles (Figure 2.8(f) through 2.10(i)).

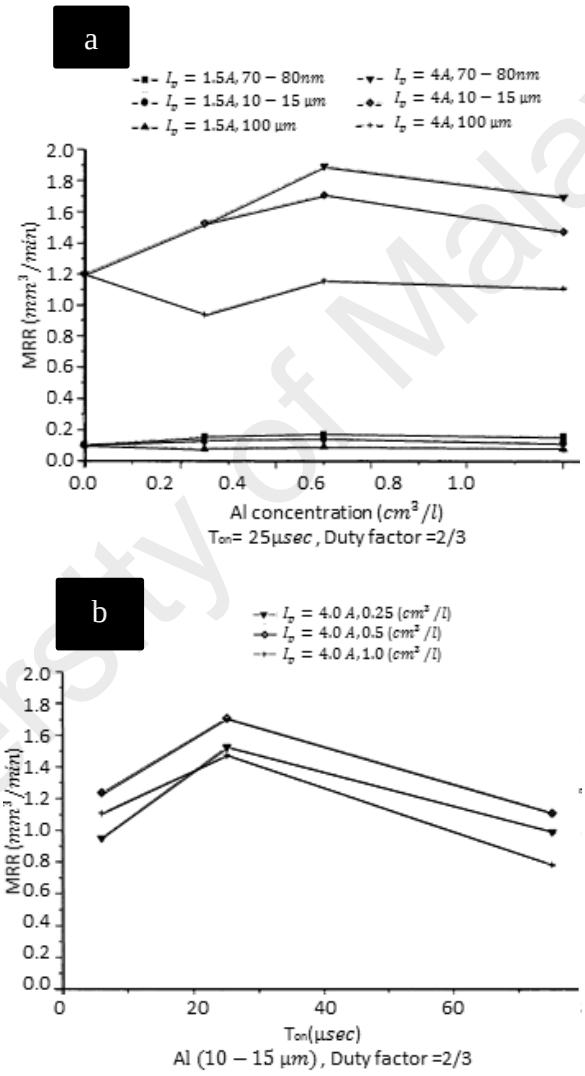

University of Malaya

Figure 2.8 continued

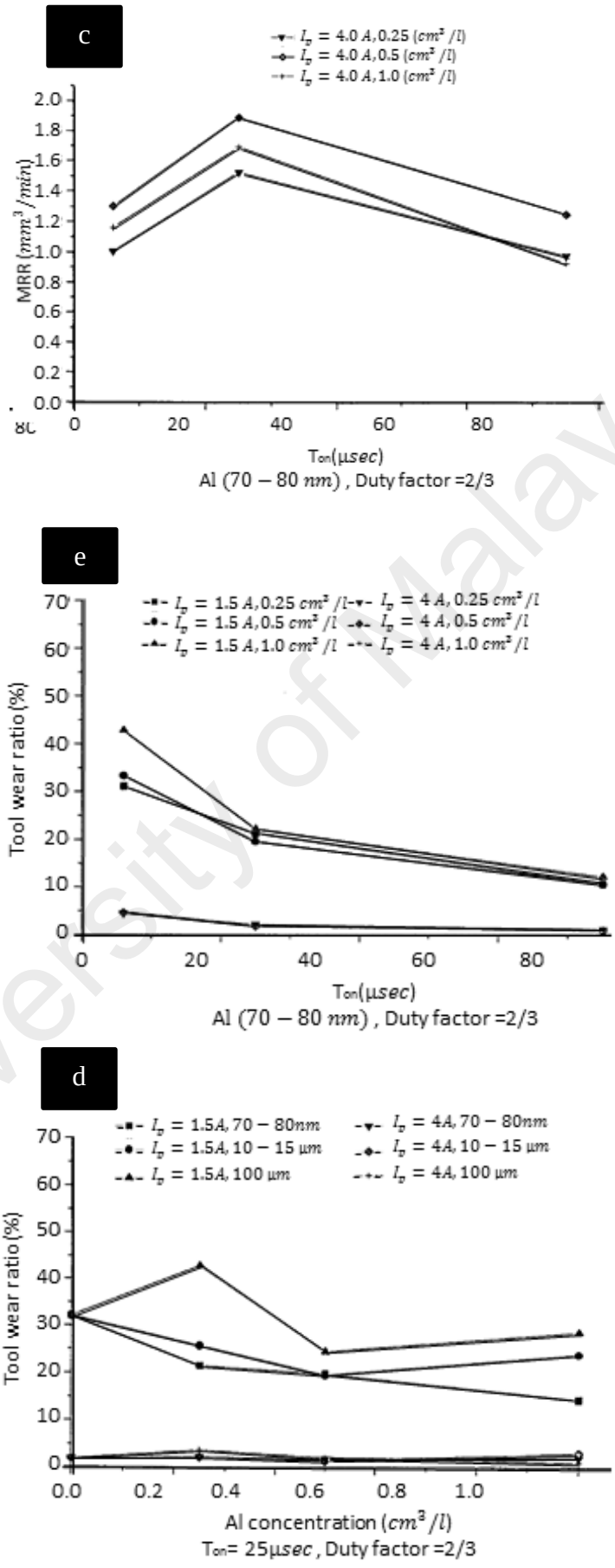

University of Malaya

Figure 2.8 continued

f

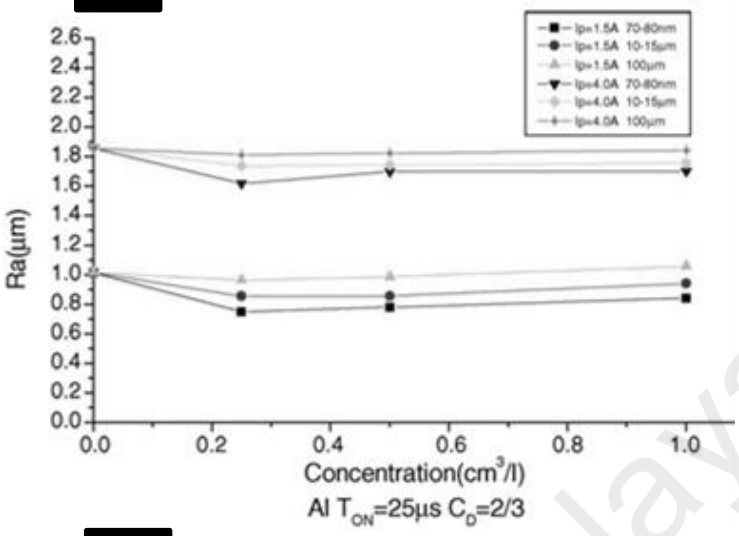

g

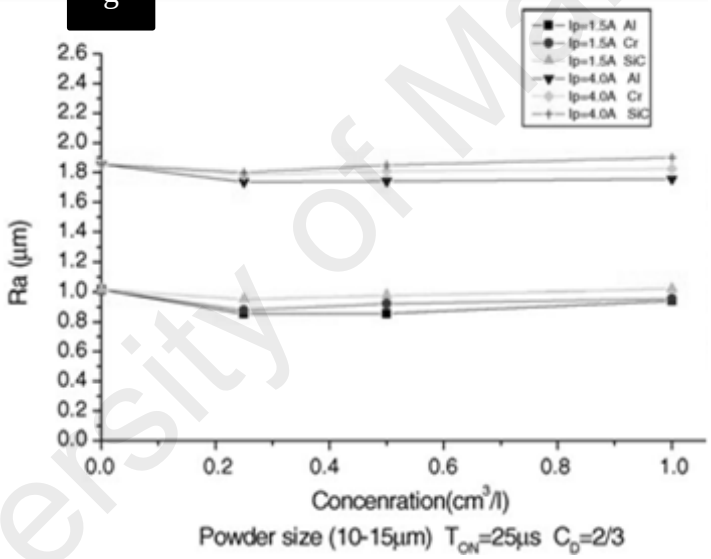

h

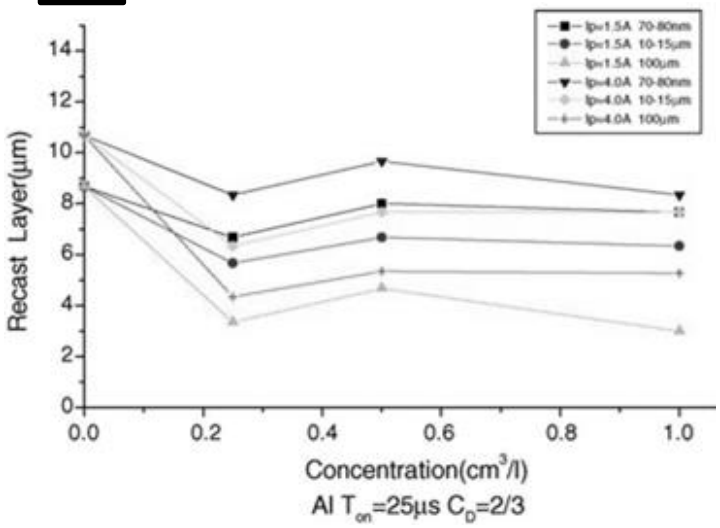

University of Malaya

Figure 2.8 continued

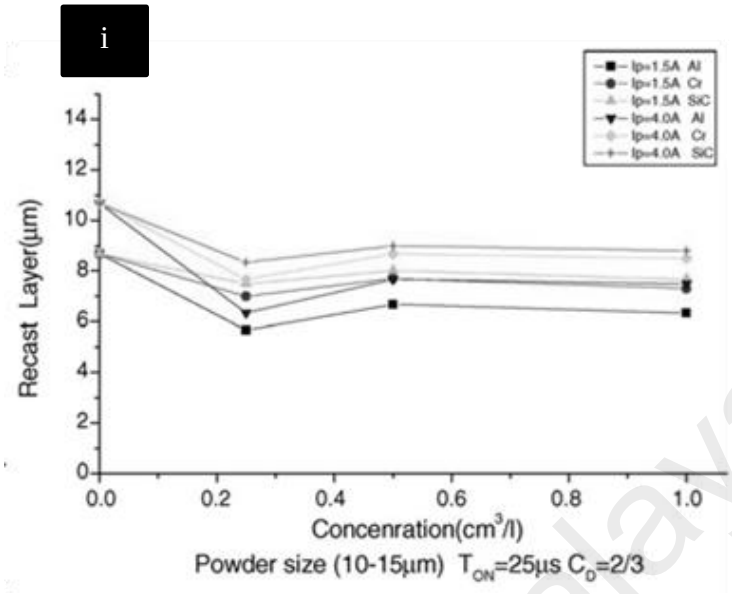

Figure 2.8: Effect of Al powder addition on (a-c), (d-e) TWR (Tzeng & Lee, 2001), (f-g) R_a, (h-i) recast layer (Yih-fong & Fu-chen, 2005)

Addition of Al powder (1 μm) to dielectric through micro-slit EDM of Ti-6Al-4V was found to increase the discharge gap and improve the material removal depth by around 30% at 5g/l powder concentration (Chow et al., 2000). However, Al powder mixed dielectric deteriorated the machined slit accuracy as a consequence of excessive overcut (Figure 2.9). Introducing surfactant (Polyoxythylene-20-sorbitan monooleate) to dielectric with Al powder increased the homogeneity of Al particles in dielectric (Wu et al., 2005). Adding surfactant (0.25 g/l) and Al powder (0.1 g/l) led to increased gap distance (Figure 2.10(a)), fabrication of mirror-like surface in machining SKD-61, increased material removal depth by 60% (Figure 2.10(b)) and thinner recast layer (Figure 2.10(c)). Wong et al. (1998) found that addition of 2 g/l of Al powder (45±3 μm) to dielectric also produced a mirror finish of SKH-51 -- a finishing quality not evident for SKH-54.

University of Malaya

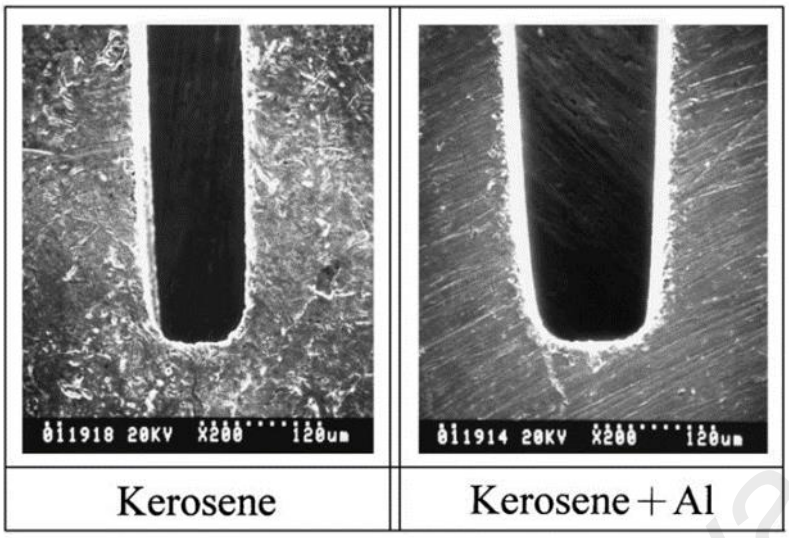

Figure 2.9: SEM photographs of micro-slits before and after powder addition to dielectric (Chow et al., 2000)

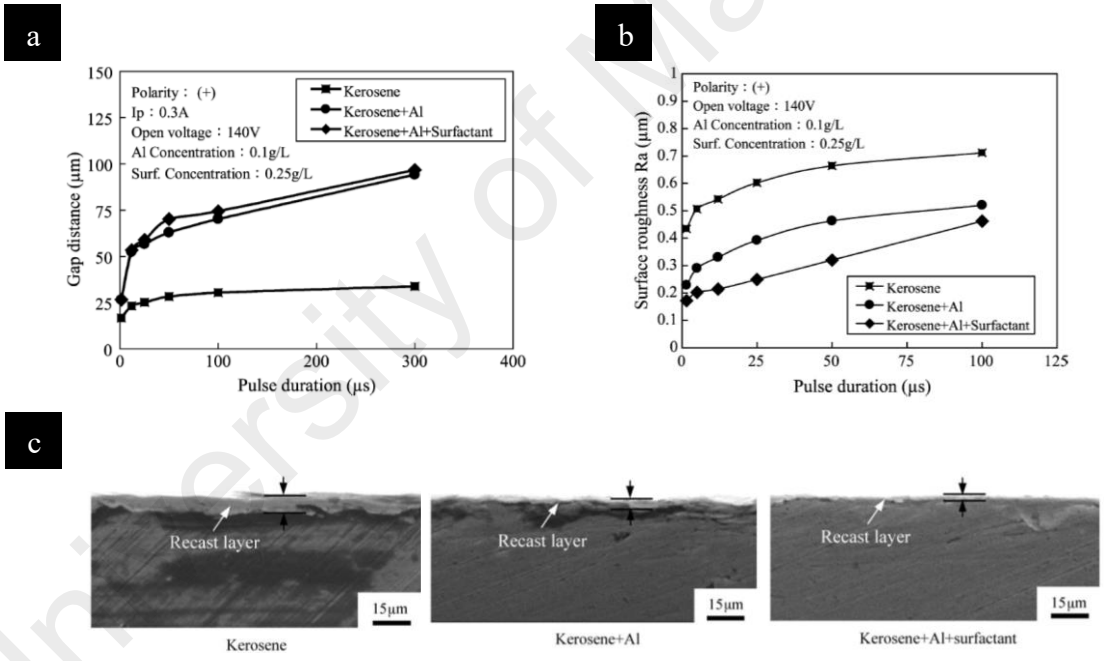

Figure 2.10: Effect of Al powder and surfactant addition on (a) gap distance, (b) R_a, (c) recast layer (Wu et al., 2005)

Al powder was added to mineral oil dielectric to improve the machining efficiency of a WC-Co workpiece (Kung et al., 2007); the optimal powder concentration to maximize MRR was 17.5 g/l. The electrode wear ratio tended to decrease with reduced Al powder concentration to a minimum of 15 g/l, after which it tended to increase. Another study carried out by Hu et al. (2013) indicated that adding Al powder (<2 μm particle size) to

University of Malaya

kerosene dielectric in machining A1 matrix composites improved the R_a by approximately 31.5% in 10 measurement trials. Additionally, this composite's micro-hardness and wear resistance improved by 40 and 100% respectively, as a result of using Al powder.

Kansal et al. (2007a) specified the important parameters and their effects on PMEDM of AISI D2 with Si powder in kerosene dielectric. The optimum machining condition to obtain the highest MRR found was: I_p=16 A, T_{on}=100 µss, T_{off}=15 µs, feed rate=0.83 mm/s and particle concentration=4 g/l. Si powder concentration and I_p were the most influential parameters on MRR. Molinetti et al. (2015) observed that addition of Si powder to dielectric (average size of less than 5 µm) reduce the surface roughness by factor of 5 at 2 A current compared to pure dielectric (Figure 2.11). Presence of Si powder in dielectric results in adherence of Si particles to the surface, where with negative polarity at low discharge currents the machined surface properties can modify forming silicon carbides.

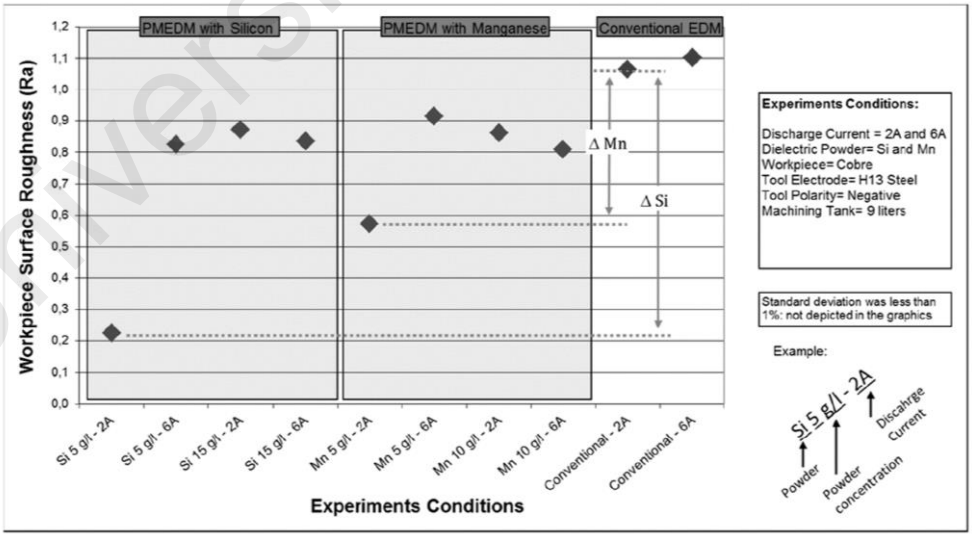

Figure 2.11: R_a for the machined surface roughness by EDM and PMEDM (Molinetti et al., 2015)

University of Malaya

In PMEDM parametric optimization using response surface methodology, adding up to 2 g/l of Si powder to dielectric improved both MRR and R_a (Kansal et al., 2005). However, these performance measures were still expected to increase for higher particle concentrations in dielectric according to response surface. Confirmation tests showed that the error between experimental and predicted MRR and SR values was within ±8% and -7.85% to 3.15%, respectively. Paulo Peças and Henriques (2007) added Si powder (10 µm) to dielectric at a concentration of 2 g/l. This method provided the lowest surface roughness (considering the highest peak-to-valley distance) (Figure 2.12(a)) and crater depth (Figure 2.12(b)). Moreover, increasing the powder concentration decreased the crater width and white-layer thickness (Figure 2.12(c) and 2.13(d)).Figure 2.12(e) and 2.13.(f) show that roughness increased for larger tool areas, but had a different trend after adding 2 g/l of Si powder to dielectric. In accordance to the above study findings (Paulo Peças & Henriques, 2007), P. Peças and Henriques (2003) showed that although Si powder in dielectric noticeably decreased the surface roughness, in larger areas the surface quality slightly dropped due to the capacitive effect. The capacitive effect implies higher current than the one set on the discharge generator, causing the formation of deeper and more irregular craters.

University of Malaya

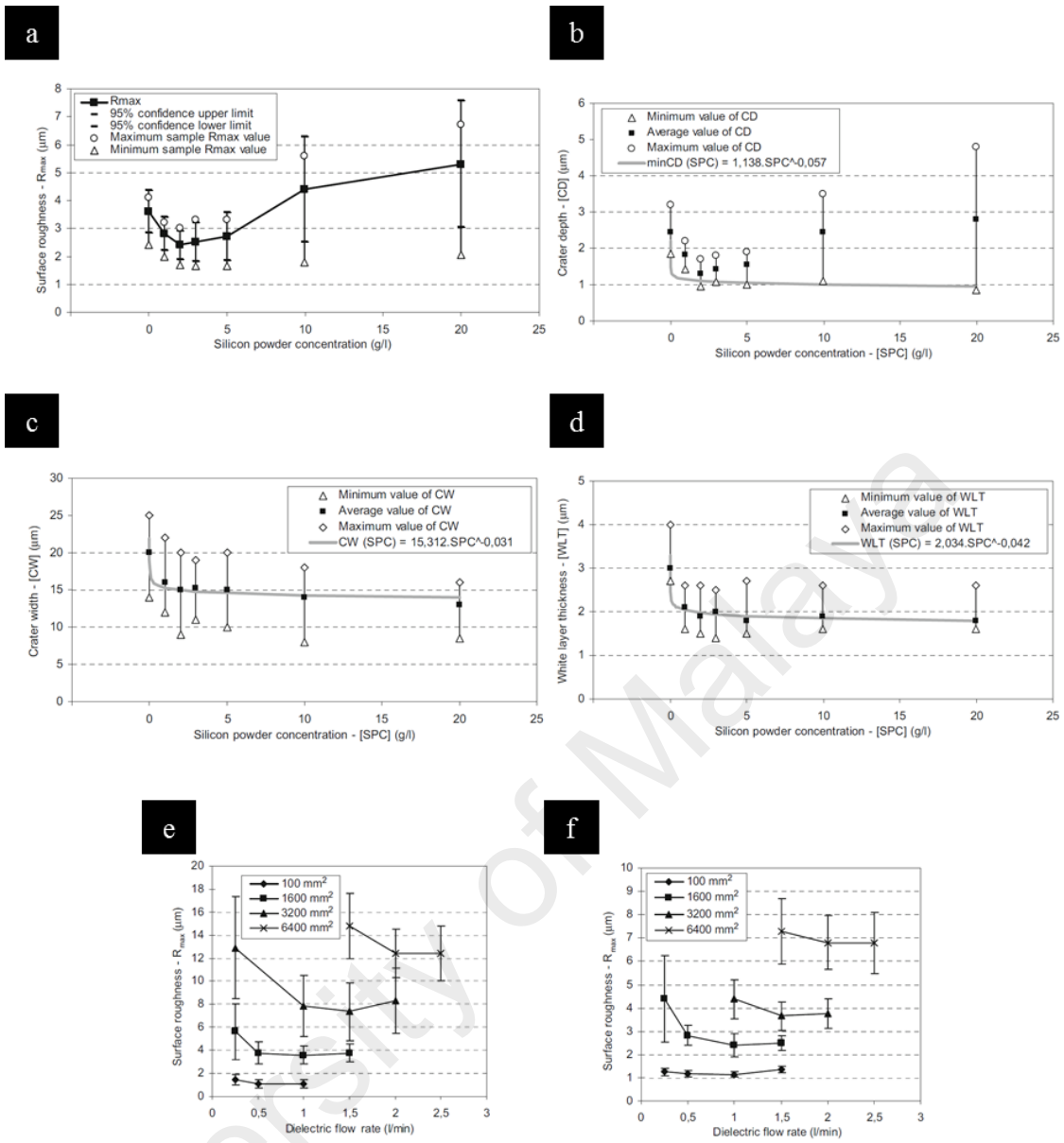

Figure 2.12: Effect of Si powder concentration on (a) surface roughness, (b) crater depth, (c) crater width and (d) white layer thickness; and the effect of dielectric flow rate on surface roughness for (e) pure and (f) Si powder mixed dielectrics (Paulo Peças & Henriques, 2007)

Si powder has been also used in powder mixed near-dry EDM. Bai, Zhang, Zhang, et al. (2013) considered the influence of I_p, T_{on}, T_{off}, flow rate, Si powder concentration, air pressure and tool rotational speed on MRR. They showed that under all machining conditions, a W18Cr4V workpiece and brass electrode resulted in higher MRR, whereas addition of 9 g/l of Si powder to the three-phase dielectric was necessary to obtain the highest MRR with around 40% enhancement compared to pure dielectric. An additional

University of Malaya

study on powder mixed near-dry EDM using Si powder was reported by Bai, Zhang, Yang, et al. (2013). The results indicated that I_p, T_{on}, T_{off}, flow rate and powder concentration are more influential on the MRR of powder mixed near-dry EDM than tool rotational speed and air pressure.

Tzeng and Lee (2001) observed that SiC powder mixed kerosene dielectric leads to a very small machining gap increase and about 30% increase in MRR at I_p=4A and T_{on}=25 µs with $\frac{2}{3}$ duty cycle. However, MRR did not notably change at lower I_p (1.5 A). Additionally, larger SiC particles (2.36±0.08 mm) failed to form a mirror-finish surface due to the formation of very distinct and deep craters with high density of global appendage (Wong et al., 1998). In micro-slit EDM of Ti-6Al-4V with a copper diskette tool, adding 25 g/l of SiC powder to kerosene resulted in the greatest material removal depth at T_{on}=10 µs (Chow et al., 2000). Nevertheless, electrode wear and slit expansion increased at all pulse durations and particle concentrations, respectively. Regarding the influence of electrode revolution speed, the highest material removal depth was attained at 20 rpm. Similar to the optimum concentration obtained by Chow et al. (2000), 25 g/l of SiC mixed deionized water dielectric resulted in the greatest material removal depth for both average particle sizes of 3 and 5 µm in micro-slit EDM (Chow et al., 2008). Moreover, the SiC particles reduced the gap distance, increased the electrode wear and material removal depth, and enhanced the surface roughness compared to pure water dielectric.

According to Yih-fong and Fu-chen (2005), SiC powder produced greater explosion force for normal pulse discharge, leading to formation of deeper craters owing to the high electrical resistivity and low thermal conductivity. Although SiC did not considerably change the R_a, it reduced the recast layer thickness. Conversely, Ekmekci and Ersöz (2012) studied the effects of SiC powder mixed in tap water and oil dielectric on the surface topology and structure of interstitial free (IF) steel. They found that suspended particles

University of Malaya

around the discharge column accelerated and gained sufficient velocity to penetrate to the molten pool before solidification by means of electrophoresis and negative pressure induced after discharge cessation, producing a surface embedded with suspended particles. Therefore, SiC powder particle penetration into the machined surface modified the surface. SiC powder in both water and hydrocarbon oil also increased the recast layer thickness, but more pronounced when the powder was mixed with water.

Titanium is another metallic powder used in PMEDM for performance measure enhancement as well as surface modification. Houriyeh Marashi et al. (2015) observed that Ti particles (40-60 nm) added to dielectric in machining AIDI D2 improved MRR and R_a by ~69% and ~35% at 6 and 12 A current, respectively. Furthermore, the AISI D2 surface morphology was enhanced as a result of shallower craters and the formation of low ridges. Furutania et al. (2001b), Janmanee and Muttamara (2012) and S.-L. Chen et al. (2014) considered Ti powder suspended dielectric fluid for machined surface modification. Furutania et al. (2001b) studied the accretion of Ti on a carbon steel surface machined by EDM with 50 g/l of Ti powder (<36 µm) suspended in oil dielectric. A good condition for accretion specified was $2 \leq T_{on} \leq 5$ µs, $T_{off}=1024$ µs and $1 \leq I_p \leq 7$ A with negative polarity. Ti powder suspended in oil dielectric produced a TiC layer with 150 µm thickness and 1600 Hv hardness.

Janmanee and Muttamara (2012) enhanced machined surface hardness by 76.76% from 990 Hv to 1750 Hv with improved surface quality and TiC surface completeness using PMEDM. At 20 A current and 50% duty factor, a 5µm coated layer of Ti and C with lower R_a and less surface cracks was achieved. Additionally, fewer micro-cracks were observed on the surface since the micro-cracks were filled and substituted by Ti particles and C that decomposed from the dielectric and acted as a combiner (TiC). S.-L. Chen et al. (2014) employed Ti powder addition at various input parameters to deionized

University of Malaya

water in micro-current EDM of Ti workpiece, which led to formation of a recast layer containing TiO. A 6 g/l powder concentration demonstrated no micro-crack formation on the modified surface at I_p=0.1 A for short-pulse durations (≤50 s), and a thinner recast layer 4-11 μm thick was attained. Machining Ti workpiece at I_p=0.1 A for 30 and 50 μs in dielectric with 6 g/l Ti powder concentration generated a hydrophilic surface. Hence, appropriate Ti powder concentration not only prevents surface crack formation but can also promote machined surface wettability.

Copper powder added to dielectric is ineffective in terms of MRR, TWR, R_a and recast layer thickness due to its high density, which causes settling (Tzeng & Lee, 2001; Yih-fong & Fu-chen, 2005). However, Sidhu et al. (2014) employed Cu powder mixed dielectric and copper electrolyte for surface modification of metal matrix composite, which increased the machined surface micro-hardness.

Chromium powder mixed dielectric significantly reduced the tool wear ratio and increased the MRR by about 50% at 0.5 cm^3/l concentration, T_{on}=25 μs and 2/3 duty factor (Tzeng & Lee, 2001). Furthermore, addition of Cr to dielectric also enhanced the R_a and recast layer thickness (Figure 2.8.g and 13.i) (Yih-fong & Fu-chen, 2005). Ojha et al. (2011) used response surface methodology for parametric optimization of MRR and TWR. They employed Cr powder mixed dielectric for machining EN-8. The results indicated that increasing the powder concentration to 6 g/l and I_p to 8 A significantly increased the MRR, while TWR slightly varied with increasing concentration.

Tungsten powder has been mainly applied for surface modification purposes. S. Kumar and Batra (2012) investigated the influence of W powder mixed dielectric in machining OHNS, D2 and H13. The effect of W particles and rise in amount of carbon on the machined surface indicated that suspended powder particles can react with carbon (from the hydrocarbon dielectric breakdown) at high plasma channel temperatures to form

University of Malaya

WC, increasing the micro-hardness of all three workpiece materials by over 100%. The rise in surface hardness directly influences abrasion resistance, which increases the life of dies and other press tools. Bhattacharya et al. (2013) stated that employing brass and W-Cu electrodes with W powder mixed dielectric results in good surface finish and higher micro-hardness, respectively.

Prihandana et al. (2009) studied the addition of MoS_2 powder (2 µm) mixed dielectric and ultrasonic vibration of the machining tank with 43 KHz frequency in micro-PMEDM. They reported superior surface quality and MRR increase by ~85%. Furthermore, the profile depth and machined surface quality substantially improved. Wong et al. (1998) claimed that adding MoS_2 to dielectric led to a mirror-finish SKH-54 surface. Furutani and Shiraki (2002) observed that under friction testing, a surface machined with MoS_2 powder mixed dielectric had a smaller friction coefficient than one machined in pure dielectric.

Boron carbide is an extremely hard ceramic, which Kibria and Bhattacharyya (2010) used as an additive powder. They mixed 4 g/l of B_4C powder (~13-16 µm) with kerosene and deionized water dielectrics. The results indicated that B_4C mixed deionized water dielectric generated more accurate micro-holes in Ti-6 Al-4V with respect to taperness and circularity compared to deionized water. Although B_4C mixed kerosene did not significantly increase the MRR, B_4C mixed deionized water increased the MRR remarkably owing to the efficient discharge distribution and increased machining efficiency (Kibria et al., 2009).

Titanium carbide powder mixed kerosene with ultrasonic tool vibration appeared to be a significant factor in improving the Al-Zn-Mg machining characteristics (Y.-F. Chen & Lin, 2009). Substantial MRR increase and surface roughness and TWR decrease were noticed at high I_p values. Decomposed Ti element from the TiC mixed dielectric medium

University of Malaya

migrated to the Al-Zn-Mg surface, producing fine grain consolidation during solidification. Furthermore, some Ti particles penetrating the machined surface during the process enhanced the hardness and wear resistance through alloying of the workpiece's external layer.

Baseri and Sadeghian (2015) investigated the addition of TiO_2 powder (average particle size of 20 nm) to kerosene in machining H13 steel with rotary copper tool. It was found that increasing the rotational speed up to 200 rpm causes the centrifugal force to get the debris away from the machining gap and MRR increases. Increasing the speed more than 200 rpm creates bubbles and the plasma channel influences and MRR decreases. Addition of up to 1 g/l of TiO_2 powder to dielectric escalate the MRR due to increasing the gap and facilitating the expulsion of the debris from machining gap.

Molinetti et al. (2015) used manganese powder with particle size of less than 10 μm to enhance the machined surface quality of AIDI H13 steel. It was found that addition of Mn to dielectric reduce the surface roughness by factor of two and enhanced the machined surface hardness by about 40%.

University of Malaya

2.4.4 Research trends of PMEDM

The trend of the collected key research studies in PMEDM over the past years is indicated in Figure 2.13. Thirty five years ago, Jeswani (1981) introduced the addition of impurities (graphite powder) to dielectric to enhance the machining performance. Later in 1995, Ming and He (1995) observed that adding conductive and inorganic oxide particles to dielectric leads to higher MRR, lower TWR and superior surface quality. The indistinct stage of this technology continued until 1998 that Wong et al. (1998) compared the utilization of various powder materials in dielectric disclosing explicitly the influence of powder properties on performance measures of EDM. This research revealed the great potential of powder addition to dielectric for improvement of machining performance which led to an increase in number of researches toward PMEDM in coming years. From 1998 to 2008 was the cognition phase of this technology where researchers mainly used same powder materials (Al, Si and SiC) as the previous studies to confirm their effectiveness in machining performance improvement. Since 2008, PMEDM investigations became even more attractive because cognition phase indicated that addition of powder to dielectric increases the dielectric's electrical conductivity and subsequently the spark frequency. Therefore, PMEDM technology is found to be a promising research area. The increasing trend of PMEDM studies since 2008 is evident with higher variety of employed powder materials which is expected to continue in the next coming years. In addition, utilization of nano-size powder has become popular recently since the smaller particle size has shown to have a better performance in terms of MRR, least TWR (Tzeng & Lee, 2001) and surface finish (Yih-fong & Fu-chen, 2005).

University of Malaya

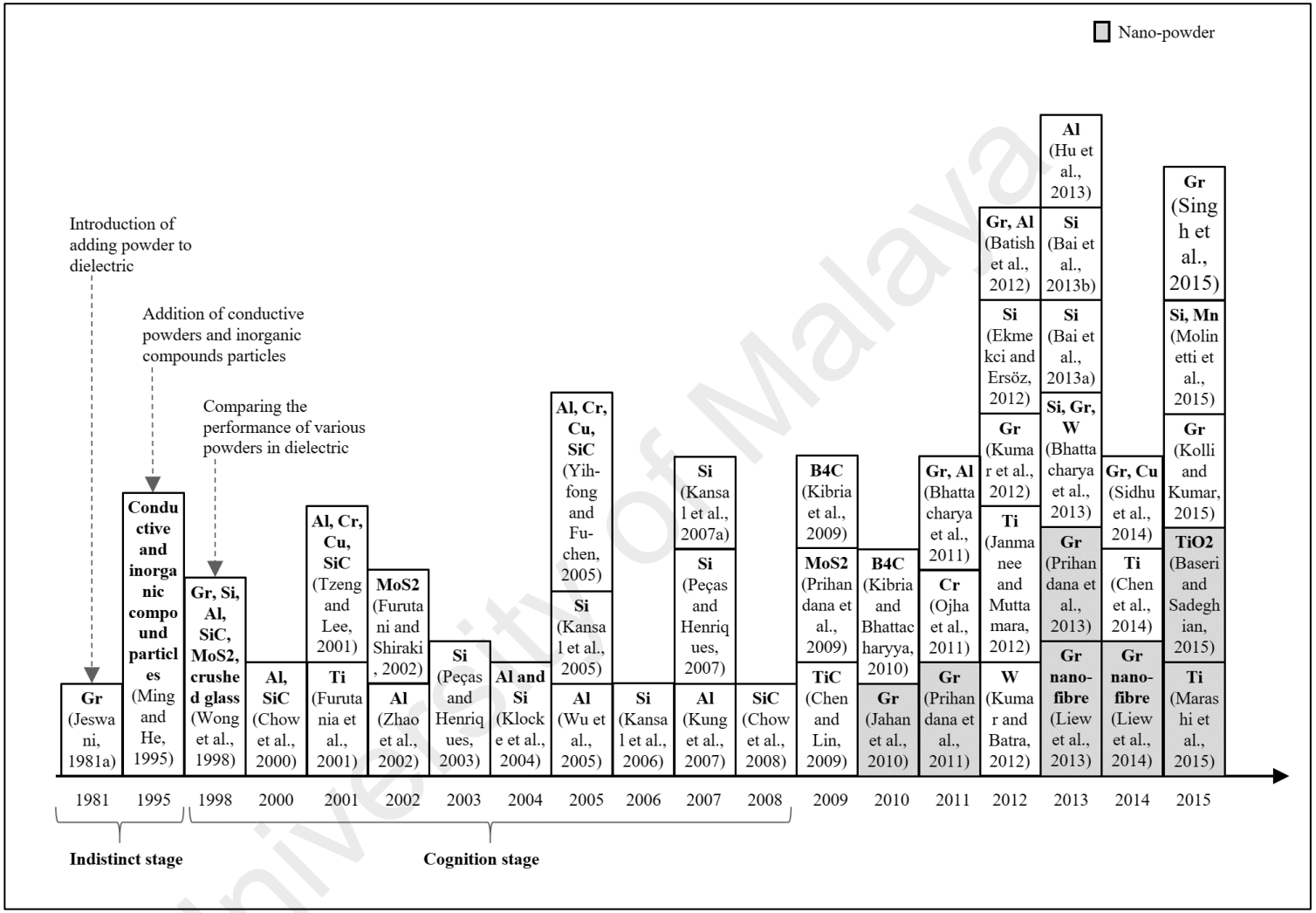

Figure 2.13: Distribution of collected research studies on PMEDM from 1981 to 2015

University of Malaya

The variety and popularity of powder materials used in PMEDM studies are demonstrated in Figure 2.14. Among the considered additives, graphite and Al powders that were also among the earlier research studies, have captured the most research attentions. These two powders have shown to provide higher improvements compared to other powders as it was explained in sections 5 and 6. Despite the fact that there is a large number of publications on PMEDM studies, the unique answer to the question of what is the most effective powder material for enhancing machining characteristics still remains disputed. Incoherency in the selection of machining input parameters, machining scale, tool or workpiece material among the available research studies, impedes an appropriate comparison of findings.

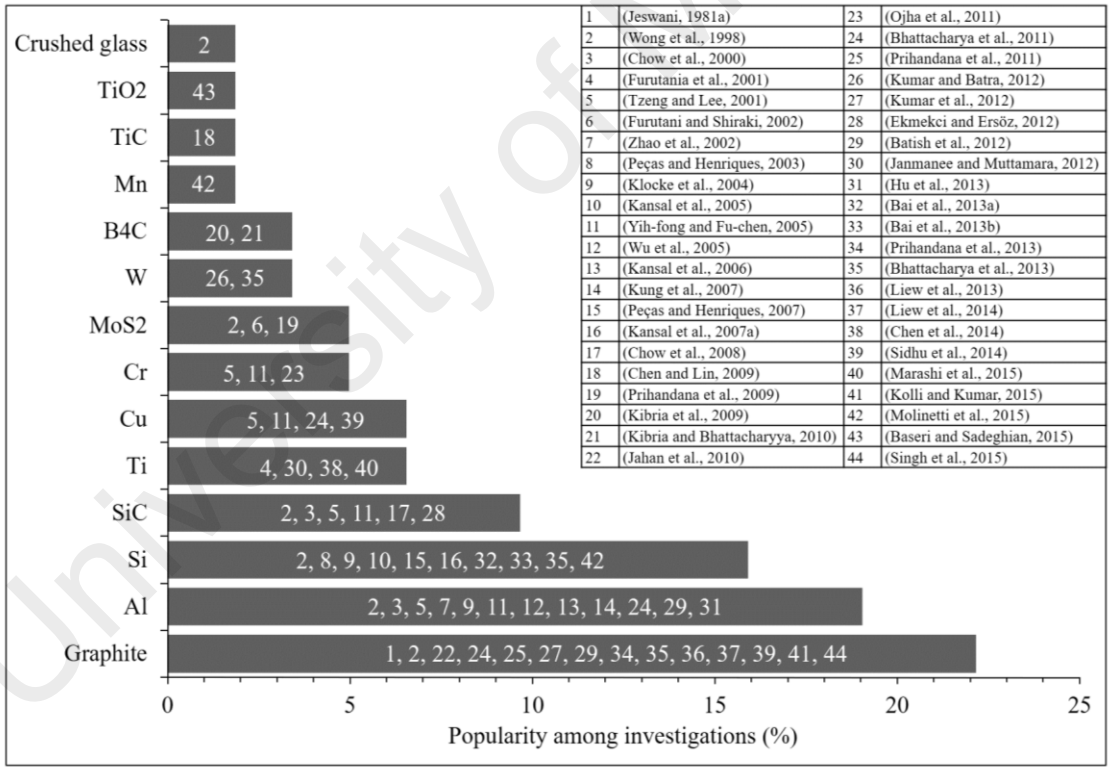

1	(Jeswani, 1981a)	23	(Ojha et al., 2011)
2	(Wong et al., 1998)	24	(Bhattacharya et al., 2011)
3	(Chow et al., 2000)	25	(Prihandana et al., 2011)
4	(Furutania et al., 2001)	26	(Kumar and Batra, 2012)
5	(Tzeng and Lee, 2001)	27	(Kumar et al., 2012)
6	(Furutani and Shiraki, 2002)	28	(Ekmekci and Ersöz, 2012)
7	(Zhao et al., 2002)	29	(Batish et al., 2012)
8	(Peças and Henriques, 2003)	30	(Janmanee and Muttamara, 2012)
9	(Klocke et al., 2004)	31	(Hu et al., 2013)
10	(Kansal et al., 2005)	32	(Bai et al., 2013a)
11	(Yih-fong and Fu-chen, 2005)	33	(Bai et al., 2013b)
12	(Wu et al., 2005)	34	(Prihandana et al., 2013)
13	(Kansal et al., 2006)	35	(Bhattacharya et al., 2013)
14	(Kung et al., 2007)	36	(Liew et al., 2013)
15	(Peças and Henriques, 2007)	37	(Liew et al., 2014)
16	(Kansal et al., 2007a)	38	(Chen et al., 2014)
17	(Chow et al., 2008)	39	(Sidhu et al., 2014)
18	(Chen and Lin, 2009)	40	(Marashi et al., 2015)
19	(Prihandana et al., 2009)	41	(Kolli and Kumar, 2015)
20	(Kibria et al., 2009)	42	(Molinetti et al., 2015)
21	(Kibria and Bhattacharyya, 2010)	43	(Baseri and Sadeghian, 2015)
22	(Jahan et al., 2010)	44	(Singh et al., 2015)

Figure 2.14: Popularity of powder materials in PMEDM studies

Under different machining conditions, adding Gr, Al, Ti, W, TiC, Si or SiC powders to dielectric results in surface modification. Through external surface alloying, the

University of Malaya

existence of Al, Ti, W or TiC increases the surface hardness and wear resistance. These powder materials find substantial application in surface modification which was investigated in detail by S. Kumar, Singh, Singh, and Sethi (2009). It is recommended for future investigations to consider both metallurgical surface compounds and the influence of powder addition on EDM performance measures to realize the effect of powder addition on the process and machined surface properties. This will clarify that whether the addition of powder to dielectric always results in surface modifications and what are the contributing factors of powder in occurrence of surface modification. For instance, addition of Cu powder particles makes no difference into the process (Mohd Abbas et al., 2007) because it deposits at the bottom of the tank and does not contribute into the discharge process. However, another research study mixed Cu powder with dielectric to attain surface modification (Sidhu et al., 2014).

Based on the collected literature, Figure 2.15 is drawn in order to demonstrate the range of concentration, size, and powder materials used in PMEDM investigations. Figures show that up to 75 g/l concentration of powder in dielectric have been investigated, where mostly used concentrations were less than 20 g/l. Also for nanopowders addition, the maximum employed concentration was found to be 20 g/l. Furthermore, the graphs show that 1 to 55 µm and 20 to 150 nm particle size range have been used in PMEDM investigations. Nano powders were used in few studies which shown to have a great potential which needs to be investigated in a greater extend. Besides the materials properties stated in this research, such as powder material, size and concentration, shape has been addressed as an influential property of powder material (Kansal et al., 2007a). As it has been also addressed by (Bajaj, Tiwari, & Dixit, 2015) as well, very little or no investigation has been undertaken to realize the effect of particle shape on performance measures. Moreover, it is recommended for future studies to establish comparative studies using various powder materials, size and concentration to

University of Malaya

clearly reveal a piece of a puzzle from the big picture of PMEDM performance. In addition, findings to date indicate that the smallest particles cause less gap expansion, higher MRR, lower TWR (Tzeng & Lee, 2001) and better surface finish and thicker recast layer (Yih-fong & Fu-chen, 2005) which in overall increase EDM performance and surface finish. However, the influence of particle size of different materials on EDM performance and the relationship between particle size and optimum concentration necessitate further attention. Furthermore, according to Figure 2.15(b), the average particle concentration of 2 g/l is used for nano-size powder additives.

2.4.5 Powder material, size and concentration selection criteria

Variety of powder materials have been used in PMEDM applications. In this research, titanium is selected due to its active nature and positive reputation in enhancing the machined surface properties. Powder particle size is emphasized as an important powder parameter to obtain desirable results in the PMEDM process. It is observed that larger particles result in greater gap expansion; this effect is more pronounced for higher T_{on} values, probably owing to greater contamination and lower deionization between workpiece and tool (Tzeng & Lee, 2001). According to Tzeng and Lee (2001), the smallest particles (70-80 nm) generated the smallest discharge gap increase, the highest MRR and the least TWR. In another study, Yih-fong and Fu-chen (2005) claimed that additive particle size is determinative in machined surface quality. The smallest particles (70–80 nm) produced the best surface finish while simultaneously increasing the recast layer thickness. Additionally, Boilard (2013) stated that smaller Ti particles have higher potential of ignition. Thus nano-sized Ti additive in dielectric may result in higher spark intensity in the discharge process due to its ignition potential. Therefore, Ti nano powder of 40-60 nm size have been selected in this study that is shown in Figure 3.1.

University of Malaya

Powder particles concentration is another influential parameter in PMEDM. The appropriate concentration leads to process efficiency and stability and increasing the concentration beyond the optimum value causes short circuiting, arcing and unstable machining due to the existence of excessive particles similar to debris particles, whereby too much debris is generally deemed the dominant cause of spark concentration (Tzeng & Lee, 2001). Furthermore, the presence of excessive particles in the discharge gap causes a settling problem and bridging effect, which lead to surface deterioration (Muhammad Pervej Jahan et al., 2010). Figure 2.15 indicates the concentration and particle size of the used powder in the PMEDM studies included in this survey. It is evident that the nano-size powder particles were used mostly at 2 g/l. Therefore, 2g/l concentration is designated as the appropriate Ti powder concentration in this research.

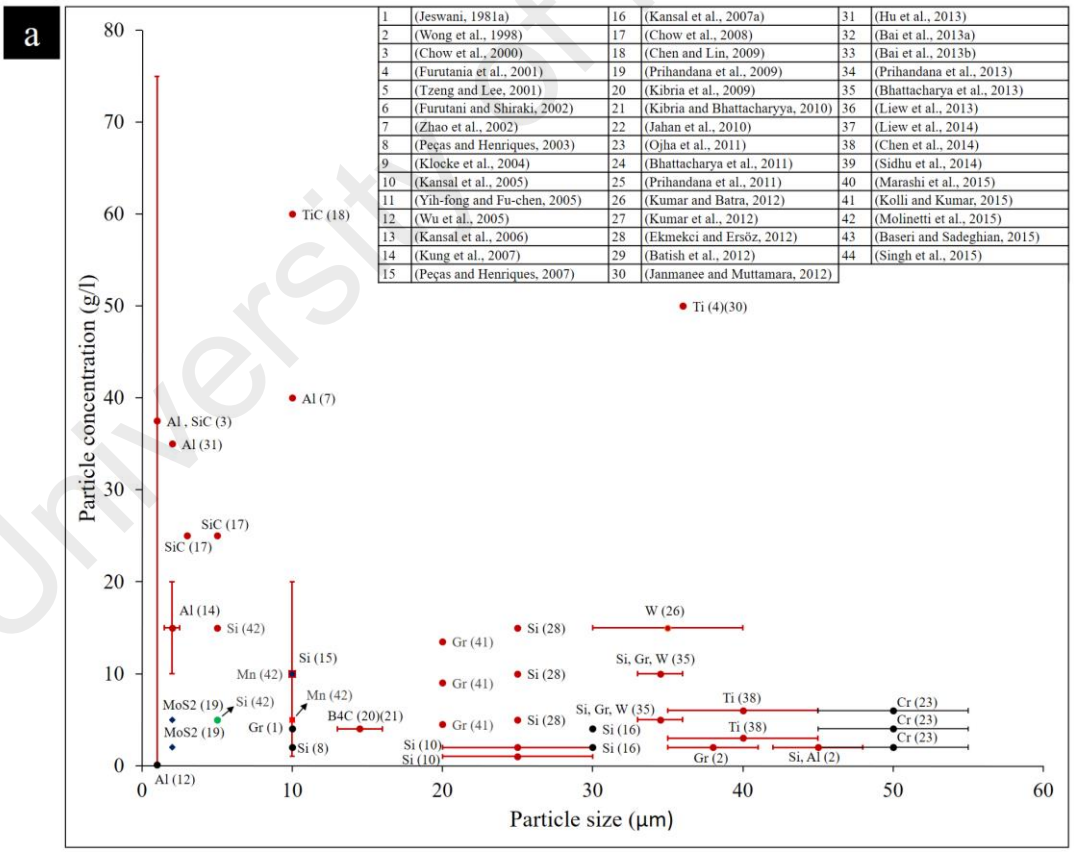

1	(Jeswani, 1981a)	16	(Kansal et al., 2007a)	31	(Hu et al., 2013)
2	(Wong et al., 1998)	17	(Chow et al., 2008)	32	(Bai et al., 2013a)
3	(Chow et al., 2000)	18	(Chen and Lin, 2009)	33	(Bai et al., 2013b)
4	(Furutania et al., 2001)	19	(Prihandana et al., 2009)	34	(Prihandana et al., 2013)
5	(Tzeng and Lee, 2001)	20	(Kibria et al., 2009)	35	(Bhattacharya et al., 2013)
6	(Furutani and Shiraki, 2002)	21	(Kibria and Bhattacharyya, 2010)	36	(Liew et al., 2013)
7	(Zhao et al., 2002)	22	(Jahan et al., 2010)	37	(Liew et al., 2014)
8	(Peças and Henriques, 2003)	23	(Ojha et al., 2011)	38	(Chen et al., 2014)
9	(Klocke et al., 2004)	24	(Bhattacharya et al., 2011)	39	(Sidhu et al., 2014)
10	(Kansal et al., 2005)	25	(Prihandana et al., 2011)	40	(Marashi et al., 2015)
11	(Yih-fong and Fu-chen, 2005)	26	(Kumar and Batra, 2012)	41	(Kolli and Kumar, 2015)
12	(Wu et al., 2005)	27	(Kumar et al., 2012)	42	(Molinetti et al., 2015)
13	(Kansal et al., 2006)	28	(Ekmekci and Ersöz, 2012)	43	(Baseri and Sadeghian, 2015)
14	(Kung et al., 2007)	29	(Batish et al., 2012)	44	(Singh et al., 2015)
15	(Peças and Henriques, 2007)	30	(Janmanee and Muttamara, 2012)		

University of Malaya

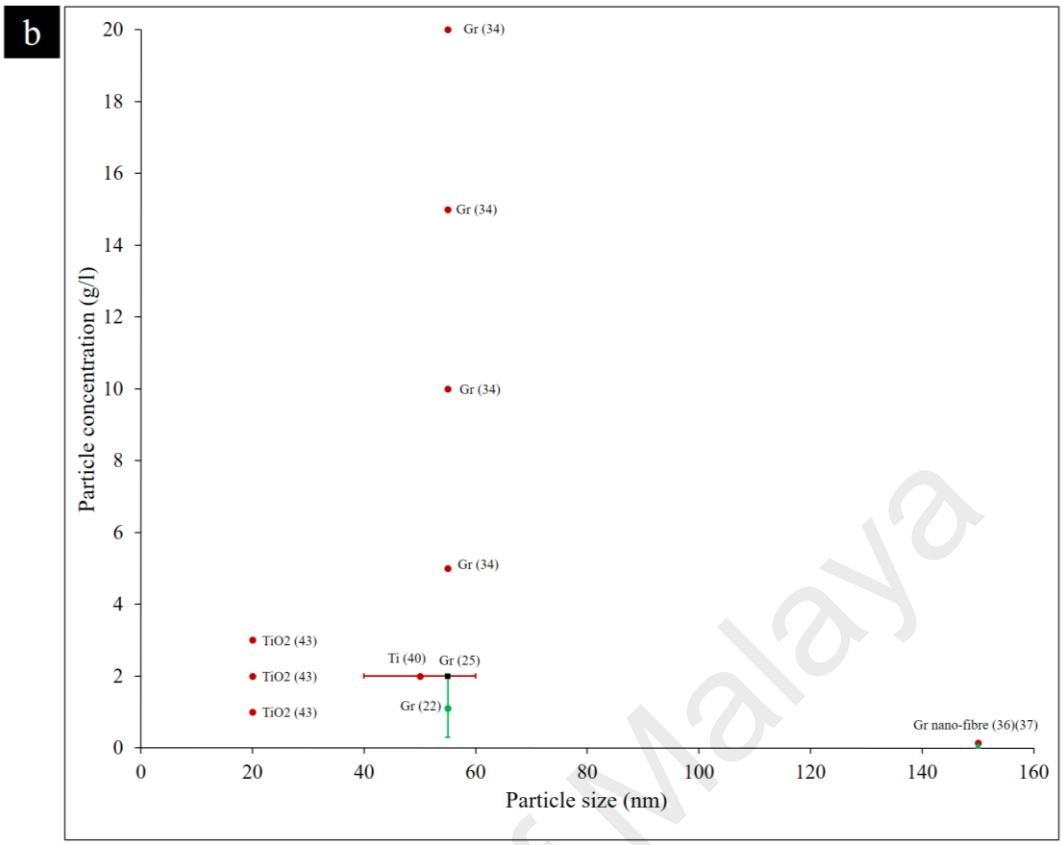

Figure 2.15: Particle material, size and concentration in PMEDM studies for (a) micro- and (b) nano-level particle size

2.5 Tool electrode EDM and tool wear phenomena

Electrode material properties as a non-electrical parameter plays a decisive role in EDM performance. The material is required to have high electrical and thermal conductivity to facilitate the charging, and high wear resistance to diminish erosion caused by repetitive quenching during the EDM process. Furthermore, easy machinability to any shape, high MRR, resistance against deformation during the erosion process, low wear considered are other important properties (Rao, 2009). Erosion is a factor of many parameters including melting point, hardness, and structural integrity which leads to longer service life and lower replacement frequency of electrode.

Wear phenomena in EDM appears in three forms of end, side and corner wear. End wear can be partially controlled through input parameters, however, corner and side wear

University of Malaya

are contingent on the electrode material wear resistance. As shown in Figure 2.16, electrode side and corner wear deteriorates the geometrical accuracy of the produced part.

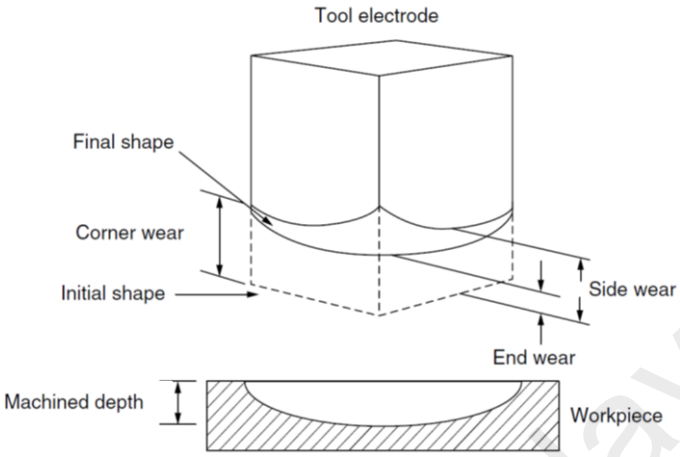

Figure 2.16: Electrode wear forms (El-Hofy, 2005)

Electrode material selection with appropriate aforementioned properties is dependent on the job criteria. EDM electrodes are mainly fabricated from copper (Cu), graphite (C), tungsten (W), brass (alloy of copper and zink) and silver (Ag) (Gaitonde, Karnik, Faustino, & Davim, 2010). Among these materials, copper and graphite are broadly employed in die and mold manufacturing owing to their high MRR (Davim, Maranhão, Cabral, & Grácio, 2009), where copper remains the most engaged material for electrodes when fine finishes are required. Despite the high MRR, high sensitivity to wear reduces final workpiece accuracy and surface integrity. To overcome these concerns, copper tungsten (Cu-W) is often used in precision EDM for the combination of high hardness and wear resistance provided by W and high thermal and electrical conductivity of Cu (S. H. Lee & Li, 2001). However, low melting temperature of Cu increases the wear during EDM, on the other hand to compensate this drawback, increasing the W content leads to formation of porosity during sintering process due to insolubility of W and Cu, which significantly increase the production cost of Cu-W electrodes (Li Li, Wong, Fuh, & Lu, 2001). Furthermore, application of this electrode material is limited due to low formability.

University of Malaya

Moreover, electrodes produced through powder metallurgy (P/M) that are categorized as green compact and sintered types are attracting great attention as a result of the promising surface integrity of workpieces after EDM machining (Patowari, Mishra, Saha, & Mishra, 2011). In machining medium carbon steel, composite electrode fabricated using copper and Chromium (Cr) powders improves finished surface wear resistance (H. C. Tsai, Yan, & Huang, 2003). WC-Cu electrodes produced by P/M used for machining C-40 steel led to higher surface integrity and reduced heat-affected zone (Patowari et al., 2011). The accretion of wear-resistant materials such as TiC on carbon steel was done by injecting Ti powder into dielectric through a copper electrode (Furutania, Saneto, Takezawa, Mohri, & Miyake, 2001a). Mainly, application P/M electrode is limited to surface modification through deposition of electrode material on the workpiece. Despite the advantages of P/M electrodes, drawbacks, for instance, under certain machining conditions P/M electrodes can cause workpiece material addition rather than material removal (Samuel & Philip, 1997).

2.6 Severe plastic deformation

Several methods have been introduced to modify the yield strength, ductility, and toughness of both crystalline and amorphous materials. These strengthening methods provides the ability to adjust the mechanical properties of materials to suit for various applications namely grain size reduction, solid solution strengthening, precipitation hardening and strain hardening (cold working).

Severe plastic deformation (SPD) is a generic term describing a group of metalworking techniques involving very large strains typically involving a complex stress state or high shear, resulting in a high defect density and equiaxed grains with high-angle boundaries. High-angle grain boundaries block slip and increase strength of the material. SPD techniques are not associated with powder related issues such as residual porosity,

University of Malaya

contamination in final product and have higher potential for industrialization (Azushima et al., 2008; R. Valiev, 2004).

2.6.1 Severe plastic deformation as a strengthening method

2.6.1.1 Effect of grain boundaries on strength of materials

Atoms and ions of a solid are arranged in a repeating pattern in three dimensions which form a solid called crystalline solid with long range order such as metals and alloys. Generally, engineering alloys are polycrystalline containing many crystallites (grains) with different size and orientation. Grain boundaries increase the strength of materials acting as barriers to dislocations, except at high temperature where they act as weak areas. Generally, fine grain materials are stronger, harder, tougher, and more susceptible to strain hardening at room temperature and also results in more uniform and isotropic behaviors of materials (Smith & Hashemi, 2003). Thus, two component made of same alloy, the one with smaller average grain diameter is stronger. Hall-Patch equation indicates the influence of grain size on strength of materials as follow (Dunstan & Bushby, 2014):

$$\boldsymbol{\sigma_y = \sigma_0 + kd^{-1/2}} \tag{2.1}$$

where, σ_0 is the frictional stress due to work-hardening and k is related to the material of interest called Patch parameter. The equation indicates that decrease in grain size diameter increase the yield strength of material. It is important to check that the hall-patch equation does not apply to extremely fine or extremely course grain sizes and metals at elevated temperature (Smith & Hashemi, 2003).

2.6.1.2 Grain shape and dislocation arrangements

Plastic deformation occurs due to the motion of a large number of dislocations called slip. Slip lines change direction at grain boundaries. Therefore, each grain has its own set of dislocations and slip planes with different orientation. Increasing the number of grains

University of Malaya

leads to smaller travel of dislocation within each grain before encountering grain boundary at which point their movement is terminated. Thus, materials with finer grain structure have higher strength (Smith & Hashemi, 2003).

As a result of formation of dislocations in the workpiece, which are uniformly distributed in the crystal in the form of a plane, multipoles or polygon walls. Thus, smaller grain areas form by high-density dislocations due to split of inner part of the grains. Taking advantage of dislocation motions, the mechanical properties of materials are modified by making it harder and tougher using a group of strethening techniques including solid solution strengthening, dispersion hardening, precipitation hardening and grain size reduction (Suzuki, Takeuchi, & Yoshinaga, 2013).

2.6.2 Severe plastic deformation methods

Various types of SPD techniques have been proposed over the past three decades (Estrin & Vinogradov, 2013). Among those, three methods of high pressure torsion (HPT) (R. Z. Valiev, Krasilnikov, & Tsenev, 1991), accumulative roll bonding (ARB) (Saito, Utsunomiya, Tsuji, & Sakai, 1999) and equal channel angular pressing (ECAP) (Segal, 1999) have the capability for industrial applications.

High-pressure torsion (HPT) as a severe plastic deformation technique, processes a thin disk-shape workpiece which will undergo torsional straining by applying high hydrostatic pressure throughout the process (R.Z. Valiev et al., 2006). In HPT, an ingot is held between anvils and strained in torsion under the applied pressure (P) of several GPa. A lower holder rotates and surface friction forces deform the ingot by shear. Owing to the sample's geometry, the main volume is strained in quasi hydrostatic compression situation under the pressures of the outer layer of workpiece and the applied force. In this technique, although large strain values are applied to the workpiece, the deformed sample is not destroyed (R.Z. Valiev et al., 2006).

University of Malaya

Accumulative roll bonding (ARB) represents the process of conventional cold rolling operation for processing a metallic sheet to modify the grain structure to ultrafine, where the sheets are compressed until the sheet thickness downs to ½ of its original condition.

Equal channel angular pressing is another sever plastic deformation technique which is explained in the next section.

2.6.3 Equal channel angular pressing

A rectangular to circular workpiece will be pressed using a punch through an angled channel, consists of two sections with equal cross section, intersect by an arbitrary angle, namely channel angle (φ). The outer arc of the die channel can be curved with an inclination angle called corner angle (ψ) (Segal, 1999).

Figure 2.17 shows the illustration of ECAP. An strong shear stress will be applied on the workpiece when it passes through the ECAP channel, while the workpiece diameter will remain the same. During the pressing process, the extreme shear increases the dislocations as explained in section 2.6.1.2, which leads to formations of finer grain structure. Since SPD is applicable for hardening of large billets, it can be implemented for wider range of applications in variety of industries. Furthermore, this technique has a relatively simple procedure imposable on variety of metals and their alloys. Besides, a practical homogeneity can be obtained over most of the processed billets owing to adequately high strain. Also, the process may be increased for the extrusion of moderately bulky samples which leads to higher industrialization of ECAP for use in commercial metal-processing procedure.

University of Malaya

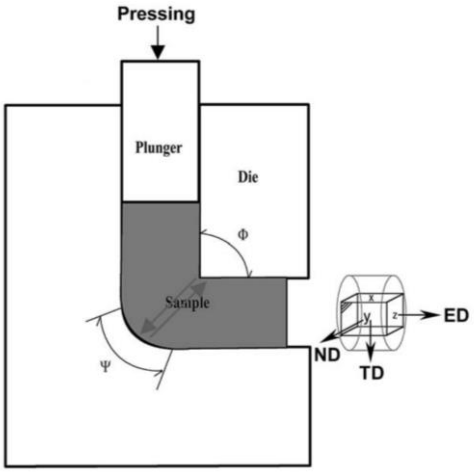

Figure 2.17: The principle of equal channel angular extrusion (ECAP) (W. Kim et al., 2003)

Repetitive extrusion results in buildup of shear strain in the sample and eventually workpiece with finer grain structure and increased hardness. Further extrusion passes of ECAP treatment can be achieved through dissimilar strain paths which is attained by consecutively rotating the sample between pressing cycles (Ruslan Z Valiev & Langdon, 2006). Four main paths have been established that regulate the grain structure of the workpiece due to their dissimilar slip systems. Figure 2.18 schematically indicates these pressing paths. Route A states a repetitive pressing of workpiece without rotating it. Route B is the consecutive pressing workpiece after 90° rotation between cycles which categorized as routes B_a (90° rotation in opposite sense) and B_c (90° rotation in same sense). The processing route C represents the 180° workpiece rotation followed by every extrusion cycle (Langdon, Furukawa, Nemoto, & Horita, 2000).

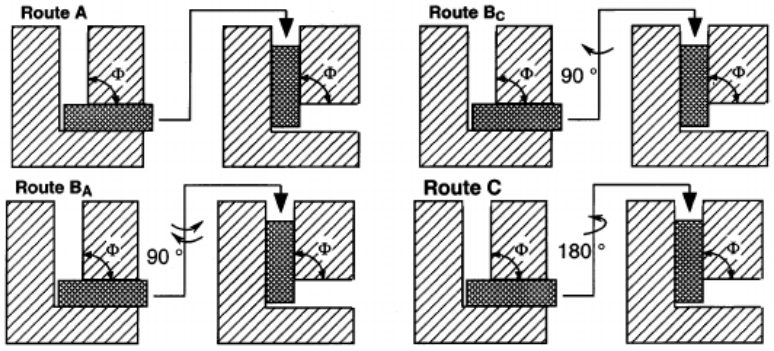

Figure 2.18: Various ECAP passes (Y. T. Zhu & Lowe, 2000)

University of Malaya

Slip systems for four different processing routes of ECAP is indicate in Figure 2.19. Route C and B_c entails continues shearings on the same plane in each consecutive passage through the die but the direction of shear is revered in each pass route. Therefore, the strain is restored after every even number of passes. On contrary, routes A and B_A, there are two separate shearing planes intersecting at an angle of 90 in route A and four distinct shearing planes intersecting at angles of 120 in route B_A. Therefore, these routes result in cumulative buildup of additional strain on each separate pass through the die (Ruslan Z Valiev & Langdon, 2006).

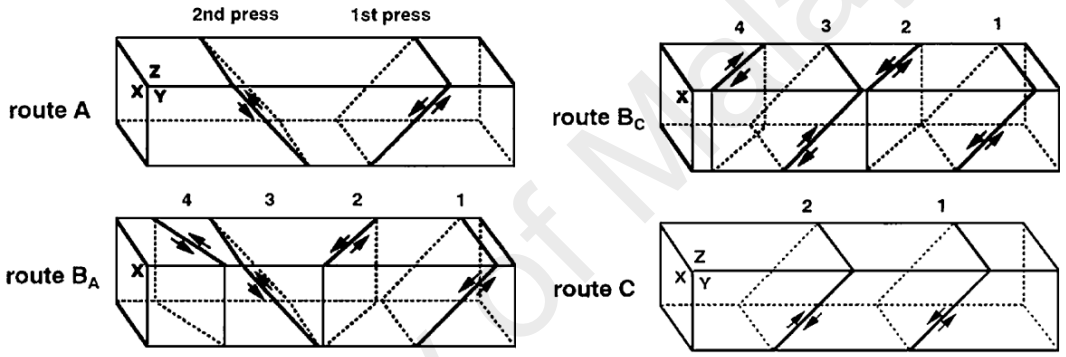

Figure 2.19: The slip systems viewed on the X, Y and Z planes for consecutive passes using processing routes A, B_A, B_C and C (Ruslan Z Valiev & Langdon, 2006)

2.6.4 ECAP process parameters

Microstructure evolution followed by SPD has been considered widely over the last few decades (Sevillano, Van Houtte, & Aernoudt, 1980). It is believed that grain size of metallic materials declines by strain accumulation. ECAP deformation represents pure shear where the deformation occurs in the immediate vicinity of plane pass through the intersection of the two die's channel (H. S. Kim, Hong, & Seo, 2001). As shown schematically in Figure 2.17, since deformation behavior in ECAP is through pure shear, the highest influence on the process is the effect of die geometry. The equivalent plastic strain ε_{equ} accumulated in the workpiece through ECAP with channel angle of (φ) and corner angle (ψ) is presented in (2.2) after P pressing passes is calculated as:

University of Malaya

$$\varepsilon\_equ = P/\sqrt{3}(2cot(\varphi / 2 + \psi / 2) + \psi cosec(\varphi / 2 + \psi / 2)) \quad (2.2)$$

The assumptions in this geometrical analysis is frictionless die surfaces and workpiece fills the channel which indicates that the material behavior is close to ideal (S. Li, Bourke, Beyerlein, Alexander, & Clausen, 2004).

The most influential parameter regarding the ECAP process is the die geometry (channel angle and corner angle), However, there are other factors that increase the temperature during the process namely pressing pressure, pressing speed, die initial temperature, friction factor and backpressure. The heat produced can be transfered to die and cause detrimental effect on the process if being neglected. Extrusion pressure is an important factor for successful ECAP process design. It determines the capacity of required press and gives the estimation of forces imposed to die and punch throughout the process. Pressing speed is one of the important factor which affects heat generation pattern through ECAP, which in turn induces phase transformation or change in micro structure significantly in grain boundaries. As a result of this variation, flow stress of the workpiece material as well as other mechanical properties may change regarding different pressing speeds. In ECAP, friction influential parameter which affects the overall deformation behavior, load requirement and strain evolution. According to Prangnell et al (Prangnell, Harris, & Roberts, 1997), strain and inhomogeneous deformation increase by friction. Moreover, friction state indicates whether the dies internal corner is filled and affects the shear magnitude accumulated in the workpiece deformed section homogeneously. Employment of backpressure in ECAP process results in slight increase of the sample hardness, nevertheless it leads to increase in the process temperature (Y. L. Wang, Lapovok, Wang, Qi, & Estrin, 2015).

University of Malaya

2.7 EDM Electrode Mechanical Properties

EDM electrodes are mainly fabricated from copper (Cu), graphite (C), tungsten (W), brass and silver (Ag) (Gaitonde et al., 2010). Of these materials, copper and graphite are broadly employed in die and mold manufacturing owing to their high MRR (Davim et al., 2009). Despite the high MRR, high sensitivity to wear reduces final workpiece accuracy and surface integrity. To overcome these concerns, copper tungsten (Cu-W) is often used in precision EDM for the combination of high hardness and wear resistance provided by W and high thermal and electrical conductivity of Cu (S. H. Lee & Li, 2001). However, low melting temperature of Cu increases the Cu-W electrode wear during EDM, on the other hand to compensate this drawback, increasing the W content leads to formation of porosity during sintering process due to insolubility of W and Cu, which significantly increase the production cost of Cu-W electrodes (Li Li et al., 2001). Furthermore, application of this electrode material is limited due to low formability.

Moreover, electrodes produced through powder metallurgy (P/M) that are categorized as green compact and sintered types are attracting great attention as a result of the promising surface integrity of workpieces after EDM machining (Patowari et al., 2011). In machining medium carbon steel, composite electrode fabricated using copper and Chromium (Cr) powders improves finished surface wear resistance (H. C. Tsai et al., 2003). WC-Cu electrodes produced by P/M used for machining C-40 steel led to higher surface integrity and reduced heat-affected zone (Patowari et al., 2011). The accretion of wear-resistant materials such as TiC on carbon steel was done by injecting Ti powder into dielectric through a copper electrode (Furutania et al., 2001a). Mainly, application P/M electrode is limited to surface modification through deposition of electrode material on the workpiece. Despite the advantages of P/M electrodes, drawbacks, for instance, under certain machining conditions P/M electrodes can cause workpiece material addition rather than material removal (Samuel & Philip, 1997).

University of Malaya

Copper with ultrafine grain structure exhibits a superior combination of mechanical and physical properties (RZ Valiev et al., 2015). Severe plastic deformation (SPD) is the most appropriate choice for fabricating bulk material with ultrafine grain structure. The main feature of SPD is the imposition of large plastic strain under high pressure without altering the initial workpiece shape. Among the SPD methods, ECAP has attracted particular attention for its exceptional potential to be scaled up for various industrial applications in addition to its ability to impose high plastic strain (Ruslan Z Valiev & Langdon, 2006). The mechanical properties of pure copper processed by ECAP highlight significant improvement as a consequence of grain refinement and evolution of high-angle grain boundaries (C. Zhu et al., 2013).

The characteristics of ECAP-treated copper are problematic when both mechanical and electrical features are essential. A number of research works have been carried out in this regard and results have shown that the mechanical properties of copper, including yield and ultimate strength and hardness significantly improved, but the electrical conductivity moderately decreased as a consequence of electron scattering due to crystal lattice defects (RZ Valiev et al., 2015).

Evaluation of mechanical properties of pure copper after one pass ECAP indicated significant improvement in tensile strength and hardness, while ductility decreases due to work hardening (Salimyanfard, Toroghinejad, Ashrafizadeh, Hoseini, & Szpunar, 2013). The improvement in tensile strength and hardness saturate after first two passes due to the limitation in grain refinement (Mishra, Kad, Gregori, & Meyers, 2007), however the ductility of copper moderately increase after second pass in compare with first pass (Ruslan Z Valiev & Langdon, 2006). These enhancements in mechanical properties of ECAP treated copper are attributed to its microstructure evolution mainly as a result of grain refinement. Study on microstructure evolution of pure copper subjected to 1-16

University of Malaya

ECAP passes showed the formation of microstructure dominated by lamellar boundaries which is oriented parallel to shear direction after first two passes. The maximum grain refinement was reported for first pressing pass and remains almost constant in successive passes; however microstructure transmits to an equiaxed grain structure by increasing its misorientation angles without indication of previous shear planes (Torre et al., 2004). Pure copper processed by ECAP showed insignificant reduction in electrical conductivity in the early stages of ECAP, while hardness increased by ~270% (Edalati, Imamura, Kiss, & Horita, 2012). Moreover the electrical conductivity of Cu-0.5%Cr was reportedly independent of ECAP passes and a moderate ~10% reduction was recorded in IACS (International Annealed Copper standard), while the microhardness increased by ~85% and ~114% after the first and second pressing passes (Wei et al., 2011).

2.8 Conclusion

This section provided a detailed review of the available investigations with comprehensive categorization to build a clear mapping of the EDM enhancement. The concluded points from the literature review is presented. Addition of powder to dielectric is the most common method for improving the EDM performance factors. Ti powder have shown to have a great ability in surface modification purposes when added to the dielectric fluid. This results in increased surface hardness, wear resistance, coating, etc. These powder materials can have substantial application for coating to address the steel oxidization issues in steel mold and die production manufacturing. However, the influence of Ti nanopowder have not been investigated till date. Ti has low density and has active nature which might assist in discharge process in PMEDM. Since the smallest particle size results in the highest improvement on the surface, this research considers the influence adding Ti nanopowder to dielectric on productivity and machined surface characteristics.

University of Malaya

As explained before, this research proposes an electrode with superior characteristics for EDM applications. Accordingly, ECAP is engaged to process pure copper as the electrode material for EDM of D2 tool steel. Compared to other high-hardness materials explained in section 2.7, severe plastic deformation enhances the mechanical properties of electrode which can reduce the TWR and the machined cavity's accuracy.

University of Malaya

CHAPTER 3: METHODOLOGY

3.1 Introduction

This chapter describes the methodology deployed in this study. First in section 3.2 details of the base materials that are used in the research and their preparation procedure are provided. The investigations in this thesis is divided into three main section of Ti nanopowder mixed EDM, EDM with ECAP treated electrodes and mutual implementation of these technologies. The process of Ti nano PMEDM of AISI D2 steel alloy including the machining apparatus and construction of system capable of providing the machining gap with Ti nanopowder and powder selection criteria are described in section 3.3. EDM with ECAP treated electrodes concerning ECAP treatment procedure and preparation of electrode is explained in section 3.4, whereas section 3.5 clarifies the nano-titanium PMEDM of AISI D2 steel alloy with ECAP treated electrodes. At last, sections 3.5 and 3.6 provide the machining conditions and mechanical and metallurgical testing, analysis and machining performance evaluation employed throughout the thesis.

3.2 Electrical Discharge Machining Equipment and Base Materials

A Sodick die sinking EDM with maximum travel range of 300 mm longitude, 250 latitude and 250 mm vertical travel was used to conduct the experiment with the various electrode and dielectric types. A hydrocarbon oil dielectric as a pure dielectric and Ti nanopowder mixed dielectric served to directly flush the machining gap to provide more effective ejection of debris and reduce machined surface crack density (Wong, Lim, & Lee, 1995).

AISI D2 steel is selected as the workpiece material which has an excellent resistance against adhesive and abrasive wear, high compressive strength and good dimensional stability. This combination of properties renders this grade of steel suitable for the fabrication of cutting, bending, drawing and extrusion die sets. The D2 steel utilized in

University of Malaya

this study has the chemical composition tabulated in Table 3.1. At first, Wire-EDM was used to cut the steel alloy into pieces measuring 20x20x6 mm and afterwards the removal of the layer of burnt surface was undertaken by with the help of the surface grinding machine.

Table 3.1: The chemical composition of the workpiece

AISI D2	Fe	C	Si	Mn	P	S	Cu	Ni	Cr	Mo	V
Percentage	≥ 82	1.4 ~ 1.6	≤ 0.40	≤ 0.60	≤ 0.03	≤ 0.03	≤ 0.25	≤ 0.50	11.0 ~ 13.0	0.8 ~ 1.2	0.2 ~ 0.5

The base materials utilized as electrode is commercial pure copper (99.9 wt. %) for the electrode. Pure copper, a widely-known electrode substrate, is the material of choice on account of its low cost and superior electrical and thermal conductivity (Gaitonde et al., 2010). The material was supplied in the form of an extruded bar and then machined with a CNC lathe machine to the 9 mm diameter, then underwent tip grinding and polishing to remove any potential oxidised layer that might have adversely affected electrical conductivity. For electrodes that underwent ECAP treatement, the preparation procedure is explained in detail in section 3.4.

Clear colourless hydrocarbon oil with properties tabulated in Table 3.2 was used as dielectric medium in conventional EDM process when investigating the influence of various electrodes on process performance measures.

Table 3.2: Dielectric oil properties

Type	**Density (15°c)**	**Viscosity (cSt)**	**Colour**	**Boiling point (°c)**
Hydrocarbon oil	0.799 kg/cm^3	2.2	Clear colourless liquid	Between 200 and 250

University of Malaya

As it is explained in detail in section 2.4.5, Ti nanopowder dielectric is selected due to its active nature and low density. Ti nanopowder indicated in Figure 3.1 was 99.9% pure titanium particles of round shape and with a mean size of 40-60 nm. 2 g/l concentration of this powder was mixed with hydrocarbon oil with properties stated in Table 3.2 by means of a stirrer, followed by ultrasonication (240 W, 40 KHz, 500 W) to ensure homogeneous distribution of powder in dielectric.

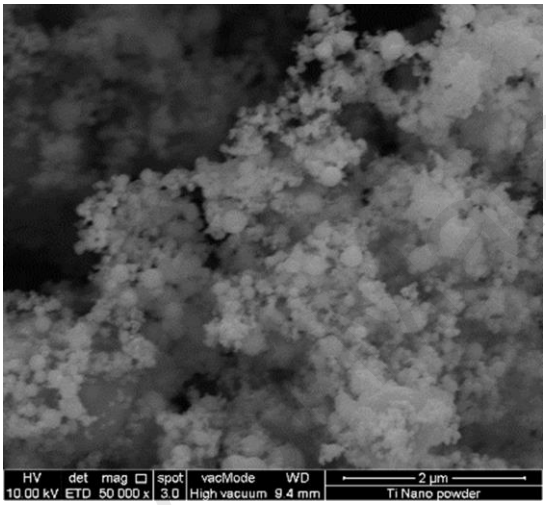

Figure 3.1: Titanium nanopowder (40-60 nm)

3.3 Nano titanium PMEDM of AISI D2 steel alloy

3.3.1 Dielectric and powder mixed dielectric circulation system

To facilitate the employment of powder mixed dielectric, a custom-made external circulation system with eight litres liquid capacity was designed which aimed at diminishing the quantity of required powder and facilitating the constant reuse of the powder over experimentation. Furthermore, it prevents the penetration of powder in the original EDM filtration system. This system was developed according to the system developed by Yih-fong and Fu-chen (2005) that is depicted in Figure 3.2, however, the magnetic filtration was replaced with paper filter. To assure the powder concentration in dielectric during experimentation, the performance of filtration system has been monitored using ESEM and EDX with details explained in section 3.3.2.

University of Malaya

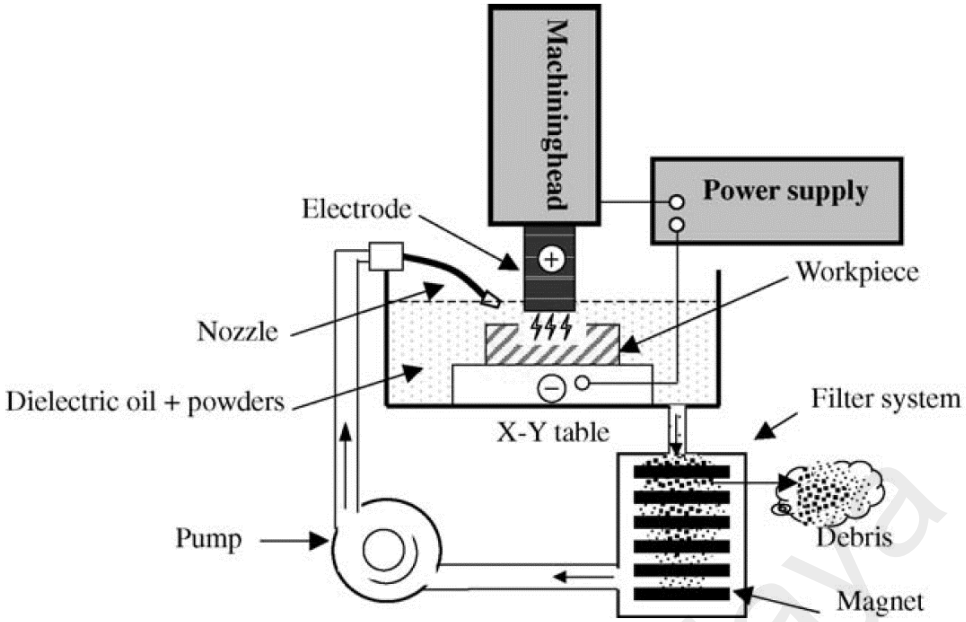

Figure 3.2: Schematic diagram of filter system for the EDM used for the experiments by (Yih-fong & Fu-chen, 2005)

Figure 3.3 and Figure 3.4 show respectively the schematic and actual demonstration of PMEDM circulation system used to carry out the experimentation in this study. During the experiment, workpiece stability was ensured by machining chamber integrated with a holder. Dielectric liquid is extracted by pump via a filter from the machining chamber and subsequently expelled through the nozzle at the rear of the chamber. The implemented PMEDM machining chamber during the machining process is shown in Figure 3.4. Direct flushing was installed to make sure that the dielectric medium was present in the machining gap.

University of Malaya

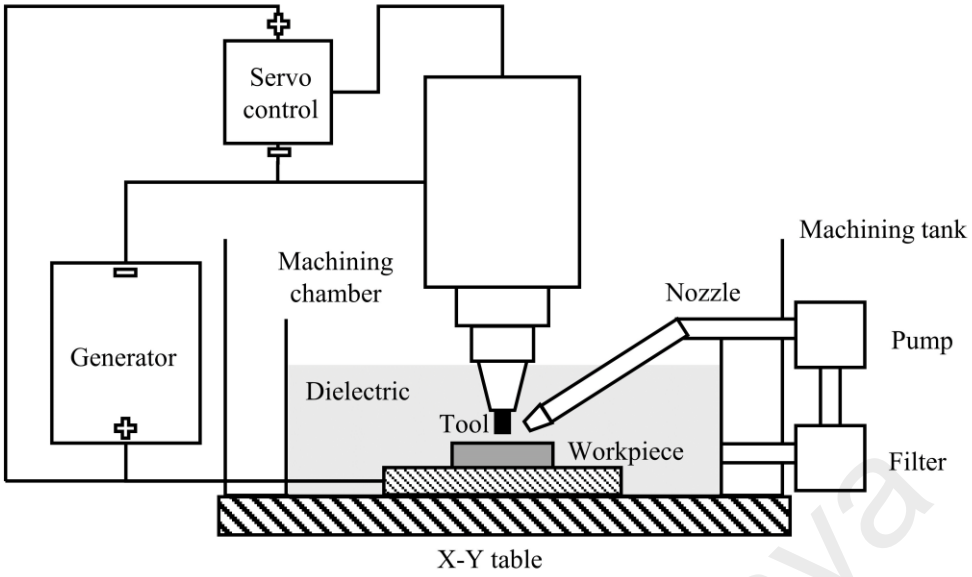

Figure 3.3: The powder-mixed EDM circulation system

University of Malaya

a

b

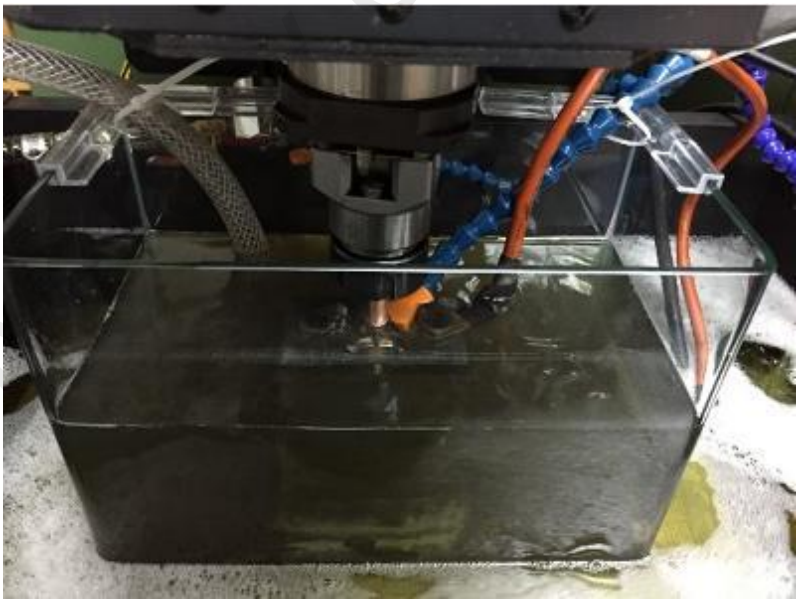

Figure 3.4: PMEDM machining (a) full set-up (b) small machining chamber

University of Malaya

3.3.2 Evaluation of PMEDM circulation system performance

Micrographs of nanopowder particles in oil prior to and following machining are depicted in Figure 3.5 and they certify that titanium nanopowder was available in dielectric. EDX was derived from each of the two samples to make sure that the tank contained the correct powder concentration and debris particle percentage.

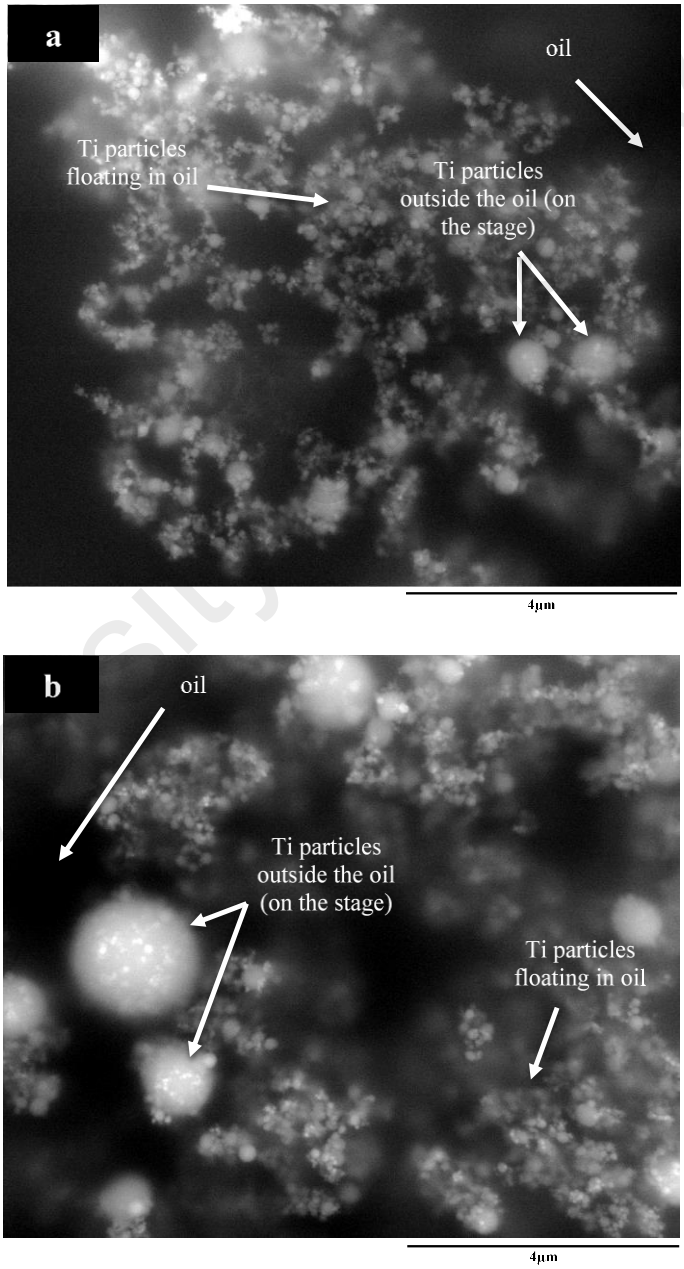

Figure 3.5: EDX spectrum of oil samples (a) before and (b) after 30 minutes of machining

University of Malaya

The EDX spectrum for the two oil samples is shown in Figure 3.6 and Figure 3.7 prior and following 30 minutes of machining. Following machining, there was a decrease of around 25% in the atomic percentage of titanium, from 4.12 to 3.02%. Possible reasons for this include deposition of particles in the circulation components or the filtration process. Therefore, replacement of dielectric liquid was undertaken after every half an hour of machining to ensure that the machining conditions remained the same all through the experiment. Since the sample was derived immediately following machining, the amount of debris elements evidently increased. Both samples exhibited high concentration of C element due to the presence of hydrocarbon oil.

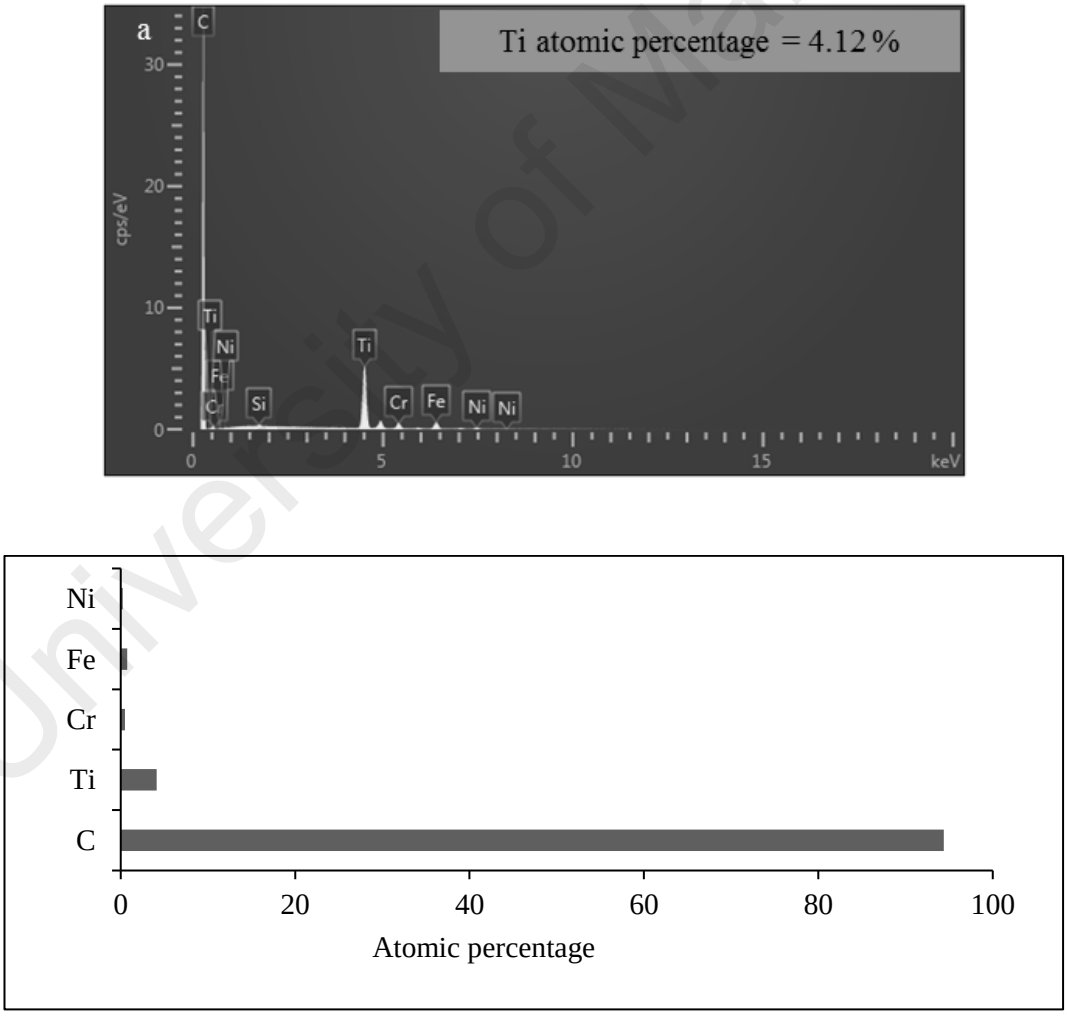

Figure 3.6: EDX spectrum of Ti nanopowder mixed dielectric samples prior to machining

University of Malaya

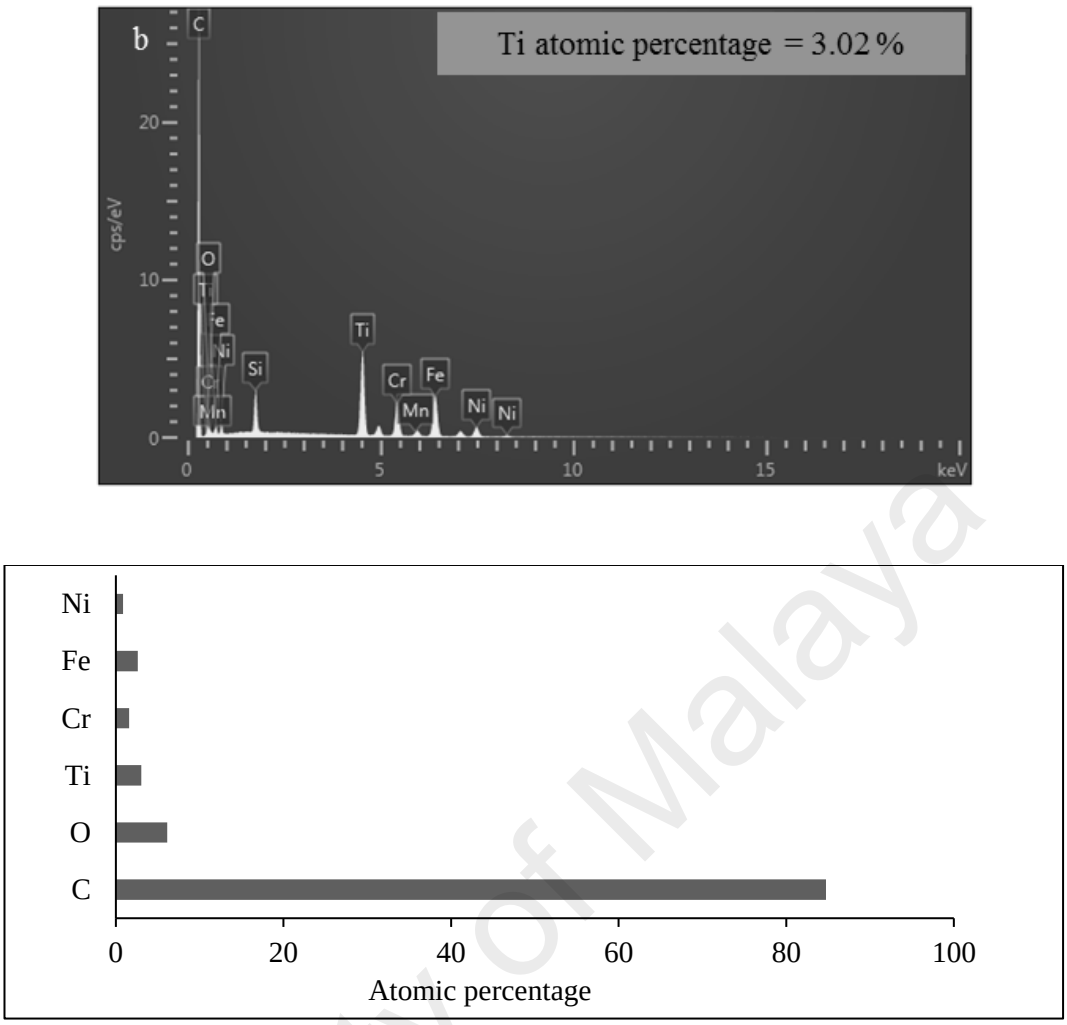

Figure 3.7: EDX spectrum of Ti nanopowder mixed dielectric samples following 30 min of machining

3.3.3 Machining conditions

Three levels of current and three levels of discharge duration, were chosen for the impact of Ti nanopowder mixed dielectric on machining efficiency (Table 3.3). The experimental matrix with three distinct parameter values was employed to develop eighteen experiments (Table 3.4). For every experiment, three samples were obtained under time-regulated condition. Once the circulation began, a vertical feed was implemented for ten minutes (Figure 3.8).

University of Malaya

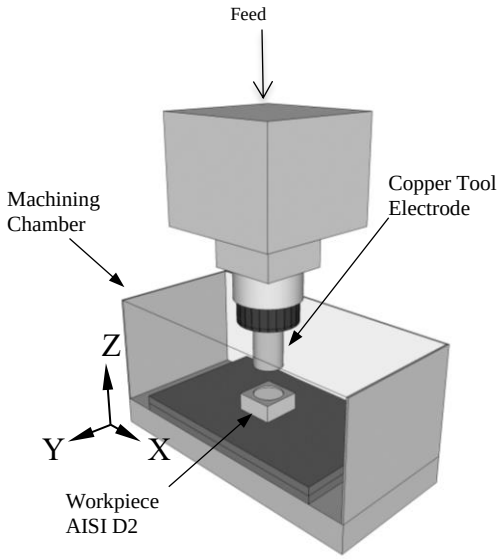

Figure 3.8: Machining chamber

Table 3.3: Parameters and levels

Parameters		Levels		
		Level 1	Level 2	Level 3
A	I_a (A)~	1	1.5	2
B	T_{on} (µs)-T_{off} (µs)	60	100	140
C	Dielectric	Oil	2 g/l Ti+oil	-

Table 3.4: The experimental matrix

Experiment No.	**A**	**B**	**C**
1	1	1	1
2	2	1	1
3	3	1	1
4	1	2	1
5	2	2	1
6	3	2	1
7	1	3	1
8	2	3	1
9	3	3	1
10	1	1	2
11	2	1	2
12	3	1	2
13	1	2	2
14	2	2	2
15	3	2	2
16	1	3	2
17	2	3	2
18	3	3	2

Table 3.5: Condition for machining nano titanium PMEDM of AISI D2 steel alloy

University of Malaya

Parameter	Value
Powder Concentration (g/l)	~2
Average voltage (V)~	45
Machining condition	Time-controlling
Machining Time (min)	10
Electrode (mm)	Pure Cu, ϕ9
Workpiece	Die Steel D2
Dielectric	Hydrocarbon oil
Powder Material	Titanium
Powder Size (nm)	40-60
Polarity	Workpiece (+), electrode (-)

3.4 EDM with electrodes treated through Equal Channel Angular Pressing

Since ECAP treatment is the only SPD technique which can process rod shape workpieces, it was selected among other SPD techniques to enhance the mechanical properties of electrode. The ECAP was carried out by means of a die set designed according to Figure 3.9. Channel angle (φ) as the most determinative specification of die set was 90° which indicated to cause a very intense plastic strain resulting in ultrafine microstructure of essentially equiaxed grains, separated by high angle grain boundaries (Nakashima, Horita, Nemoto, & Langdon, 1998). Furthermore, the corner angle (ψ) was designed as 20° which was indicated to result in the optimal distribution of effective plastic strain in the ECAP treated workpiece which channel angle of 90°. The employed die set (Figure 3.10) was fabricated from cold-worked steel, machined to a R_a of 0.6 μm, and heat treated to 60 HRC hardness. Since appropriate friction between the electrode sample and die channel facilitates accomplishment of grain size homogeneity, before inserting the electrode (pure copper) into the die channel inlet, sample surfaces and the channel surface were covered with molybdenum disulfide lubricant to diminish the friction. Afterwards, at room temperature, the ECAP was done by pressing the electrode into the die channel by means of a 100 kN press with pressing speed of 1 mm/s to minimize the effect of rising heat during the process. Figure 3.10 demonstrates the final ECAP-treated copper sample after passing through the ECAP die channel and its relative

University of Malaya

die set. The second ECAP process pass was completed according to the aforementioned process parameters without rotating the sample after the first pass (route A). The electrodes stated in Table 3.6 were then prepared for experimentation.

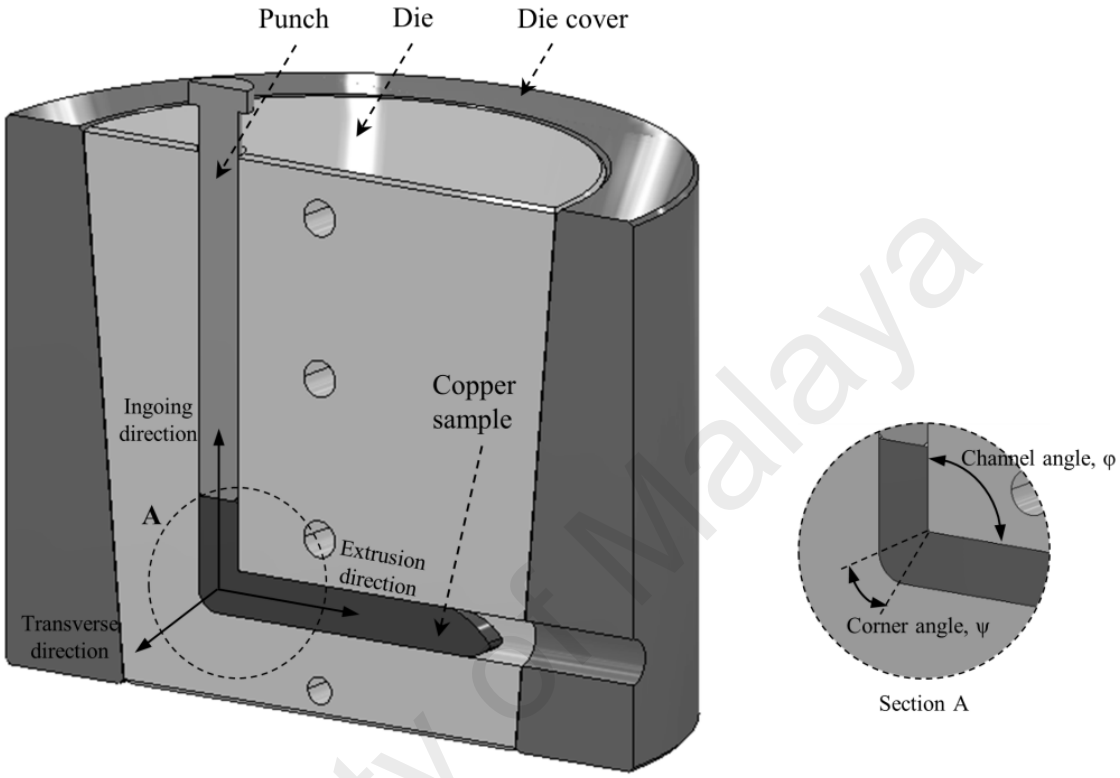

Figure 3.9: Schematic illustration of ECAP die set (H. Marashi, Jafarlou, Sarahan, & Mardi)

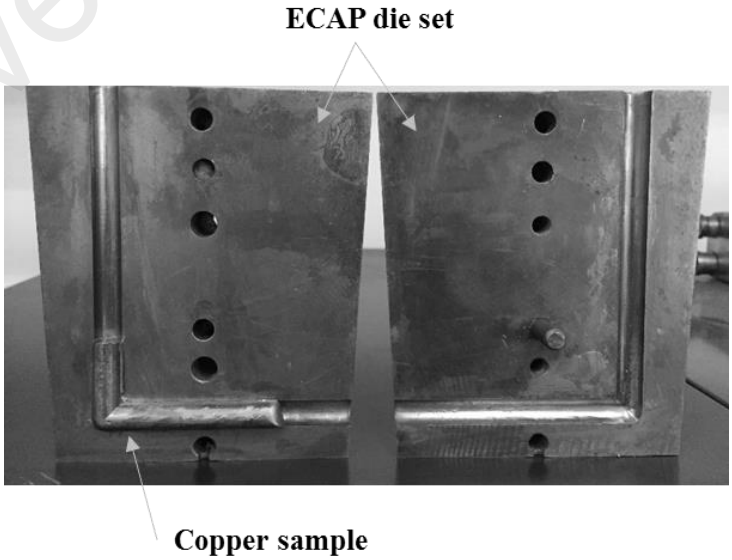

Figure 3.10: Copper sample after the ECAP process and relative ECAP die set

University of Malaya

Table 3.6: Electrode types employed for experimentation

C0	As-received copper electrode
C1	Copper electrode treated with one cycle ECAP pass
C2	Copper electrode treated with one cycle ECAP passes

Figure 3.11(a) demonstrate a schematic view of the electrode with its dimensions and Figure 3.11(b) represents the final workpiece after EDM. The electrodes were machined according to the dimensions illustrated in Figure 3.11(a) using a lathe machine. They were subsequently polished with 800-2400 grit silicon carbide paper followed by ultrasonic rinsing in acetone to remove surface contamination. As seen in Figure 3.11(b), a square cavity was considered for machining. To produce this cavity, an electrode was fed downwards (Z-direction) under the servo control with conditions tabulated in Table 3.7 into the workpiece for 3 mm. The electrical parameters stated in Table 3.7 were selected according to the most recommended condition for machining steel workpiece using copper electrode. Feeding in the ±X and ±Y directions continued until the machining plan was achieved.

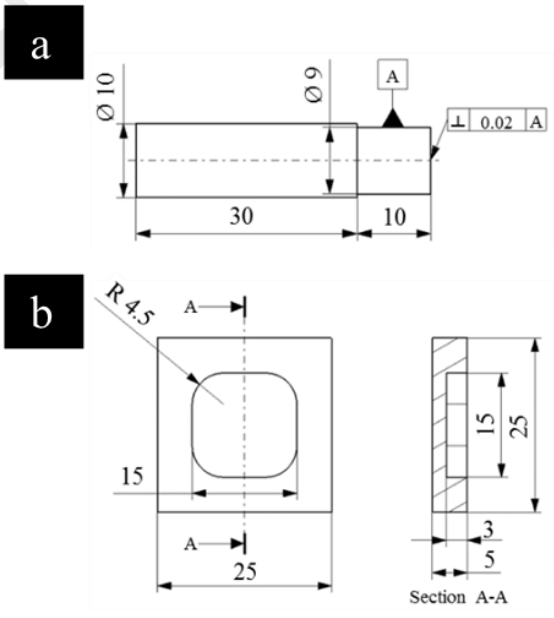

Figure 3.11: Illustration of (a) tool (electrode) and (b) workpiece

University of Malaya

Table 3.7: Condition for EDM of AISI D2 steel with ECAP-treated electrodes

Parameter	Value
I_a (A)~	4.5
Pulse on-time (T_{on}), µs	60
Pulse off-time (T_{off}), µs	20
V_a (V)~	95
Polarity	Workpiece (+), electrode (-)
Machining condition	Depth-controlling
Electrode (mm)	Pure Cu, ϕ9
Workpiece	Die Steel D2
Dielectric	Hydrocarbon oil

3.5 Nano Titanium PMEDM of AISI D2 steel alloy with ECAP treated electrodes

To investigate the mutual impact of Ti nanopowder addition to dielectric and ECAP treatment of electrode, the machining condition was set at the most common condition for machining steel workpiece using copper electrode. The T_{on} and T_{off} were increased to 100 µs and 40 µs respectively to increase the influence spark energy on electrode. The experimentation procedure was carried out using the abovementioned PMEDM setup explained in section 3.3.1 and ECAP treatment technique described in section 3.4 under the machining condition stated in Table 3.8.

Table 3.8: Condition for Ti nano PMEDM of AISI D2 steel with ECAP-treated electrodes

Parameter	Value
I_a (A)~	1
Pulse on-time (T_{on}), µs	100
Pulse off-time (T_{off}), µs	40
V_a (V)~	85
Polarity	Workpiece (+), electrode (-)
Machining condition	Depth-controlling
Electrode (mm)	Pure Cu, ϕ9
Workpiece	Die Steel D2
Dielectric	Hydrocarbon oil

University of Malaya

3.6 Mechanical and metallurgical testing, analysis and machining performance evaluation

Immediately after completion of every experiment, samples were cleaned with acetone in an ultrasonic bath, after which they were left to dry in warm air. Subsequently, to identify the properties of the machined surface, several devices, including scanning electron microscope (SEM), field emission scanning electron microscope (FESEM), energy dispersive X-ray (EDX), Mitutoyo surface profilometer and atomic force microscope (AFM), were used to weigh and analyse various properties of electrodes.

To evaluate the effect of process adjustments on the machining characteristics, MRR and TWR were selected as the EDM response variables. MRR was calculated as the wear weight of the workpiece over machining time as:

$$MRR = \frac{1}{t}(w_{wb} - w_{wa}) \tag{3.1}$$

where w_{wb} is the weight of the workpiece before machining, w_{wa} is the workpiece weight after machining, and t is the machining time. The wear weight of electrodes treated by ECAP is calculated as follows:

$$TWR = \frac{1}{t}(w_{tb} - w_{ta}) \tag{3.2}$$

where w_{tb} is the weight of the tool before machining, w_{ta} is the weight of the tool after machining and t is the machining time.

It was found that in the materials with average grain size of 1μm, nanohardness is more suited than microhardness in order to evaluate the hardness distribution (Suś-Ryszkowska, Wejrzanowski, Pakieła, & Kurzydłowski, 2004). Furthermore, this method provides the possibility for significant increase in the numbers of indentation and avoids the strain hardening effect between adjacent indentations. In this regard, the

University of Malaya

nanomechanical characteristics of the original and ECAP-treated copper electrodes were investigated across the plane perpendicular to the tool axis using a Hysitron TI-750D Ubi nanoindenter, which is powered by a diamond indenter which has 150 nm curvature radius. 30 seconds loading and unloading durations were established with 12 mN/min constant rate and the maximum 6 mN indentation load and 3 sec indentation time.

Furthermore, the workpieces were visually investigated after EDM using SEM. Additionally, the elemental analysis was undertaken on the crack propagation zone (visible from the cross-sectional view) using energy dispersive X-ray (EDX) on the mapping module.

University of Malaya

Besides MRR and TWR for samples fabricated a geometry in Figure 3.11(b), the volumetric overcut (VOC) was investigated to measure machining accuracy. This response variable is introduced as the percentage ratio of the difference between the designed volume V_D and the actual machined volume V_m over the designed volume. The VOC is expressed as:

$$VOC\ (\%) = \frac{V_D - V_m}{V_D} \times 100 \tag{3.3}$$

Electrode corner wear is an essential matter when it comes to the production of geometrically complex shapes with close tolerance. It is expected during cavity machining for the electrode corner wear to be always considerably larger than the electrode end wear because the corners are struck by a multitude of sparks from many directions simultaneously (Figure 4a), compromising the machined corner sharpness (S. Singh et al., 2004). Prior to corner inspection, the workpiece was cut using a Bohler precision cutter along the planes that is schematically illustrated in Figure 3.12. Then the curve that formed in the workpiece corners were observed by SEM and measured with an appropriate scale. Afterwards, the areas under the curves were calculated to quantify the corner sharpness using the following equation:

$$A = \int_0^{x_i} f(x)dx \tag{3.4}$$

where A is the area under the curve with function $f(x)$ in a domain from 0 to x_i as indicated in Figure 3.12(a).

University of Malaya

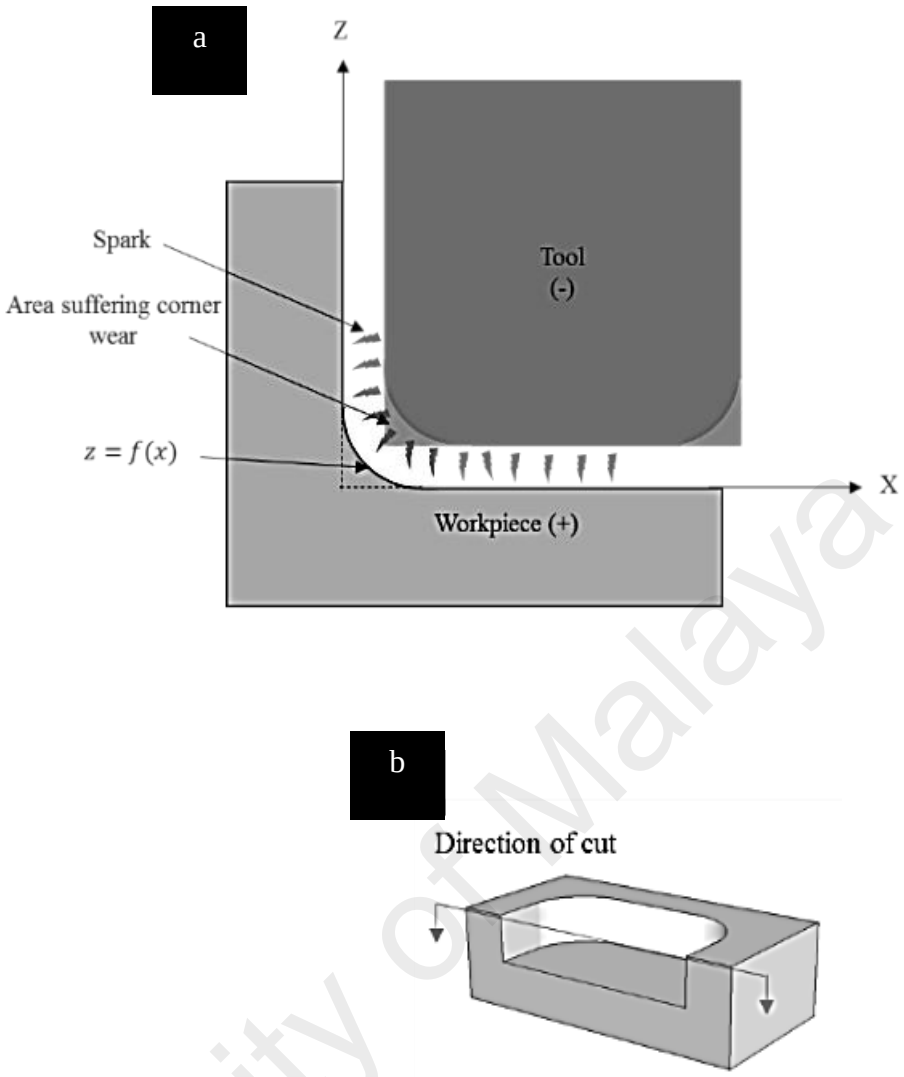

Figure 3.12: Schematic illustrations of (a) corner wear (b) the cutting direction of workpiece

Furthermore, the electrode wear ratio, which is defined as the ratio of the weight of material removed from the electrode to the weight of material removed from the workpiece, is a very suitable factor for considering the simultaneous effect of TWR and MRR. This ratio was calculated using the following equation:

$$Electrode\ wear\ ratio = \frac{w_{tb} - w_{ta}}{w_{wb} - w_{wa}} \tag{3.5}$$

University of Malaya

To examine the finished surface quality, a Mitutoyo surface profilometer measured the R_a. Several measurements were carried out along 3 and 5 lines with a length of 7.5 mm respectively on the circular and squared workpiece surfaces as indicated in Figure 3.13. The formation of voids, droplets and cracks as three factors deteriorating EDM machined surface were considered in the analysis of surface micro-graphs obtained from SEM.

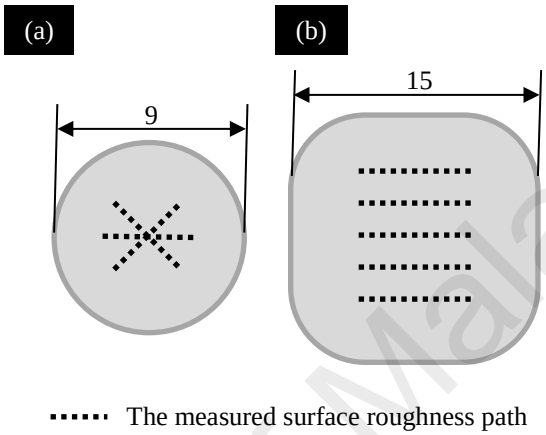

Figure 3.13: Machined surfaces and their relative measured roughness path (a) circular, (b) squared

Regarding surface cracks, the complexity of a qualitative comparison is addressed using crack density as a quantitative measurement as introduced in (Hasçalık & Çaydaş, 2007) and expressed as follows:

$$crack\ density = \frac{\sum_1^n l_i}{A_m} \tag{3.6}$$

where l is the crack length, n is the number of cracks and A_m represents the area of the surface micrograph. Crack density and number of cracks have been calculated using image measurement software. The cracks were measured by straight fitted lines with length *l*. The major shift of crack direction was fitted with a new line and counted as a separate crack.

In order to evaluate the titanium concentration in dielectric, environmental scanning electron microscope (ESEM) and EDX was used to analyse the titanium-mixed oil

University of Malaya

dielectric and verify that Ti nanopowder was available for the process. The ESEM chamber and liquid sample prior to assessment are presented at Figure 3.14. To facilitate investigation, an absorbent stick was used to diminish the hydrocarbon oil content of the sample once the powder particles attached to each other. The samples of choice were titanium-mixed oil from the tank prior to machining and following half an hour of machining, respectively.

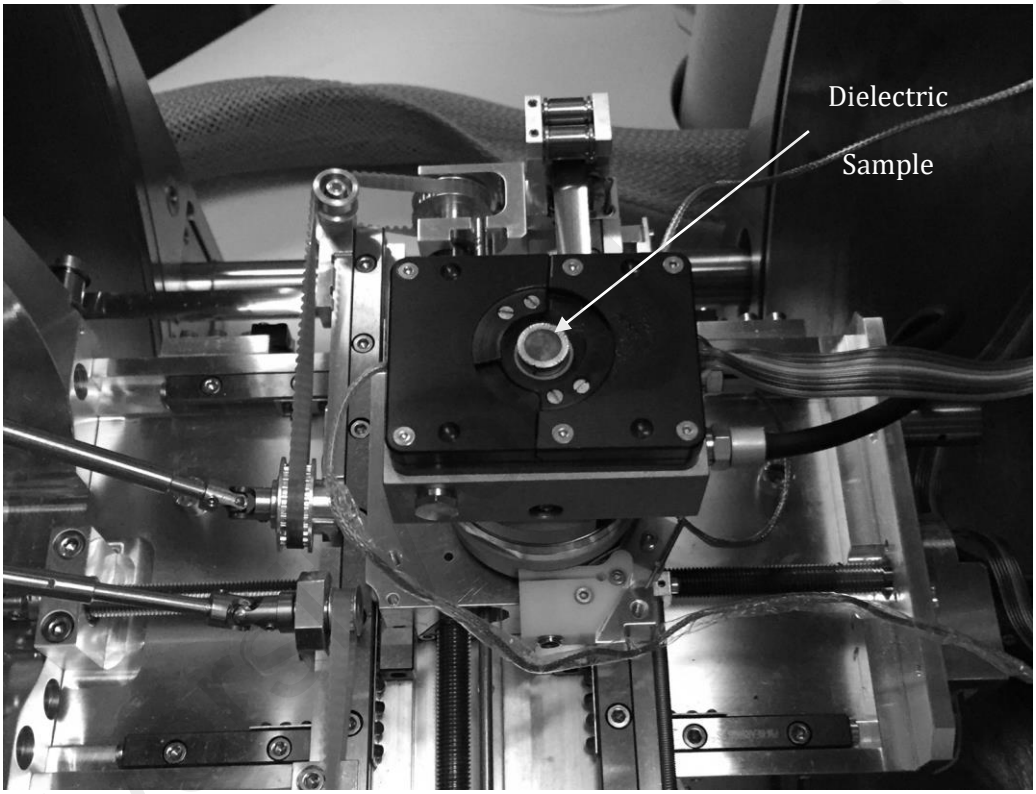

Figure 3.14: The ESEM Chamber

3.7 Conclusion

In this chapter, utilization of Ti nanopowder mixed dielectric approach in EDM is presented and the related base materials, preparation, experimental conditions, evaluation techniques were demonstrated. Also, this chapter outlines the various research components required to develop the external circulation system which facilitates the employment of Ti nanopowder mixed dielectric. Additionally, the SPD approach to enhance the mechanical properties of electrode and the method associated with the process was introduced with its related base materials, preparation, experimental conditions, evaluation techniques.

University of Malaya

CHAPTER 4: RESULTS AND DISCUSSION

4.1 Introduction

Followed by data collection in section 3, analysis and graphical representation of data is undertaken in this chapter. The collected results are demonstrated and discussion is oriented in three sections of 4.2, 4.3 are evaluating the nano titanium PMEDM of AISI D2 steel alloy and EDM with ECAP-treated electrodes. Lastly in section 4.4, the mutual impact of Ti nanopowder mixed dielectric and ECAP treatment of electrodes are investigated.

4.2 Nano titanium PMEDM of AISI D2 steel alloy

4.2.1 Machined surface morphology analysis

Influence of Ti nanopowder dielectric utilization on the machined surface characteristics is evaluated using FESEM, surface roughness profilometer and AFM analysis. The micrograph of the machined surfaces in pure and Ti nanopowder mixed dielectric are exhibited in Figure 4.1, Figure 4.2 and Figure 4.3 which were subjected to machining at average current of 1, 1.5 and 2 A, respectively. The clear dissimilarities in the surface texture of the machined surfaces highlight the importance of dielectric in spark attribute and subsequently surface quality. Observably, employing Ti nanopowder dielectric seem to produce smoother surface owing to formation of relatively more even overlapping craters at all discharge durations especially at 1.5 A and 2 A current and 100 and 140 µs discharge duration compared to pure dielectric. In pure dielectric, electrical discharge occurs directly between tool and workpiece resulting in formation of crater with deeper centre and high-level ridges at border, whilst in Ti nanopowder mixed dielectric, the surface texture seemed smoother due to discharge dispersion (Liew et al., 2013). Increased electrical conductivity of dielectric after addition of powder leads to reduced breakdown voltage which results in more even distribution of spark energy, thus reducing the magnitude of impact force on each spark (Bhattacharya et al., 2013).

University of Malaya

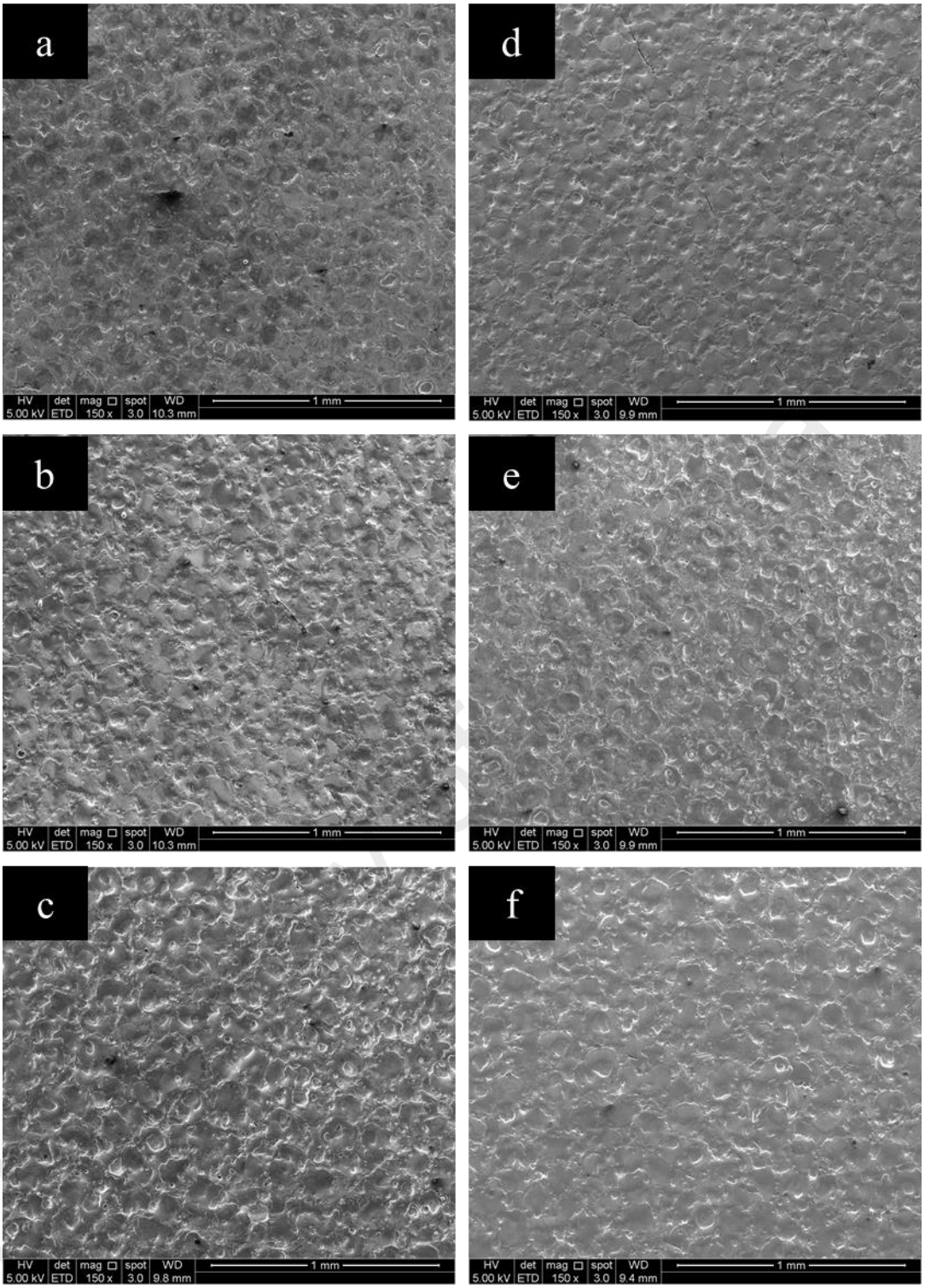

Figure 4.1: Micrograph of machined surface obtained by FESEM at 150X magnification, I_a= 1 A, T_{off}=40, (a)T_{on}=60 µs (b) T_{on}=100 µs, (c) T_{on}=140 µs in pure dielectric and (d) T_{on}=60 µs, (e) T_{on}=100 µs, (f) T_{on}=140 µs machined in Ti nanopowder mixed dielectric

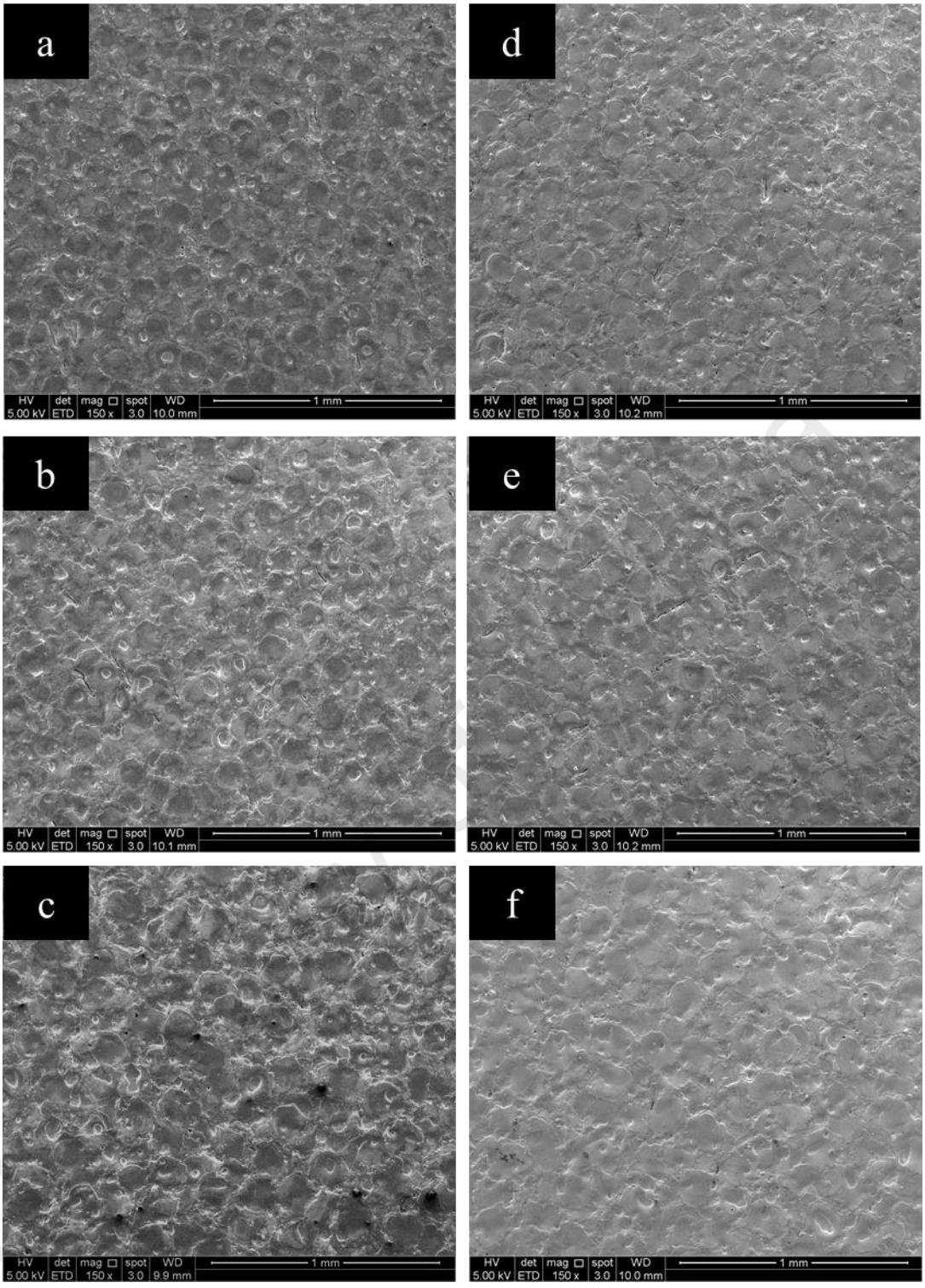

Figure 4.2: Micrograph of machined surface obtained by FESEM at 150X magnification, I_a= 1.5 A, T_{off}=40, (a)T_{on}=60 µs (b) T_{on}=100 µs, (c) T_{on}=140 µs in pure dielectric and (d) T_{on}=60 µs, (e) T_{on}=100 µs, (f) T_{on}=140 µs machined in Ti nanopowder mixed dielectric

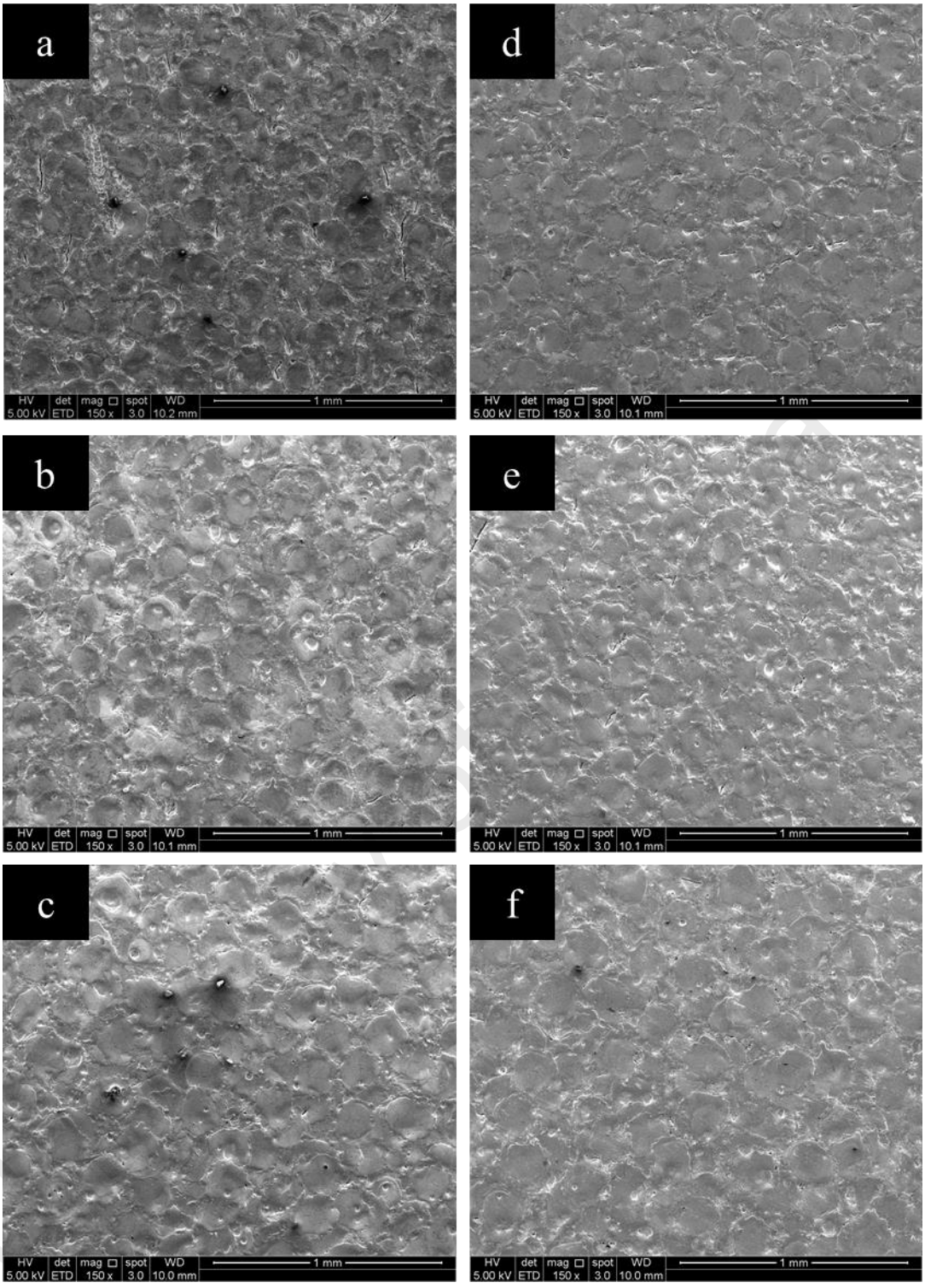

Figure 4.3: Micrograph of machined surface obtained by FESEM at 150X magnification, I_a= 2 A, T_{off}=40, (a)T_{on}=60 µs (b) T_{on}=100 µs, (c) T_{on}=140 µs in pure dielectric and (d) T_{on}=60 µs, (e) T_{on}=100 µs, (f) T_{on}=140 µs machined in Ti nanopowder mixed dielectric

As explained previously, material removal mechanism of EDM is mainly through melting and evaporation of surface followed by dielectric washing and cooling effect. This leads to formation of surface irregularities namely high-level ridges, micro-voids, micro-droplets, and micro-cracks (Figure 4.4) specially at higher discharge energies. Micro-void is the consequence of gas bubbles entrapment in the discharge gap which are produced due to deionisation of hydrocarbon pure dielectric induced by high plasma temperature. In addition, gas bubbles are also expelled from the molten material during the solidification (Guu, 2005).

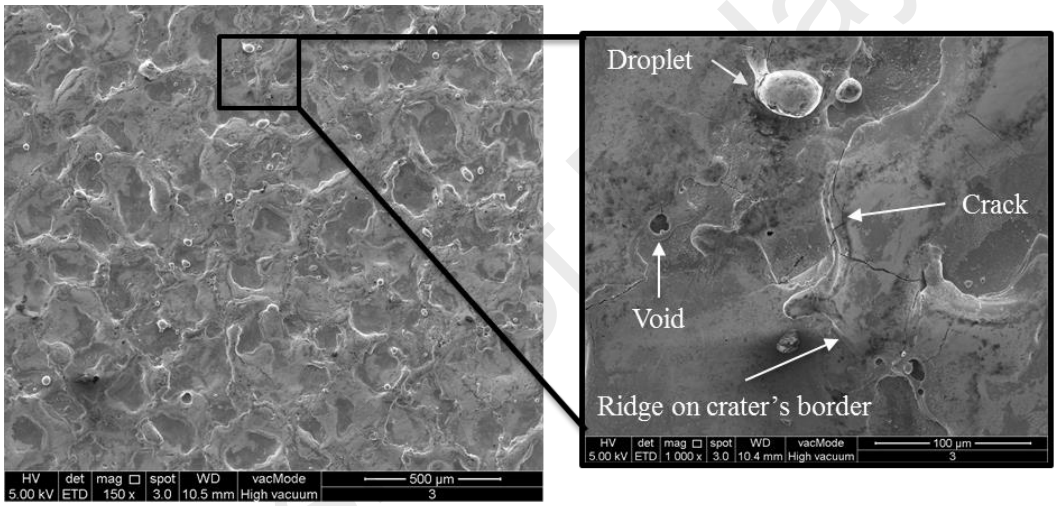

Figure 4.4: Micro-defects on surface machined by EDM

Better visualization of machined surface features is attained through micrographs at higher magnifications indicated in Figure 4.5 through Figure 4.7. The first to notice is the increase in crater size at higher currents or discharge duration, since elevating either of these factors increase spark energy. Furthermore, at low spark energy of 1 A current and 60 µs, density of micro-voids is higher on the surface machined as demonstrated in Figure 4.5. This effect does not seem to persist when using mixed dielectric though, owing to higher dielectric conductivity followed by adding Ti nanopowder, which leads to discharge gap expansion and subsequently facilitates easier expulsion of gas as well as debris. More, the effect of powder addition on decreasing the high-level ridges is more

pronounced at current of 1.5 and 2 A indicated in Figure 4.6 and Figure 4.7, respectively. Contribution of powder in dielectric leads to surface quality enhancement, since the Ti particles trigger multiple dissipated sparks instead of one intense spark.

Followed by the explosion in the gap, melted/evaporated material is pushed away by shock wave triggered by a heat-producing blast. The molten material moves on the surface which initially forms ridges on crater's border and gives rise to a ligament affixed to the droplet until the explosion force or dielectric washing effect causes complete detachment as indicated in Figure 4.4. However, because of the low dielectric temperature, complete detachment of the molten material before re-solidification is sometimes unsuccessful. Consequently, micro-droplets form and cause surface quality to deteriorate.

Figure 4.8 schematically shows the current and voltage waveform for a single spark during the EDM process. Most electrical parameters affect the MRR mainly through discharge energy (E_d) and pulse signal frequency (F_p). E_d is the mean value of electrical energy per one impulse, which is converted into heat and is expressed as (Gostimirovic, Kovac, Sekulic, & Skoric, 2012):

$$E_d = \int_0^{t_d} u(t)\, i(t) dt \cong U.I_d.t_d \tag{4.1}$$

where t_d, U and I_d are discharge duration, voltage and current, and variables $u(t)$ and $i(t)$ indicate the instantaneous voltage and current, respectively.

Selecting proper machining conditions leads to instantaneous electrical discharge and is independent from other electrical values. In this case, the ignition delay time (t_{delay}) can be neglected, thus the discharge duration t_d is equal to the pulse duration or pulse on time (t_{on}) and E_d expressed as (Gostimirovic et al., 2012):

University of Malaya

$$E_d = U.I_d\,.t_{on} \tag{4.2}$$

Equation (4.2) indicates higher spark energy with the increase of either U, I_d or t_{on}, which subsequently leads to higher MRR, TWR and surface roughness due to higher energy impacting both the tool and workpiece.

According to the abovementioned equations, increasing either of current or discharge durations, leads to higher discharge energy. As indicated in the figures, the appearance of micro-droplets is seldom due to low spark energy which cause small blasts with faster re-solidification.

University of Malaya

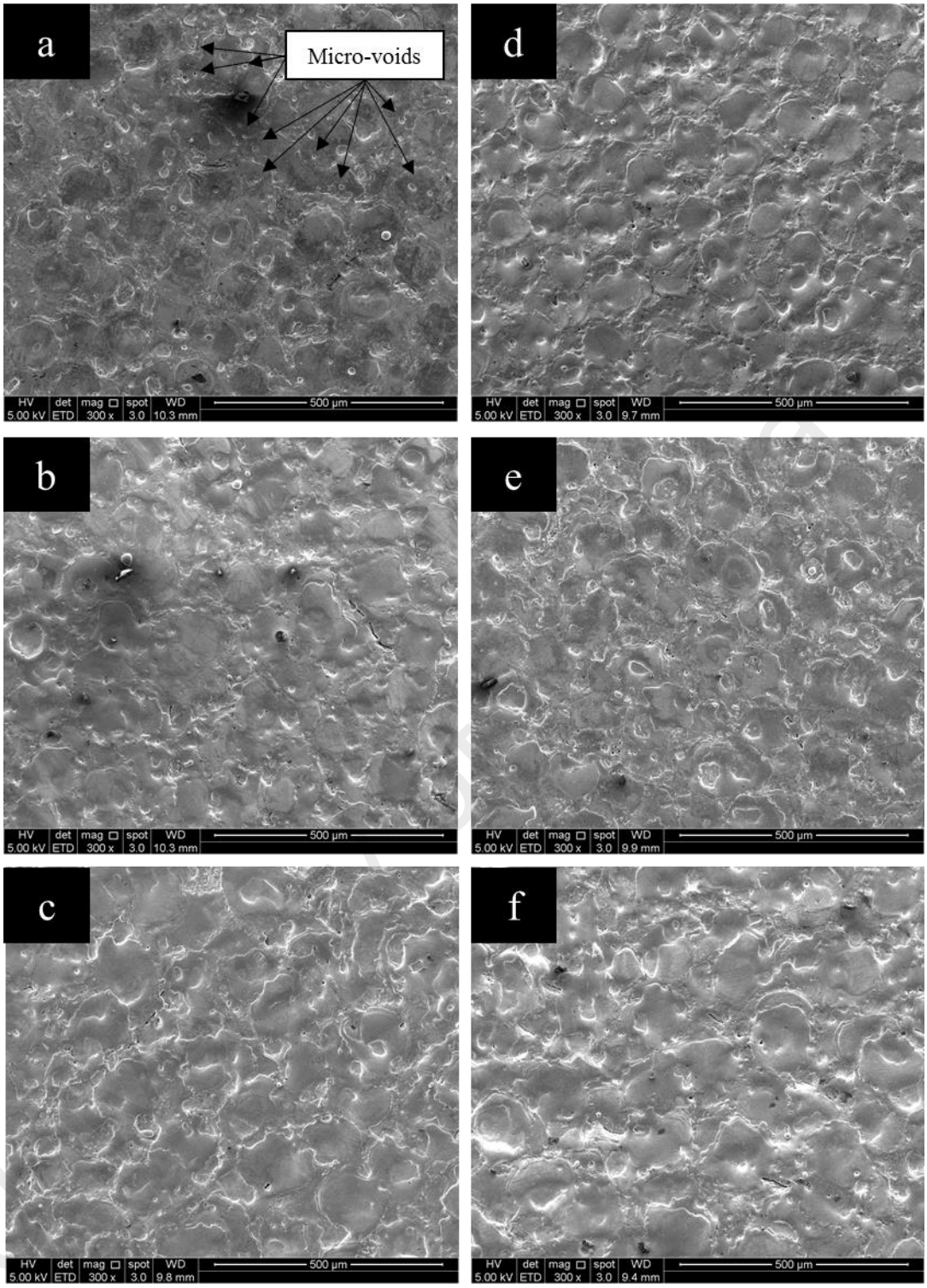

Figure 4.5: Micrograph of machined surface obtained by FESEM at 300X magnification, I_a= 1 A, T_{off}=40, (a)T_{on}=60 µs (b) T_{on}=100 µs, (c) T_{on}=140 µs in pure dielectric and (d) T_{on}=60 µs, (e) T_{on}=100 µs, (f) T_{on}=140 µs machined in Ti nanopowder mixed dielectric

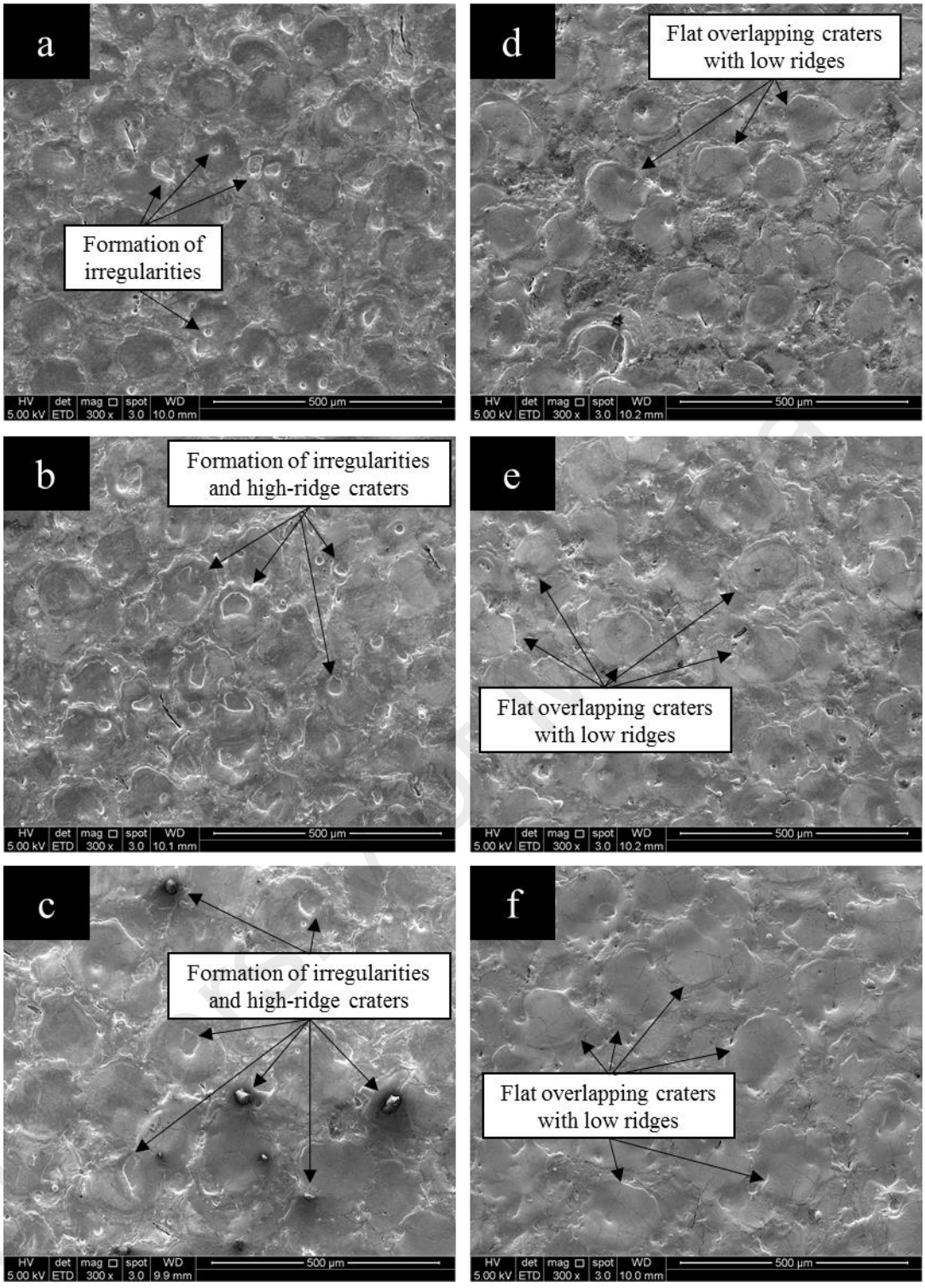

Figure 4.6: Micrograph of machined surface obtained by FESEM at 300X magnification, I_a= 1.5 A, T_{off}=40, (a)T_{on}=60 µs (b) T_{on}=100 µs, (c) T_{on}=140 µs in pure dielectric and (d) T_{on}=60 µs, (e) T_{on}=100 µs, (f) T_{on}=140 µs machined in Ti nanopowder mixed dielectric

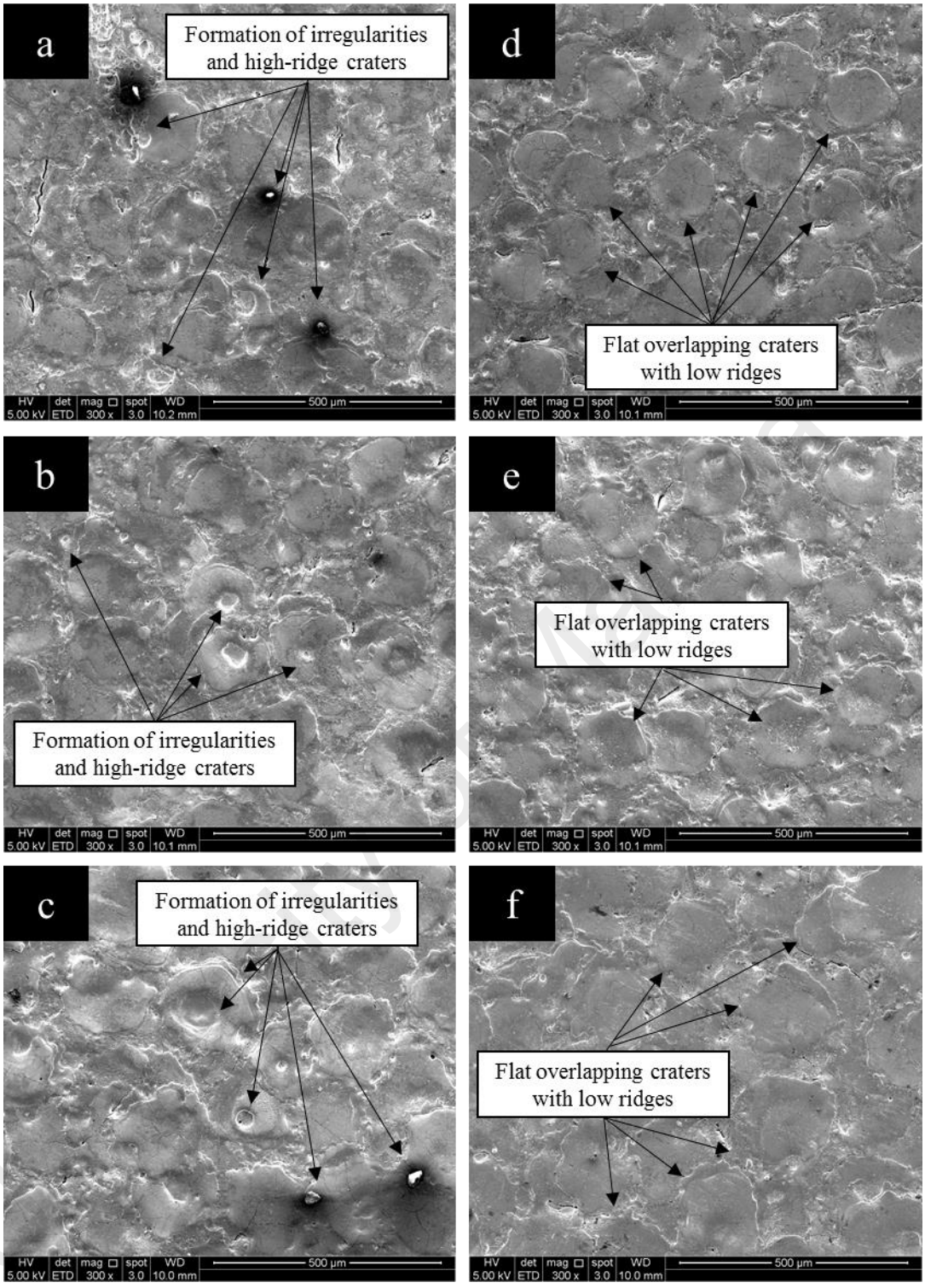

Figure 4.7: Micrograph of machined surface obtained by FESEM at 300X magnification, I_a= 2 A, T_{off}=40, (a)T_{on}=60 µs (b) T_{on}=100 µs, (c) T_{on}=140 µs in pure dielectric and (d) T_{on}=60 µs, (e) T_{on}=100 µs, (f) T_{on}=140 µs machined in Ti nanopowder mixed dielectric

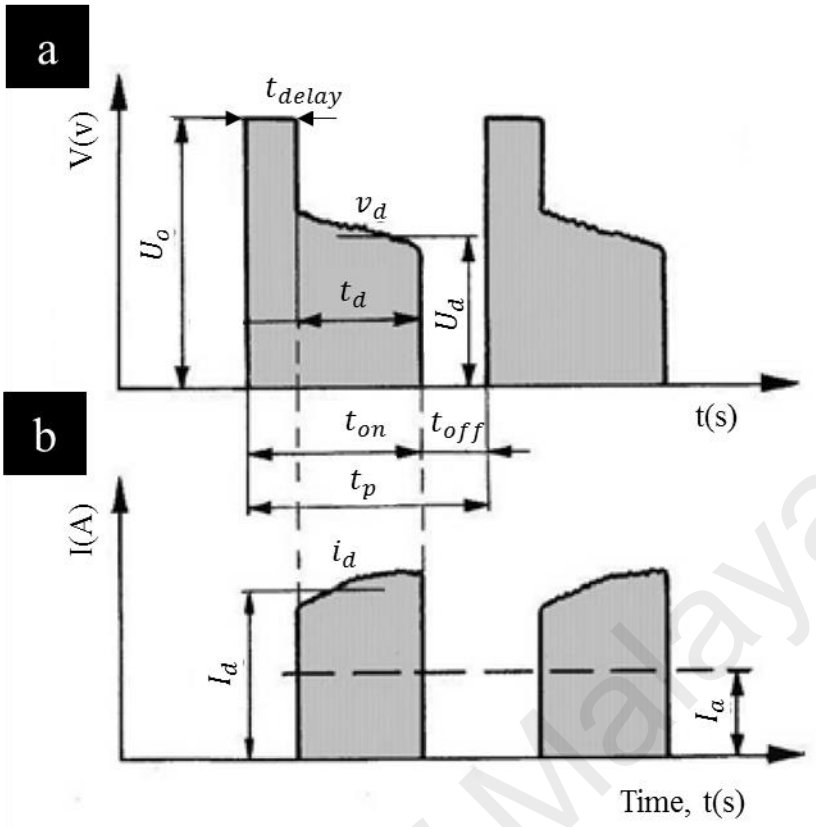

Figure 4.8: Characteristic values of (a) voltage and (b) current impulses according to (Gostimirovic et al., 2012)

Another type of irregularity observable on the FESEM micrographs is presence of black spots mainly when machining with pure dielectric. Evaluation of black spots components is undertaken by means of EDX analysis which is indicated in Figure 4.9. As expected, the elements in the EDX target area contain AISI D2 steel workpiece which confirms that black spots presence is due to debris particles adhering to surface. Unlike machining in pure dielectric, this phenomenon was less appeared when machining with Ti nanopowder mixed dielectric since addition of Ti nano-powder to dielectric leads to wider discharge gap. Furthermore, debris attachment to surface is more observable at current of 2 A. According to equation (4.1), the explosion size is expanded by increasing current and/or discharge duration which results in debris particles of larger size leading to more difficult flushing of debris from discharge gap. Thus, at 2 A current, formation of the heavier debris particles leads to improper ejection of the debris from the gap, deteriorating the surface quality.

University of Malaya

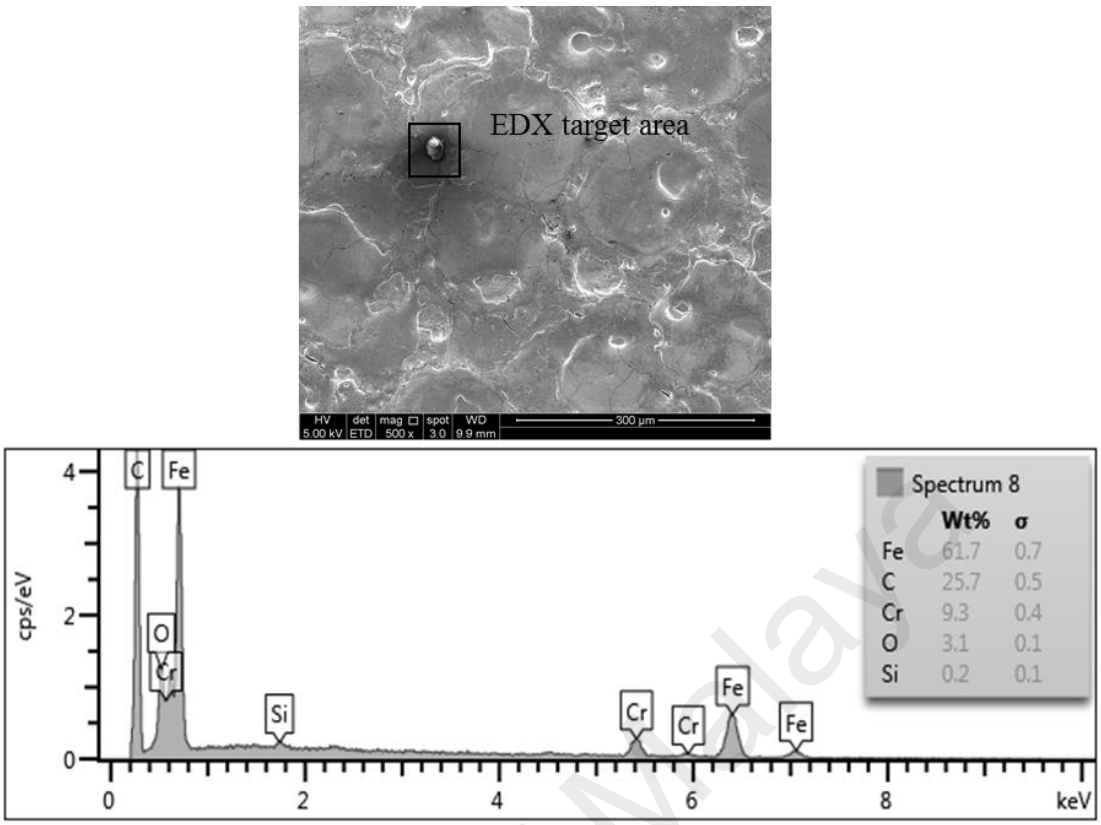

Figure 4.9: Debris elemental analysis target area and its relative EDX spectrum

4.2.2 Machined surface topography analysis

In order to quantitatively measure the surface variations, the profile roughness associated with 1, 1.5, and 2 A current with 60, 100 and 140 µs discharge duration for pure dielectric and Ti nanopowder dielectric were measured and illustrated in Figure 4.10(a) through Figure 4.10(i). The surface variation wavelength (distance separating one peak and valley from the following peak and valley) over a measured length of 4.5 mm was expanded when discharge duration or current was increased due to formation of larger craters at higher discharge energies leading to less variation of surface over 4.5 mm measured length. Furthermore, compared to pure dielectric medium, Ti nanopowder mixed dielectric was associated with lower peaks and shallower valleys.

University of Malaya

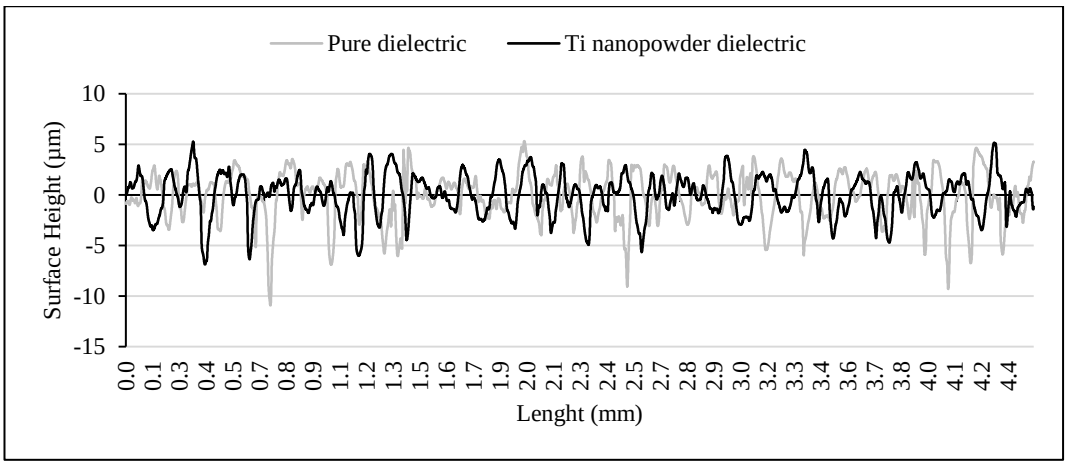

(a) T_{on}=60 µs, T_{off}=40 µs, I_a= 1 A

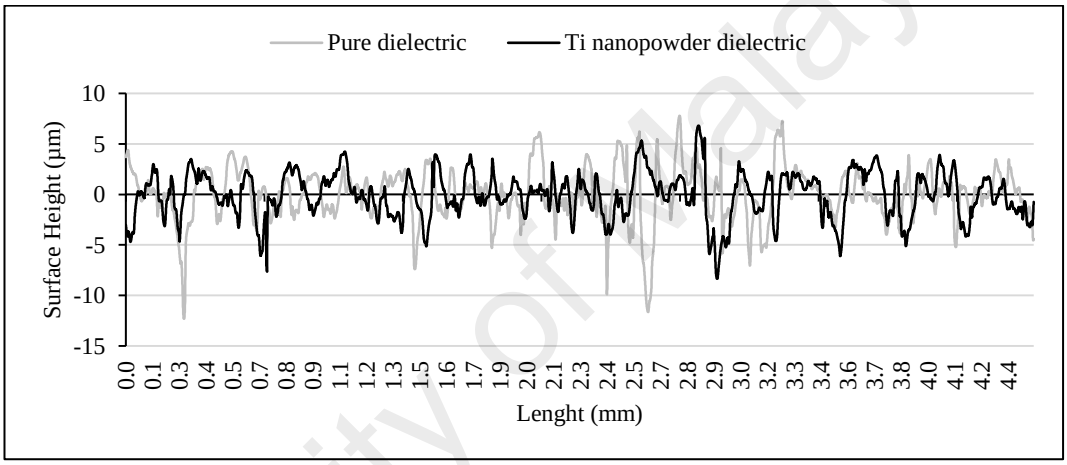

(b) T_{on}=60 µs, T_{off}=40 µs, I_a= 1.5 A

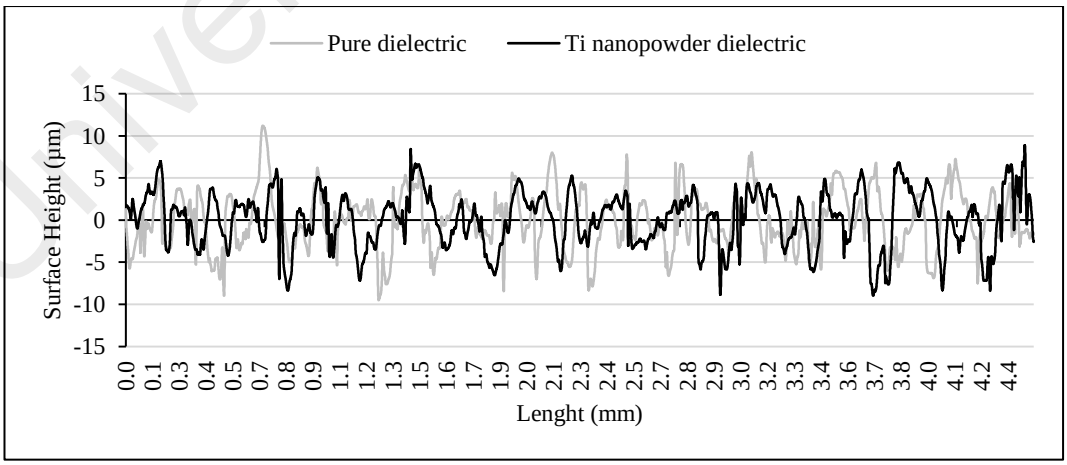

(c) T_{on}=60 µs, T_{off}=40 µs, I_a= 2 A

University of Malaya

Figure 4.10 continued.

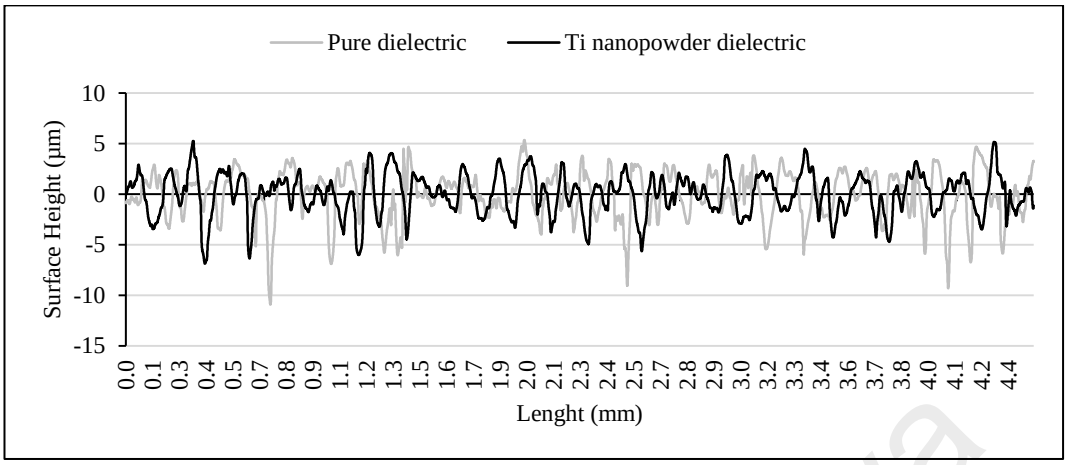

(d) T_{on}=100 µs, T_{off}=40 µs, I_a= 1 A

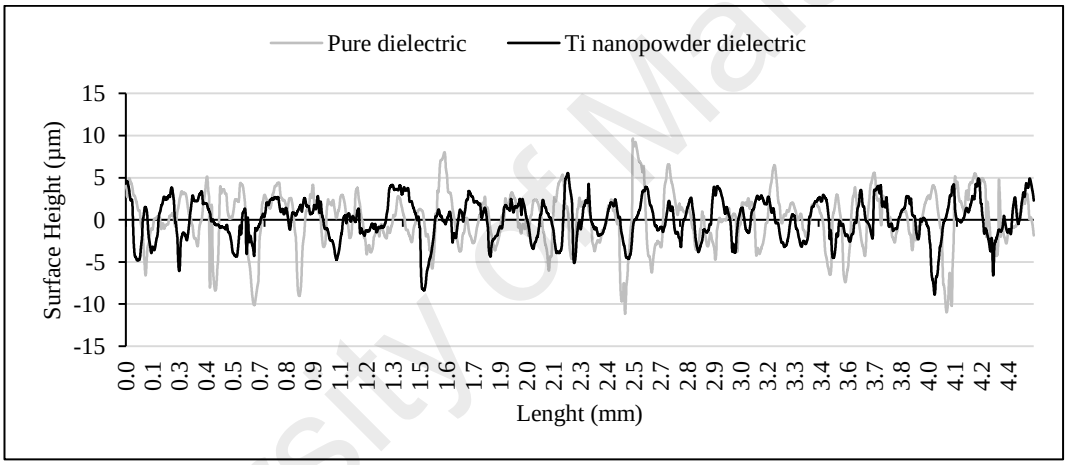

(e) T_{on}=100 µs, T_{off}=40 µs, I_a= 1.5 A

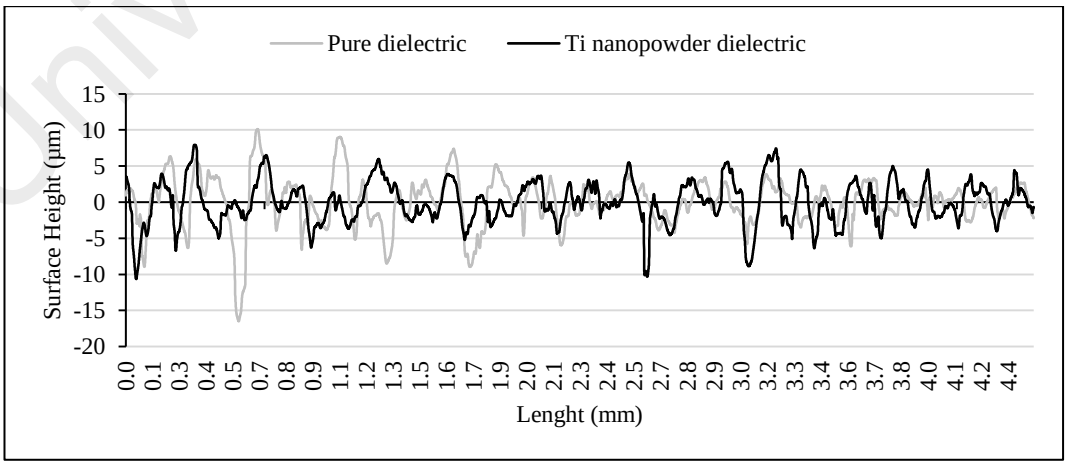

(f) T_{on}=100 µs, T_{off}=40 µs, I_a= 2 A

University of Malaya

Figure 4.10 continued.

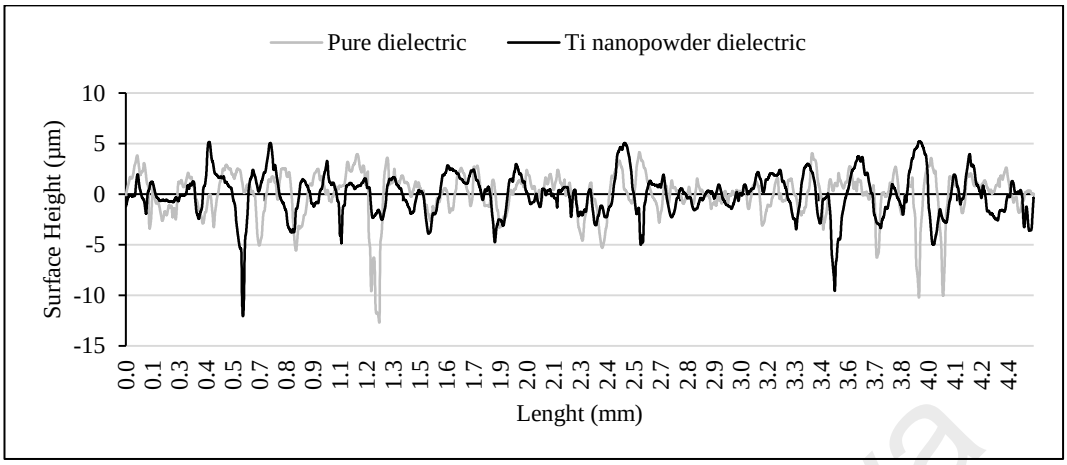

(g) T_{on}=140 µs, T_{off}=40 µs, I_a= 1 A

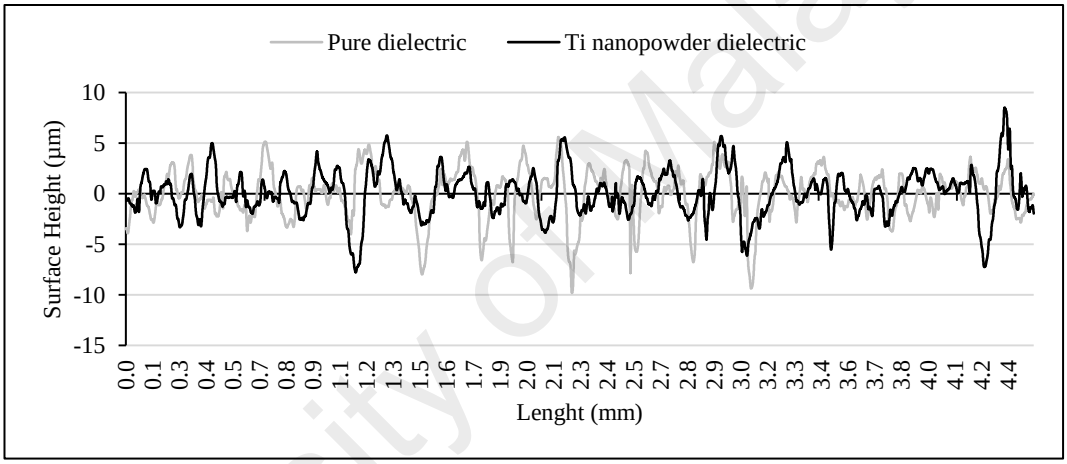

(h) T_{on}=140 µs, T_{off}=40 µs, I_a= 1.5 A

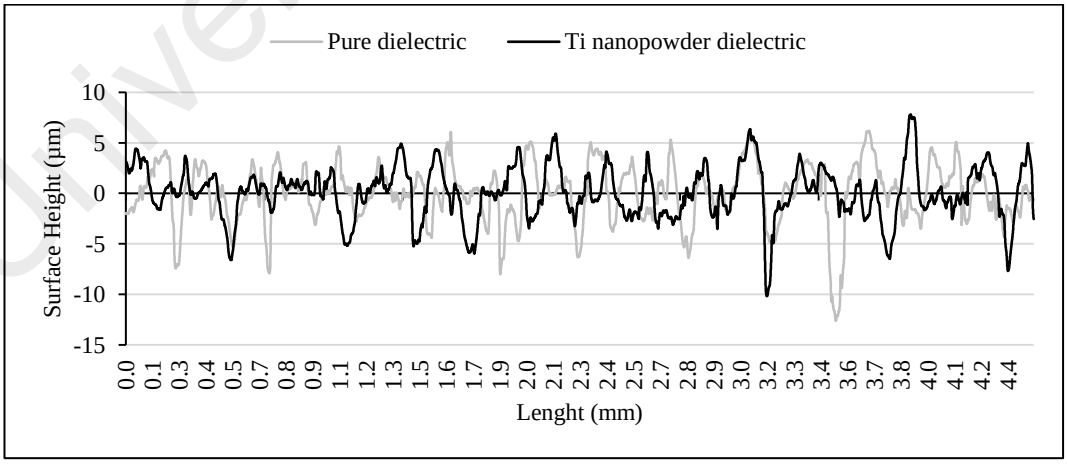

(i) T_{on}=140 µs, T_{off}=40 µs, I_a= 2 A

Figure 4.10: Graphs showing surface roughness of samples machined with pure and Ti nanopowder mixed dielectrics

University of Malaya

The Ra and Rz values extracted from above diagrams (Figure 4.10) are indicated in Figure 4.11. Although both Ra and Rz reflect the surface roughness, formation of irregular defects is more pronounced in Rz. Therefore, both indicators of Ra and Rz are considered in this research. The Ra graphs in Figure 4.11 have alike improvement trend at all discharge durations, while Rz graphs show improvement at only 60 and 100 µs and no significant change on Rz value at discharge duration of 140 µs.

Adding Ti nanopowder reduce Ra at all machining conditions with the highest decrease of ~23% at I=1 A and 100 µs followed by 13% at 1.5 A and 100 µs and 1 A and 140 µs. The most improvement in terms of Rz was observed at discharge duration of 100 µs and current of 1 A that Rz decreased by about 24%, while at 60 µs discharge duration and the same current, Rz decreased by around 22% by addition of powder to dielectric. It can be concluded that at 1 A current, Ti nanopowder had the highest improvement effect on both Ra and Rz, as shown by Figure 4.11. The least improvement is evident at 2 A current, whereas Ra improved by around 6, 4 and 2% at 60, 100 and 140 µs discharge duration, respectively. As shown in both Figure 4.11(a) and Figure 4.11(b), Ra and Rz exhibited the greatest improvement at 1 A. However, at higher discharge duration of 140 µs lower improvement was evident (Figure 4.11(c)). It seems that the additive does not determine considerable enhancement in surface roughness at high discharge durations.

The need to monitor both parameters of Ra and Rz is emphasised when the decrease in Ra and no remarkable change in Rz is observable at discharge duration of 140 µs. This validates that surface texture is adequately represented by Ra while surface major irregularities that form deep peaks and valleys are not appropriately specified. In order to gain understanding of this complications, further investigations on the machined surface is conducted using AFM of machined surface.

University of Malaya

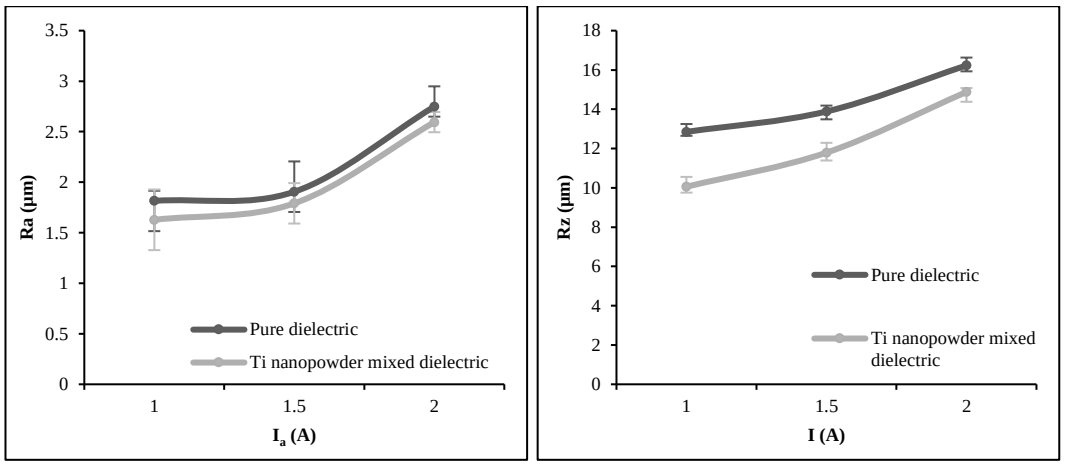

(a) T_{on} = 60 µs T_{off} =40 µs

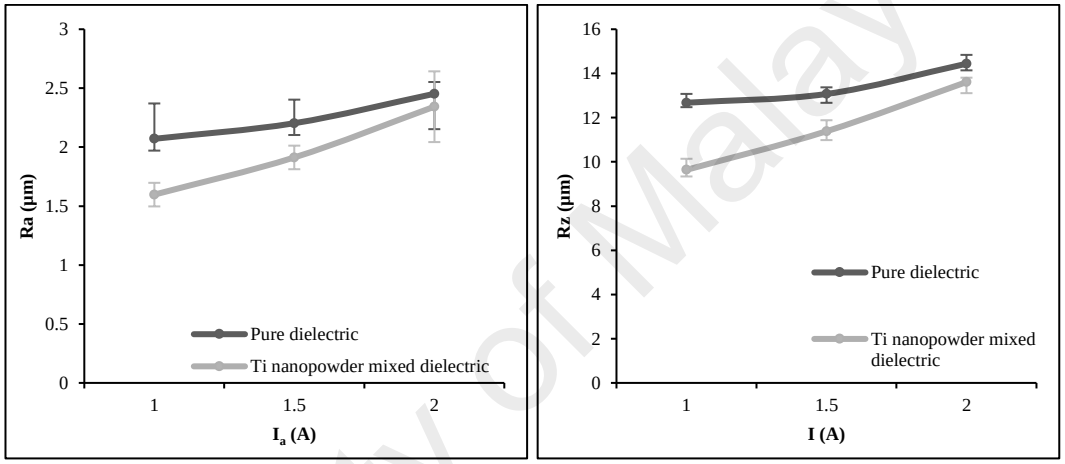

(b) T_{on} = 100 µs T_{off} =40 µs

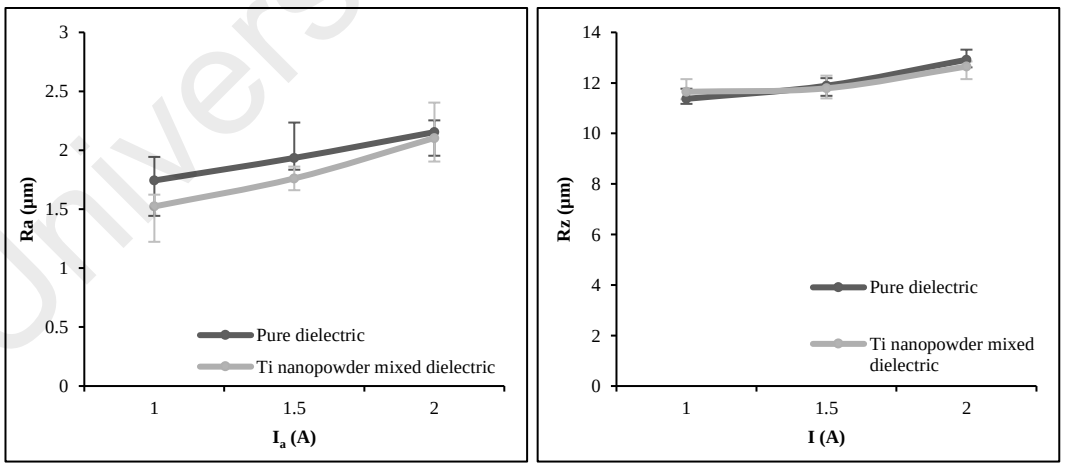

(c) T_{on} = 140 µs T_{off} =40 µs

Figure 4.11: Ra and Rz of surfaces machined with pure and Ti nanopowder mixed dielectric

University of Malaya

4.2.3 Influence of PMEDM machining characteristics on surface texture

The discrepancy between improvements of Ra and Rz in previous section highlighted the necessity to investigate the surface texture which was undertaken using AFM. The 3D representation of surfaces machined in pure dielectric and Ti nanopowder mixed dielectric is exhibited in Figure 4.12, Figure 4.13, and Figure 4.14.

The 3D image of surfaces machined at 60 µs discharge duration is demonstrated in Figure 4.12. The first to notice is the more uniform texture of the surface when Ti nanopowder is present in dielectric. Comparing the surfaces machined at 1 A in pure and Ti nanopowder mixed dielectric in Figure 4.12(a) and Figure 4.12(b), shows that addition of powder to dielectric reduced the level of high-ridges on crater's border from 10 µm to 6 µm and crater's center from -16 to -14 µm. For the case of surfaces obtained at 1.5 and 2 A, the highest peak and deepest valley found to be the same, however, the surfaces machined in Ti nanopowder mixed dielectric are more even with fewer deep craters on the surface.

University of Malaya

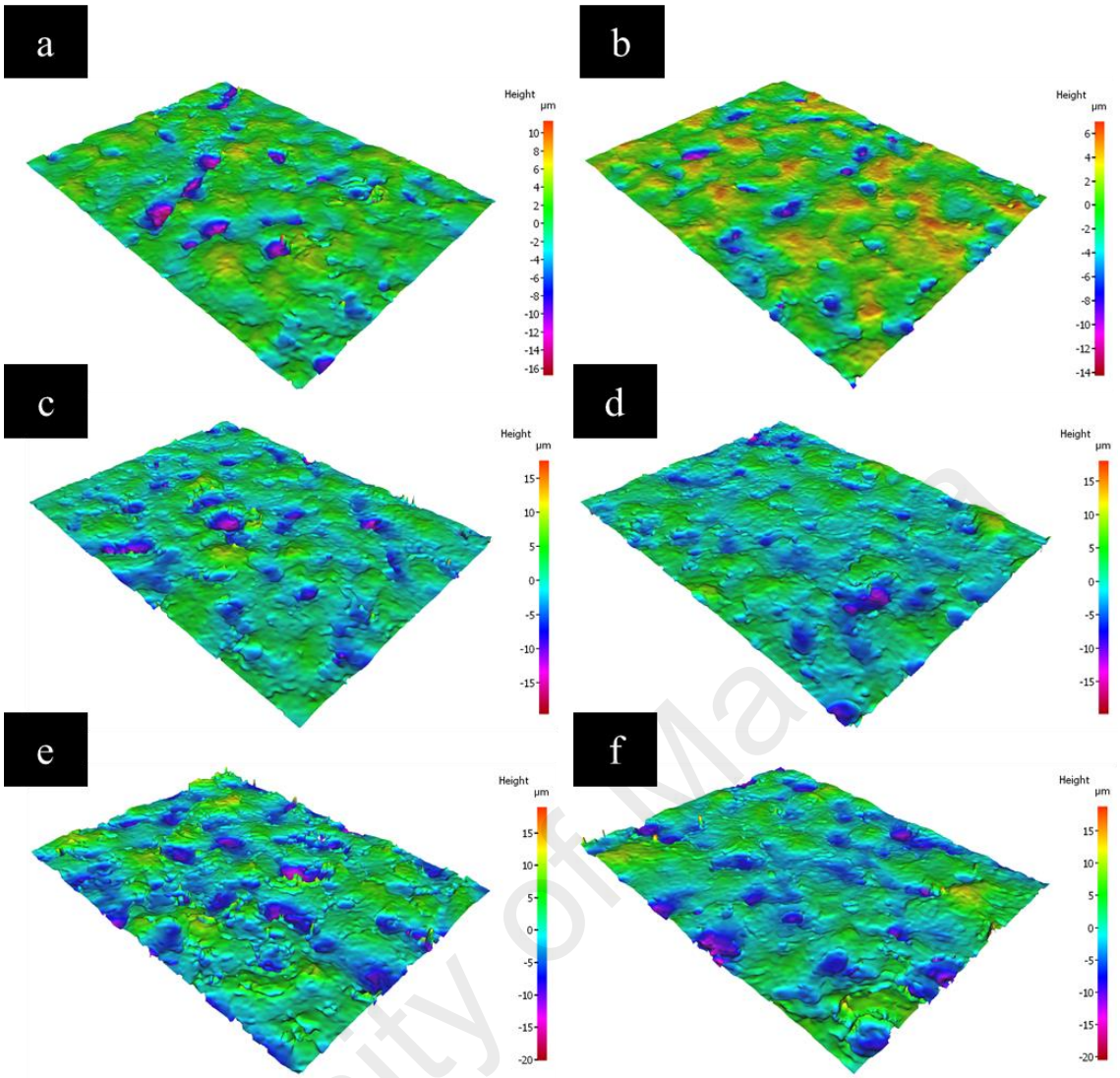

Figure 4.12: 3D representation of machined surface at T_{on}=60 µs, T_{off}=40, (a) I_a=1.5 A (b) I_a=2 A, (c) I_a=2.5 A in pure dielectric and (d) I_a=1, (e) I_a=2 A, (f) I_a=2.5 A in Ti nanopowder mixed dielectric

The 3D representation of surfaces machined at 100 µs discharge duration (Figure 4.13) shows that the use of Ti nanopowder dielectric is associated with a distinct surface texture. At 1 A current indicated in Figure 4.12(a), the red colour at the crater centre has approximately -20 µm depth and the high ridges of up to 10 µm indicate that crater depth was greater in the case of surface machined in pure dielectric than in surface machined in Ti nanopowder dielectric (Figure 4.12(b)). Similar improvement in surface is observable for surfaces machined at 1.5 and 2 A. In the case of the surface machined in pure dielectric at 1.5 A, the red colour denotes that the centre of the crater can reach -18 µm; whereas in the case of the surface machined in Ti nanopowder dielectric, the red indicates -12 µm.

University of Ma

Not only the crater depth was reduced, but also the orange colour indicating the highest points on the surface was reduced from 12 to 8 µm when Ti nanopowder was mixed with dielectric. Furthermore, at 2 A current, although the deepest valley has 16 µm depth in compare with -20 µm in Ti nanopowder dielectric, the highest surface level has dropped by 10 µm, from 16 µm in pure dielectric to 10 µm after addition of powder.

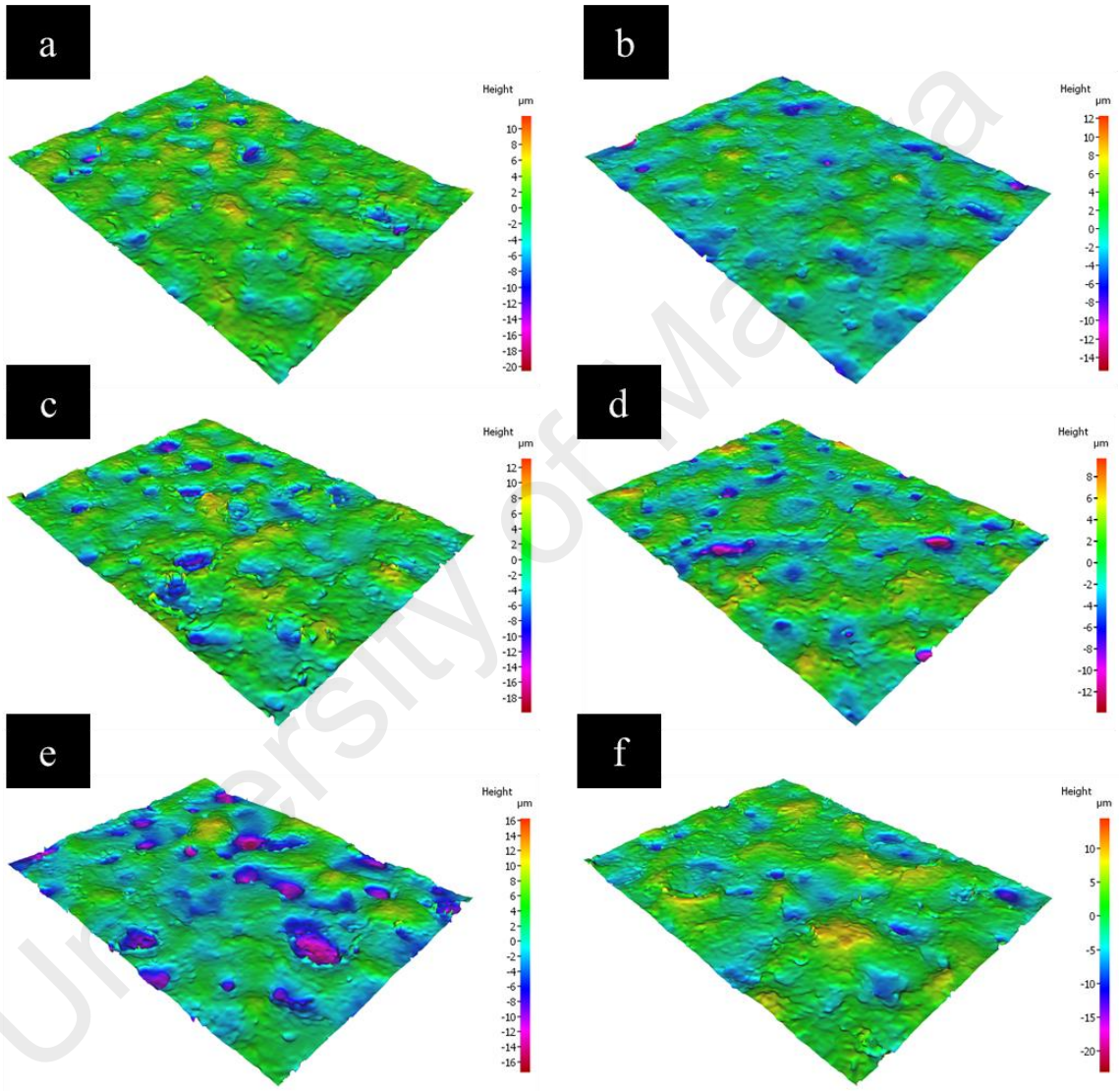

Figure 4.13: 3D representation of machined surface at T_{on}=100 µs, T_{off}=40, (a) I_a=1.5 A (b) I_a=2 A, (c) I_a=2.5 A in pure dielectric and (d) I_a=1.5, (e) I_a=2 A, (f) I_a=2.5 A in Ti nanopowder mixed dielectric

Alike the surfaces obtained at 60 and 100 µs, the surface machined at 140 µs (Figure 4.14) shows lower levels of peaks and valleys at 1, 1.5 and 2 A current.

University of Malaya

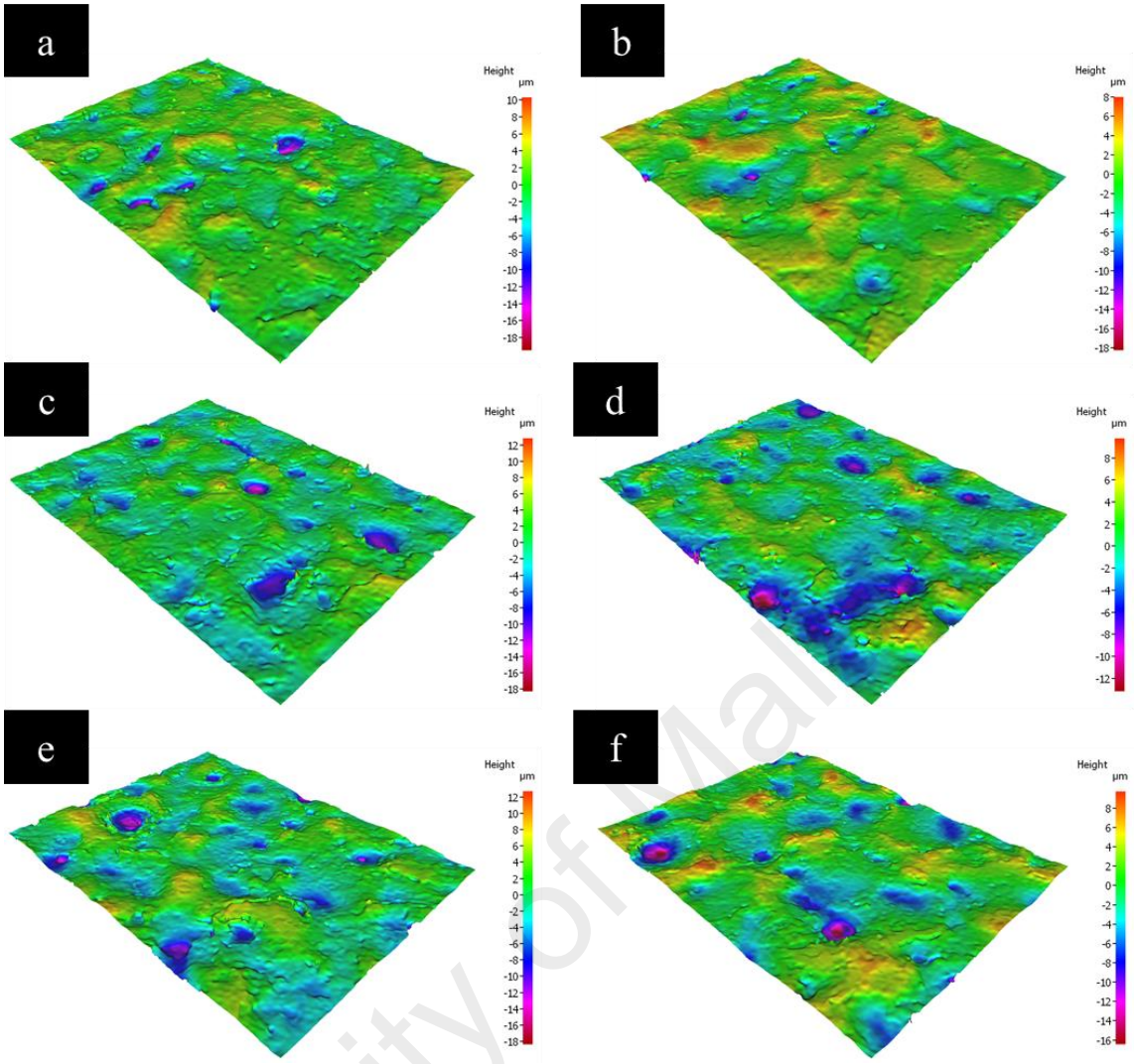

Figure 4.14: 3D representation of machined surface at T_{on}=140 µs, T_{off}=40, (a) I_a=1 A (b) I_a=1.5 A, (c) I_a=2 A in pure dielectric and (d) I_a=1, (e) I_a=1.5 A, (f) I_a=2 A in Ti nanopowder mixed dielectric

According to the abovementioned observations, the use of Ti nanopowder dielectric enhance the machined surface texture through formation of smaller craters on the machined surface. The results derived from R_a and R_z are corroborated by the surface texture micrographs. This means that, by comparison to the surface machined in Ti nanopowder dielectric, craters of greater depth form on the surface machined in pure dielectric.

Figure 4.15 schematically illustrates the surface formation in EDM before and after adding powder to the dielectric. Since impurities contaminate the plasma channel in the

University of Mal

EDM gap (Descoeudres, Hollenstein, Demellayer, & Wälder, 2004), the discharge process and plasma channel formation are influenced by the addition of conductive powder to dielectric. Is well-established that adding powder to dielectric increases the dielectric constant (κ), resulting in discharge gap expansion.

On one hand, larger gap width means decreased heat flux, which reduces the MRR and surface roughness (Guu & Hou, 2007). On the other hand, higher dielectric electrical conductivity accelerates dielectric ionization and the spark frequency between tool and workpiece (Bhattacharya et al., 2013; Muthuramalingam & Mohan, 2015). It seems that the higher discharge frequency overcomes the lower MRR effect resulting from the gap expansion, because the sparks do not hit the workpiece surface directly; instead, the primary discharge takes place between the tool and additive particles. Moreover, discharge dispersion markedly reduces ridges emerging on the surface. The reason for this is the shallower craters with lower borders caused by the added powder.

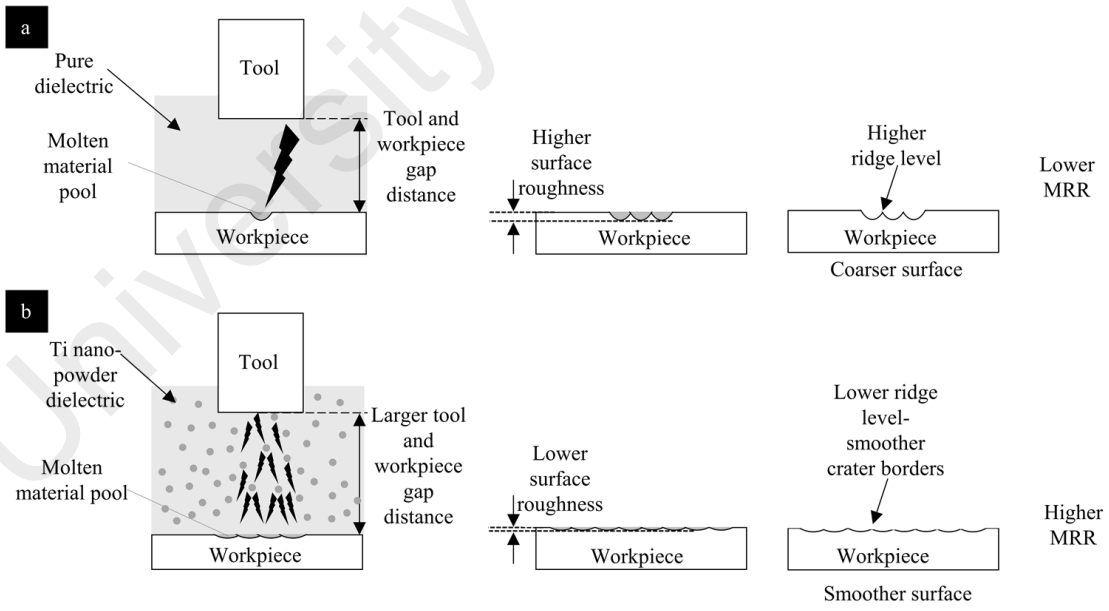

Figure 4.15: Diagram of surface development in (a) EDM and (b) PMEDM

4.2.4 Machining productivity concerning material removal

In EDM, MRR is indirectly proportional with surface roughness, meaning that when one increases, the other decreases. Because higher material removal rate is associated

University of Malaya

with higher spark energy (equations (4.1) and (4.2)) which results in formation of bigger craters on the machined surface. Formation of large craters on the surface eventually lead to production of surface with higher roughness. Spark energy in EDM represents the quantity of electrical power present in every spark multiplied by the duration of flow of the electrical power (Jameson, 2001).

MRR can be the highest priority to achieve since it affects the economical aspect of production. Thus, MRR has also been addressed along with surface quality in this research, to ensure the achievement of higher surface quality without decreasing the machining efficiency. MRR for 60, 100 and 140 µs discharge durations is illustrated in Figure 4.16(a), Figure 4.16(b) and Figure 4.16(c). The figure clearly shows that at all discharge durations of 60, 100 and 140 µs the graphs follow the similar improvement trend in all the conditions after addition of Ti nanopowder additive to dielectric. The highest improvement was ~34% attained at 60 µs discharge duration and 1 A current as a result of powder addition which is shown in Figure 4.16(a). In overall the highest improvement was at 60 µs discharge duration, while the lowest improvement was evident at 140 µs discharge duration. The increase in MRR value is attributed to the energy dispersion promoted by the Ti nanopowder particles in dielectric.

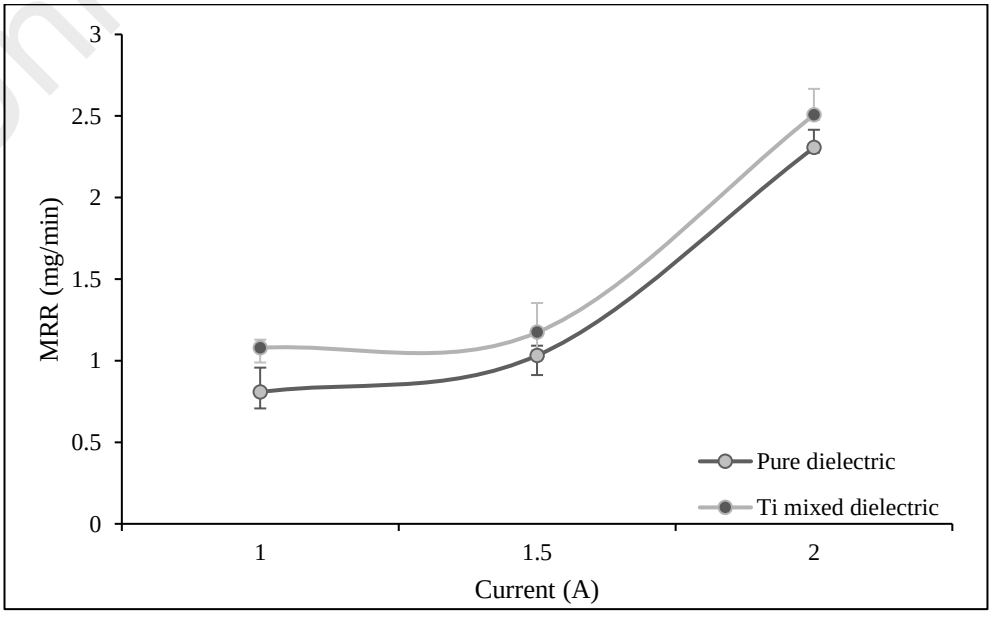

University of Malaya

(a) T_{on} = 60 µs T_{off} =40 µs

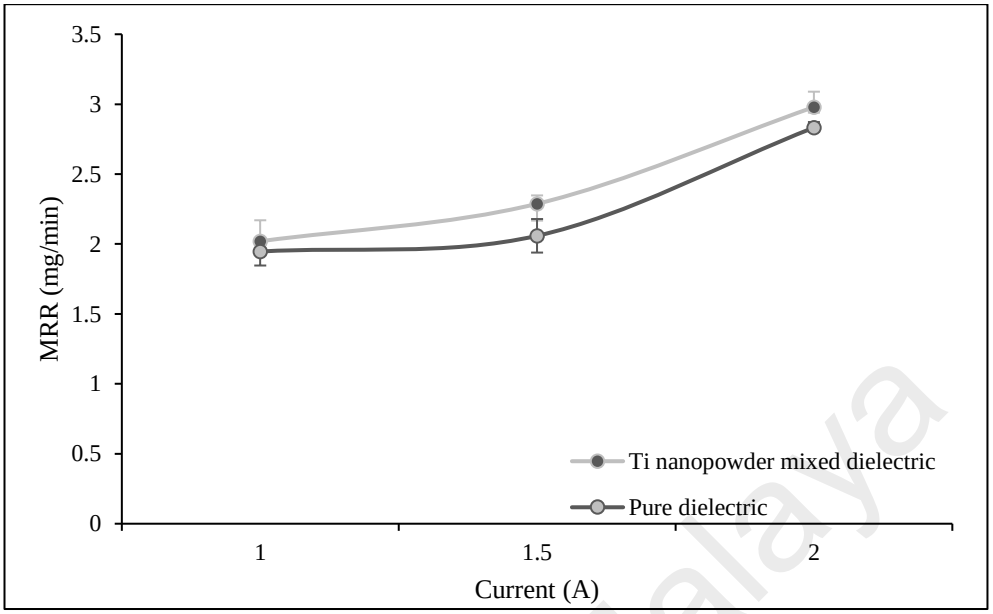

(b) T_{on} = 100 µs T_{off} =40 µs

University of Malaya

Figure 4.16 Continued.

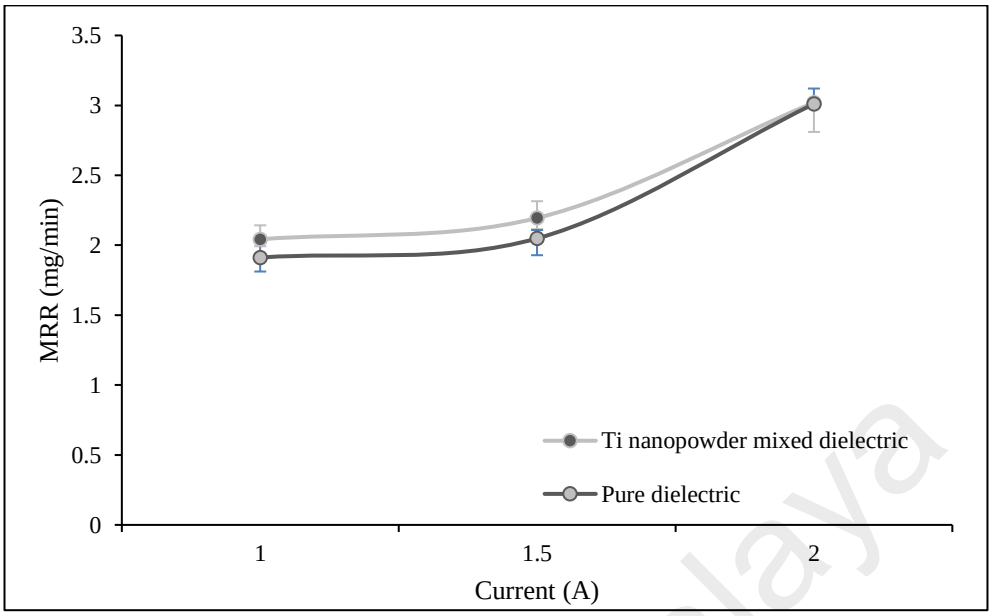

(c) T_{on} = 140 µs T_{off} =40 µs

Figure 4.16: MRR for 10 min machining time

4.2.5 Influence of powder addition on EDM process

In conventional EDM, normal pulse discharges regularly cause arcing due to insufficient pure dielectric deionization and excessive local debris (Luo, 1997). However, adding sufficient powder to the dielectric decreases the electrical resistivity and expands the gap, subsequently stabilizing the process through better flushing and servo-hunting (Wong et al., 1998). A wider discharge gap also decreases the heat flux (Kojima et al., 2008), which reduces the material removal of a single spark and enhances the surface quality. However, such gap expansion is not possible with all powder materials, since powder density, electrical resistivity, and thermal conductivity along with particle size and concentration are highly determinative.

Upon addition of conductive powder, the reduced electrical resistivity of the dielectric enhances the ionization and spark frequency between the tool and workpiece. The increased spark frequency appears to overcome the lower MRR of a single spark resulting from gap expansion. Therefore, multiple discharge patterns are evident from a single

University of Malaya

input pulse due to multiple discharge paths created, leading to discharge energy dispersion (Chow et al., 2000; Wu et al., 2005) in contrast to pure dielectric that produces a consistent waveform pattern (Figure 2.5). Moreover, discharge dispersion reduces the emergence of surface ridges due to the formation of shallower craters with lower borders (Ekmekci, 2009). Subsequently, smaller discharge craters and debris particles ease gap exhaust and accelerate the MRR (Chow et al., 2008).

Therefore, as a result of using powder added dielectric, the heat flux magnitude incident on the workpiece by a single spark reduces accordingly. Consequently, a smaller crater forms on the surface from a single spark, which is compensated by higher spark frequency.

To describe the effect of powder addition on the dielectric's breakdown voltage, the electrode and workpiece resemble a capacitor with potential difference of *V* between them. *V* is correlated to the system charge through the surrounding medium properties and is expressed as:

$$V = \frac{1}{C} Q \tag{4.3}$$

where, *Q* refers to the charge separation of the system and the capacitance *C* depends on the geometry of the electrode and workpiece as well as the properties of the medium between them (dielectric). The value of *C* for two parallel plates with surface area *A* and separation distance *d* is expressed as (Bird, 2013):

$$C = \frac{\varepsilon_0 \varepsilon_r A}{d} \tag{4.4}$$

University of Malaya

where, d is the distance between the two plates, ε_0 is the permittivity in free space (flux density of the field in vacuum) and ε_r is the relative permittivity, which is equal to dielectric constant (κ) and is defined as the flux density of the field in dielectric ε_d over ε_0.

Assuming that the field line between the plates is straight, the magnitude of the potential difference between the plates is (Liao, Dourmashkin, & Belcher, 2004):

$$|\Delta V| = Ed \tag{4.5}$$

where, E is the electric field in capacitor.

Above a critical magnitude of the electric field at which dielectric breakdown takes place is called the breakdown strength, where the dielectric in capacitor becomes conductive. In case of a homogeneous electric field, the field intensity is the same at full breakdown trajectory length; therefore, electric breakdown strength is defined as (Marci & Csanyi):

$$E_b = \frac{U_b}{d} \tag{4.6}$$

where, E_b is the breakdown strength and U_b is the breakdown voltage.

Breakdown voltage limits the maximum energy that can be stored in capacitor, which is particularly depends on the dielectric material. It was shown that adding impurities (in our case powder particles) alter the magnitude of electrical field (Haynes, 2010) and subsequently according to equation (4.6) reduces the breakdown voltage as a result of bridge formation.

University of Malaya

In order to explain the formation of bridge in discharge gap in detail, assume that the additive particles are spheres with higher permittivity than dielectric. The powder particles in the gap get polarized in an electric field and experience force equal to toward the place of maximum stress, and in a uniform electric field that can usually be developed by a small sphere gap, the field is the strongest in the uniform field region (Wadhwa, 2007). Thus, the force on the particle is zero and the particle remains in equilibrium. Therefore, the particles will be dragged into the uniform field region. Since the permittivity of the particles is higher than that of the liquid, the presence of particles in the uniform field region will cause flux concentration at its surface. Other particles also tend to move towards the higher flux concentration. If the present particles are large, they become aligned due to these forces and form a highly conductive bridge across the gap. The electric field in the liquid in the gap will increase and if it reaches a critical value E_b breakdown will take place. If the number of particles is not sufficient to bridge the gap, the particles will give rise to local field enhancement; if the field exceeds the dielectric strength of the liquid, local breakdown will occur near the particles and consequently, gas bubbles will form, which have much lower dielectric strength. Hence, this will ultimately lead to easier liquid breakdown (Haynes, 2010; Wadhwa, 2007).

4.2.6 Material migration phenomena and elemental analysis

Elemental analysis of the machined surface was conducted using EDX to evaluate the titanium transfer in atomic scale from the mixed dielectric to the machined surface (Figure 4.17). As schematically demonstrated in Figure 4.19, as a result of spark, plasma channel forms, which leads to ionization and decomposition of atoms, particles and other species present in discharge gap. Eventually, the released particles are either washed away from the gap by dielectric flow or may be transferred to the machined surface. The thermal energy released from the discharge incident leads to the melting and deposition of Ti atoms onto the surface (Janmanee & Muttamara, 2012). This energy also facilitates the

University of Malaya

diffusion of Ti atoms according to the Arrhenius principle (Askeland, Phulé, & Wright, 2003).

As shown in Figure 4.17, discharge duration and current are influential in deposition of Ti atoms due to thermal energy possessed by the atoms and ions. 140 µs discharge duration was associated with the highest amount of Ti deposition on the machined surface with the maximum deposition of about 0.25% Ti atomic percentage recorded at 2 A current.

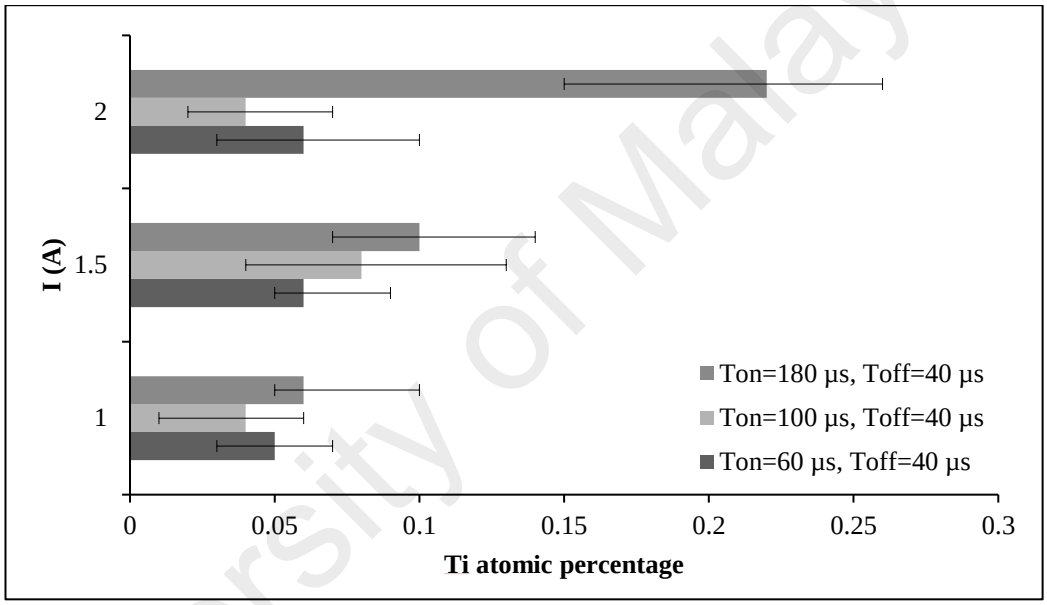

Figure 4.17: Deposition of Ti nanopowder on the machined surface

Moreover, Ti atomic concentration was investigated in more detail using EDX analysis around the crack areas, as these are susceptible to higher deposition. It was found that the concentration of Ti atoms transferred around the crack area significantly varies from the Ti atomic concentration on the surface demonstrated in Figure 4.17. A typical example of a surface crack selected for elemental analysis and the EDX spectrum are presented for discharge duration of 140 µs and current of 2 A in Figure 4.18. It is clear that the peaks related to Ti element are considerably high. The results show approximately 1.9% deposition of Ti atoms, which is significantly higher than around 0.25% on the surface

University of Malaya

(Figure 4.17). Also, by closely observing the crack edges in Figure 4.18 the workpiece colour slightly differs account the crack area, which might be due to Ti deposition. As indicated in Figure 4.19, this observation could be attributed to the higher local accumulation of Ti particles around the crack zones and ingress of Ti particles into the crack area where C acts as a bonder that increases the Ti deposition concentration (Janmanee & Muttamara, 2012). This reveals the ability of Ti nanopowder to reduce machined surface cracks and ultimately improve the surface quality.

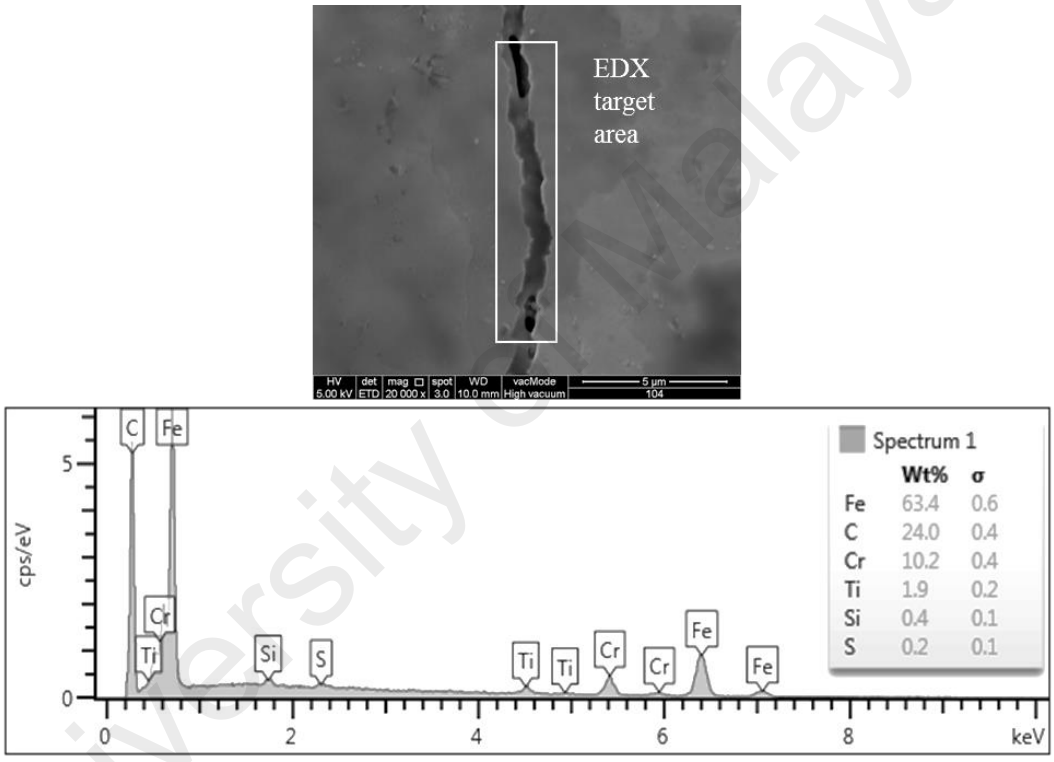

Figure 4.18: Typical micrograph of crack on the machined surface and its related EDX spectrum (T_{on}=140 µs and I=2 A)

University of Malaya

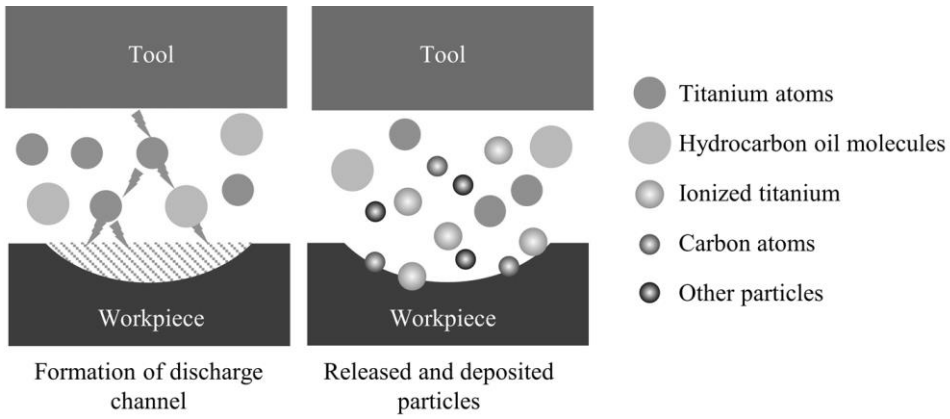

Figure 4.19: Schematic illustration of particles decomposition and deposition on the machined surface

University of Malaya

4.3 EDM with ECAP-treated electrodes

4.3.1 Improved Nano-hardness of electrode

In order to investigate the nanomechanical properties of ECAP-treated electrodes, a series of nanoindentation tests were carried out across the plane perpendicular to the electrode axis which 16 nano-indentation points (Figure 4.20). The typical load-displacement curves for C0, C1 and C2 are shown in Figure 4.21. As seen from the curves, none exhibited any notable discontinuity during loading and un-loading time which indicate the absence of any crack formation or phase transformation during nanoindentation testing (Fischer-Cripps, 2000).

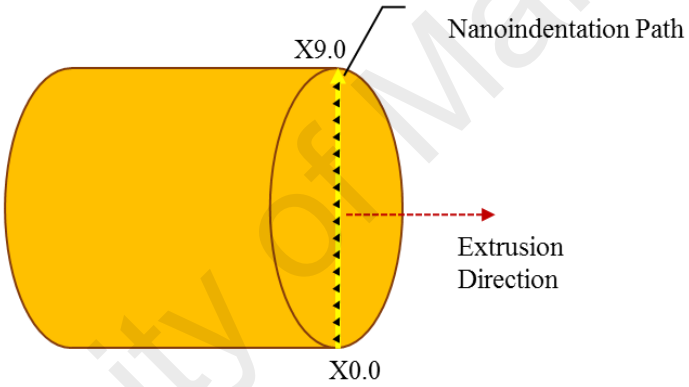

Figure 4.20: Schematic representation of nano-indentation path

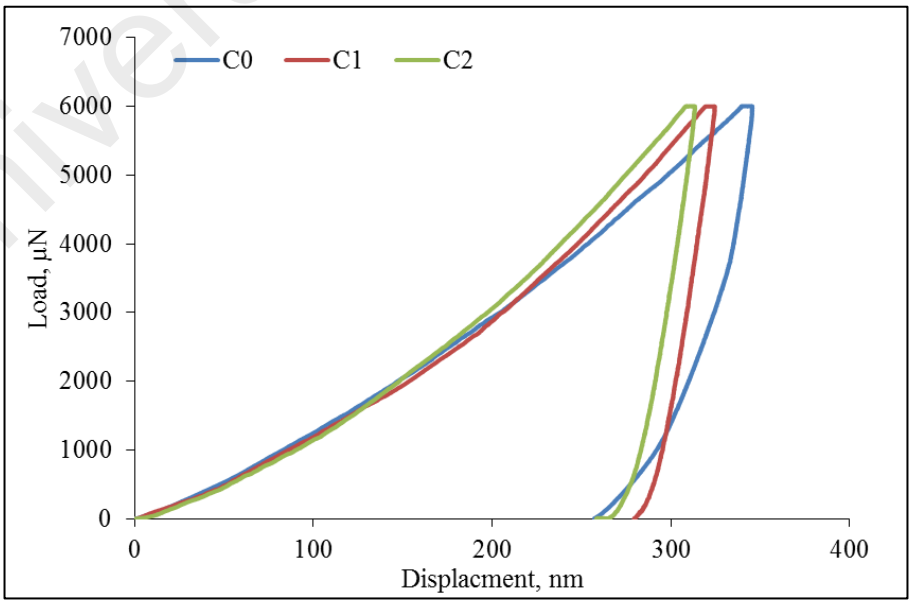

Figure 4.21: Load-displacement responses of copper electrodes including as-received (C0), subjected to one ECAP pass (C1) and two ECAP passes (C2)

University of Malaya

It is apparent from Figure 4.21 that under a same load, lower displacement for electrodes C1 and C2 compared with electrode C0 was evident. The hardness values measured on electrodes C0, C1 and C2 signify that ECAP processing improved the samples' hardness on a nanoscale as a result of strain accumulation in the copper electrode.

According to the path indicated in Figure 4.20, the hardness of electrodes C0, C1 and C2 is exhibited in Figure 4.22, which was measured along the ingoing direction defined in Figure 3.9. The hardness values confirm the effectiveness of ECAP in improving electrode hardness and also to evaluate the amount of inhomogeneity imposed on the electrode after ECAP.

A mean hardness value of 1.7 GPa was measured for electrode C0. After the first pressing pass, the hardness value increased as a result of strain accumulation in the electrode, reaching a mean value of 1.9 GPa; however, the inhomogeneity slightly increased over the electrode's cross section. For the second pressing pass, 2.12 GPa hardness was calculated for the electrode C2, which indicates that the second pressing pass enhanced the electrode's hardness. In Figure 4.22, the hardness variation along the diametric path specifying that the hardness of the ECAP-treated electrodes in the region adjacent to the channel angle had the lowest values. By moving toward the electrode core, these values increased and reached the maximum hardness in the region adjacent to the corner angle.

University of Malaya

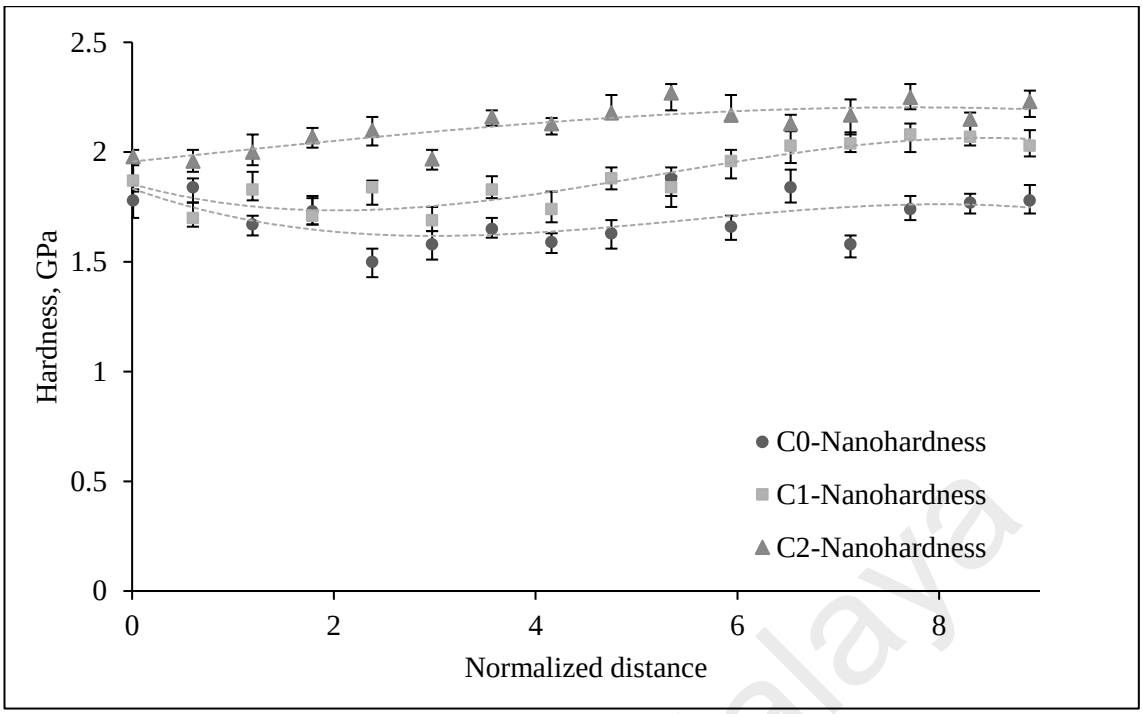

Figure 4.22: Distribution nanohardness along the diametric path at the cross section of the electrode after the first and second pressing passes

4.3.2 Geometrical accuracy concerning corner sharpness and overcut phenomena

It is well-established that electrode corner wear notably affects the corner of machined cavity in EDM which subsequently decrease the machining accuracy. Therefore, the area under the corner curve of electrode (A_{Ti}) and workpiece (A_{Ci}) and VOC of the workpiece were measured using equations (3.3) and (3.4), respectively. To observe the corners' sharpness, the cross-section of workpiece micrographs was investigated (Figure 4.23).

University of Malaya

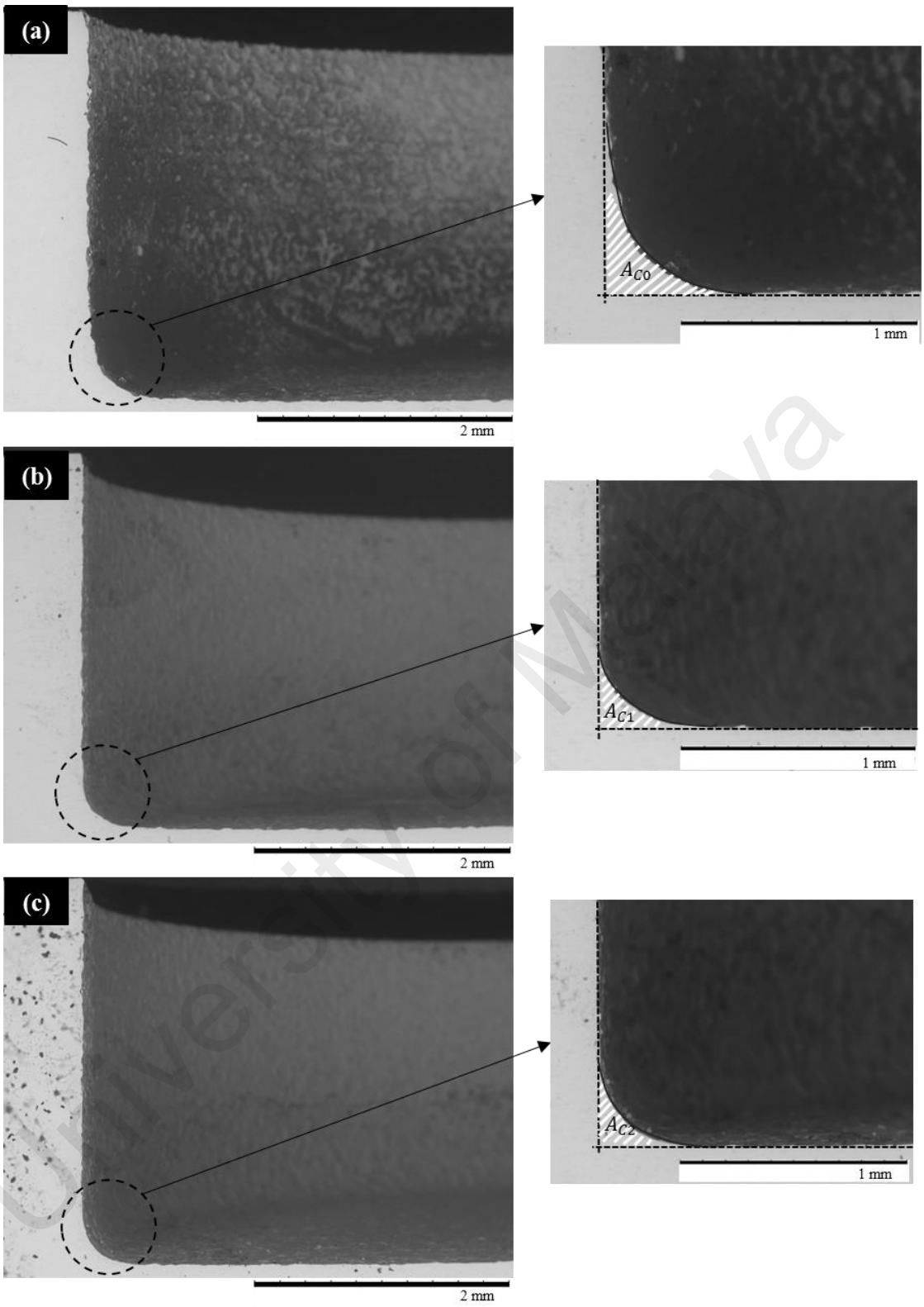

Figure 4.23: Cross-sectional view of cavity corner machined by electrodes (a) C0, (b) C1 and (c) C2

University of Malaya

According to equation (3.4) and analysis of Figure 4.23, electrode C1 demonstrated the lowest corner wear ($A_{T1} = 27700\mu m^2$), while this value increase by almost 10 and 4% for electrodes C0 and C2, respectively. It is clear that the overall shape of the cavity enhanced in terms of the wall deviation and corner sharpness caused by lower electrode corner wear as the electrodes underwent ECAP treatment. The detailed corner views in Figure 4.23 show that A_{ci} decreased when using ECAP-treated electrodes.

A_{ci} was measured by fitting a curve on each corner as demonstrated in Figure 4.23. Then the following equations that define the aforementioned curves relating to electrodes C0, C1 and C2 were extracted, respectively:

$$z = 72.15x^6 - 238.4x^5 + 309.62x^4 - 200.78x^3 + 68.59x^2 - 12.13x + 1.01 \quad (4.7)$$

$$z = 15044x^6 - 18415x^5 + 8835.6x^4 - 2107x^3 + 263.2x^2 - 17.3x + 0.63 \quad (4.8)$$

$$z = 437.71x^6 - 886.7x^5 + 698.22x^4 - 271.35x^3 + 55.64x^2 - 6.35x + 0.4 \quad (4.9)$$

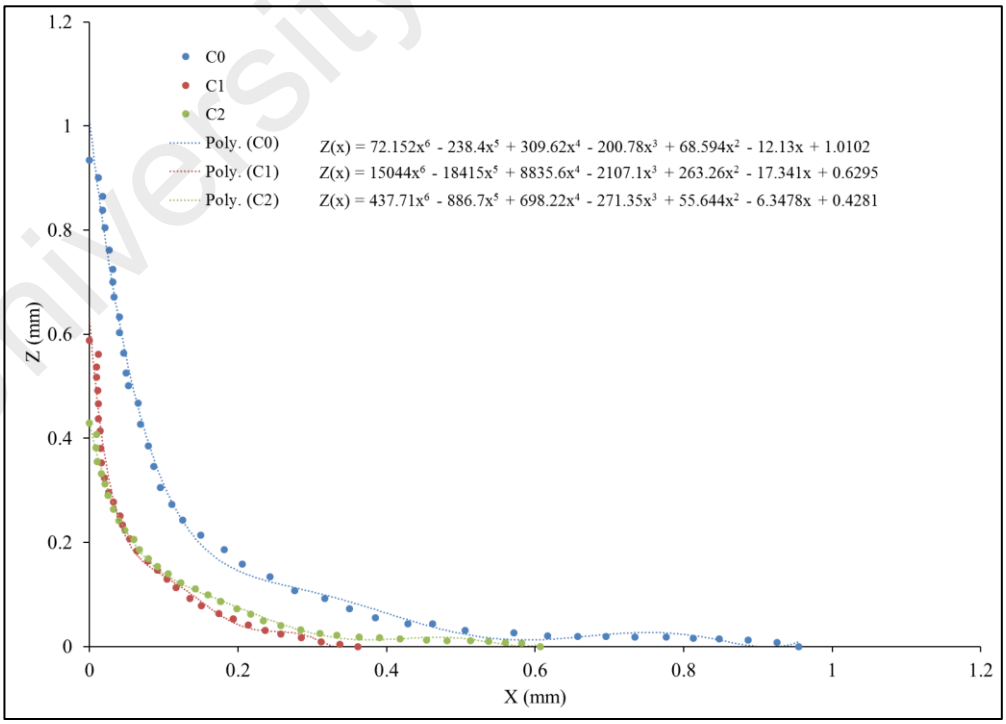

Figure 4.24: Workpiece corner shapes machined in pure dielectric (Z: cavity wall, Y:cavity bottom)

University of Malaya

The above equations were substituted into equation (3.4) with their respective domains to measure the area under the curve (Figure 4.23). According to the results, EDM with electrode C2 resulted in nearly 61% reduction in area under the curve compare with electrode C0. Machining with the C1 electrode produced roughly 66% improvement in corner sharpness compared to electrode C0. These results indicate that electrode C0 presented more severe wear than the other two electrodes, which led to the production of a cavity with the poorest geometry.

The values of VOC were calculated for all electrodes according to (3.3) and are summarized in Figure 4.25. Following a similar trend to the area under the curve, the results showed that using electrodes C1 and C2 reduced the VOC by 13 and 5% compared with electrode C0. The reduction in A_{ci} is due to the reduction in electrode corner wear when the nanohardness of electrodes increased as a result of ECAP treatment. However, it seems that the state of stress in the electrodes after ECAP treatment plays a crucial role in electrode wear during EDM. Electrode C2 experienced higher corner wear than C1 with effect on workpiece corner sharpness.

University of Malaya

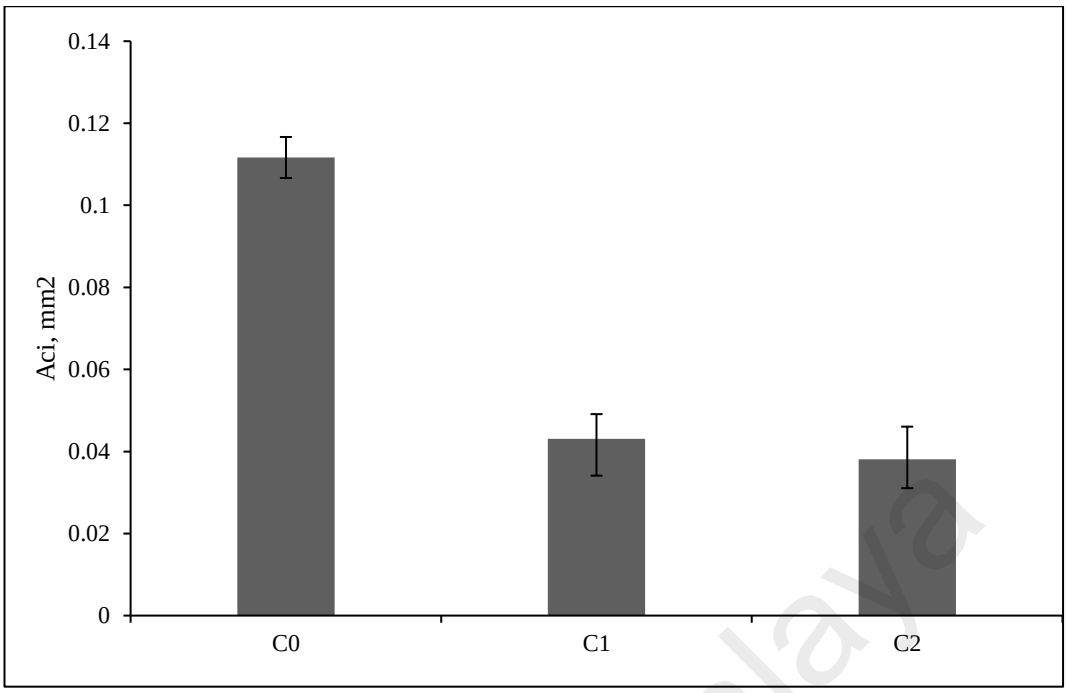

Figure 4.25: Area under the curve (A_{ci}) for the cavity machined by electrodes C0, C1 and C2

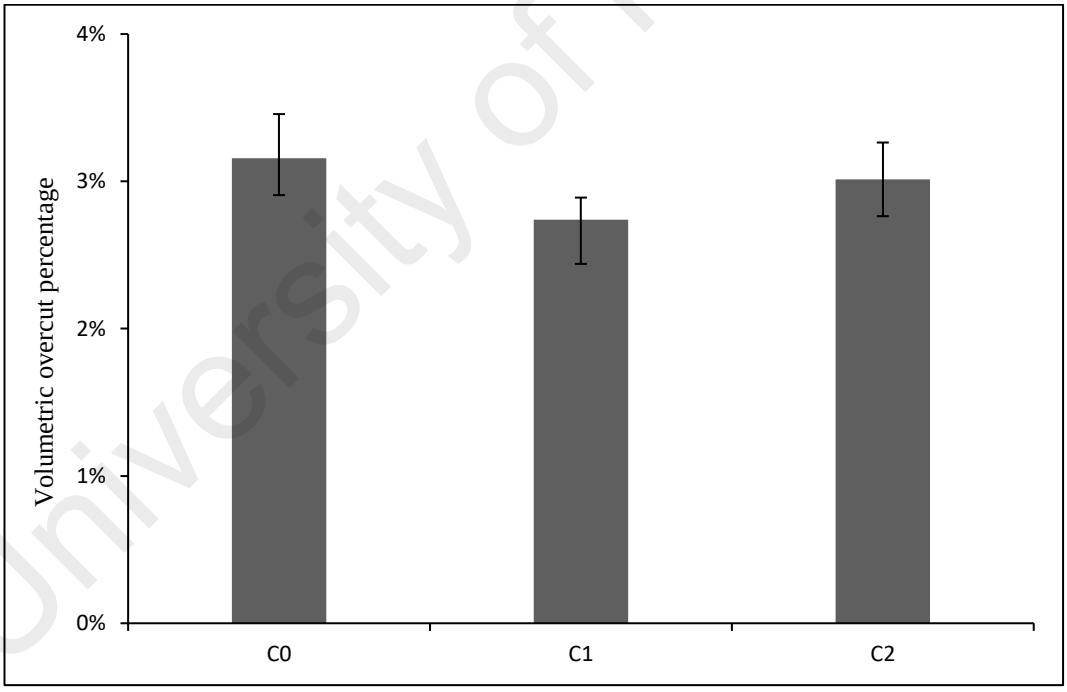

Figure 4.26: Volumetric overcut (VOC) for the cavity machined by electrodes C0, C1 and C2

University of Malaya

4.3.3 Influence of ECAP treatment of Electrode properties

ECAP treatment increases the electrode hardness. As indicated in Figure 4.27, for all types of materials and bonds, higher hardness is associated with higher melting point. ECAP treatment increasing the melting point of the electrode. Thus, the electrode wear during the discharge process will be reduced owing to its higher melting point.

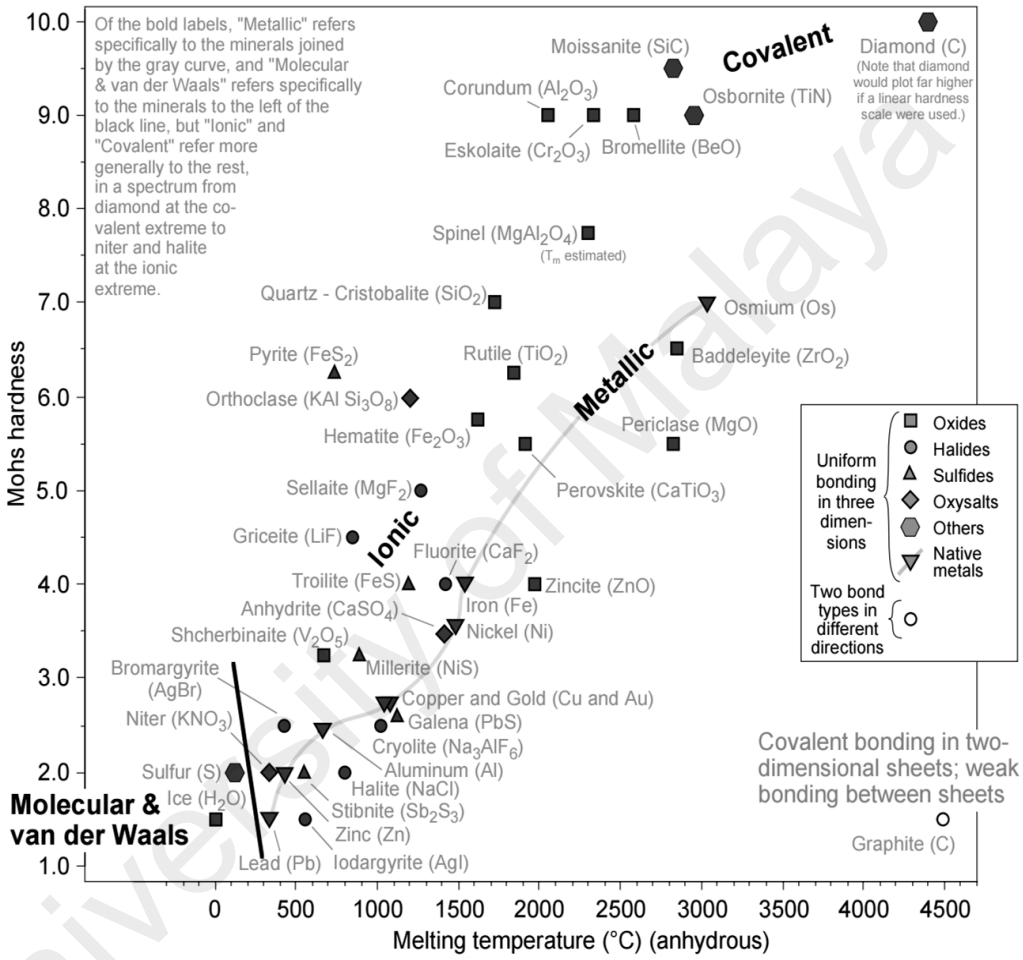

Figure 4.27: Melting point and hardness of minerals (Railsback, 2008)

4.3.4 Surface topography and morphology analysis of machined cavity

The effect of different electrode types on workpiece was initially investigated by means of surface profilometer. Typical measurements of surface roughness for machined surfaces with electrodes C0, C1 and C2 is illustrated in Figure 4.28. Comparing the surface roughness waveforms for different electrodes the distance between each peak and valley is reduced for electrodes C1 and C2 compared to the surface machined by C0. This

University of Malaya

indicates formation of smaller craters as a result of diminished electrical conductivity of electrodes after ECAP treatment.

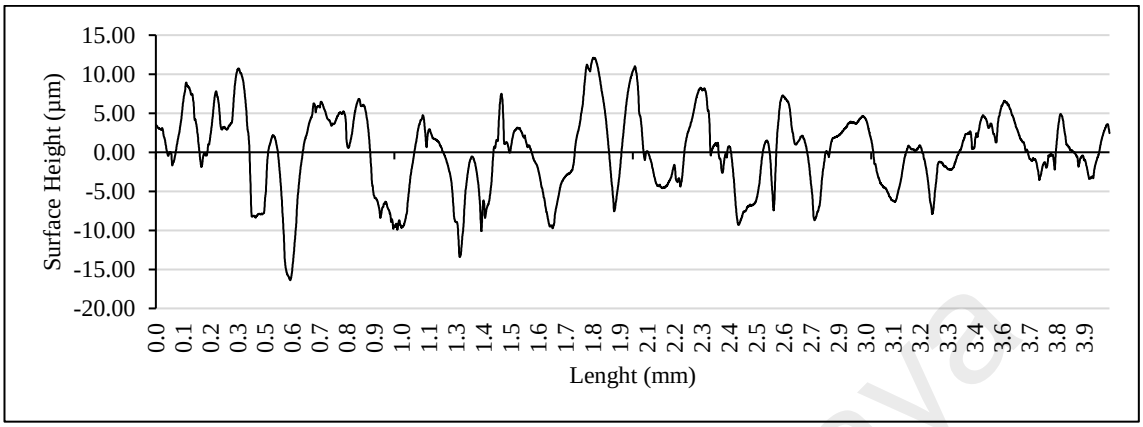

(a) Machined surface roughness using electrode C0

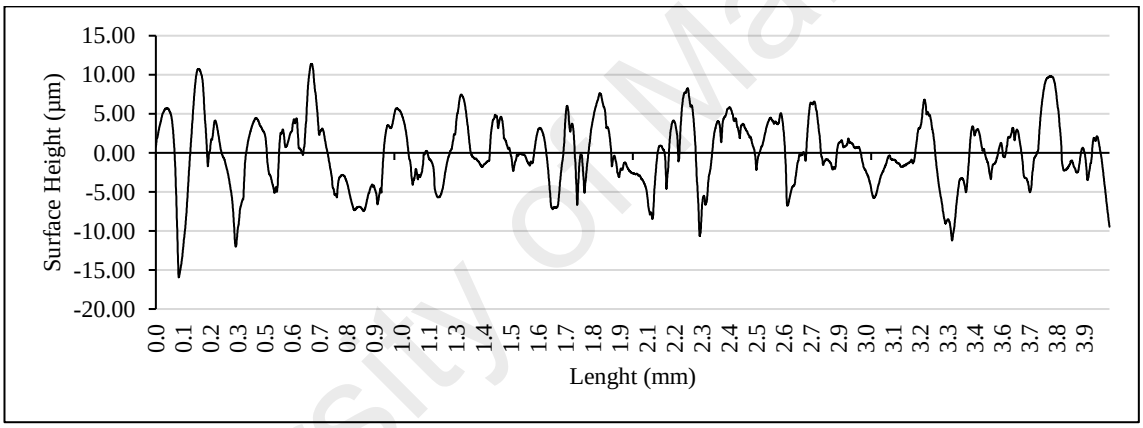

(b) Machined surface roughness using electrode C1

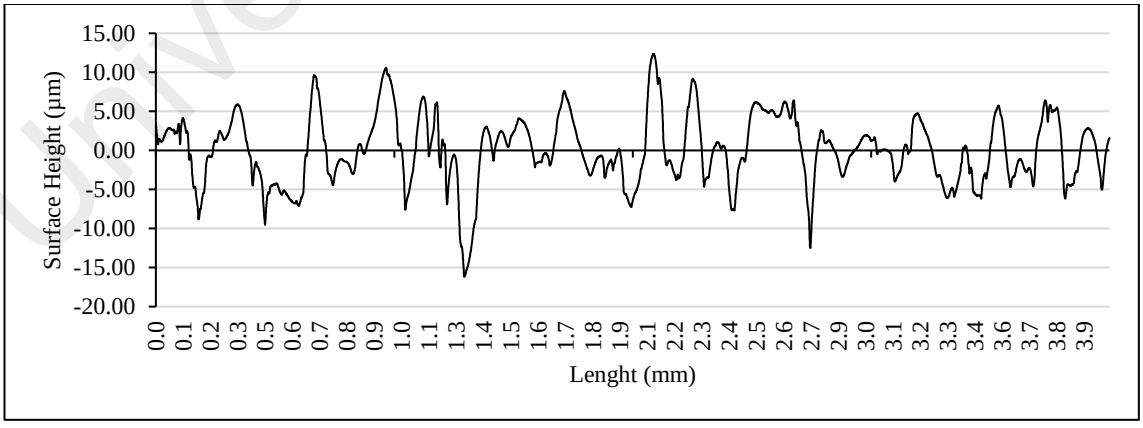

(c) Machined surface roughness using electrode C2

Figure 4.28: Machined surface roughness using electrodes C0, C1 and C2

University of Malaya

Intense amounts of heat during EDM melted and evaporated some workpiece material, which led to the formation of an uneven and non-etchable layer called a recast layer (white layer) on the top-most surface of the workpiece(Guu, 2005). In the early stage of ECAP treatment for pure copper, a minor increase in resistivity reportedly occurred (RZ Valiev et al., 2015); which affects the magnitude of energy induced on the workpiece. Therefore, the lower surface roughness in the case of electrode C2 is explainable by its slightly lower electrical conductivity. Additionally, higher surface roughness was accompanied by higher MRR due to the formation of larger craters (Gopalakannan & Senthilvelan, 2012). Since the MRR of samples undergoing ECAP treatment seemed to be lower due to the slight reduction in electrical conductivity, the discharge energy was not identical for all three electrodes, which affected the surface morphology and defects.

The value of surface roughness indicator Ra was extracted from multiple waveform measurements (such as Figure 4.28) and is shown in Figure 4.29. It was revealed that electrode C2 produced the finest surface compared with electrodes C0 and C1. Electrode C0 produced a surface with R_a of 4 µm, which remained constant for 4.14 µm for C1 and decreased to 3.36 µm for C2. These notable variations in R_a could have originated from the crater shape (S. Singh et al., 2004) as well as microscopic defects. Investigating the R_z indicator, it follows similar variation trend, whereas C2 has the lower value. This indicate the consistency of surface texture. Nevertheless, the workpieces' micrographs were further investigated to identify the cause of R_a variation.

University of Malaya

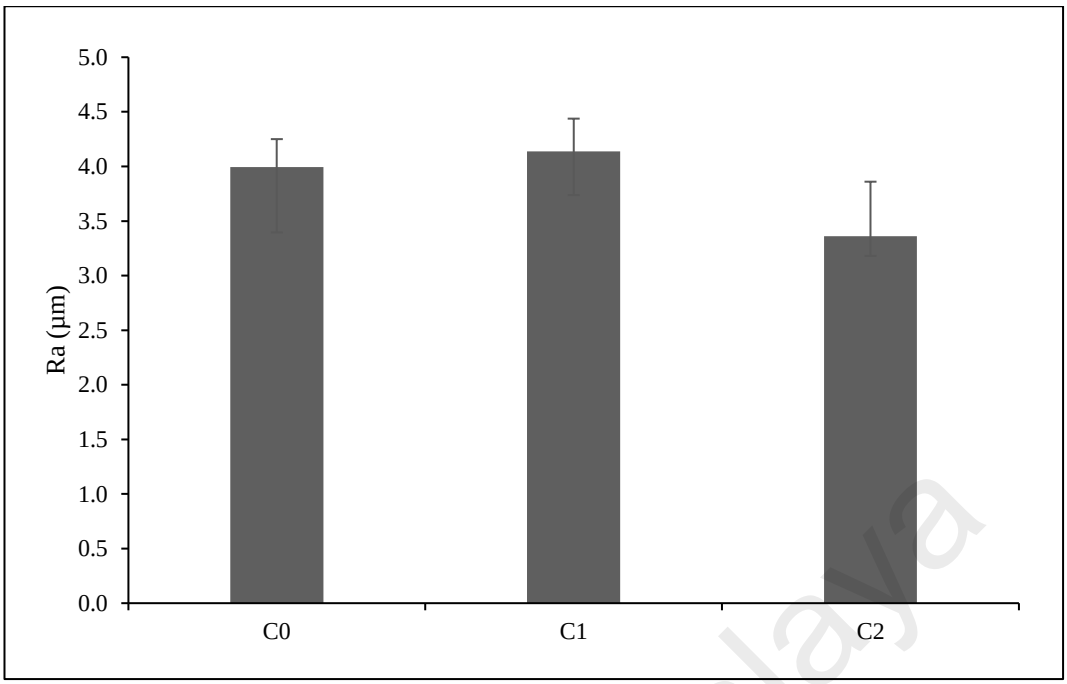

Figure 4.29: Average surface roughness's (Ra) of surfaces machined by electrodes C0, C1 and C2

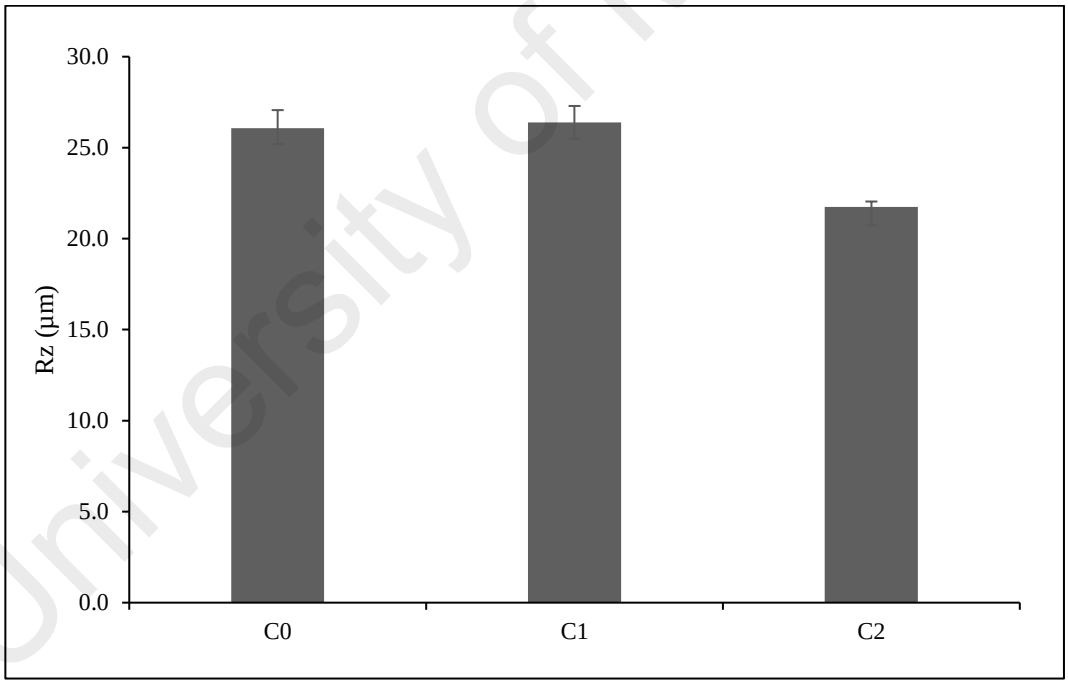

Figure 4.30: Peak-to-valley surface roughness's (Rz) of surfaces machined by electrodes C0, C1 and C2

University of Malaya

Figure 4.31 illustrates typical images of machined workpiece surfaces with different electrode types. It is clear from the micrographs that the finished surfaces vary from each other due to the existence of different types of micro-defects such as voids, droplets and cracks. Micro-voids formed due to gas bubbles expelled from the molten material during solidification, deteriorating the surface quality (Guu, 2005). Moreover, micro-droplets appeared due to the improper detachment of molten material from the surface. The molten material moved on the surface forming droplets until the dielectric's low temperature re-solidified the material on the surface (Patel, Patel, & Patel, 2012).

Figure 4.31(a) through Figure 4.31(c) indicated surfaces machined using electrodes C0,C1 and C2, respectively. The higher density of micro-voids is observable on the machined surface when using electrode C2. In contrast, electrode C1 exhibited the poorest surface quality by forming the highest number of droplets density. This finding is in accordance with the R_a measurements (Figure 4.29), whereby the R_a value slightly increased for electrode C1 owing to the existence of surface defects like micro-droplets and micro-voids on the machined surface. Note that the machined surface morphology is dependent on the discharge energy applied (Guu, 2005). Since the MRR of samples undergoing ECAP treatment seemed to be lower due to the slight reduction in electrical conductivity (Edalati et al., 2012), the discharge energy was not identical for all three electrodes, thus affecting the surface morphology and defects.

University of Malaya

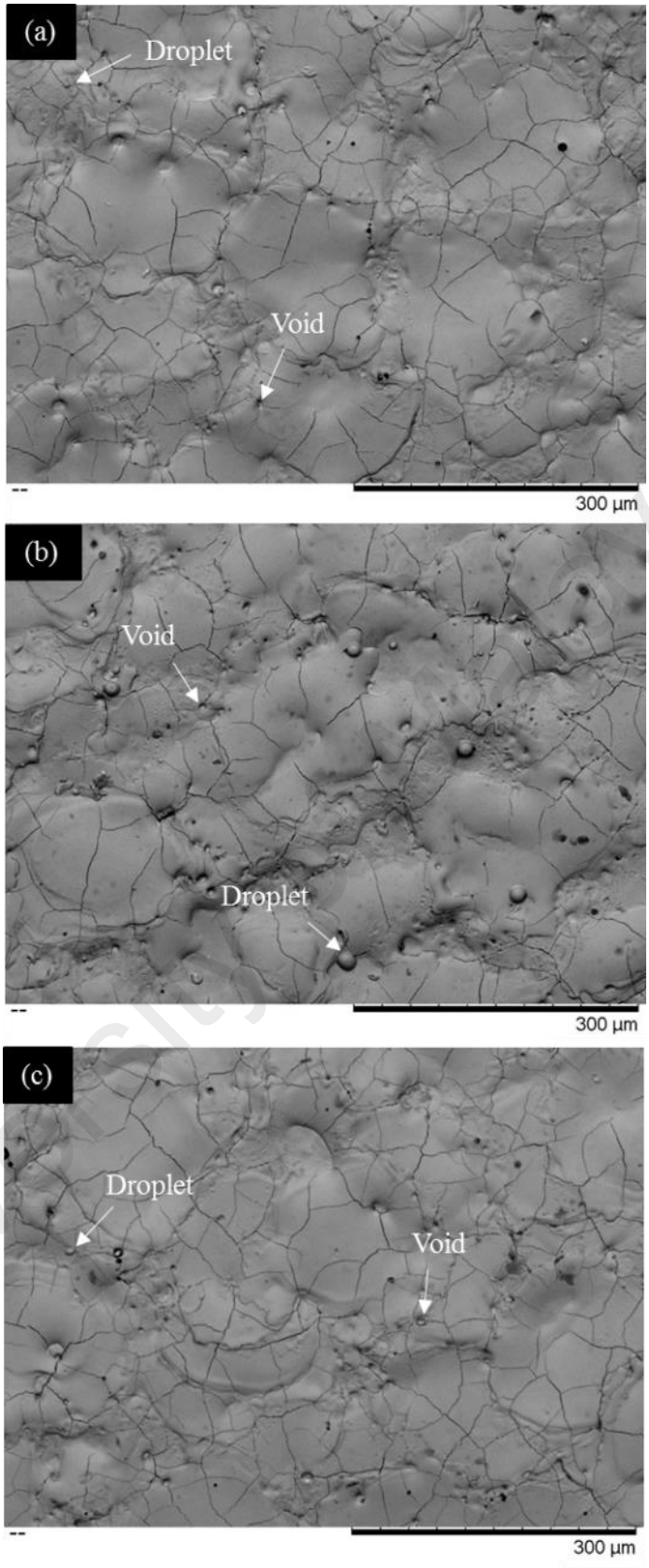

Figure 4.31: SEM of surface machined using (a) original copper tool (b) one ECAP pass and (c) two ECAP passes

University of Malaya

4.3.5 Surface crack susceptibility

To quantitatively measure the effect of different types of electrodes on crack distribution over the surface, the density and numbers of cracks for each workpiece were measured and summarized in Figure 4.31. It was revealed that electrode C1 produced the lowest density and number of cracks on the finished workpiece surface. The density reduced by more than 26% when employing electrode C1 compared with electrode C0. Electrode C1 had the lowest MRR among the electrodes, thus produced less debris particles which not only swept more easily from the gap, but also formed lower amount carbon that act as two factor decelerating crack generation (H. T. Lee & Tai, 2003). The electrical conductivity of electrodes after two cycles of ECAP treatment reduces even more, which results in bigger explosions during time. Bigger discharges mean higher discharge impact on the machined surface and higher generation of carbon, increasing the crack density for electrode C2. From these data it is concluded that the electrode crystallographic microstructure had significant effect on crack distribution similar to the dielectric flashing rate (Wong et al., 1995), discharge current and pulse on-time (Hasçalık & Çaydaş, 2007).

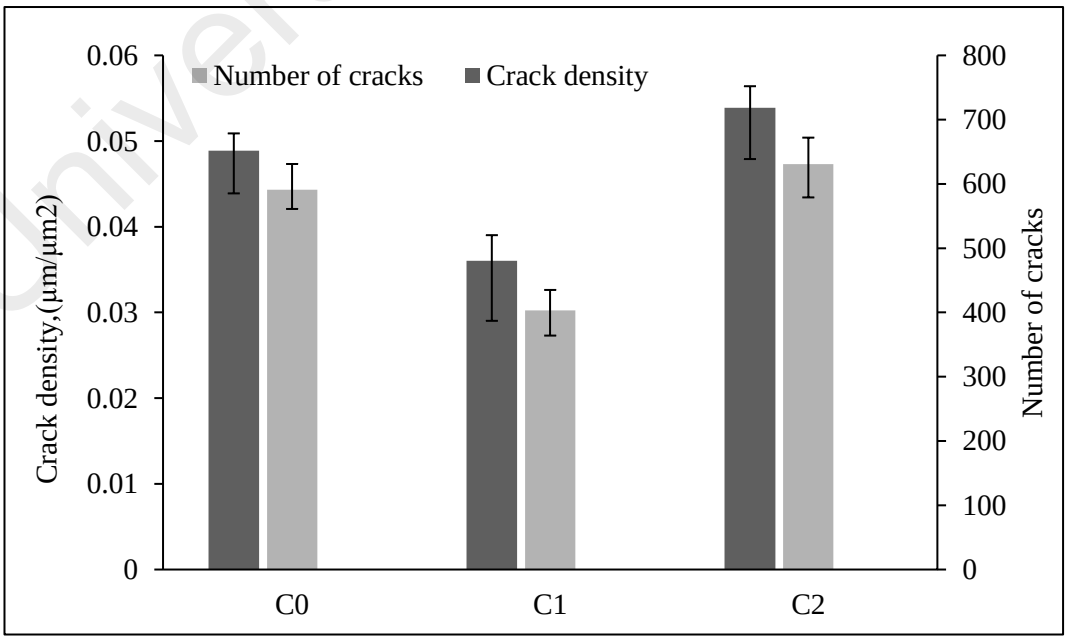

Figure 4.32: Machined surface crack density after using electrodes C0, C1 and C2

University of Malaya

The development of micro-cracks in recast and heat-affected zones is a prevalent issue as a result of thermal stress during EDM. Under mechanical stress such cracks propagate into the substrate, ultimately leading to premature failure (H. T. Lee & Tai, 2003). Therefore, it is important to analyze the density and number of micro-cracks in the workpiece after EDM.

Following crack density analysis, workpiece cross sections were prepared for crack propagation inspection by optical microscope and SEM (Figure 4.33). Typical micrographs demonstrating the recast layer of machined surfaces are depicted in Fig. Figure 4.33(a) through Figure 4.33(c). Quantitative measurements of the recast layer thickness attained from analyzing several sections along a workpiece cross section indicated that ECAP-treated electrodes are associated with approximately 30% reduction in recast layer thickness. Since the molten material after discharge was rapidly quenched by the dielectric, the surface metallurgical structure and characteristics changed, which led to the formation of a brittle re-solidified layer with high hardness (S. Kumar et al., 2009) that is a suitable medium for crack formation. The cracks obviously followed different paths and penetration depths in the workpiece. As illustrated in Figure 4.33(d) through Figure 4.33(f), the workpieces indicated crack propagation in a specific pieces of material in workpiece. In overall electrodes C1 and C2 are produce thinner recast layer of around (7 μm).

University of Malaya

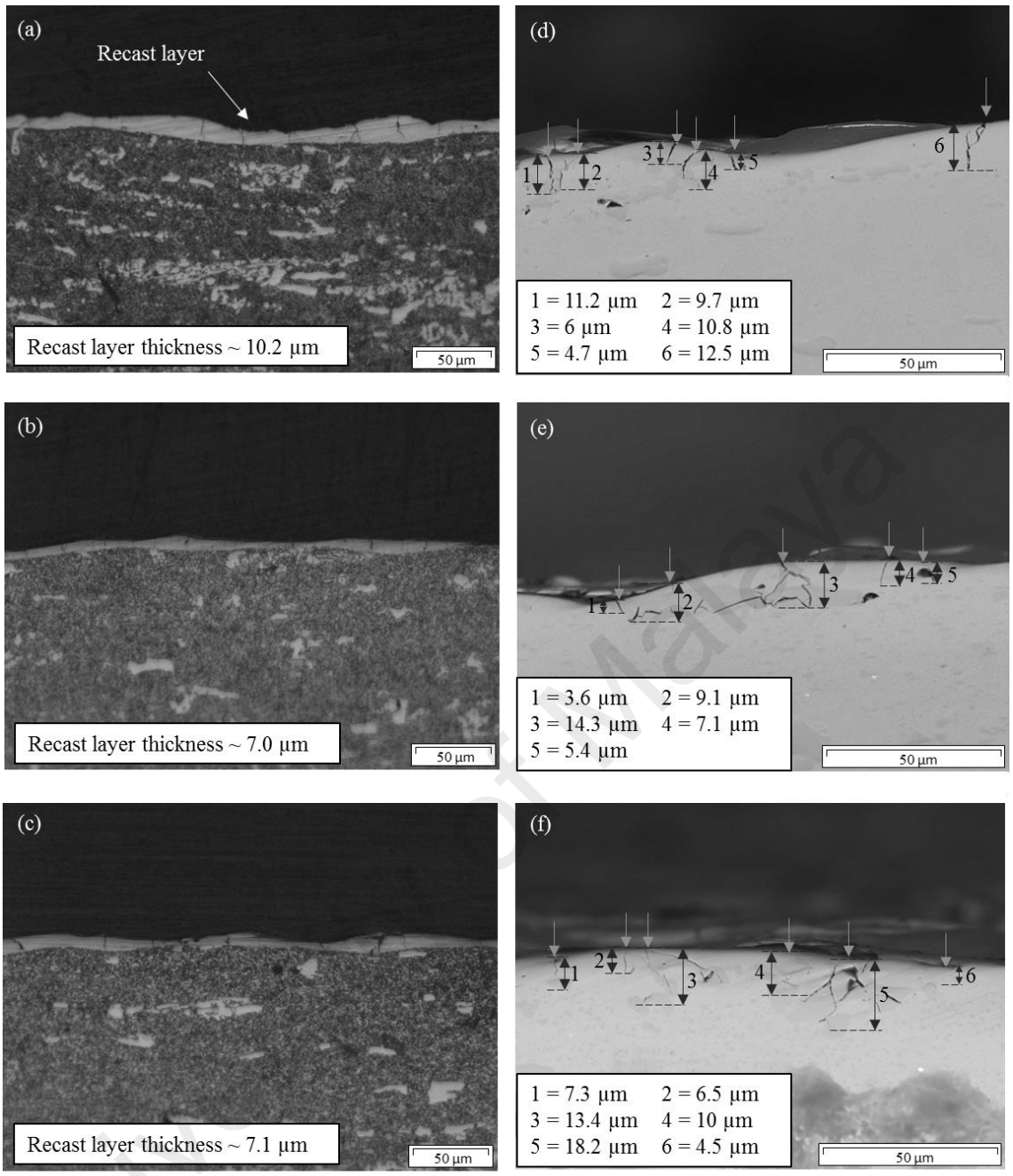

Figure 4.33: Surface cross sections after machining using electrodes (a) C0 (b) C1 and (c) C2

Figure 4.34(a) through Figure 4.34(f) demonstrate a selective crack and its relative EDX mapping on the cross-section of workpiece machined with electrode C0, C1 and C2. As seen from Figure 4.34(d) though Figure 4.34(f), the area containing Chromium (Cr) is the favorite for crack propagation. This finding implies that the influence of heat generated during pulse on-time was stronger on Cr than other elements. It is worth mentioning that steel with high amounts of Cr, Ni and Mo is susceptible to intergranular

fracture (Lima & Sankaré, 2014). This phenomenon originates as a result of strain localization and stress concentration at the grain boundaries (Farkas, Van Swygenhoven, & Derlet, 2002). During pulse on-time, ultra-high temperature is imposed on the workpiece, followed by instantaneous quenching that significantly increases the possibility of intergranular fracturing. Therefore, it is important to control MRR by selecting an appropriate electrode type to minimize this type of fracture.

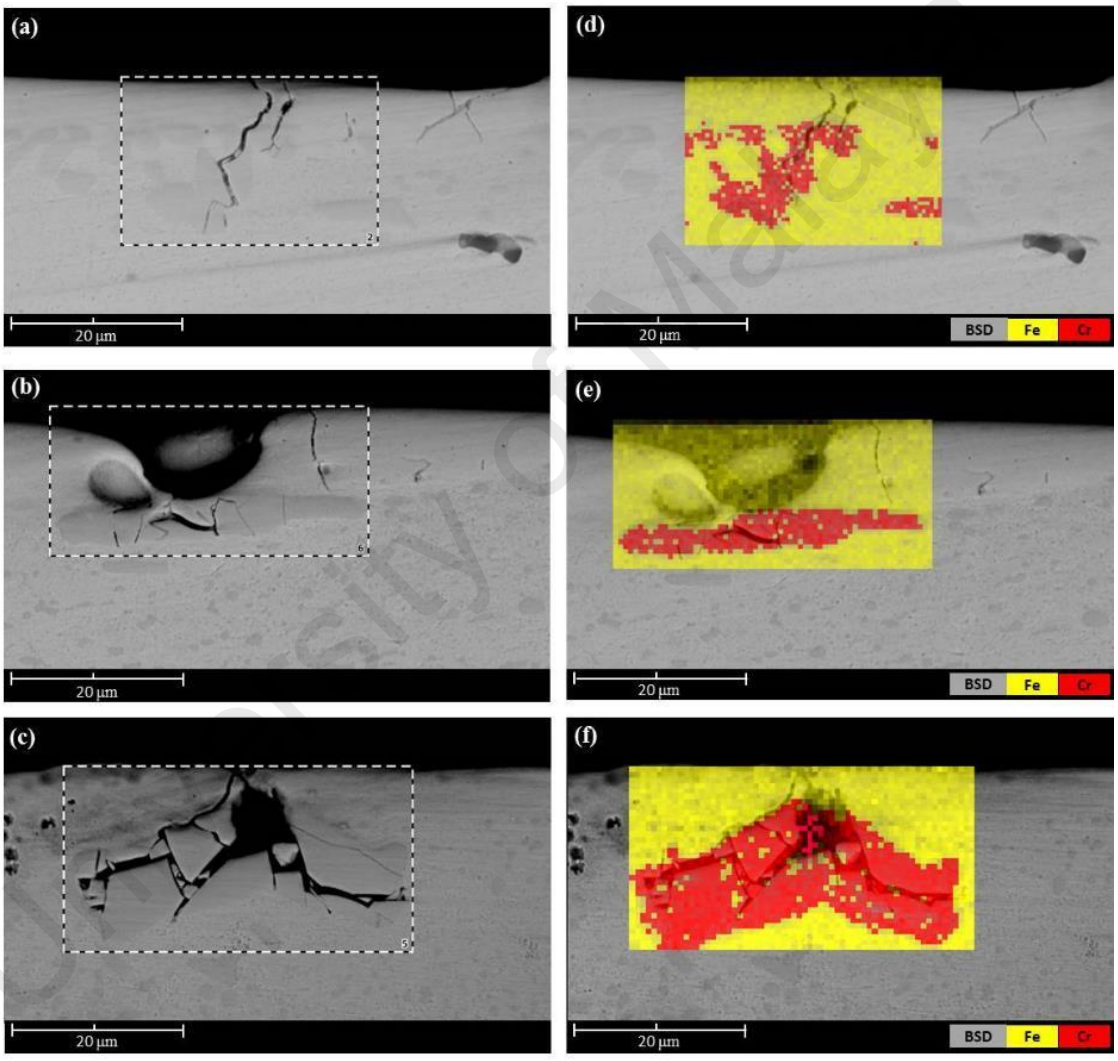

Figure 4.34: Cross-section of surface machined with electrode (a) C0, (b) C1 and (c) C2 and the relative EDX mapping for electrodes (d) C0 (e) C1 and (f) C2

Investigating the elemental analysis results and correlating them to Cr's mechanical properties was undertaken using nanoindentation on the workpiece cross section. Typical

images of nanoindentation impressions and their relative load-displacement curves are depicted in Figure 4.35.

According to Figure 4.35(a), the first indentation (point 1) is in a Cr-rich area and the five other points (points 2 to 6) are positioned in other areas that mainly contain Fe. Remarkably higher displacement for points (2) to (5) was evident compared with point 1. Therefore, the hardness values measured in the Fe-rich regions (from 4.2 to 4.5 GPa) were significantly lower than the Cr-rich area (18.1 GPa). This extremely high nanohardness in the Cr-rich area is due to the formation of Cr-containing compositions. This results are in accordance with what was observed in earlier in Figure 4.34 that demonstrated the existence of brittle Cr-rich zones. The extremely high brittleness of the Cr-rich zones explains the higher sensitivity of these regions to crack propagation. The extremely high hardness of Cr indicates its high brittleness, which specifies lower energy absorption ability and explains the higher impact of heat on Cr and the surface crack propagation into areas containing Cr.

It is worth mentioning that steel with high amounts of Cr, Ni and Mo is susceptible to intergranular fracturing (Lima & Sankaré, 2014), specially for operating and melting temperatures higher than 0.25 (Riedel, 1987). This phenomenon is a result of strain localization and stress concentration at the grain boundaries (Farkas et al., 2002). During pulse on time, ultra-high temperature is imposed on the workpiece, followed by instantaneous quenching that significantly increases the possibility of intergranular fracturing. Therefore, it is important to control MRR by selecting an appropriate electrode type to minimize this type of fracture.

University of Malaya

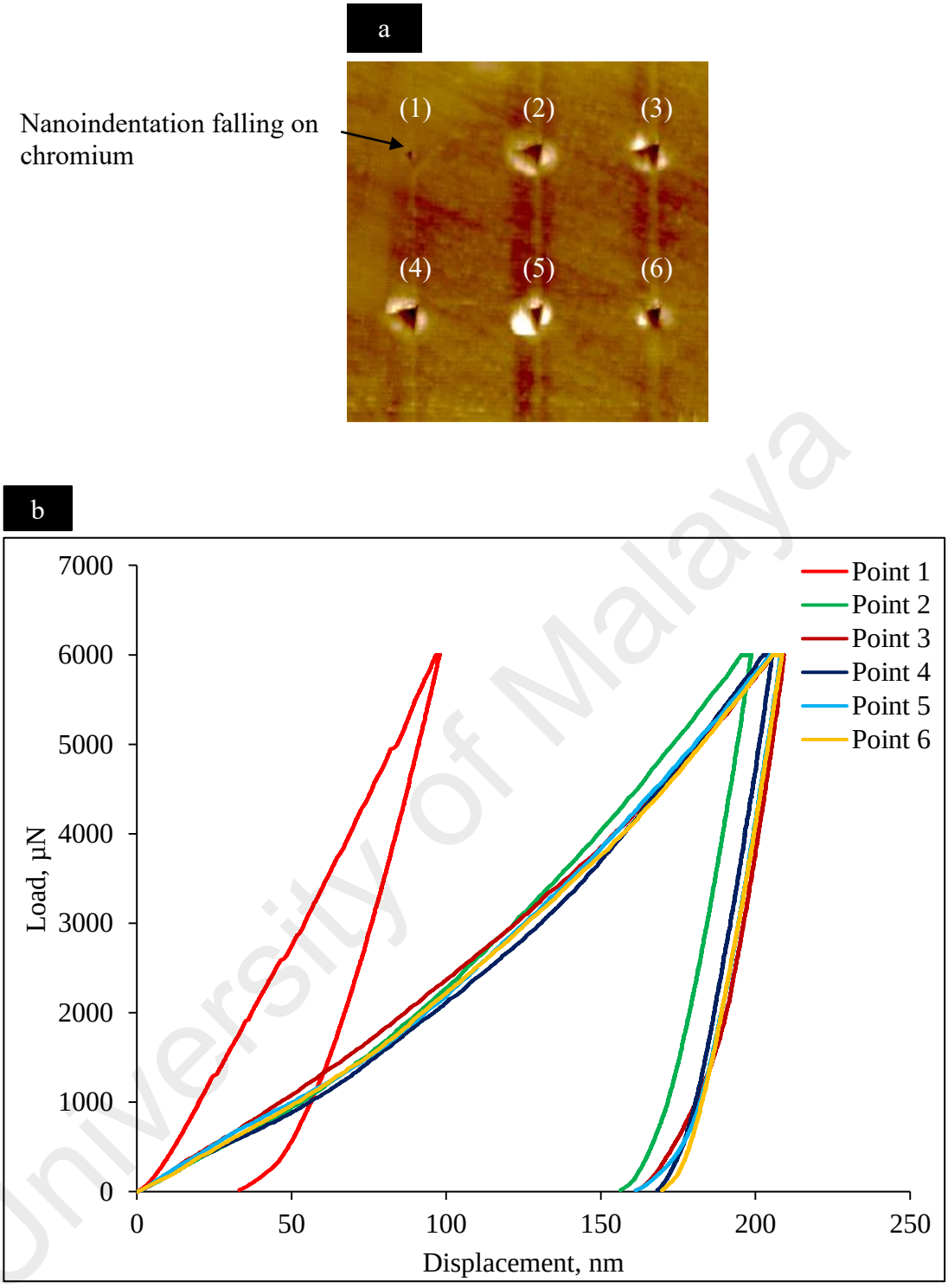

Figure 4.35: (a) Nanoindentation of AISI D2 steel and (b) its relative load-displacement graph

University of Malaya

4.3.6 Machining productivity concerning material removal and electrode wear

MRR and TWR were inspected to obtain a more comprehensive understanding of the impact of ECAP treatment on EDM efficiency. Figure 4.36 illustrates the MRR and TWR for the different electrode. The MRR almost remained constant for electrode C1 compared to C0. A negligible reduction in MRR for ECAP-treated electrodes can be attributed to the decrease in copper conductivity when subjected to ECAP treatment. The conductivity reduction reported after one pass of ECAP treatment was about 3% and 2% IACS for Cu-0.5%Cr and pure copper, respectively (Edalati et al., 2012; Wei et al., 2011). Moreover, it was explained that the average values and distribution ranges of MRR and discharge gap "within grain" and "on boundary" are different (J. Z. Li, Shen, Yu, & Natsu, 2013). This explains why grain refinement can be influential on machinability by exposing more grain boundaries over the electrode surface.

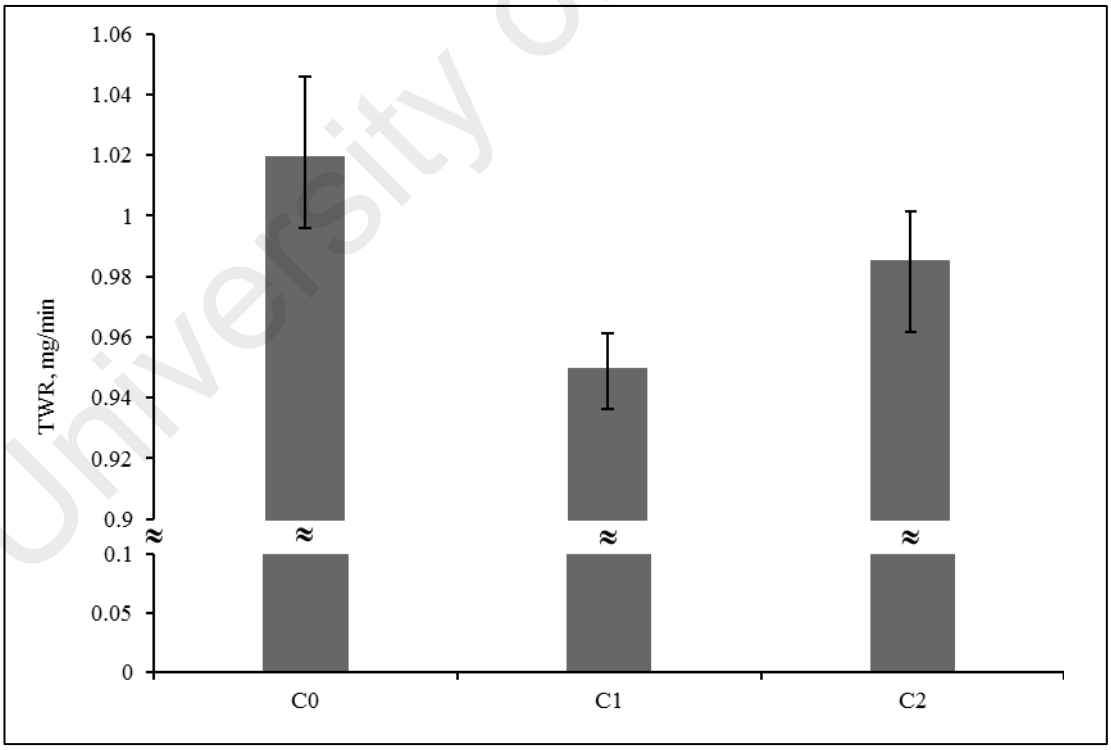

Figure 4.36: Influence of electrode ECAP treatments on TWR under depth control condition

University of Malaya

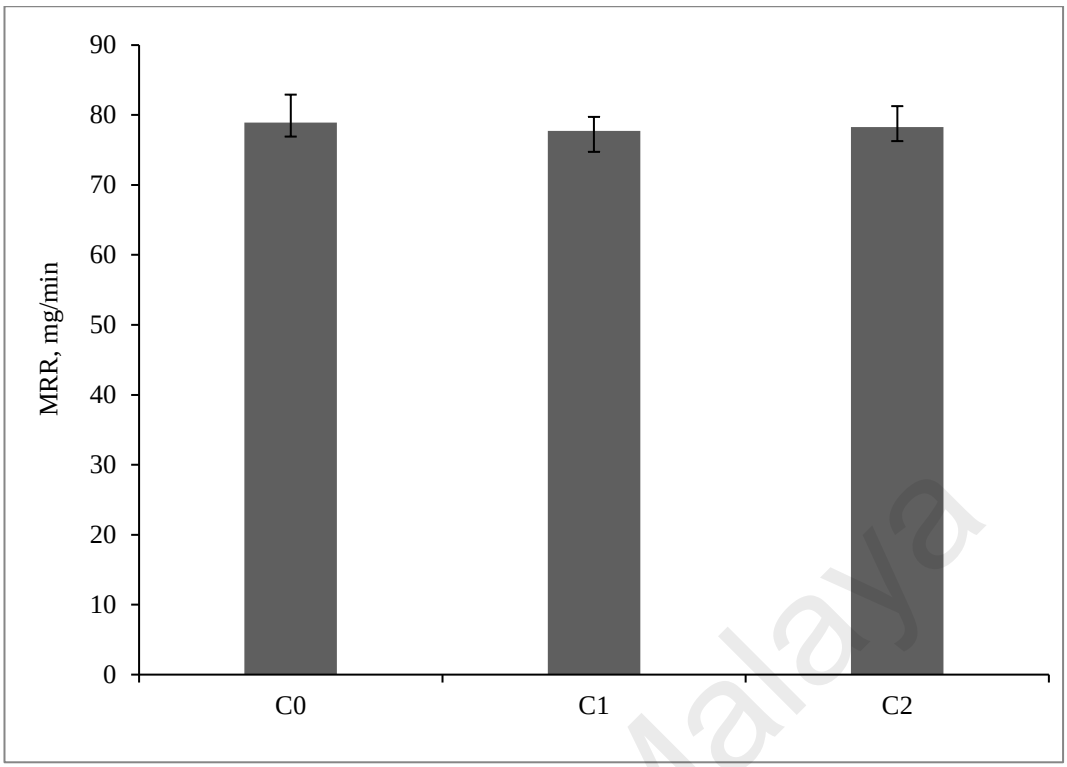

Figure 4.37: Influence of electrode ECAP treatment on TWR under depth control condition

ECAP treatment successfully decreased wear of electrode C1 by almost 7% compared to C0. Since the Cu-W electrode with approximately 225 MPa hardness reportedly had good wear resistance during EDM (Gaitonde et al., 2010), the decrease in TWR was attributed to the higher hardness of C1 (1.9 GPa) compared with pure copper with 1.7 GPa. Although the hardness was higher than C1, the C2 electrode was found to have less TWR reduction of nearly 5% compared to electrode C0. The higher amount of stress as a result of the second pressing pass for electrode C2 may neutralize the hardness improvement and subsequently increase the effect of spark heat on the electrode.

To comprehend the overall effectiveness of ECAP treatment in terms of both MRR and TWR, electrode wear ratio was deliberated. The electrode wear ratio showed an improvement of more than 5% in the case of electrode C1 and almost 3% for electrode C2 compared with electrode C0. Despite the fact that the measured MRR was slightly

University of Malaya

lower when electrode C1 was employed, the electrode wear ratio of this electrode appeared to be the most efficient.

4.4 Nano titanium PMEDM of AISI D2 steel alloy with ECAP treated electrodes

4.4.1 Geometrical accuracy concerning corner sharpness and overcut phenomena

Geometrical accuracy is investigated in terms of corner sharpness and overcut phenomena. In order to evaluate the sharpness of the machined corner at the bottom of the cavity, SEM analysis was undertaken to capture micrographs from cross-section of machined cavity (Figure 4.38). Visual inspection of micrographs in Figure 4.38(a) through (c) indicate that the corner sharpness increase when ECAP treatment was engaged to enhance the electrode's mechanical properties. Similar to the samples machined in oil dielectric, inspection of cavity machined in Ti nano-powder mixed dielectric in Figure 4.38 (d), (e) and (f) demonstrates higher sharpness for electrodes C1 and C2. Generally, the corner sharpness seems to be the finest when electrode C1 is employed for machining the cavity, whereas the worst results seems to be associated with electrode C0.

University of Malaya

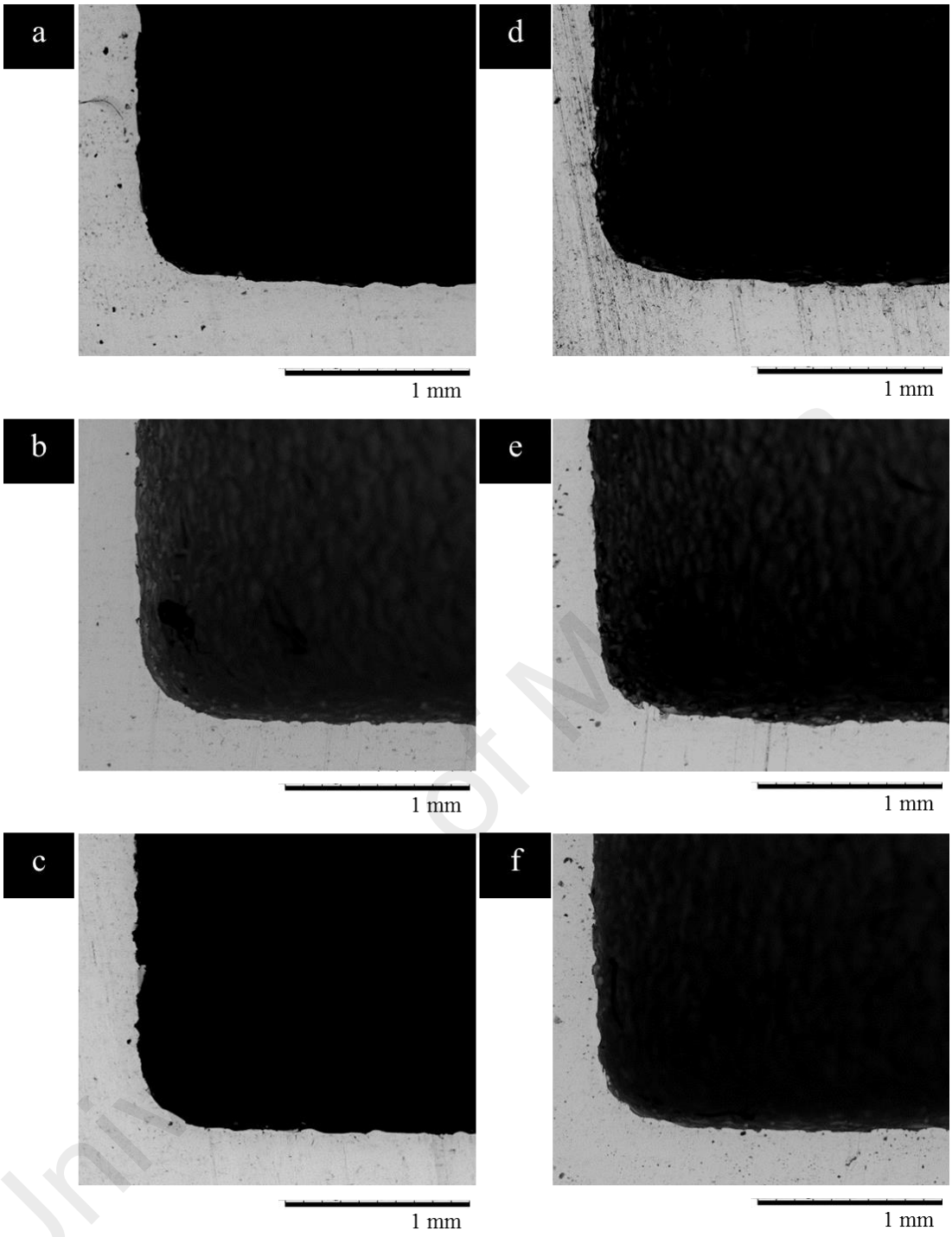

Figure 4.38: Cross-sectional view of cavity corner machined by electrodes (a) C0, (b) C1 and (c) C2 in pure dielectric, and (d) C0, (e) C1 and (f) C2 in Ti nanopowder mixed dielectric

Using a digitizer software, the cavity's corner micrograph captured with SEM has been plotted as depicted in Figure 4.39 and Figure 4.40. For the cavities machined in pure dielectric (Figure 4.39), the corner sharpness is higher for electrodes C1 and C2 due to higher hardness of electrodes as a result of ECAP treatment. The equation of the most

fitted lines on the corner of the cavities machined in pure dielectric (Figure 4.39) with electrodes C0, C1 and C2 are presented in (4.10), (4.11) and (4.12), respectively.

$$y_{C0} = 152.09x^6 - 371.21x^5 + 360.76x^4 - 179.23x^3 + 48.587x^2 - 7.1287x + 0.5346 \quad (4.10)$$

$$y_{C1} = 713.67x^6 - 1394.3x^5 + 1055.3x^4 - 390.24x^3 + 74.073x^2 - 7.3878x + 0.4365 \quad (4.11)$$

$$y_{C2} = 500.59x^6 - 1045.3x^5 + 851.18x^4 - 342.91x^3 + 72.403x^2 - 8.0872x + 0.4666 \quad (4.12)$$

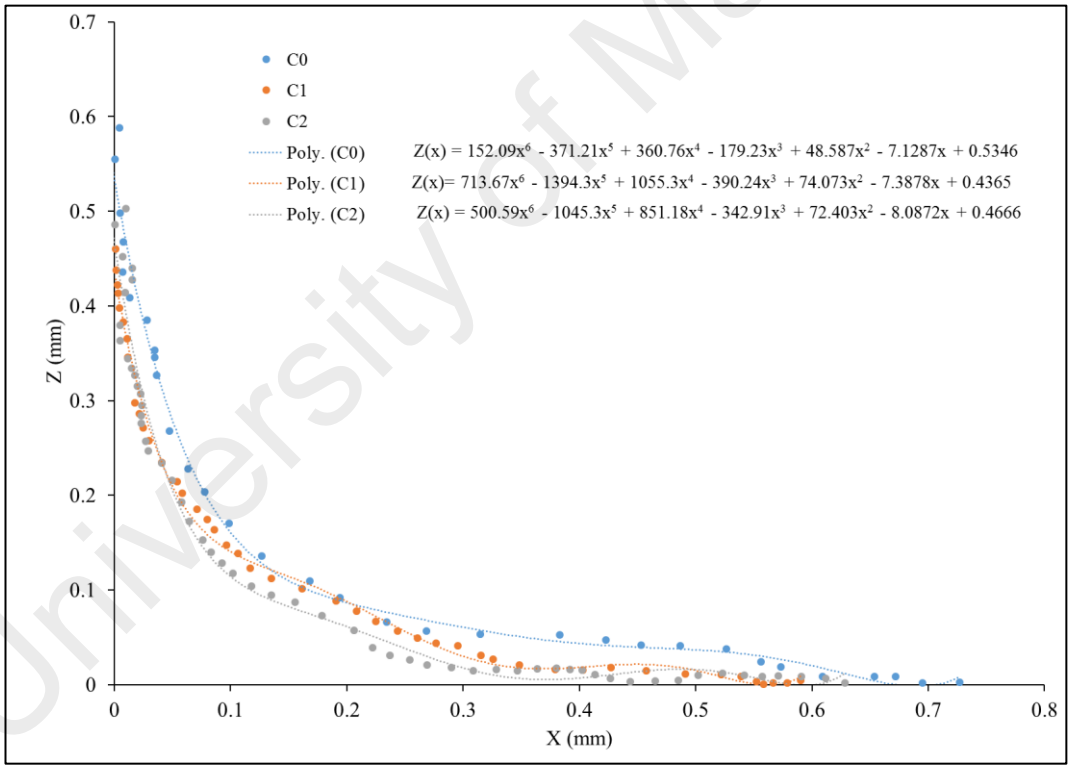

Figure 4.39: Workpiece corner shapes machined in pure dielectric (Z: cavity wall, X:cavity bottom)

University of Malaya

Unlike the cavities machined in pure dielectric, the corner sharpness does not specify an obvious difference when various electrodes are employed with Ti nanopowder mixed dielectric as dielectric (Figure 4.40). The equation of the most fitted lines on the corner of the cavities machined in pure dielectric with electrodes C0, C1 and C2 are presented in equations (4.13), (4.14) and (4.15), respectively.

$$y_{C0} = 345.74x^6 - 694.78x^5 + 565.8x^4 - 237.59x^3 + 54.252x^2 - 6.6914x + 0.4347 \quad (4.13)$$

$$y_{C1} = 523.42x^6 - 1164.6x^5 + 1010.6x^4 - 431.28x^3 + 94.305x^2 - 10.246x + 0.5269 \quad (4.14)$$

$$y_{C2} = 232.05x^6 - 529.1x^5 + 476.09x^4 - 214.97x^3 + 51.648x^2 - 6.6504x + 0.4483 \quad (4.15)$$

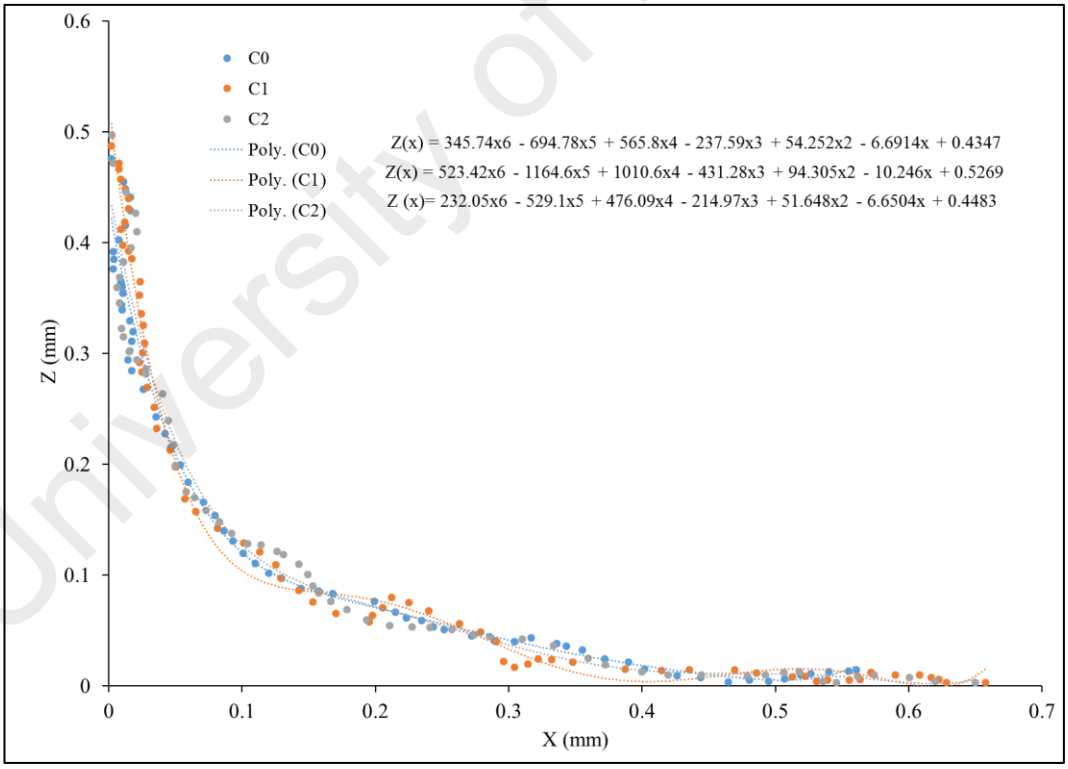

Figure 4.40: Workpiece corner shapes machined in Ti nanopowder dielectric (Z: cavity wall, X:cavity bottom)

University of Malaya

Figure 4.41 indicates the values calculated from the above mentioned curves using equation Figure 3.1 to quantify the value under the machined curve. A_{ci} was measured by fitting a curve on each corner as demonstrated in Figure 4.39 and Figure 4.40. Then the abovementioned equations that define the aforementioned curves relating to electrodes C0, C1 and C2 were extracted, respectively: Over all machining conditions, electrode C2 demonstrated the lowest corner wear achieved in pure dielectric which is 38% lower than C0 electrode which indicated the highest corner wear. It is clear that the overall shape of the cavity enhanced in terms of the wall deviation and corner sharpness caused by lower electrode corner wear as the electrodes underwent ECAP treatment. Employment of Ti nanopowder mixed dielectric does not seem to deteriorate the effect of ECAP treatment on reducing the electrode corner wear. As shown in Figure 4.41, area under the machined corner in Ti nanopowder mixed dielectric for all electrodes of C0, C1 and C2 remains constant. This behavior is due to higher dielectric ionization or might be attributed to surface of electrode getting influenced after addition of powder to dielectric.

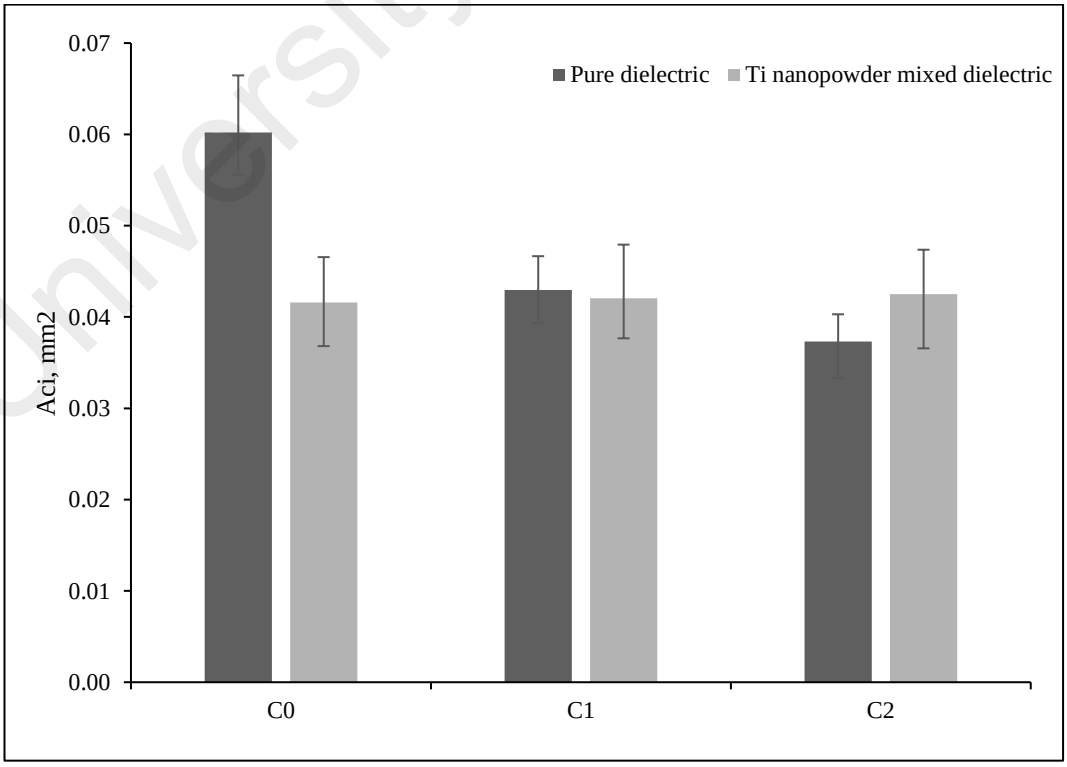

University of Malaya

Figure 4.41: Area under the curve (A_{ci}) for the cavity machined by electrodes C0, C1 and C2

The values of VOC were calculated for all electrodes according to equation (3.3) and are summarized in Figure 4.42. The results show that in pure dielectric, using electrodes C1 and C2 reduced the VOC by approximately 35 and 24% compared with electrode C0. As it was explained previously, this reduction is attributed to lower electrical conductivity of electrodes as a result of ECAP treatment.

Dissimilar trend is observable for the case Ti nanopowder dielectric, since contribution of powder leads to higher conductivity and ionization of dielectric, after penetration of tool into the workpiece the corner is attached by higher number of sparks compensating the lower electrical conductivity of electrodes C1 and C2.

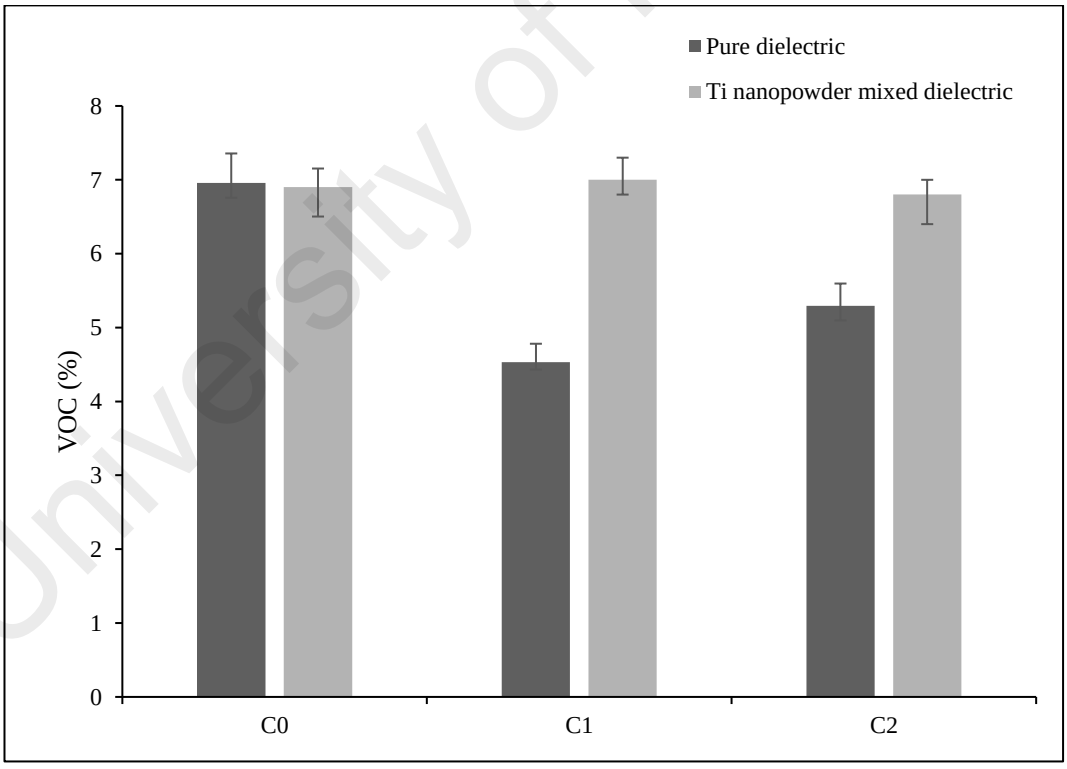

Figure 4.42: Volumetric overcut (VOC) for the cavity machined by electrodes C0, C1 and C2 in pure and Ti nanopowder mixed dielectric

University of Malaya

4.4.2 Surface topography and morphology analysis of machined cavity

The effect of different electrode types on workpiece surface roughness was calculated using R_a and R_z as shown in Figure 4.43 and Figure 4.44, respectively. A quick look at the figures reveal that contribution of nanopowder to dielectric leads to lower surface roughness in terms of R_a and R_z for any electrode type of C0, C1 or C2, whereas highest improvement concerns C2 electrode in pure and powder mixed dielectric. Employment of C0 in pure dielectric indicates the highest R_z value as the highest number of irregularities form on the machined surface due to direct spark between tool and workpiece. Electrode C0 produced a surface with R_a of around 5.3 µm, while this value almost remained constant for C1 and reduced to 4.7 C2. Furthermore, when machining with Ti nanopowder mixed dielectric, all Ra values experienced alight reduction. Seams that in this machining condition, the influence of adding Ti nanopowder is not significant. These variations in R_a could have originated from the crater shape (S. Singh et al., 2004) as well as microscopic defects. Thus, the workpieces' micrographs were further investigated to identify the cause of R_a variation. Regarding the R_z, addition of Ti nanopowder to dielectric slightly reduced the R_z. According to the aforementioned discussion in section 4.2, the existence of surface droplets and defects is more pronounced in R_z value than R_a. Thus, after the engagement of Ti nanopowder mixed dielectric, contribution of powder particles in discharge prevents the direct discharge between tool and workpiece which results in formation of surface with lower roughness.

University of Malaya

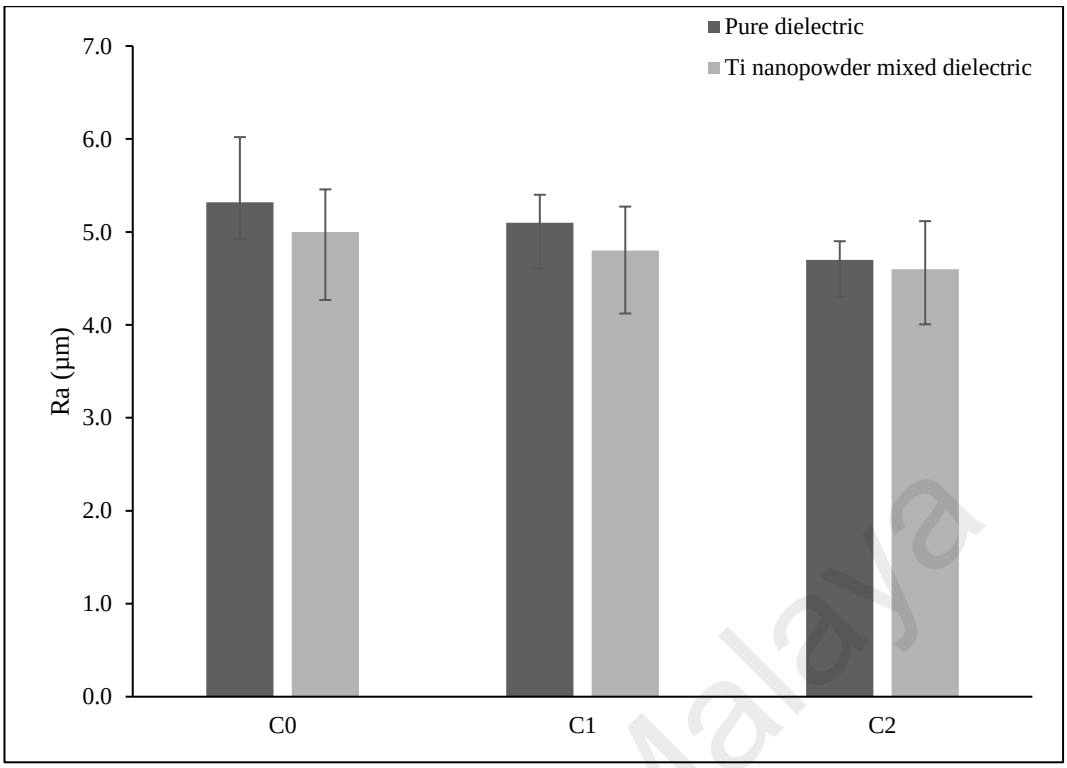

Figure 4.43: Average surface roughness (Ra) of surfaces machined by electrodes C0, C1 and C2 in pure and Ti nanopowder mixed dielectric

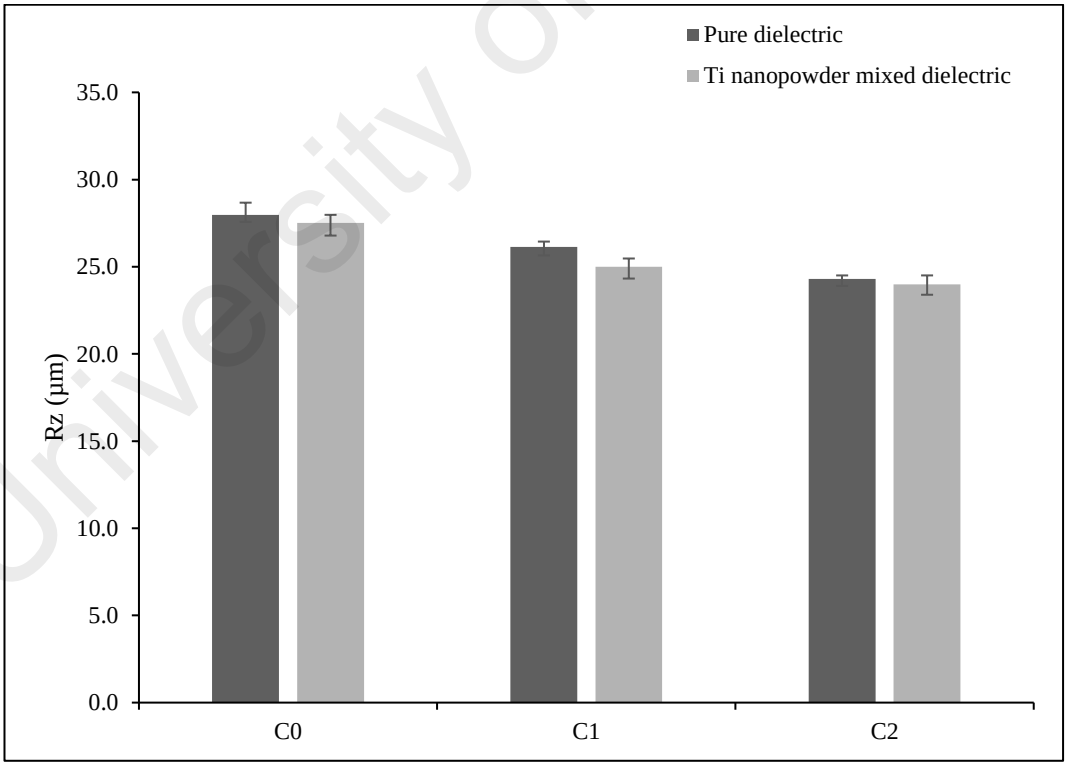

Figure 4.44: Surface roughness's (Rz) of surfaces machined by electrodes C0, C1 and C2 in pure and Ti nanopowder mixed dielectric

University of Malaya

Surface quality was also investigated by means of FESEM through attaining micrograph of the machined surface at the center of the cavity demonstrated in Figure 4.45 and Figure 4.46 in pure and Ti nanopowder mixed dielectric, respectively. It is evident that electrode C2 produced the finest surface compared with electrodes C0 and C1 which is in accordance with surface roughness results in both dielectrics. Comparing Figure 4.45 and Figure 4.46 indicates that using all electrode types, the machined surface has more irregularities and higher density of micro-droplets when machining in pure dielectric using C0. However, employment of electrodes C1 and C2 is shown to enhance the machined surface topography, since lower number of micro-droplets and less high-level ridges are evident in their related micrographs. This is attributed to the relatively lower electrical conductivity of electrodes following ECAP treatment which leads to smaller machining gap and discharge energy. Electrode C2 is shown to provide the best machined surface for cavity machining in pure dielectric.

University of Malaya

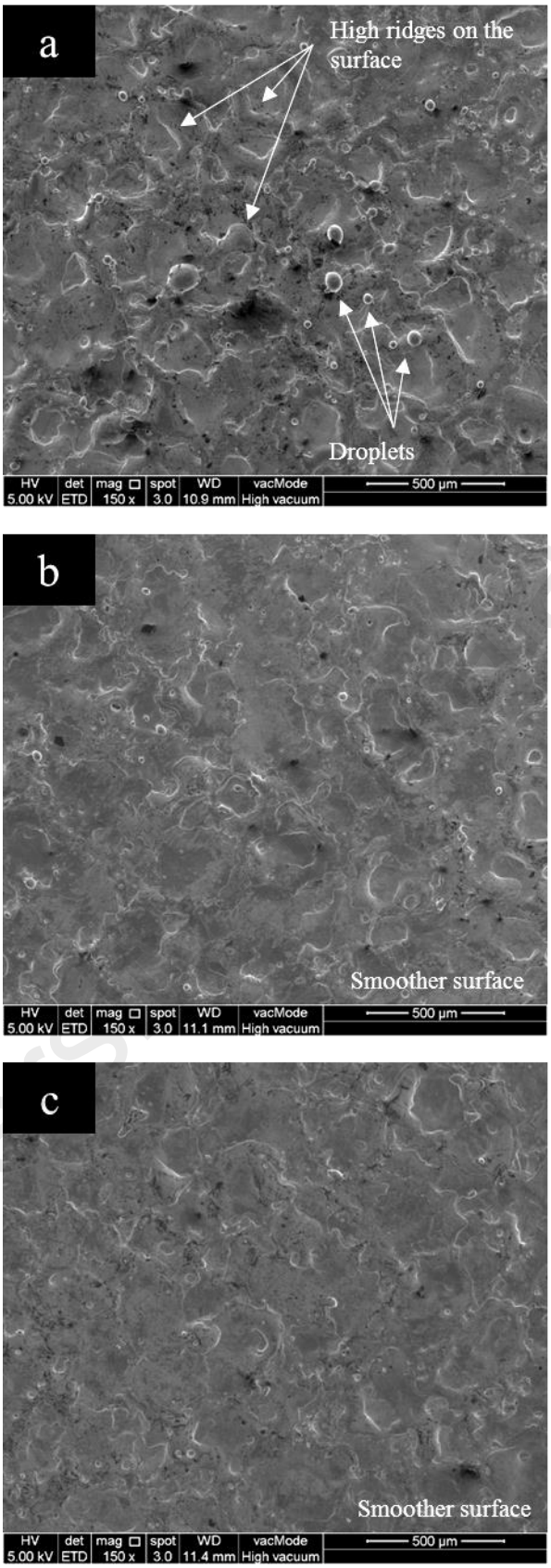

Figure 4.45: FESEM of machined surfaces in pure dielectric with electrodes (a) C0, (b) C1 and (c) C2

Universiti Malaya

Figure 4.46 illustrates the micrograph of surfaces machined in Ti nanopowder mixed dielectric using electrodes C0, C1 and C2. The first to notice is formation of relatively smoother surface compared to the surface machined in pure dielectric for all electrode types, however, micro-droplets still form on the machined surface for electrode C0. Due to higher density of Ti nanopowder mixed dielectric, escape of liquidified workpiece material and gas bubble from machining gap is difficult. That is the reason for formation of more micro-voids for electrodes C1 and C2 on the machined surface.

Beside center of the cavity, the machined surface around the corners has been also investigated using FESEM indicated in Figure 4.47 and Figure 4.48 for pure and powder mixed EDM, respectively. Due to existence of 3 mm high walls around the fabricated cavity, the flushing is interrupted around the cavity's edges resulting in surface quality deterioration due to formation of higher number of droplets when C0 is employed in pure dielectric (Figure 4.47(a)). However, this effect does not seem to persist for the case of electrodes C1 and C2 due to formation of smaller sparks on the machined surface (Figure 4.47(b) and (c)).

University of Malaya

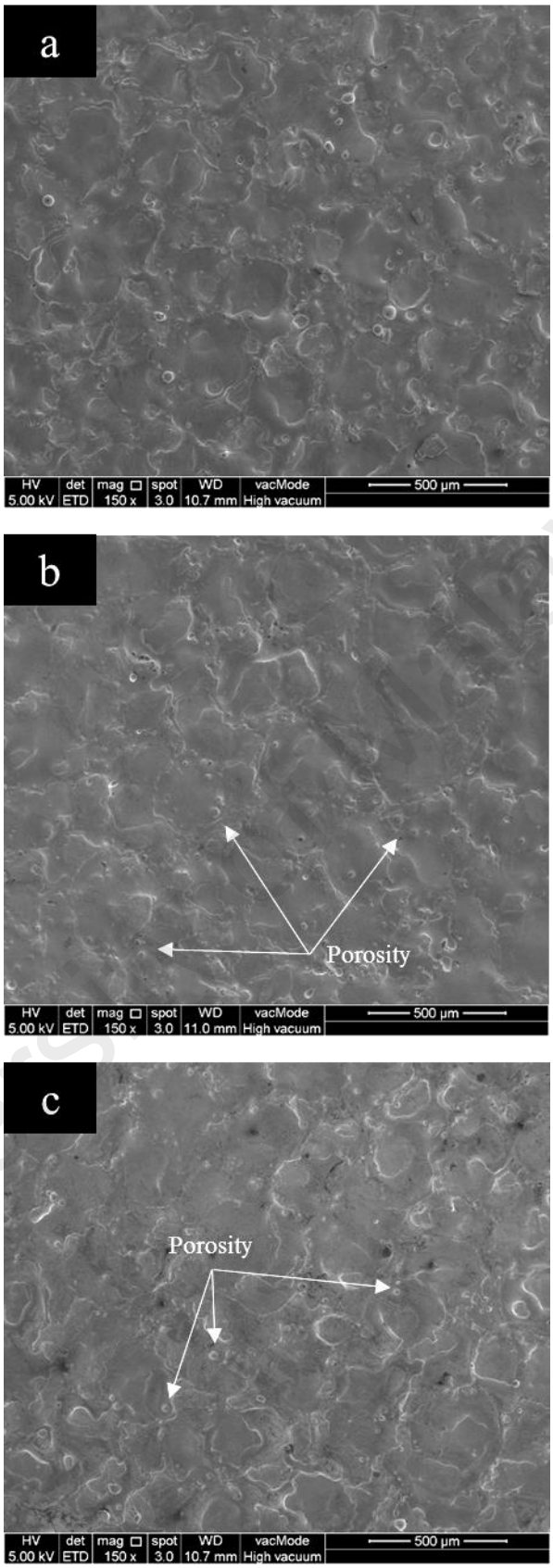

Figure 4.46: FESEM of machined surfaces in Ti nanopowder mixed dielectric with electrodes (a) C0, (b) C1 and (c) C2

Universiti Malaya

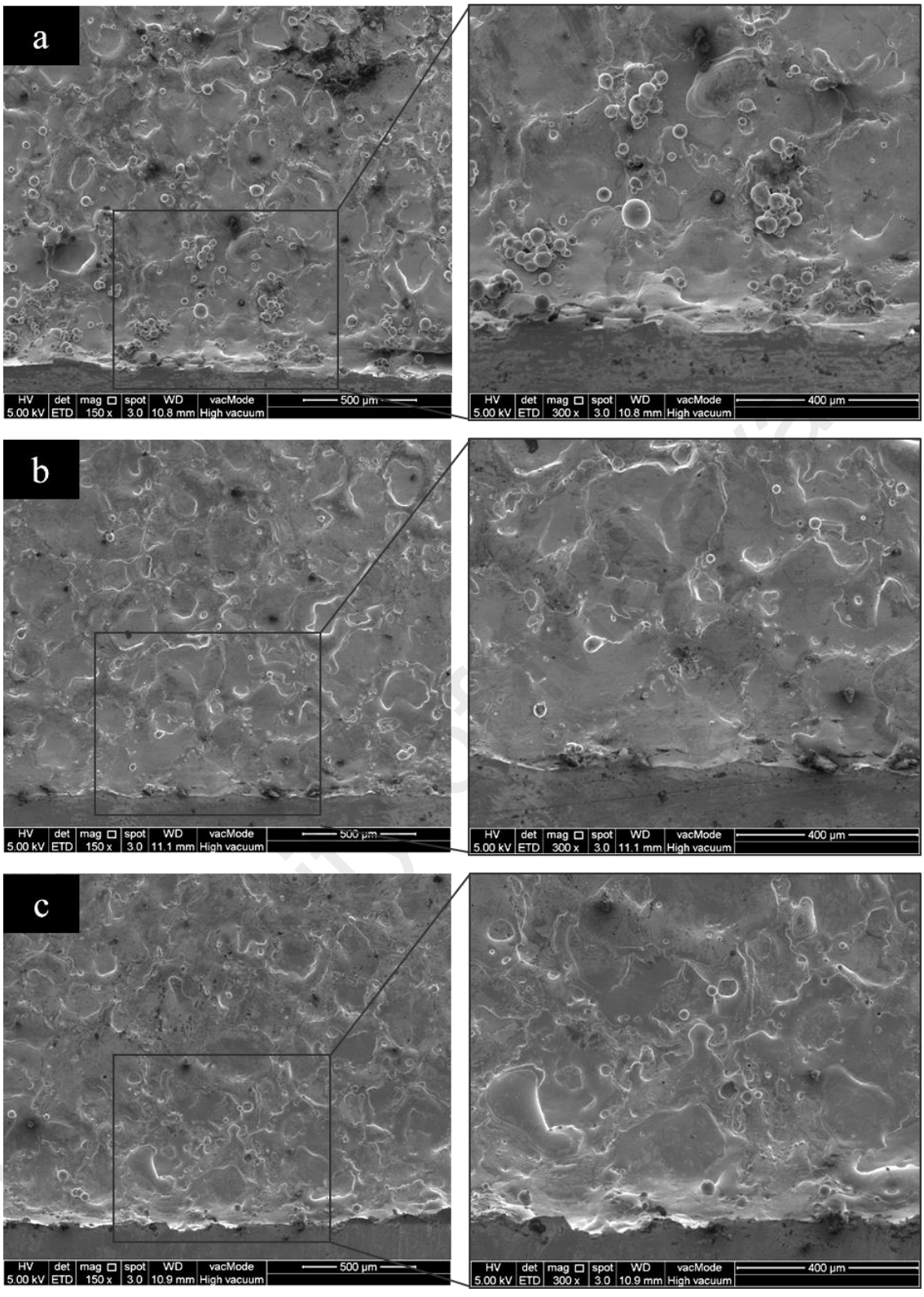

Figure 4.47: FESEM of machined surfaces close by the edge in pure dielectric with electrodes (a) C0, (b) C1 and (c) C2

Performance of C0, C1 and C2 in Ti nanopowder dielectric seems alike and improving. Yet micro-voids on the machined surface is more pronounced. This is attributed to the higher density of Ti nanopowder mixed dielectric that aborts the expelled gases escape from machining gap.

University of Malaya

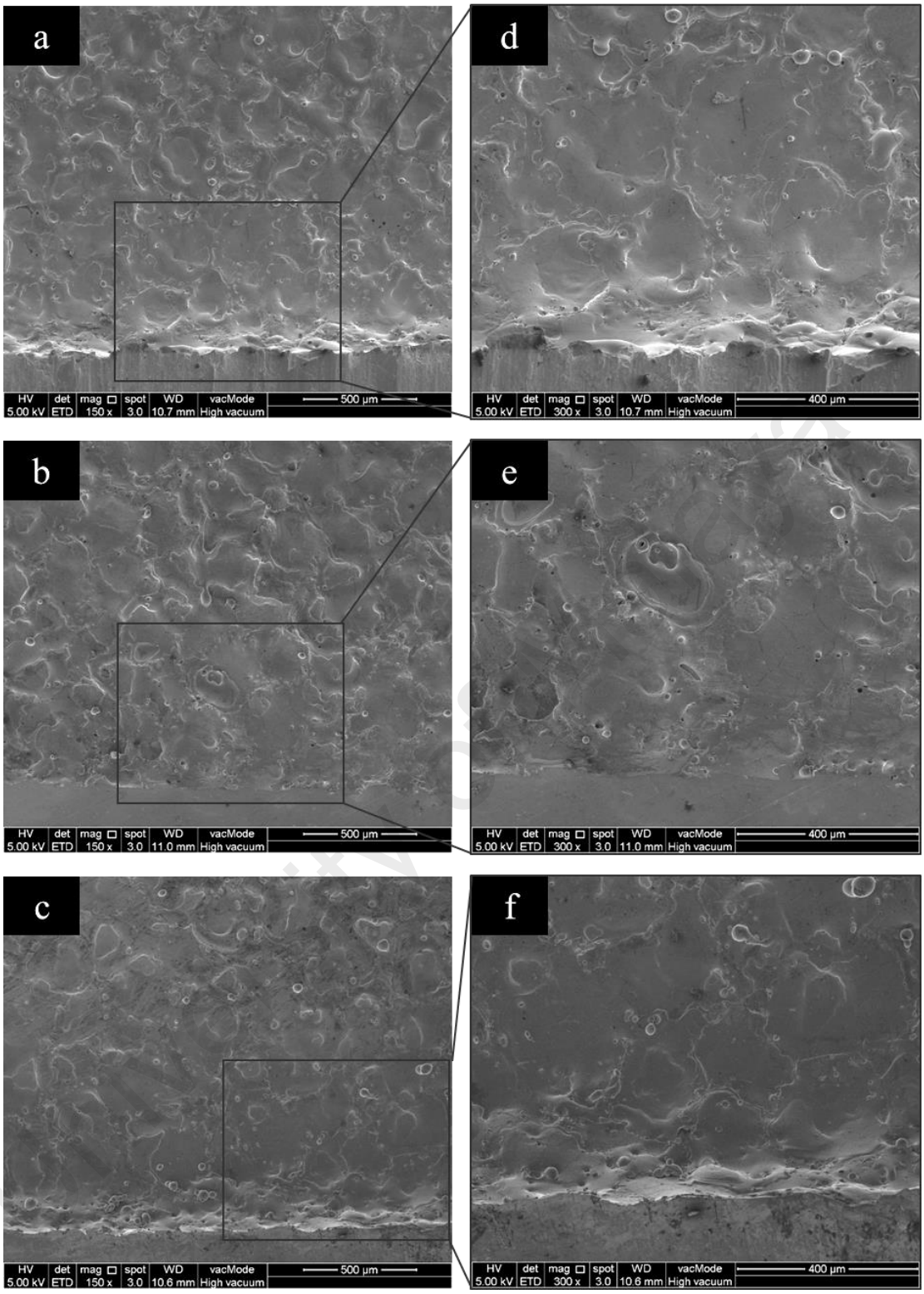

Figure 4.48: FESEM of machined surfaces close by the edge in Ti nanopowder mixed dielectric with electrodes (a) C0, (b) C1 and (c) C2

4.4.3 Surface crack susceptibility

To quantitatively measure the effect of different types of dielectric and electrodes on crack distribution over the surface, the density and numbers of cracks for workpiece

micrograph in Figure 4.49 were measured and summarized in Figure 4.50. It was revealed that electrode C2 produced the lowest density on the finished workpiece surface in pure dielectric. It was observed in section 4.3.5 that at 60 µs discharge duration and 4.5 A current, crack density was reduced by more than 26% when employing electrode C1 compared with electrode C0. However, it is evident in Figure 4.50 that employment of ECAP treated electrodes does not reduce the surface cracks at 100 µs and 1 A. Employment of Ti nanopowder mixed dielectric shown to lead to higher density of surface cracks due to higher ionization and spark frequency which leads to extra quenching effect on the surface.

University of Malaya

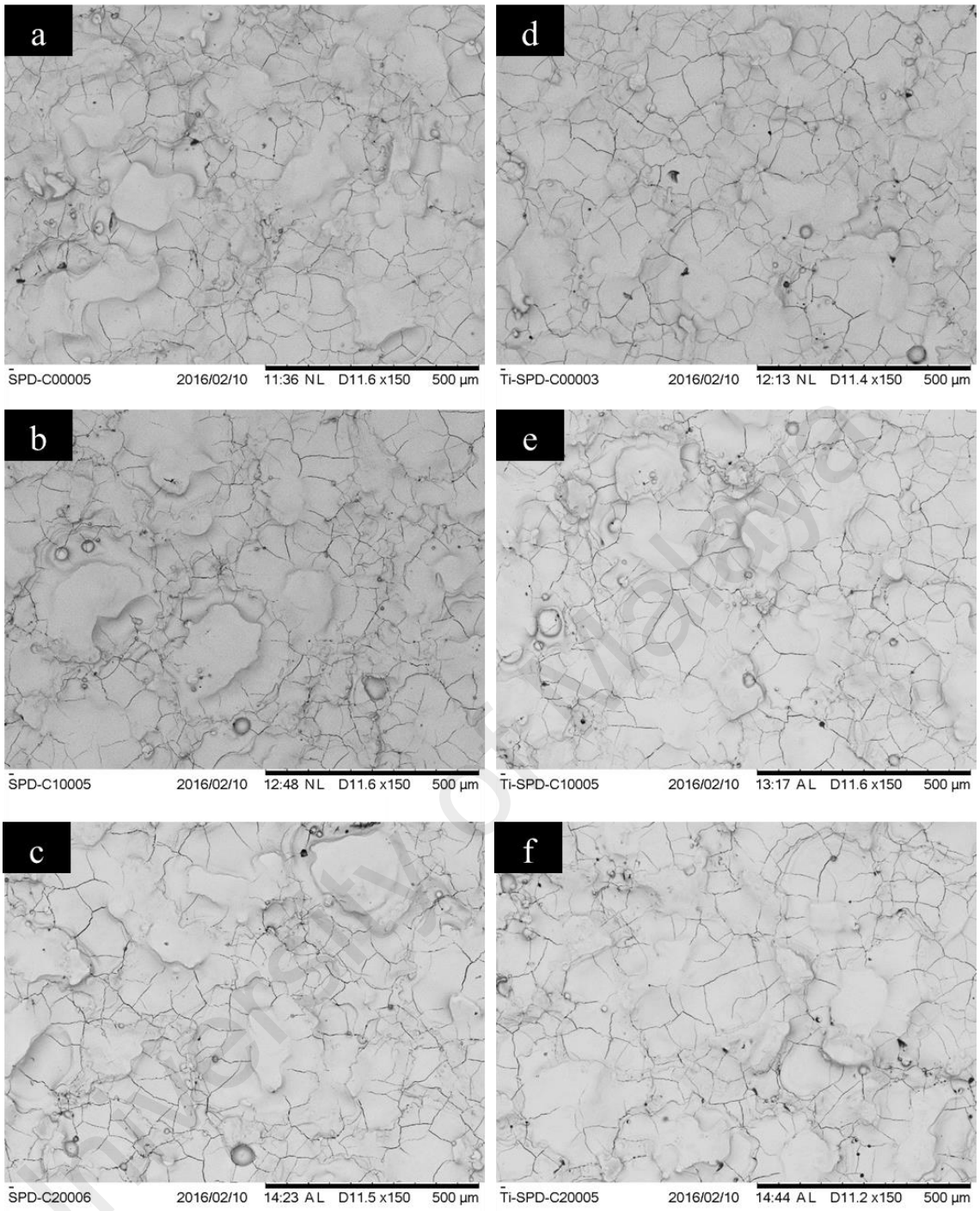

Figure 4.49: Micrograph of surfaces machined by electrodes (a) C0, (b) C1 and (c) C2 in pure and (d) C0, (e) C1 and (f) C2 in Ti nanopowder mixed dielectric

University of Malaya

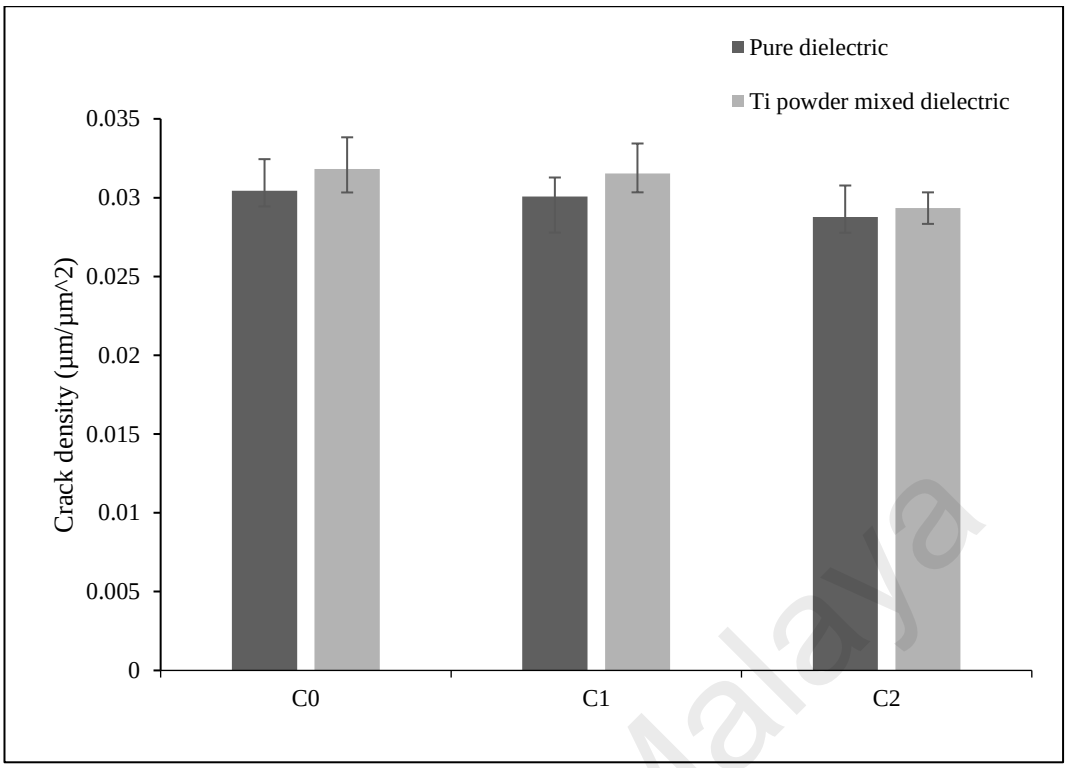

Figure 4.50: Crack density of surface machined by electrodes C0, C1 and C2 in pure and Ti nanopowder mixed dielectric

4.4.4 Machining productivity concerning material removal and electrode wear

To evaluate the machining process efficiency, MRR, TWR and electrode wear ratio are deliberated. Figure 4.51 and Figure 4.52 demonstrate the MRR and TWR for machining cavities in pure and Ti mixed dielectric using electrodes C0, C1 and C2. Influence of using different types of electrodes on TWR in pure and Ti nanopowder mixed dielectric demonstrate different trends. Machining a cavity using electrode C1 shown to reduce the TWR by more than 10% compared to electrode C0 in pure dielectric, which can be considerably cost saving when it comes to long machining hours in die and mold production industry. However, the influence of using electrodes C0, C1 and C2 in Ti nanopowder mixed dielectric is diminished due to higher ionization and spark frequency between tool and workpiece after addition of powder to dielectric. This also leads to higher TWR when Ti nanopowder dielectric is selected as the working fluid.

University of Malaya

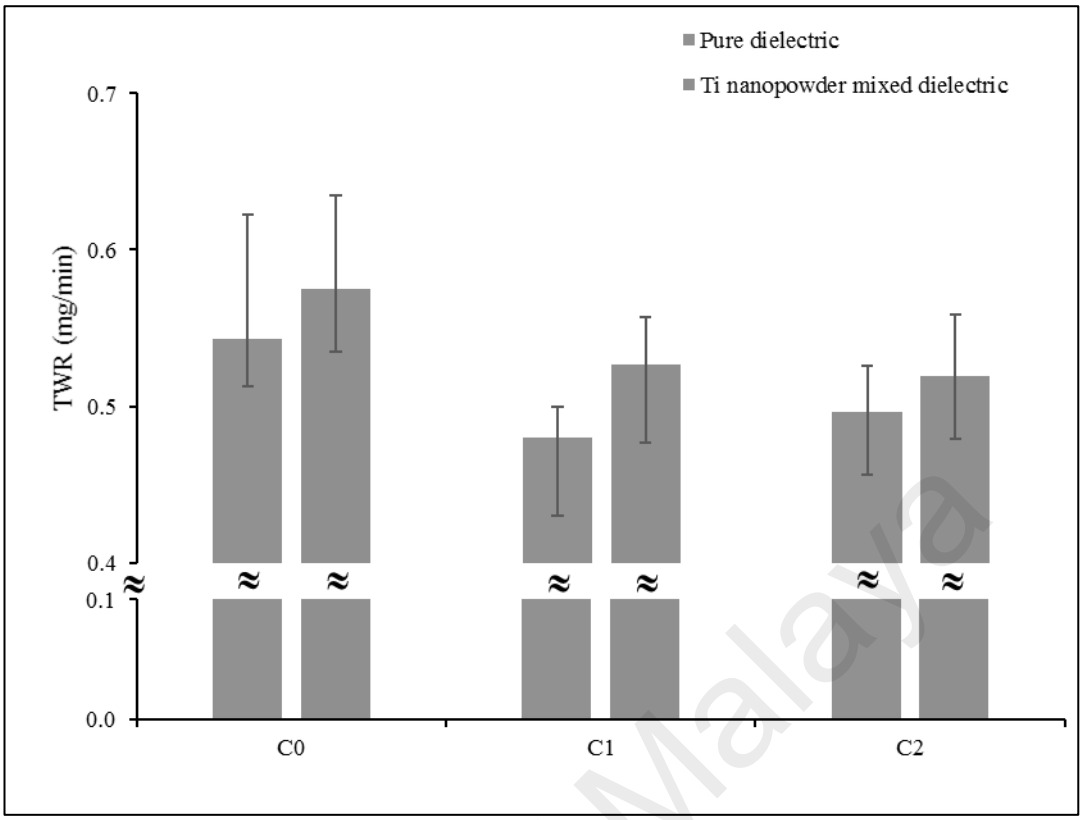

Figure 4.51: Influence of electrode ECAP treatment and dielectric fluid on TWR

As an important machining factor, MRR did not experience a considerable fluctuation at this machining condition by using various types of electrode (C0, C1 and C2) to machine the workpiece in pure dielectric. As it was expected, for all types of electrode, addition of powder to dielectric has led to slightly higher MRR. This behavior was also evident at 60 µs spark duration and 4.5 A current discussed in section 4.2.4.. Furthermore, severe plastic deformation of electrode did not indicate to have any considerable effect on MRR.

University of Malaya

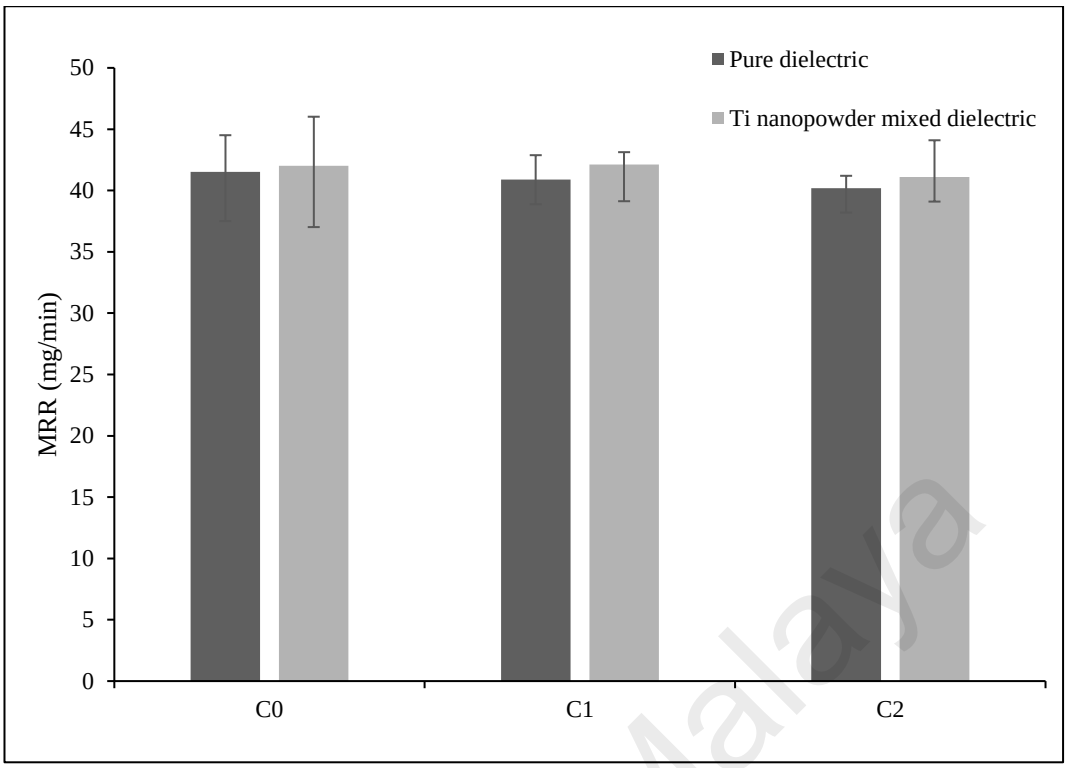

Figure 4.52: Influence of electrode ECAP treatment and dielectric fluid on MRR

4.4.5 Material migration phenomena and elemental analysis

Material migration and elemental analysis of the machined surface is important since the change in surface chemical composition alters the component's mechanical properties. In EDM, contamination of discharge gap leads to inclusion of external molecules and atoms in the recast layer as explained in section 4.2.6. The EDX analysis and quantification of elemental content on workpiece is charted in Figure 4.53. Results depicted in Figure 4.53 show that deposition of Ti on workpiece is insignificant. However, slightly lower conductivity of C1 and C2 than C0 led to smaller gap size which results in entrapment of Ti nanoparticles in the recast layer during solidification. Although the deposition of Ti on machined surface is negligible, the effect of ECAP treatment on the amount of deposited Ti on the machined surface is evident.

University of Malaya

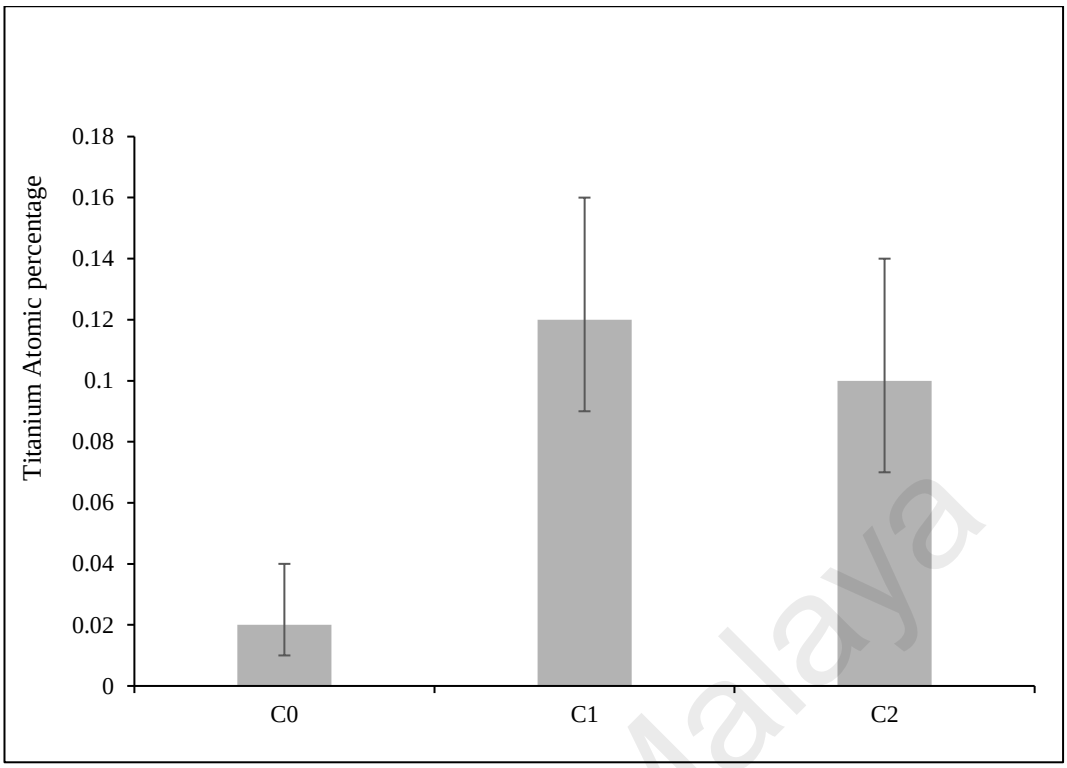

Figure 4.53: Atomic percentage of titanium on the machined surface

University of Malaya

CHAPTER 5: CONCLUSION AND RECOMMENDATION

5.1 Nano titanium PMEDM of AISI D2 steel alloy

In this research, the influence of adding Ti nanopowder to dielectric was investigated considering discharge durations (T_{on}) of 60, 100 and 140 µs and current (I) of 1, 1.5 and 2 A. To utilize the Ti nanopowder dielectric in the machining area, a made-in-house circulation system was developed. To check the efficiency of the developed system, environmental scanning electron microscopy (ESEM) and energy dispersive x-ray spectroscopy (EDX) analyses were carried out to examine the concentration of Ti nano-particles. Furthermore, the surface characteristics were evaluated using a surface roughness profilometer, field emission scanning electron microscopy (FESEM), EDX and AFM. The following findings were derived from the analysis:

- It was observed that due to addition of Ti nanopowder to dielectric the surface roughness significantly improved in all selected machining conditions. Ti nanopowder dielectric presented the highest enhancement at 1 A current and 100 µs discharge duration, where the Ra and Rz improved the most by ~23% and ~24%, respectively.
- Using Ti nanopowder dielectric enhanced the morphology of D2 steel surface because of shallower craters and the formation of low-height ridges. Furthermore, surface micro-defects and debris attachment to the machined surface decreased.
- According to the EDX results, a negligible amount of Ti atoms deposited on the machined surface, which is important to maintain the properties of the AISI D2 steel. However, the concentration of Ti atoms around the crack areas appeared higher than other surface areas due to local accumulation of Ti nanopowder.

University of Malaya

5.2 EDM with ECAP-treated electrodes

Pure Cu is a popular material for producing EDM electrodes. However, electrode wear due to machining is a major drawback, as it deteriorates machined component accuracy. In this research, ECAP as the most effective SPD method was employed to improve the mechanical properties of pure copper electrodes in order to achieve superior EDM performance. ECAP processing of up to two passes was performed successfully at room temperature. The nanohardness evolution after the first and second pressing passes were obtained. Afterwards, a series of experiments were conducted to evaluate the influence of ECAP-treated copper electrodes on the machining characteristics of AISI D2 tool steel. Based on experimental studies, the following findings are outlined:

- Nanoindentation testing indicated an increase in nanohardness of approximately 12 and 25% after the first and second ECAP passes, respectively.
- Electrodes that underwent one and two passes of ECAP treatment improved corner sharpness by 66% and 61%, and decreased the VOC by 13% and 5% respectively, compared to the as-received electrodes. Furthermore, it was observed that using ECAP-treated electrodes reduced the wall deviation of the fabricated cavity.
- As a result of hardness improvement after ECAP processing, tool wear was reduced by almost 7% compared with the as-received electrodes. Since the MRR remained nearly constant, the electrode wear ratio was the lowest in the case of one treatment pass.
- Recast layer thickness was reduced by around 30% when ECAP-treated electrodes were employed for machining. Two ECAP treatment passes presented the best surface quality in terms of Ra. However, one pass of treatment reduced the crack density of the machined surface by more than 26%.

University of Malaya

It was revealed that Cr-rich zones on the D2 steel workpiece are the favored locations for crack propagation due to the high Cr brittleness.

- The one-pass ECAP-treated electrode (C1) facilitated achieving the best machining performance in terms of TWR, machining accuracy and surface crack formation.

5.3 Nano titanium PMEDM of AISI D2 steel alloy with ECAP treated electrodes

After investing the influence of Ti nanopowder mixed dielectric and ECAP treatment of electrode on the machining, combination of these techniques have been employed to realize their mutual impact. Followings have been concluded from the investigation:

- Addition of powder to dielectric for all electrode types leads to enhancing the machined surface quality in terms of morphology and average surface roughness.
- TWR was reduced by about 11% while MRR was almost remained constant when pure dielectric was used. Addition of powder to dielectric led to slightly higher MRR and TWR.
- In overall, ECAP treatment of electrode slightly improve the corner sharpness of produced components, however, addition of powder to dielectric deteriorates this effect through increasing the dielectric ionization. Addition of powder to dielectric increase the tool wear rate for original and ECAP-treated electrodes due to increasing the ionization of dielectric fluid.
- Formation of droplets on the surface close to the cavity walls was reduced after employment of Ti nanopowder mixed dielectric or/and ECAP treatment of electrode. There is a negligible amount of Ti element deposited on the machined surface when electrodes C0, C1 or C2 were employed.

University of Malaya

5.4 Overall conclusion

Addition of Ti nanopowder to dielectric enhanced the EDM performance in terms of surface roughness and morphology during finishing owing to formation of smaller craters compared to oil dielectric. Furthermore, the MRR was improved without deposition of Ti nanopowder on the machined surface. EDM performance was improved in terms of TWR, white layer thickness and machined cavity corner sharpness after employment of severe plastic deformation to improve electrode's mechanical properties. The mutual impact of adding Ti nanopowder to dielectric and severe plastic deformation of electrode is not very effective, since they reduce each other's effect. It worth mentioning that Ti nanopowder mixed dielectric is mainly suitable for finishing regime, while severe plastic deformation of electrode is suitable for rough machining due to high TWR at this condition.

5.5 Future studies and recommendation

Addition of Ti nanopowder to dielectric for PMEDM applications is found to be promising. Furthermore, it was observed that ECAP treatment of electrode can be cost-saving particularly for machining complex shape components. It is recommended for future research to consider the addition of Ti nanopowder in other types of dielectric such as water. Furthermore, future research investigations can consider the ECAP treatment in micro-manufacturing, to produce copper electrode with superior mechanical properties and lower wear rate. This is where the electrode wear will be even more sensitive.

University of Malaya

REFERENCES

Ao, S. I., Rieger, B. B., & Amouzegar, M. (2010). *Machine Learning and Systems Engineering*: Springer Netherlands.

Askeland, D. R., Phulé, P. P., & Wright, W. J. (2003). *The science and engineering of materials* (Sixth ed.): Cengage Learning.

Azushima, A., Kopp, R., Korhonen, A., Yang, D. Y., Micari, F., Lahoti, G. D., . . . Yanagida, A. (2008). Severe plastic deformation (SPD) processes for metals. *CIRP Ann., 57*, 716–735.

Bai, X., Zhang, Q.-H., Yang, T.-Y., & Zhang, J.-H. (2013). Research on material removal rate of powder mixed near dry electrical discharge machining. *The International Journal of Advanced Manufacturing Technology, 68*(5-8), 1757-1766. doi:10.1007/s00170-013-4973-2

Bai, X., Zhang, Q., Zhang, J., Kong, D., & Yang, T. (2013). Machining efficiency of powder mixed near dry electrical discharge machining based on different material combinations of tool electrode and workpiece electrode. *Journal of Manufacturing Processes, 15*(4), 474-482. doi:10.1016/j.jmapro.2013.09.005

Bajaj, R., Tiwari, A. K., & Dixit, A. R. (2015). Current Trends in Electric Discharge Machining Using Micro and Nano Powder Materials- A Review. *Materials Today: Proceedings, 2*(4-5), 3302-3307. doi:10.1016/j.matpr.2015.07.147

Baseri, H., & Sadeghian, S. (2015). Effects of nanopowder TiO2-mixed dielectric and rotary tool on EDM. *International Journal of Advanced Manufacturing Technology*. doi:10.1007/s00170-015-7579-z

Batish, A., Bhattacharya, A., Singla, V. K., & Singh, G. (2012). Study of Material Transfer Mechanism in Die Steels Using Powder Mixed Electric Discharge Machining. *Materials and Manufacturing Processes, 27*(4), 449-456. doi:10.1080/10426914.2011.585498

Benbow, D. W., Elshennawy, A. K., & Walker, H. F. (2003). *The Certified Quality Technician Handbook*: ASQ Quality Press.

Bhattacharya, A., Batish, A., & Kumar, N. (2013). Surface characterization and material migration during surface modification of die steels with silicon, graphite and tungsten powder in EDM process. *Journal of Mechanical Science and Technology, 27*(1), 133-140. doi:10.1007/s12206-012-0883-8

Bhattacharya, A., Batish, A., Singh, G., & Singla, V. K. (2011). Optimal parameter settings for rough and finish machining of die steels in powder-mixed EDM. *The International Journal of Advanced Manufacturing Technology, 61*(5-8), 537-548. doi:10.1007/s00170-011-3716-5

Bird, J. (2013). *Science for Engineering*: Taylor & Francis.

Boilard, S. (2013). Explosibility of Micron- and Nano-Size Titanium Powders.

University of Malaya

Chen, S.-L., Lin, M.-H., Huang, G.-X., & Wang, C.-C. (2014). Research of the recast layer on implant surface modified by micro-current electrical discharge machining using deionized water mixed with titanium powder as dielectric solvent. *Applied Surface Science, 311*, 47-53. doi:10.1016/j.apsusc.2014.04.204

Chen, Y.-F., & Lin, Y.-C. (2009). Surface modifications of Al–Zn–Mg alloy using combined EDM with ultrasonic machining and addition of TiC particles into the dielectric. *Journal of Materials Processing Technology, 209*(9), 4343-4350. doi:10.1016/j.jmatprotec.2008.11.013

Chow, H.-M., Yan, B.-H., Huang, F.-Y., & Hung, J.-C. (2000). Study of added powder in kerosene for the micro-slit machining of titanium alloy using electro-discharge machining. *Journal of Materials Processing Technology, 101*(1–3), 95-103. doi:http://dx.doi.org/10.1016/S0924-0136(99)00458-6

Chow, H.-M., Yang, L.-D., Lin, C.-T., & Chen, Y.-F. (2008). The use of SiC powder in water as dielectric for micro-slit EDM machining. *Journal of Materials Processing Technology, 195*(1-3), 160-170. doi:10.1016/j.jmatprotec.2007.04.130

Davim, J. P., Maranhão, C., Cabral, G., & Grácio, J. (2009). Performance of cutting tools in machining Cu/W alloys for application in EDM electrodes. *International Journal of Refractory Metals and Hard Materials, 27*(4), 676-682. doi:10.1016/j.ijrmhm.2008.10.018

Descoeudres, A., Hollenstein, C., Demellayer, R., & Wälder, G. (2004). Optical emission spectroscopy of electrical discharge machining plasma. *Journal of Materials Processing Technology, 149*(1), 184-190.

Dunstan, D. J., & Bushby, A. J. (2014). Grain size dependence of the strength of metals: The Hall–Petch effect does not scale as the inverse square root of grain size. *Int. J. Plast., 53*, 56–65.

Edalati, K., Imamura, K., Kiss, T., & Horita, Z. (2012). Equal-Channel Angular Pressing and High-Pressure Torsion of Pure Copper: Evolution of Electrical Conductivity and Hardness with Strain. *Materials Transactions, 53*(1), 123-127. doi:10.2320/matertrans.MD201109

Ekmekci, B. (2007). Residual stresses and white layer in electric discharge machining (EDM). *Applied Surface Science, 253*(23), 9234-9240. doi:10.1016/j.apsusc.2007.05.078

Ekmekci, B. (2009). White Layer Composition, Heat Treatment, and Crack Formation in Electric Discharge Machining Process. *Metallurgical and Materials Transactions B, 40*(1), 70-81. doi:10.1007/s11663-008-9220-0

Ekmekci, B., & Ersöz, Y. (2012). How Suspended Particles Affect Surface Morphology in Powder Mixed Electrical Discharge Machining (PMEDM). *Metallurgical and Materials Transactions B, 43*(5), 1138-1148. doi:10.1007/s11663-012-9700-0

El-Hofy, H. (2005). *Advanced Machining Processes: Nontraditional and Hybrid Machining Processes*: McGraw-Hill Education.

University of Malaya

Estrin, Y., & Vinogradov, A. (2013). Extreme grain refinement by severe plastic deformation: a wealth of challenging science. *Acta Materialia, 61*(3), 782-817.

Farkas, D., Van Swygenhoven, H., & Derlet, P. (2002). Intergranular fracture in nanocrystalline metals. *Physical Review B, 66*(6), 060101.

Fischer-Cripps, A. C. (2000). *Factors Affecting Nanoindentation Test Data*: Springer.

Furutani, K., & Shiraki, K. (2002). Deposition of Lubricant Layer during Finishing Process by Electrical Discharge Machining with Molybdenum Disulfide Powder Suspended in Working Fluid. *JSME Materials and Processing Conference (M&P), 10*(2), 468-473.

Furutania, K., Saneto, A., Takezawa, H., Mohri, N., & Miyake, H. (2001a). Accretion of titanium carbide by electrical discharge machining with powder suspended in working fluid. *Precision Engineering, 25*(2), 138–144.

Furutania, K., Saneto, A., Takezawa, H., Mohri, N., & Miyake, H. (2001b). Accretion of titanium carbide by electrical discharge machining with powder suspended in working fluid. *Precision Engineering, 25*(2), 138-144. doi:10.1016/s0141-6359(00)00068-4

Gaitonde, V. N., Karnik, S. R., Faustino, M., & Davim, J. P. (2010). Machinability analysis in turning tungsten–copper composite for application in EDM electrodes. *International Journal of Refractory Metals and Hard Materials, 28*(2), 221-227. doi:http://dx.doi.org/10.1016/j.ijrmhm.2009.10.002

Garg, R. K., Singh, K. K., Sachdeva, A., Sharma, V. S., Ojha, K., & Singh, S. (2010). Review of research work in sinking EDM and WEDM on metal matrix composite materials. *The International Journal of Advanced Manufacturing Technology, 50*(5-8), 611-624. doi:10.1007/s00170-010-2534-5

Gopalakannan, S., & Senthilvelan, T. (2012). Effect of Electrode Materials on Electric Discharge Machining of 316 L and 17-4 PH Stainless Steels *Journal of Minerals and Materials Characterization and Engineering*.

Gostimirovic, M., Kovac, P., Sekulic, M., & Skoric, B. (2012). Influence of discharge energy on machining characteristics in EDM. *Journal of Mechanical Science and Technology, 26*(1), 173-179. doi:10.1007/s12206-011-0922-x

Guu, Y. H. (2005). AFM surface imaging of AISI D2 tool steel machined by the EDM process. *Applied Surface Science, 242*(3-4), 245-250. doi:10.1016/j.apsusc.2004.08.028

Guu, Y. H., & Hou, M. T.-K. (2007). Effect of machining parameters on surface textures in EDM of Fe-Mn-Al alloy. *Materials Science and Engineering: A, 466*(1-2), 61-67. doi:10.1016/j.msea.2007.02.035

Hasçalık, A., & Çaydaş, U. (2007). Electrical discharge machining of titanium alloy (Ti–6Al–4V). *Applied Surface Science, 253*(22), 9007-9016. doi:10.1016/j.apsusc.2007.05.031

Haynes, W. M. (2010). *CRC Handbook of Chemistry and Physics, 91st Edition*: Taylor & Francis.

University of Malaya

Ho, K. H., & Newman, S. T. (2003). State of the art electrical discharge machining (EDM). *International Journal of Machine Tools and Manufacture, 43*(13), 1287-1300. doi:10.1016/s0890-6955(03)00162-7

Hockenberry, T. (1967). Geometrical formation of the discharge channel in narrow gaps. *SME Paper*.

Hu, F. Q., Cao, F. Y., Song, B. Y., Hou, P. J., Zhang, Y., Chen, K., & Wei, J. Q. (2013). Surface Properties of SiCp/Al Composite by Powder-Mixed EDM. *Procedia CIRP, 6*, 101-106. doi:10.1016/j.procir.2013.03.036

Jahan, M. P. (2013). Micro-Electrical Discharge Machining. 111-151. doi:10.1007/978-1-4471-5179-1_4

Jahan, M. P., Rahman, M., & Wong, Y. S. (2010). Study on the nano-powder-mixed sinking and milling micro-EDM of WC-Co. *The International Journal of Advanced Manufacturing Technology, 53*(1-4), 167-180. doi:10.1007/s00170-010-2826-9

Jain, P. V. K. (2009). *Advanced Machining Processes*: Allied Publishers Pvt Limited.

Jameson, E. C. (2001). *Electrical Discharge Machining*: Society of Manufacturing Engineers.

Janmanee, P., & Muttamara, A. (2012). Surface modification of tungsten carbide by electrical discharge coating (EDC) using a titanium powder suspension. *Applied Surface Science, 258*(19), 7255-7265. doi:10.1016/j.apsusc.2012.03.054

Jeswani, M. L. (1981). Effect of the addition of graphite powder to kerosene used as the dielectric fluid in electrical discharge machining. *Wear, 70*(2), 133-139. doi:http://dx.doi.org/10.1016/0043-1648(81)90148-4

Joshi, S., Govindan, P., Malshe, A., & Rajurkar, K. (2011). Experimental characterization of dry EDM performed in a pulsating magnetic field. *CIRP Annals - Manufacturing Technology, 60*(1), 239-242. doi:10.1016/j.cirp.2011.03.114

Kansal, H. K., Singh, S., & Kumar, P. (2005). Parametric optimization of powder mixed electrical discharge machining by response surface methodology. *Journal of Materials Processing Technology, 169*(3), 427-436. doi:10.1016/j.jmatprotec.2005.03.028

Kansal, H. K., Singh, S., & Kumar, P. (2006). An experimental study of the machining parameters in powder mixed electric discharge machining of Al–10%SiCP metal matrix composites. *International Journal of Machining and Machinability of Materials, 1*(4), 396-411. doi:10.1504/IJMMM.2006.012349

Kansal, H. K., Singh, S., & Kumar, P. (2007a). Effect of Silicon Powder Mixed EDM on Machining Rate of AISI D2 Die Steel. *Journal of Manufacturing Processes, 9*(1), 13-22. doi:10.1016/s1526-6125(07)70104-4

Kansal, H. K., Singh, S., & Kumar, P. (2007b). Technology and research developments in powder mixed electric discharge machining (PMEDM). *Journal of Materials Processing Technology, 184*(1-3), 32-41. doi:10.1016/j.jmatprotec.2006.10.046

University of Malaya

Kibria, G., & Bhattacharyya, B. (2010). *Analysis on Geometrical Accuracy of Microhole during Micro-EDM of Ti-6Al-4V using Different Dielectrics*. Paper presented at the International Conference on Advances in Material and Processing Technologies.

Kibria, G., Sarkar, B. R., Pradhan, B. B., & Bhattacharyya, B. (2009). Comparative study of different dielectrics for micro-EDM performance during microhole machining of Ti-6Al-4V alloy. *The International Journal of Advanced Manufacturing Technology, 48*(5-8), 557-570. doi:10.1007/s00170-009-2298-y

Kim, H. S., Hong, S. I., & Seo, M. H. (2001). Effects of strain hardenability and strain-rate sensitivity on the plastic flow and deformation homogeneity during equal channel angular pressing. *Journal of Materials Research, 16*(03), 856-864.

Kim, W., Hong, S., Kim, Y., Min, S., Jeong, H., & Lee, J. (2003). Texture development and its effect on mechanical properties of an AZ61 Mg alloy fabricated by equal channel angular pressing. *Acta Materialia, 51*(11), 3293-3307.

Klocke, F., Lung, D., Antonoglou, G., & Thomaidis, D. (2004). The effects of powder suspended dielectrics on the thermal influenced zone by electrodischarge machining with small discharge energies. *Journal of Materials Processing Technology, 149*(1–3), 191-197. doi:http://dx.doi.org/10.1016/j.jmatprotec.2003.10.036

Kojima, A., Natsu, W., & Kunieda, M. (2008). Spectroscopic measurement of arc plasma diameter in EDM. *CIRP Annals - Manufacturing Technology, 57*(1), 203-207. doi:10.1016/j.cirp.2008.03.097

Kolli, M., & Kumar, A. (2015). Effect of dielectric fluid with surfactant and graphite powder on Electrical Discharge Machining of titanium alloy using Taguchi method. *Engineering Science and Technology, an International Journal, 18*(4), 524-535. doi:10.1016/j.jestch.2015.03.009

Kumar, A., Maheshwari, S., Sharma, C., & Beri, N. (2012). Machining Efficiency Evaluation of Cryogenically Treated Copper Electrode in Additive Mixed EDM. *Materials and Manufacturing Processes, 27*(10), 1051-1058. doi:10.1080/10426914.2011.654151

Kumar, S., & Batra, U. (2012). Surface modification of die steel materials by EDM method using tungsten powder-mixed dielectric. *Journal of Manufacturing Processes, 14*(1), 35-40. doi:10.1016/j.jmapro.2011.09.002

Kumar, S., Singh, R., Singh, T. P., & Sethi, B. L. (2009). Surface modification by electrical discharge machining: A review. *Journal of Materials Processing Technology, 209*(8), 3675-3687. doi:10.1016/j.jmatprotec.2008.09.032

Kung, K.-Y., Horng, J.-T., & Chiang, K.-T. (2007). Material removal rate and electrode wear ratio study on the powder mixed electrical discharge machining of cobalt-bonded tungsten carbide. *The International Journal of Advanced Manufacturing Technology, 40*(1-2), 95-104. doi:10.1007/s00170-007-1307-2

Langdon, T. G., Furukawa, M., Nemoto, M., & Horita, Z. (2000). Using equal-channel angular pressing for refining grain size. *JOM, 52*(4), 30-33.

University of Malaya

Lee, H. T., & Tai, T. Y. (2003). Relationship between EDM parameters and surface crack formation. *Journal of Materials Processing Technology, 142*, 676–683.

Lee, S. H., & Li, X. P. (2001). Study of the effect of machining parameters on the machining characteristics in electrical discharge machining of tungsten carbide. *Journal of Materials Processing Technology, 115*(3), 344–358.

Li, J. Z., Shen, F. H., Yu, Z. Y., & Natsu, W. (2013). Influence of microstructure of alloy on the machining performance of micro EDM. *Surface and Coatings Technology, 228*, S460-S465. doi:10.1016/j.surfcoat.2012.05.025

Li, L., Wong, Y. S., Fuh, J. Y. H., & Lu, L. (2001). Effect of TiC in copper–tungsten electrodes on EDM performance. *Journal of Materials Processing Technology, 113*(1–3), 563-567. doi:http://dx.doi.org/10.1016/S0924-0136(01)00622-7

Li, L., Zongwei, N., & Guangming, Y. (2009) Effect of ultrasonic vibration of tool on electrical discharge machining of sintered NdFeB magnet. *Vol. 407-408. Key Engineering Materials* (pp. 628-631).

Li, S., Bourke, M., Beyerlein, I., Alexander, D., & Clausen, B. (2004). Finite element analysis of the plastic deformation zone and working load in equal channel angular extrusion. *Materials Science and Engineering: A, 382*(1), 217-236.

Liao, S., Dourmashkin, P., & Belcher, J. (2004). Capacitance and DielectricsElectricity and Magnetism: Massachusetts Institute of Technology.

Liew, P. J., Yan, J., & Kuriyagawa, T. (2013). Carbon nanofiber assisted micro electro discharge machining of reaction-bonded silicon carbide. *Journal of Materials Processing Technology, 213*(7), 1076-1087. doi:10.1016/j.jmatprotec.2013.02.004

Liew, P. J., Yan, J., & Kuriyagawa, T. (2014). Fabrication of deep micro-holes in reaction-bonded SiC by ultrasonic cavitation assisted micro-EDM. *International Journal of Machine Tools and Manufacture, 76*, 13-20. doi:10.1016/j.ijmachtools.2013.09.010

Lima, M. S. F. d., & Sankaré, S. (2014). Microstructure and mechanical behavior of laser additive manufactured AISI 316 stainless steel stringers. *Materials & Design, 55*, 526–532.

Liu, Y., Li, X., Bai, F., Chen, J., Wang, Y., & Liu, N. (2014). Effect of system parameters on the size distributions of hollow nickel microspheres produced by an ultrasound-aided electrical discharge machining process. *Particuology, 17*(0), 36-41. doi:http://dx.doi.org/10.1016/j.partic.2013.11.002

Liu, Y., Wang, J., Zhao, F., & Wang, Y. (2010, 23-25 Nov. 2010). *Research on dielectric breakdown mechanism of micro EDM.* Paper presented at the Advanced Technology of Design and Manufacture (ATDM 2010), International Conference on.

Luo, Y. F. (1997). The dependence of interspace discharge transitivity upon the gap debris in precision electrodischarge machining. *Journal of Materials Processing Technology, 68*(2), 121-131. doi:http://dx.doi.org/10.1016/S0924-0136(96)00019-2

University of Malaya

Maradia, U., Boccadoro, M., Stirnimann, J., Kuster, F., & Wegener, K. (2015). Electrode wear protection mechanism in meso–micro-EDM. *Journal of Materials Processing Technology, 223*, 22-33. doi:10.1016/j.jmatprotec.2015.03.039

Marashi, H., Jafarlou, D. M., Sarahan, A. A. D., & Mardi, N. A. Employing severe plastic deformation to the processing of electrical discharge machining electrodes. *Precision Engineering*. doi:http://dx.doi.org/10.1016/j.precisioneng.2016.05.012

Marashi, H., Jafarlou, D. M., Sarhan, A. A., & Hamdi, M. (2016). State of the art in powder mixed dielectric for EDM applications. *Precision Engineering*.

Marashi, H., Sarhan, A. A. D., & Hamdi, M. (2015). Employing Ti nano-powder dielectric to enhance surface characteristics in electrical discharge machining of AISI D2 steel. *Applied Surface Science, 357, Part A*, 892-907. doi:http://dx.doi.org/10.1016/j.apsusc.2015.09.105

Marci, M., & Csanyi, L. *Electric breakdown strength measurement of liquid dielectric samples exposed to the weather effect*.

Masuzawa, T. (2000). State of the Art of Micromachining. *CIRP Annals - Manufacturing Technology, 49*(2), 473-488. doi:10.1016/s0007-8506(07)63451-9

Meena, V. K., & Azad, M. S. (2012). Grey Relational Analysis of Micro-EDM Machining of Ti-6Al-4V Alloy. *Materials and Manufacturing Processes, 27*(9), 973-977. doi:10.1080/10426914.2011.610080

Ming, Q. Y., & He, L. Y. (1995). Powder-suspension dielectric fluid for EDM. *Journal of Materials Processing Tech., 52*(1), 44-54. doi:10.1016/0924-0136(94)01442-4

Mishra, A., Kad, B., Gregori, F., & Meyers, M. (2007). Microstructural evolution in copper subjected to severe plastic deformation: Experiments and analysis. *Acta Materialia, 55*(1), 13-28.

Mohd Abbas, N., Solomon, D. G., & Fuad Bahari, M. (2007). A review on current research trends in electrical discharge machining (EDM). *International Journal of Machine Tools and Manufacture, 47*(7-8), 1214-1228. doi:10.1016/j.ijmachtools.2006.08.026

Molinetti, A., Amorim, F. L., Soares, P. C., Jr., & Czelusniak, T. (2015). Surface modification of AISI H13 tool steel with silicon or manganese powders mixed to the dielectric in electrical discharge machining process. *International Journal of Advanced Manufacturing Technology*. doi:10.1007/s00170-015-7613-1

Muthuramalingam, T., & Mohan, B. (2015). A review on influence of electrical process parameters in EDM process. *Archives of Civil and Mechanical Engineering, 15*(1), 87-94. doi:10.1016/j.acme.2014.02.009

Nakashima, K., Horita, Z., Nemoto, M., & Langdon, T. G. (1998). Influence of channel angle on the development of ultrafine grains in equal-channel angular pressing. *Acta Materialia, 46*(5), 1589-1599. doi:http://dx.doi.org/10.1016/S1359-6454(97)00355-8

University of Malaya

Ojha, K., Garg, R. K., & Singh, K. K. (2011). Parametric Optimization of PMEDM Process using Chromium Powder Mixed Dielectric and Triangular Shape Electrodes. *Journal of Minerals & Materials Characterization & Engineering*.

Patel, V., Patel, C., & Patel, U. (2012). Analysis of Different Tool Material on MRR and Surface Roughness of Mild Steel in EDM. *International Journal of Engineering Research & Application, 1*, 394-397.

Patowari, P. K., Mishra, U. K., Saha, P., & Mishra, P. K. (2011). Surface Integrity of C-40 Steel Processed with WC-Cu Powder Metallurgy Green Compact Tools in EDM. *Materials and Manufacturing Processes, 26*, 668–676.

Peças, P., & Henriques, E. (2003). Influence of silicon powder-mixed dielectric on conventional electrical discharge machining. *International Journal of Machine Tools and Manufacture, 43*(14), 1465-1471. doi:10.1016/s0890-6955(03)00169-x

Peças, P., & Henriques, E. (2007). Effect of the powder concentration and dielectric flow in the surface morphology in electrical discharge machining with powder-mixed dielectric (PMD-EDM). *The International Journal of Advanced Manufacturing Technology, 37*(11-12), 1120-1132. doi:10.1007/s00170-007-1061-5

Prangnell, P., Harris, C., & Roberts, S. (1997). Finite element modelling of equal channel angular extrusion. *Scripta Materialia, 37*(7), 983-989.

Prihandana, G. S., Mahardika, M., Hamdi, M., Wong, Y. S., Miki, N., & Mitsui, K. (2013). Study of workpiece vibration in powder-suspended dielectric fluid in micro-EDM processes. *International Journal of Precision Engineering and Manufacturing, 14*(10), 1817-1822. doi:10.1007/s12541-013-0243-3

Prihandana, G. S., Mahardika, M., Hamdi, M., Wong, Y. S., & Mitsui, K. (2009). Effect of micro-powder suspension and ultrasonic vibration of dielectric fluid in micro-EDM processes—Taguchi approach. *International Journal of Machine Tools and Manufacture, 49*(12-13), 1035-1041. doi:10.1016/j.ijmachtools.2009.06.014

Prihandana, G. S., Mahardika, M., Hamdi, M., Wong, Y. S., & Mitsui, K. (2011). Accuracy improvement in nanographite powder-suspended dielectric fluid for micro-electrical discharge machining processes. *The International Journal of Advanced Manufacturing Technology, 56*(1-4), 143-149. doi:10.1007/s00170-011-3152-6

Railsback. (2008). Some Fundamentals of Mineralogy and Geochemistry.

Rao, P. N. (2009). *MANUFACTURING TECHNOLOGY: Metal Cutting & Machine Tools, Volume II, 2E*: McGraw-Hill Education (India) Pvt Limited.

Riedel, H. (1987). *Fracture at High Temperatures*: Springer.

Saito, Y., Utsunomiya, H., Tsuji, N., & Sakai, T. (1999). Novel ultra-high straining process for bulk materials development of the accumulative roll-bonding (ARB) process. *Acta Mater., 47*(2), 579-583.

University of Malaya

Salimyanfard, F., Toroghinejad, M. R., Ashrafizadeh, F., Hoseini, M., & Szpunar, J. A. (2013). Investigation of texture and mechanical properties of copper processed by new route of equal channel angular pressing. *Materials & Design, 44*, 374-381.

Samuel, M. P., & Philip, P. K. (1997). Power metallurgy tool electrodes for electrical discharge machining. *International Journal of Machine Tools and Manufacture, 37*(11), 1625-1633. doi:http://dx.doi.org/10.1016/S0890-6955(97)00006-0

Schumacher, B. M. (1965). *Removal behavior and wear when sparkeroding steel with condenser- and semiconductor-pulse generators.* RWTH Aachen.

Schumacher, B. M. (2004). After 60 years of EDM the discharge process remains still disputed. *Journal of Materials Processing Technology, 149*(1-3), 376-381. doi:10.1016/j.jmatprotec.2003.11.060

Segal, V. M. (1999). Equal channel angular extrusion: from macromechanics to structure formation. *Materials Science and Engineering A, 271*(1-2), 322-333.

Sevillano, J. G., Van Houtte, P., & Aernoudt, E. (1980). Large strain work hardening and textures. *Progress in Materials Science, 25*(2), 69-134.

Sidhu, S. S., Batish, A., & Kumar, S. (2014). Study of Surface Properties in Particulate-Reinforced Metal Matrix Composites (MMCs) Using Powder-Mixed Electrical Discharge Machining (EDM). *Materials and Manufacturing Processes, 29*(1), 46-52. doi:10.1080/10426914.2013.852211

Singh, A. K., Kumar, S., & Singh, V. P. (2015). Effect of the addition of conductive powder in dielectric on the surface properties of superalloy Super Co 605 by EDM process. *International Journal of Advanced Manufacturing Technology, 77*(1-4), 99-106. doi:10.1007/s00170-014-6433-z

Singh, S., Maheshwari, S., & Pandey, P. C. (2004). Some investigations into the electric discharge machining of hardened tool steel using different electrode materials. *Journal of Materials Processing Technology, 149*(1-3), 272-277. doi:10.1016/j.jmatprotec.2003.11.046

Smith, W. F., & Hashemi, J. (2003). *Foundations of Materials Science and Engineering*: McGraw-Hill.

Sommer, C., & Sommer, S. (2005). *Complete EDM Handbook*: Advance Publishing, Incorporated.

Srivastava, V., & Pandey, P. M. (2013). Study of ultrasonic assisted cryogenically cooled EDM process using sintered (Cu–TiC) tooltip. *Journal of Manufacturing Processes, 15*(1), 158-166. doi:10.1016/j.jmapro.2012.12.002

Subramanian, R., Marimuthu, K., & Sakthivel, M. (2012). Study of Crack Formation and Re-Solidified Layer in EDM Process on T90Mn2W50Cr45 Tool Steel. *Materials and Manufacturing Processes*, 121008121903005. doi:10.1080/10426914.2012.727120

Suś-Ryszkowska, M., Wejrzanowski, T., Pakieła, Z., & Kurzydłowski, K. (2004). Microstructure of ECAP severely deformed iron and its mechanical properties. *Materials Science and Engineering: A, 369*(1), 151-156.

University of Malaya

Suzuki, T., Takeuchi, S., & Yoshinaga, H. (2013). *Dislocation dynamics and plasticity* (Vol. 12): Springer Science & Business Media.

Torre, F. D., Lapovok, R., Sandlin, J., Thomson, P. F., Davies, C. H. J., & Pereloma, E. V. (2004). Microstructures and properties of copper processed by equal channel angular extrusion for 1–16 passes. *Acta Materialia*, *52*(16), 4819–4832.

Torres, A., Puertas, I., & Luis, C. J. (2014). Modelling of surface finish, electrode wear and material removal rate in electrical discharge machining of hard-to-machine alloys. *Precision Engineering*. doi:10.1016/j.precisioneng.2014.10.001

Tsai, H. C., Yan, B. H., & Huang, F. Y. (2003). EDM performance of Cr/Cu-based composite electrodes. *International Journal of Machine Tools and Manufacture, 43*(3), 245–252.

Tsai, K.-M., & Wang, P.-J. (2001). Predictions on surface finish in electrical discharge machining based upon neural network models. *International Journal of Machine Tools and Manufacture, 41*(10), 1385-1403. doi:http://dx.doi.org/10.1016/S0890-6955(01)00028-1

Tzeng, Y. F., & Lee, C. Y. (2001). Effects of Powder Characteristics on Electrodischarge Machining Efficiency. *The International Journal of Advanced Manufacturing Technology, 17*(8), 586-592. doi:10.1007/s001700170142

Valiev, R. (2004). Nanostructuring of metals by severe plastic deformation for advanced properties. *Nat. Mater., 3*(8), 511-516.

Valiev, R., Estrin, Y., Horita, Z., Langdon, T., Zehetbauer, M., & Zhu, Y. (2015). Fundamentals of superior properties in bulk nanoSPD materials. *Materials Research Letters*(ahead-of-print), 1-21.

Valiev, R. Z., Estrin, Y., Horita, Z., Langdon, T. G., Zechetbauer, M. J., & Zhu, Y. T. (2006). Producing bulk ultrafine-grained materials by severe plastic deformation. *JOM, 58*(4), 33-39.

Valiev, R. Z., Krasilnikov, N. A., & Tsenev, N. K. (1991). Plastic deformation of alloys with submicron-grained structure. *Mater. Sci. Eng., A, 137*, 35–40.

Valiev, R. Z., & Langdon, T. G. (2006). Principles of equal-channel angular pressing as a processing tool for grain refinement. *Progress in Materials Science, 51*(7), 881-981.

Wadhwa, C. L. (2007). *High Voltage Engineering*: New Age International (P) Limited.

Wang, A. C., Tsai, L., & Lin, Y.-C. (2014). Characterizing the machining effects of lateral electrodes in electrical discharge machining. *International Journal of Precision Engineering and Manufacturing, 15*(6), 1095-1100. doi:10.1007/s12541-014-0442-6

Wang, Y. L., Lapovok, R., Wang, J. T., Qi, Y. S., & Estrin, Y. (2015). Thermal behavior of copper processed by ECAP with and without back pressure. *Materials Science and Engineering: A, 628*, 21-29. doi:10.1016/j.msea.2015.01.021

University of Malaya

Wei, K. X., Wei, W., Wang, F., Du, Q. B., Alexandrov, I. V., & Hu, J. (2011). Microstructure, mechanical properties and electrical conductivity of industrial Cu–0.5%Cr alloy processed by severe plastic deformation. *Materials Science and Engineering: A, 528*(3), 1478–1484.

Wong, Y. S., Lim, L. C., & Lee, L. C. (1995). Effects of flushing on electro-discharge machined surfaces. *Journal of Materials Processing Technology, 48*(1–4), 299-305. doi:http://dx.doi.org/10.1016/0924-0136(94)01662-K

Wong, Y. S., Lim, L. C., Rahuman, I., & Tee, W. M. (1998). Near-mirror-finish phenomenon in EDM using powder-mixed dielectric. *Journal of Materials Processing Technology, 79*(1-3), 30-40. doi:10.1016/s0924-0136(97)00450-0

Wu, K. L., Yan, B. H., Huang, F. Y., & Chen, S. C. (2005). Improvement of surface finish on SKD steel using electro-discharge machining with aluminum and surfactant added dielectric. *International Journal of Machine Tools and Manufacture, 45*(10), 1195-1201. doi:10.1016/j.ijmachtools.2004.12.005

Yih-fong, T., & Fu-chen, C. (2005). Investigation into some surface characteristics of electrical discharge machined SKD-11 using powder-suspension dielectric oil. *Journal of Materials Processing Technology, 170*(1-2), 385-391. doi:10.1016/j.jmatprotec.2005.06.006

Zhao, W. S., Meng, Q. G., & Wang, Z. L. (2002). The application of research on powder mixed EDM in rough machining. *Journal of Materials Processing Technology, 129*(1–3), 30-33. doi:http://dx.doi.org/10.1016/S0924-0136(02)00570-8

Zhu, C., Du, F., Jiao, Q., Wang, X., Chen, A., Liu, F., & Pan, D. (2013). Microstructure and strength of pure Cu with large grains processed by equal channel angular pressing. *Materials & Design, 52*, 23-29.

Zhu, Y. T., & Lowe, T. C. (2000). Observations and issues on mechanisms of grain refinement during ECAP process. *Materials Science and Engineering: A, 291*(1–2), 46-53. doi:http://dx.doi.org/10.1016/S0921-5093(00)00978-3

University of Malaya

LIST OF PUBLICATIONS

1. Marashi, H.; Sarhan, A. A. D.; Hamdi, M., Employing Ti nano-powder dielectric to enhance surface characteristics in electrical discharge machining of AISI D2 steel. Applied Surface Science 2015, 357, Part A, 892-907.
2. Marashi, H.; Jafarlou, D.; Sarahan, A.; Mardi, N., Employing severe plastic deformation to the processing of electrical discharge machining electrodes. Precision Engineering 2016.
3. Marashi, H.; Jafarlou, D. M.; Sarhan, A. A.; Hamdi, M., State of the art in powder mixed dielectric for EDM applications. Precision Engineering 2016.
4. Marashi, H.; Sarhan, A. A. D.; Maher, I.; Sayuti, M., Various Techniques to Improve EDM Capabilities: A Review. In Reference Module in Materials Science and Materials Engineering, Elsevier: 2016.

University of Malaya